Ephemeral Hydrological Processes in Savannas

ES Riddell, J Nel, D Fundisi, A van Niekerk, SA Lorentz

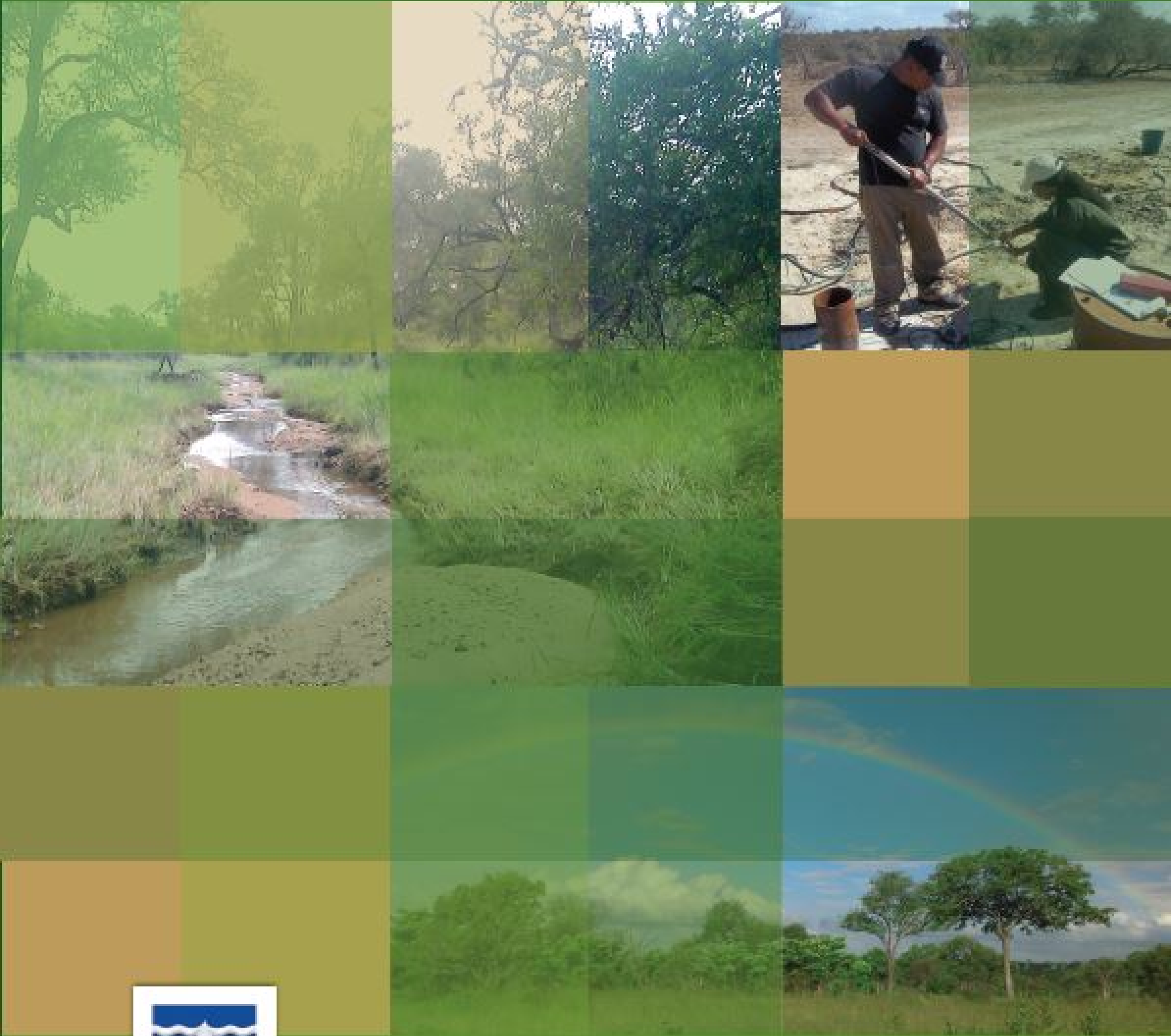

WATER RESEARCH COMMISSION

TT 619/14

Ephemeral Hydrological Processes in Savannas

ES Riddell, J Nel, D Fundisi, F Jumbi, A van Niekerk, SA Lorentz

Report to the
Water Research Commission

by

Centre for Water Resources Research
School of Agriculture, Earth and Environmental Sciences
University of KwaZulu-Natal

&

Groundwater Consulting Services with the
Department of Earth Sciences
University of the Western Cape

WRC Report No. TT 619/14

December 2014

Obtainable from

Water Research Commission
Private Bag X03
Gezina, Pretoria
0031 SOUTH AFRICA

orders@wrc.org.za or download from www.wrc.org.za

The publication of this report emanates from a project entitled: *Surface Water, Groundwater and Vadose Zone Interactions in Selected Pristine Catchments in the Kruger National Park* (WRC Project No K5/2051).

ISBN 978-1-4312-0616-2
Printed in the Republic of South Africa

EXECUTIVE SUMMARY

There is a tight coupling of hydrological, geological and ecological processes in the semi-arid setting of the lowveld savannas of South Africa. In the Kruger National Park (KNP) this has resulted in distinct landscape patterns closely organised around the hierarchical drainage network of seasonal and ephemeral streams which dominate the landscape. These patterns have resulted from a relatively stable geological template, the topographical redistribution of water and the resultant geomorphic setting one sees in the KNP today. Overtime this has led to the establishment of unique soil and vegetation assemblages in the landscape at both the hillslope and catchment scale.

South African National Parks (SANParks) embarked on a long-term research strategy to study both the biotic and abiotic components of savanna ecological interactions in an integrated, trans-disciplinary manner on un-manipulated sites. The KNP *Supersites* were established as living laboratories in order to grow this integrated ecological science and inform management in order to allow extrapolation of knowledge to other parts of the KNP, the broader lowveld landscape, and other savanna systems.

It is on this basis that the research presented in this report augments the Supersite dataset to describe a key component of the abiotic template for dominant landscapes in the KNP. Focusing on granitic and basaltic terrains the research has determined the extent of surface water, groundwater and vadose zone interactions within the drainage hierarchy of 1st-3rd order streams represented within the KNP Supersites. The research had the following core objectives centred on the concept of *hydrological connectivity*:

Quantify the role of hydrological inter-connectedness between hydrological process domains;

Determine the spatio-temporal variability of this interconnectedness in order to understand the hydrological fluxes that drive these savanna systems;

using the following conceptual framework as the basis for the research:

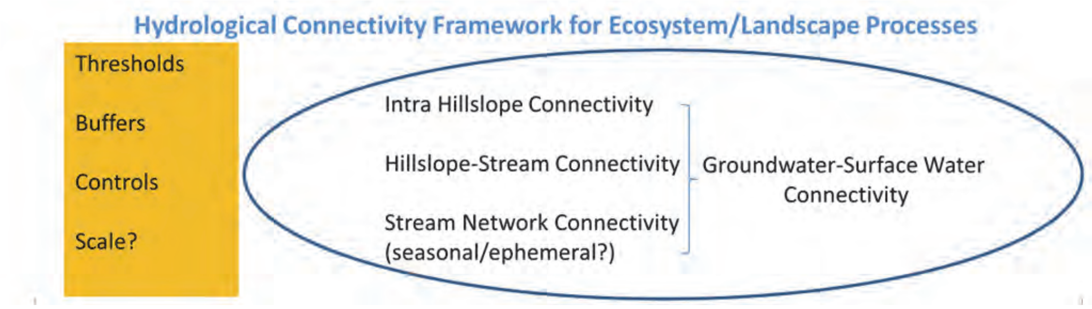

Four sites were established as Supersites in the KNP in 2011 and the research presented here focuses on two in the south of the park: Stevenson-Hamilton on granite (Southern Granites or SGR); and Nhlowa on basalt (Southern Basalt or SBAS). Both sites are situated on the hydrological divide (watershed) between the perennial Sabie and Crocodile Rivers.

The hydrological approach was the same for both sites in order to allow for inter-comparison of hydrological connectivity across geological settings and included: intensive geophysical surveys; drilling and characterisation of a piezometric borehole network; ephemeral streamflow gauging; hydro-chemical tracer sampling; hydro-pedological classification of catena sequences; associated soil moisture monitoring network; quantification of catena actual evapotranspiration through remote sensing, and a variety of other factors.

Key findings on the Southern Granite site included:

- The identification of two distinct hydrogeological zones: a shallow responsive aquifer system in the weathered zone maintaining local scale processes; and a deep aquifer system in the consolidated hard rock likely linked to regional processes with drainage toward the perennial rivers in the KNP.

- The groundwater systems do not follow the surface topography at the scale of the individual catchments investigated but rather run parallel to the surface drainage network with groundwater flow from the 1st to the 3rd order catchment.

- The 1st order stream is gaining and sustained from shallow perched aquifer contributions, whilst the 2nd order stream was found to lose water to the groundwater system along the stream conduit following significant rainfall sequences and this is likely to result from morphological changes in the catchment as one shifts scale from 1st to 2nd order. The 2nd and 3rd order stream reaches were found to experience significant transmission losses.

- It was noted that event water significantly dominates (60-100%) the intermittently connected streamflow responses at all orders.

- At the hillslope scale there are both similarities and differences moving across scales. In all 3 orders the crest soils had similar hydraulic properties, of vertical free drainage (high groundwater recharge potential) and interflow soils on the midslopes (although poorly represented at the 1st order). However the footslopes differed in their hydraulic responses with saturation excess responsive soils at the 1st order, interflow soils at the 2nd order, and freely drained potential recharge (limited interflow) soils at the 3rd order.

- Overall the 1st order catchment had the greatest actual evapotranspiration with the 3rd order the least.

Key findings on the Southern Basalt site included:

- Two distinct hydrogeological zones: a weathered zone aquifer system and deeper fractured hard rock aquifer system. Similar to the granite, the general groundwater flow direction was parallel to the stream network with a west-east sloping gradient. This was most apparent in the 1st and 2nd order catchments, which are deemed entirely disconnected from the stream network.

- At the 3rd order the groundwater flow direction is also parallel to stream network in the hard rock. However the weathered aquifer system at this order generally influences the stream network with a perpendicular orientation allowing the stream to gain.

- The 3rd order stream network intersects the regional groundwater table at the lower end of the reach. The stream here becomes an important groundwater discharge point, at the geological contact between the basalts and rhyolite geology (of the Lebombo formation)

- The 3rd order reach on the southern basalts had the most persistent event-driven flows. Event water contributions to streamflow were typically >60% at the 3rd order and ~100% at the 1st order stream.

- Hillslopes at all orders show the same hydraulic characteristics of extensive inter-fluvial areas dominated by recharge (potential groundwater recharge) soils, with relatively rapid wetting-drying cycles. Lateral connectivity to the stream network is limited to the immediate riparian zone soils by surface runoff only.

- Approximately 21% of incident rainfall following a series of rainfall sequences infiltrates beyond the root suction zone to constitute potential groundwater recharge.

- Typically all orders showed similar actual evapotranspiration, although this was ~200 mm less than on the granites, during summer. At the scale of remote sensing analysis, the crest regions in general showed the greatest actual evapotranspiration, marginally higher at lower orders, which is attributed to both lower topographic gradients and deeper soil moisture storage.

ACKNOWLEDGEMENTS

The research in this non-solicited project was initiated, managed and funded by the Water Research Commission, for whose assistance we are sincerely grateful. The project would also not have been possible had it not been for the funding and services by members of the Department of Water Affairs Limpopo drilling division for the two borehole drilling campaigns in the KNP between 2012-13. Special thanks go to the staff of South African National Parks: the Kruger National Park including Dr Izak Smit and Mr Robin Petersen as project co-ordinators and interaction on project ideas. Continuous collaborative support on this project including hydropedological survey was provided by Prof Pieter Le Roux and Dr George van Zijl (and team) at the University of the Free State. Dr Matthys Dippenaar of the University of Pretoria provided geological expertise including the characterisation of borehole logs. Mr Martin de Klerk of Cape Geophysics also provided sound geophysics support during the project. Ms Carola Cullum of the Centre for Water in the Environment at the University of the Witwatersrand for continued conceptual support and reflection. Members of the Reference Group (below) are thanked for their time and invaluable expertise:

Dr S Adams (Chairman)	Water Research Commission (WRC)
Dr R Grant	SANParks
Dr I Smit	SANParks
Dr V Chaplot	IRD
Prof K Rogers	University of the Witwatersrand-CWE
Ms C Cullum	University of the Witwatersrand-CWE
Dr I Dennis	University of the North West
Dr G Steyl	University of the Free State
Dr M Dippenaar	University of Pretoria
Prof P Le Roux	University of the Free State
Dr J Van de Merwe	University of the Free State
Mr F Fourie	Department of Water Affairs
Prof O Chadwick	University of California, Santa Barbara
Mr T Scheepers	University of the Western Cape
Prof K Witthueser	Delta H

The following people provided valuable assistance in the field: Mr Annoit Mashele, Mr Adolf Manganyi, Mr Difference Thibela, Ms Lucie Porentru, Ms Tercia Strydom, Mr Denzel Bent, Mr Thomas Rowe and Mr Raymond Minnaar.

We are also grateful to eLeaf (The Netherlands) and the Inkomati Catchment Management Agency for providing access to the SEBAL raster dataset for the Incomati basin from the EU WATPLAN project.

TABLE OF CONTENTS

1 INTRODUCTION

1.1 Problem Statement (Context of the Study) 1
1.2 Research Aims and Objectives 2
1.3 State of Knowledge of Groundwater-Surface Water Interactions and Hydrological Connectivity the in KNP 2
1.4 Surface & Vadose Zone processes in the KNP 4
1.5 Geohydrology of the KNP 5
1.6 Relevant soil and geomorphology information 9
1.7 Concepts of hydrological connectivity in groundwater and surface water and application to the study area 10
1.7.1 Hydrologic Connectivity and Catchment Function 11
1.7.2 Drivers and Controls of Hydrological Connectivity 13
1.7.3 Connecting Mechanisms of Surface and Groundwater Resources 13
1.7.4 A Review of Existing Knowledge on Hydrological Connectivity 14
1.8 Structure of the report 15

2 KNP STUDY SITE DESCRIPTION

2.1 KNP Geology drainage and climate 17
2.2 KNP Supersite Selection Process 17
2.3 Study Site Details 18
2.3.1 Southern Granites (SGR) 18
2.3.2 Southern Basalts (SBAS) 18
2.4 Development of Initial Conceptual Model of GW-SW Interactions for the two Southern KNP Supersites 23
2.4.1 Southern Granite (Stevenson-Hamilton) Supersite 23
2.4.2 Southern Basalt (Nhlowa) Supersite 24

3 KEY RESPONSES & CONCEPTUAL UNDERSTANDING OF HYDROLOGICAL CONNECTIVITY OF KNPs SOUTHERN GRANITE AND BASALT SAVANNAS

3.1 Southern Granites 27
3.2 Southern Basalts 33
3.3 Key Differences and Similarities in Hydrological Processes between the two Supersites 37
3.4 Findings: relevance to catchment management, savanna ecology and the KNP Supersites concept 38

4 METHODOLOGY

4.1 Approach 40
4.2 Characterisation datasets 40
4.2.1 Geophysical surveys 41
4.2.2 Soil and Hillslope Classification (hydropedology) 42
4.2.3 Soil Hydraulic Properties Characterisation 43
4.2.4 Soil hydrodynamics 44
4.2.5 Surface Water 45
4.2.5.1 Stream channel surveys 45
4.2.5.2 Streamflow ratings 46
4.2.5.3 Stage-Discharge relationships 47
4.2.5.4 Subsurface flow characterisation 47
4.2.6 Rainfall-Runoff Analysis 48
4.2.7 Stream and Riparian Zone Hydraulic Head Monitoring 48
4.2.8 Sampling and laboratory analyses 49
4.2.8.1 Tracer Analysis 50
4.2.8.2 Hydrograph separation 50
4.2.9 Multi-piezometer groundwater monitoring network 52
4.2.9.1 Monitoring Groundwater level trends 52
4.2.9.2 Borehole Fluid logging 53
4.2.9.3 Borehole Specific Depth Sampling 53
4.2.9.4 Aquifer properties characterisation 53
4.2.10 Meteorologic Data 54
4.2.11 Actual Evapotranspiration 54
4.2.12 Modelling 55
4.2.12.1 Catena Water Balances (HYDRUS) 55
4.2.12.1.1 Model Set-up 57
4.2.12.2 Geohydrological Processes (MODFlow) 59
4.2.12.2.1 Pre-Modelling Process and Modelling Procedure 59
4.2.12.2.2 Model construction & Governing Equations 59
4.2.12.2.3 Boundary conditions 60
4.2.12.2.4 Model Calibration 60

5 RESULTS – SOUTHERN GRANITES

5.1 Precipitation 65

5.2 Southern Granite Streamflows 66

5.2.1 Total Discharge at Southern Granites 66

5.2.2 Rainfall-Runoff Analysis Statistical Analysis 67

Runoff Coefficients 68

5.2.3 Hydrometric Analysis of Stream network and Stream-Catchment Connectivity 69

5.3 Streamflow Hydrochemistry 74

5.3.1 Isotopic trends in rainfall, subsurface and surface water samples 74

5.3.2 Tracer Analysis at Southern Granites 76

5.3.3 Quantifying contribution of different water sources to streamflow 80

5.3.3.1 2 Stage Hydrograph Separation 19 January 2013 80

5.3.3.2 2 Stage Hydrograph Separation 20 February 2013 83

5.3.3.3 3 Stage Hydrograph Separation 19 January 2013 85

5.3.4 Stream Network Connectivity at Southern Granites 86

5.4 Southern Granite 1st order hillslope 87

5.4.1 1st order Geophysics 87

5.4.2 1st order shallow unsaturated zone characterization and responses 92

5.4.3 1st order Hydrogeology: Hydraulic Responses and Parameters 95

5.5 Southern Granite 2nd order hillslope 101

5.5.1 2nd order Geophysics 101

5.5.2 2nd order shallow unsaturated zone characterization and responses 106

5.5.3 2nd order Hydrogeology: Hydraulic Responses and Parameters 109

5.6 Southern Granite 3rd order hillslope 113

5.6.1 3rd order Geophysics 113

5.6.2 3rd order shallow unsaturated zone characterization and responses 117

5.6.3 3rd order Hydrogeology: Hydraulic Responses and Parameters 120

5.7 Spatial Integration of Groundwater Data 127

5.7.1 Spatial distribution of groundwater head within the southern granite Supersite 127

5.7.2 Spatial distribution of average specific conductance for the southern granite supersite boreholes 127

5.7.3 Spatial distribution of average temperatures for the southern granite supersite boreholes 127

5.8 Hydrological Modelling 132

5.8.1 Catena Water Balances (HYDRUS) 132

5.8.1.1 Atmospheric Input Variables 132

5.8.1.2 Modelled Hydrological Fluxes 133
5.8.1.2.1 SGR1 Simulated Results 134
5.8.1.2.2 SGR2 Simulated Results 135
5.8.1.2.3 SGR3 Simulated Results 137
5.8.1.3 Updating the conceptual hillslope models on the Southern Granites 139
5.8.2 Scaled Geohydrological Processes (Modflow) on the Southern Granites 142
5.8.2.1 Model Domain Specifications, Mesh and Layers 142
5.8.2.2 Recharge 144
5.8.2.3 Hydraulic properties 145
5.8.2.4 Model Calibration 146

6 RESULTS – SOUTHERN BASALTS

6.1 Precipitation 153
6.2 Southern Basalts Streamflows 154
6.2.1 Total Discharge at Southern Basalts 154
6.2.2 Southern Basalts Rainfall-Runoff Analysis: Statistical Analysis 156
6.2.3 Runoff Coefficients 157
6.2.4 Hydrometric Analysis of Stream network and Stream-Catchment Connectivity 158
6.2.5 Streamflow Hydrochemistry 162
6.2.5.1 Isotopic trends in rainfall and surface water samples 162
6.2.5.2 Physico-chemical (EC) trends in rainfall, stream and borehole water samples 164
6.2.5.3 Hydrochemical (silica) trends in rainfall, stream and borehole water samples. 164
6.2.5.4 Tracer Analysis at Southern Basalts 164
6.2.5.5 Quantifying contributions of different water sources to streamflow 170
6.2.5.6 Two Component Hydrograph Separation 171
6.2.5.6.1 Event 1(19 January 2013) at Southern Basalts 3rd Order Reach (SBAS3) 171
6.2.5.7 Event 2 (20 February 2013) at Southern Basalts 3rd order reach (SBAS3) 172
6.2.5.8 Event 3 (29 December 2013) at Southern Basalts 3rd stream order. 173
6.2.5.9 Event 4 (28 January 2014) at Southern Basalts all stream orders 174
6.2.6 Stream Network Connectivity at Southern Basalts 175
6.3 Southern Basalt 1st order hillslope 176
6.3.1 1st order Geophysics 176

6.3.2 1st order shallow unsaturated zone characterization and responses 179

1st Order Hillslope 179

6.3.3 1st order Hydrogeology: Hydraulic Responses and Parameters 181

6.4 Southern Basalt 2nd order hillslope 186

6.4.1 2nd order Geophysics 186

6.4.2 2nd order shallow unsaturated zone characterization and responses 189

6.4.3 2nd order Hydrogeology: Hydraulic Responses and Parameters 191

6.5 Southern Basalt 3rd order hillslope 196

6.5.1 3rd order Geophysics 196

6.5.2 3rd order shallow unsaturated zone characterization and responses 199

6.5.3 Conceptual models derived from Hydropedological interpretations on southern Basalt supersite 201

6.5.4 3rd order Hydrogeology: Hydraulic Responses and Parameters 202

6.6 Spatial Integration of Groundwater Data 207

6.7 Hydrological Modelling 208

6.7.1 Catena Water Balances (HYDRUS) 208

6.7.1.1 Atmospheric Input Variables 208

6.7.1.2 Modelled Hydrological Fluxes 211

6.7.1.2.1 SBAS3 Simulated Results 211

6.7.1.3 Updating the conceptual hillslope models on the Southern Basalts 212

6.7.2 Scaled Geohydrological Processes (Modflow) on the Southern Basalts 213

6.7.2.1 Model Domain Specifications, Mesh and Layers 213

6.7.2.2 Time Discretization 216

6.7.2.3 Recharge 216

6.7.2.4 Hydraulic properties 217

6.7.2.5 Steady State Model calibration results 218

6.7.2.6 Transient Model calibration results 219

7 REFERENCES 223

LIST OF APPENDICES (on accompanying CD)

APPENDIX I	Additional Geophysics Surveys & Borehole Logs
APPENDIX II	Catena Soil Classification and installation depth of soil moisture sensors
APPENDIX III	Streamflow ratings
APPENDIX IV	Actual Evaporation (SEBAL)
APPENDIX V	Hydrograph Separation & End Member Mixing Analysis
APPENDIX VI	Borehole hydro-chemistry, in-situ parameters, pumping & slug tests data
APPENDIX VII	Borehole Logs
APPENDIX VIII	Depth v Time Isotope series
APPENDIX IX	Model Validation & Sensitivity (Hydrus)

LIST OF FIGURES

Figure 1.1: The central elements that guided 1990s research in the Kruger National Park Rivers Research Programme (KNPRRP). 3
Figure 1.2: Groundwater Drainage Regions within the KNP 8
Figure 1.3: History of water level behaviour in the KNP reflected by the cumulative rainfall departure of three rainfall stations 9
Figure 1.4: Recharge-discharge mechanisms 10
Figure 1.5: Integration of hydrology and ecosystem science 12

Figure 2.1: Location of final selected Supersites in KNP in relation to: drainage network; dominant geology; physiographic zones; and mean annual precipitation. 19
Figure 2.2: Framework for the development of conceptual models on hydrological connectivity of surface and groundwater processes in the KNP Supersites 2011-12. 23
Figure 2.3: Schematic of conceptual dominant hydrological processes at the southern Granite (Stevenson-Hamilton) Supersite. 25
Figure 2.4: Schematic of conceptual dominant hydrological processes at the southern Basalt (Nhlowa) Supersite. 26

Figure 3.1: Southern Granites stream (SGRQ) flow duration curves September 2012 to April 2013. 28
Figure 3.2: Key responses on Southern Granites first order (SGR1) September 2012 to April 2013. 29
Figure 3.3: Key responses on Southern Granites second order (SGR2) September 2012 to April 2013. 30
Figure 3.4: A hydrogeological conceptual site model of the southern granite supersite 33
Figure 3.5: Key responses on Southern Basalts first order (SBAS1) and third order (SBAS3) September 2013 to April 2014 35
Figure 3.6: A hydrogeological conceptual site model of the southern basalt supersite. 37

Figure 4.1: Methodological approach for quantifying groundwater-surface water interaction on the KNP Supersites 40
Figure 4.2: Solinst Levelogger installation and schematic 45
Figure 4.3: ALCO 20-bottle sequential sampler 49
Figure 4.4: Schematic illustration of diagnostic horizons and boundary conditions applied in this study using Hydrus 1D 57

Figure 5.1: Map of installed instrumentation at the Southern Granite 64
Figure 5.2: Southern Granite Rainfall September 2012-September 2013 65
Figure 5.3: Southern Granites (SGR) Flow Duration Curves for the period from September 2012 to March 2013. 66
Figure 5.4: Total discharge (combined surface and subsurface) hydrographs at Southern 67
Figure 5.5: Southern Granites streamflow responses following the rainfall event on the 19th of January 2013. 70
Figure 5.6: Southern Granites streamflow responses following the rainfall event on the 20th of February 2013. 71
Figure 5.7: Southern Granites monitoring points map, groundwater and stream water levels monitored from November 2012 to April 2013. 72

Figure 5.8: In-stream and riparian zone piezometer water levels at SGR3T during the month of March 2013 and at SGR3Q (from December 2012 to March 2013) at Southern Granites. 73
Figure 5.9: δO^{18} Isotopic trends in rainfall and stream samples at Southern Granites from September 2012 to March 2013 75
Figure 5.10: Isotopic ($\delta^{18}O$) delta values for three incremental spatial scales at the Southern Granites study site from September 2012 to March 2013 79
Figure 5.11: Southern Granites time series presentation of silica concentrations for three incremental spatial scales from September 2012 to March 2013 80
Figure 5.12: Isotope data for samples collected following the January 19, 2013 rainfall event at the 3rd order catchment of Southern Granites Supersites. 82
Figure 5.13: Two component hydrograph separation for 19 January 2013 at the 3rd order of Southern Granites showing rainfall, component and total stream runoff, and percentage contributions of event and pre-event water to total runoff. 82
Figure 5.14: Contribution of event and pre-event water to total runoff at SGR1 & SGR2 reaches at Southern Granites using δ18O and EC as tracers for the event of 19 January 2013 83
Figure 5.15: Isotope data for samples collected following the February 20, 2013 rainfall event at the 3rd order reach of Southern Granites study site. 84
Figure 5.16: Two component hydrograph separation for 20 February 2013 at the 3rd order of Southern Granites showing rainfall, component and total stream discharge, and percentage contributions of event and pre-event water to the stream. 84
Figure 5.17: Contribution of event and pre-event water to total runoff using $\delta^{18}O$ as tracer for the event of 20 February 2013 for SGR1 and SGR2 at Southern Granites site. 85
Figure 5.18: Three component hydrograph separation at the 1st order reach (SGR1) of Southern Granites study site for the 19 January 2013 rainfall event. 85
Figure 5.19: Initial and final interpretation of 2D ERT traverses coupled with topography data, satellite imagery and estimated and actual positions of groundwater level and weathering 89
Figure 5.20: Time-series geophysics transect southern granite 1st order hillslope 90
Figure 5.21: (a) Soil texture triangle (b) site map (c) K_{unsat} at soil surface (d) K_{sat} per soil horizon on southern granite 1st order hillslope 91
Figure 5.22: Soil matric potential responses and % ED curves along the southern granite supersite first order hillslope between September 2012 and April 2013 94
Figure 5.23: Hydrological soil types and conceptual flow paths for granite 1st order hillslope 95
Figure 5.24: 1st order crest position 103 m borehole water level response to rainfall over the hydrological season September 2012 to September 2013 97
Figure 5.25: 1st order crest position 17 m borehole water level response to rainfall over the hydrological season September 2012 to September 2013 97
Figure 5.26: 1st order riparian position 61 m borehole water level response to rainfall over the hydrological season September 2012 to September 2013 98
Figure 5.27: 1st/2nd order triangulation position 36 m and 61 m borehole water level response to rainfall over the hydrological season September 2012 to September 2013 98
Figure 5.28: Specific conductance quarterly fluid log for the 1st order crest position 103 m borehole, crest 17 m borehole, and riparian position 61 m borehole. 100
Figure 5.29: Specific conductance quarterly fluid log for the 1st/2nd order triangulation position 61 m borehole, and 36 m borehole. 101

Figure 5.30: Initial and final interpretation of 2D ERT traverses coupled with topography data, satellite imagery and estimated and actual positions of groundwater level and weathering 103
Figure 5.31: Time-series geophysics transect southern granite 2nd order hillslope 104
Figure 5.32: (a) Soil texture triangle (b) site map (c) K_{unsat} at soil surface (d) K_{sat} per soil horizon on granite 2nd order hillslope 105
Figure 5.33: Soil matric potential responses and % ED curves along the southern granite supersite second order hillslope between September 2012 and April 2013 108
Figure 5.34: Hydrological soil types and flow paths for granite 2nd order hillslope 109
Figure 5.35: 2nd order crest position 40 m and 55 m borehole water level response to rainfall over the hydrological season September 2012 to September 2013 110
Figure 5.36: 2nd order riparian position 28 m and 49 m borehole water level response to rainfall over the hydrological season September 2012 to September 2013 111
Figure 5.37: Specific conductance quarterly fluid log for the 2nd order crest position 55 m borehole, crest 40 m borehole, 2nd order riparian position 49 m boreholes, and riparian 28 m boreholes. 112
Figure 5.38: Initial and final interpretation of 2D ERT traverses coupled with topography data, satellite imagery and estimated and actual positions of groundwater level and weathering 114
Figure 5.39: Time-series geophysics transect southern granite 2nd order stream 115
Figure 5.40: (a) Soil texture triangle (b) site map (c) K_{unsat} at soil surface (d) K_{sat} per soil horizon on granite 3rd order hillslope 116
Figure 5.41: Soil matric potential responses and % ED curves along the southern granite supersite third order hillslope between September 2012 and April 2013 119
Figure 5.42: Hydrological soil types and flow paths for granite 3rd order hillslope 120
Figure 5.43: 3rd order crest position 34 m and 55 m borehole water level response to rainfall over the hydrological season September 2012 to September 2013 123
Figure 5.44: 3rd order mid-slope position 23 m, 26 m and 49 m borehole water level response to rainfall over the hydrological season September 2012 to September 2013 123
Figure 5.45: 3rd order riparian position 20 m and 43 m borehole water level response to rainfall over the hydrological season September 2012 to September 2013 124
Figure 5.46: 3rd order triangulation position 34 m and 61 m borehole water level response to rainfall over the hydrological season September 2012 to September 2013 124
Figure 5.47: Specific conductance quarterly fluid log for the 3rd order crest position 55 m borehole, crest 34 m borehole, 3rd order mid-slope position 49 m borehole, and mid-slope position 26 m borehole. 125
Figure 5.48: Specific conductance quarterly fluid log for the 3rd order riparian position 43 m borehole, riparian 20 m borehole, 3rd order triangulation position 61 m borehole, and 3rd order triangulation position 34 m borehole. 126
Figure 5.49: General groundwater contours of the deep boreholes within the southern granite Supersite. 128
Figure 5.50: The general groundwater flow direction of the shallow boreholes within the southern granite Supersite. 128
Figure 5.51: Spatial distribution of specific conductance for the southern granite supersite deep boreholes during the dry season combined averaged value fluid logs of May 2013 and August 2013. 129
Figure 5.52: Spatial distribution of specific conductance for the southern granite supersite deep boreholes during the wet season combined averaged value fluid logs of November 2012 and February 2013. 129

Figure 5.53: Spatial distribution of specific conductance for the southern granite supersite shallow boreholes during the dry season combined averaged value fluid logs of May 2013 and August 2013. 130
Figure 5.54: Spatial distribution of specific conductance for the southern granite supersite shallow boreholes during the wet season combined averaged value fluid logs of November 2012 and February 2013. 130
Figure 5.55: Spatial temperature distribution for the southern granite supersite deep boreholes during the hydrological season fluid logs of November 2012 to August 2013. 131
Figure 5.56: Spatial temperature distribution for the southern granite supersite shallow boreholes during the hydrological season fluid logs of November 2012 to August 2013. 131
Figure 5.57: ETa per catena element for granite 1st order hillslope 132
Figure 5.58: ETa per catena element for granite 2nd order hillslope 133
Figure 5.59: ETa per catena element for granite 3rd order hillslope 133
Figure 5.60: Simulated cumulative evaporation and transpiration fluxes on SGR1 hillslope catena elements 135
Figure 5.61: Simulated cumulative free drainage fluxes on SGR1 hillslope catena elements 135
Figure 5.62: Cumulative surface runoff on SGR hillslope catena elements 136
Figure 5.63: Simulated cumulative evaporation and transpiration fluxes on SGR2 hillslope catena elements 137
Figure 5.64: Simulated cumulative free drainage fluxes on SGR2 hillslope catena elements 137
Figure 5.65: Simulated cumulative evaporation and transpiration fluxes on SGR2 hillslope catena elements 138
Figure 5.66: Simulated cumulative free drainage fluxes on SGR3 hillslope catena elements 139
Figure 5.67: Initial and updated conceptual model of Vadose zone water balance for 1st order granite hillslope 140
Figure 5.68: Initial and updated conceptual model of Vadose zone water balance for 2nd order granite hillslope 141
Figure 5.69: Initial and updated conceptual model of Vadose zone water balance for 3rd order granite hillslope 141
Figure 5.70: The 3 layers of the Southern Granites MODFLOW model showing the Drain, General Head (GHB) and No Flow boundary conditions. 143
Figure 5.71: Recharge rate property in m/day for the model domain at Southern Granite site. 144
Figure 5.72: spatial distribution of 6 hydraulic property zones at Southern Granite site 145
Figure 5.73: Steady state calibration results 147
Figure 5.74: Calibrated transient groundwater flows at Southern Granite site. 149

Figure 6.1: Map of installed instrumentation at the Southern Basalt (Nhlowa) Supersite 152
Figure 6.2: Southern basalt time series rainfall from October 2012 to March 2014. 153
Figure 6.3: Southern basalt Antecedent Precipitation Index October 2012-March 2014 154
Figure 6.4: Southern Basalts (SBAS) Flow Duration Curves for the period from September 2012 to March 2013. 155
Figure 6.5: Streamflows at Southern Basalts from October 2012 to March 2013 155
Figure 6.6: Streamflow responses at Southern Basalts from October 2012 to March 2014.156
Figure 6.7: Southern Basalts streamflow responses following the rainfall event on the 19th of January 2013. 158

Figure 6.8: Southern Basalts streamflow responses following the 20th of February 2013 rainfall event. 159
Figure 6.9: Hydraulic head of SBAS1 boreholes relative to stream water levels. 160
Figure 6.10: Hydraulic head of SBAS2 boreholes relative to stream water levels. 161
Figure 6.11: Hydraulic head differences between crest boreholes, riparian boreholes and the stream at Southern Basalts 3rd order reach during the period February 2013 to March 2014. 162
Figure 6.12: Isotopic trends in rainfall and stream samples at Southern Basalts from September 2012 to March 2013. 163
Figure 6.13: Sodium (Na) signatures in boreholes and the stream at Southern Basalts site. 165
Figure 6.14: Electrical conductivity (EC) signatures in boreholes and the stream at Southern Basalts site. 166
Figure 6.15: Isotope ($\delta^{18}O$) signatures in boreholes and the stream at Southern Basalts site for the event of the 28th of January 2014. 167
Figure 6.16: Southern Basalts time series presentation of $\delta^{18}O$ delta values for the 3rd order reach from September 2012 to March 2013. 169
Figure 6.17: Southern Basalts time series presentation of silica concentrations from September 2012 to March 2013. 170
Figure 6.18: Isotope data for samples collected following the January 19, 2013 rainfall event at the 3rd order catchment of Southern Basalts study site. 171
Figure 6.19: Percentage contribution of event and pre-event water to total runoff using $\delta^{18}O$ and EC as tracers for the event of 19 January 2013 at SBAS3 reach of Southern Basalts site. 171
Figure 6.20: Isotope data for samples collected following the February 20, 2013 rainfall event at the 3rd order catchment of Southern Basalts study site. 172
Figure 6.21: Percentage contribution of event and pre-event water to total runoff using $\delta^{18}O$ and EC as tracers for the event of 20 February 2013 at Southern Basalts study site. 172
Figure 6.22: Two component hydrograph separation for Event 3 (December 29, 2013) at SBAS3 showing event and pre event components and percentage contributions of these components to the streamflow. 173
Figure 6.23: Isotope data for samples collected following the January 28, 2014 rainfall event at the 3rd order catchment of Southern Basalts study site. 174
Figure 6.24: Contribution of event and pre-event water to total runoff at SBAS1, SBAS2 & SBAS3 reaches at Southern Basalts using δ18O for the event of 28 January 2014. 175
Figure 6.25: Initial and final interpretation of 2D ERT traverses coupled with topography data, satellite imagery and estimated and actual positions of groundwater level and weathering 177
Figure 6.26: Time-series geophysics transect southern basalt 1st order hillslope 178
Figure 6.27: Unsaturated hydraulic conductivity on 1st order hillslope 180
Figure 6.28: soil moisture responses and % ED curves for 1st order hillslope 181
Figure 6.29: 1st order riparian position 67 m borehole water level response to rainfall over the hydrological season October 2012 to March 2014 182
Figure 6.30: 1st order crest position 61 m and 100 m borehole water level response to rainfall over the hydrological season October 2012 to March 2014 182
Figure 6.31: 1st order triangulation position 56 m borehole water level response to rainfall over the hydrological season October 2012 to March 2014 183
Figure 6.32: specific conductance quarterly fluid log for the 1st order riparian position 67 m borehole 184

Figure 6.33: specific conductance quarterly fluid log for the 1st order crest position 100 m borehole 184
Figure 6.34: specific conductance quarterly fluid log for the 1st order crest position 61 m borehole 185
Figure 6.35: specific conductance quarterly fluid log for the 1st order triangulation position 56 m borehole 185
Figure 6.36: Initial and final interpretation of 2D ERT traverses coupled with topography data, satellite imagery and estimated and actual positions of groundwater level and weathering 187
Figure 6.37: time-series geophysics transect southern basalt 2nd order hillslope 188
Figure 6.38: K_{unsat} on 2nd order hillslope 189
Figure 6.39: soil moisture responses and % exceedence curves for 2nd order hillslope 190
Figure 6.40: 2nd order riparian position 80 m and 8 m borehole water level response to rainfall over the hydrological season October 2012 to March 2014 192
Figure 6.41: 2nd order crest position 57 m borehole water level response to rainfall over the hydrological season October 2012 to March 2014 192
Figure 6.42: 2nd order triangulation position 80 m and 15 m borehole water level response to rainfall over the hydrological season October 2012 to March 2014 193
Figure 6.43: specific conductance quarterly fluid log for the 2nd order riparian position 80 m borehole 194
Figure 6.44: specific conductance quarterly fluid log for the 2nd order crest position 57 m borehole 194
Figure 6.45: specific conductance quarterly fluid log for the 2nd order triangulation position 80 m borehole 195
Figure 6.46: specific conductance quarterly fluid log for the 2nd order triangulation position 15 m borehole 195
Figure 6.47: Initial and final interpretation of 2D ERT traverses coupled with topography data, satellite imagery and estimated and actual positions of groundwater level and weathering 197
Figure 6.48: time-series geophysics transect southern basalt 3rd order hillslope 198
Figure 6.49: K_{unsat} on 3rd order hillslope 199
Figure 6.50: soil moisture responses and % exceedence curves for 3rd order hillslope 201
Figure 6.51: Hydrological soil types and flow paths for basalts 1st, 2nd and 3rd order hillslopes 202
Figure 6.52: 3rd order riparian position 80 m and 10 m borehole water level response to rainfall over the hydrological season October 2012 to March 2014 203
Figure 6.53: 3rd order crest position 80 m and 10 m borehole water level response to rainfall over the hydrological season October 2012 to March 2014 203
Figure 6.54: 3rd order triangulation position 61 m and 4 m borehole water level response to rainfall over the hydrological season October 2012 to March 2014 204
Figure 6.55: specific conductance quarterly fluid log for the 3rd order riparian position 80 m borehole 205
Figure 6.56: specific conductance quarterly fluid log for the 3rd order riparian position 10 m borehole 205
Figure 6.57: specific conductance quarterly fluid log for the 3rd order crest position 80 m borehole 206
Figure 6.58: specific conductance quarterly fluid log for the 3rd order crest position 10 m borehole 206
Figure 6.59: specific conductance quarterly fluid log for the 3rd order triangulation position 61 m borehole 207
Figure 6.60: General groundwater contours of the deep boreholes within the southern basalt Supersite. 208

Figure 6.61: The general groundwater flow direction of the shallow boreholes within the southern basalt Supersite. 208
Figure 6.62: ETa per catena element for basalt 1st order hillslope 209
Figure 6.63: ETa per catena element for basalt 2nd order hillslope 210
Figure 6.64: ETa per catena element for basalt 3rd order hillslope 210
Figure 6.65: Simulated cumulative evaporation and transpiration fluxes on SBAS3 catena elements 211
Figure 6.66: Simulated cumulative free drainage fluxes on SBAS3 hillslope catena elements 212
Figure 6.67: Initial and updated conceptual model for 3rd order basalt hillslope 213
Figure 6.68: The vertical cross-sections of the Southern Basalts model. 214
Figure 6.69: Maps showing No flow boundary, head targets, Drain boundary in Layer 1 and General Head Boundary (GHB) in Layer 2 for the Southern Basalts model. 215
Figure 6.70: Recharge rate property in m/day for the model domain at Southern Basalts site. 217
Figure 6.71: spatial distribution of 6 hydraulic property zones at Southern Basalts site. 217
Figure 6.72: Simulated versus observed head targets in m.amsl at Southern Basalts study site 218
Figure 6.73: Water level contours after steady calibration of the Southern Basalts model. 219
Figure 6.74: Calibrated transient groundwater flows at Southern Basalts site. 220

LIST OF TABLES

Table 2.1: Land system and land type characteristics for the locations of the KNP Supersites 20
Table 2.2: Land forms and soil characteristics for the locations of the KNP Supersites 21
Table 2.3: Hydrogeological characteristics for the regions of the KNP Supersites 22
Table 2.4: Conceptual dominant hydrological process at the southern Granite (Stevenson-Hamilton) Supersite. 25
Table 2.5: Conceptual dominant hydrological process at the southern Basalt (Nhlowa) Supersite. 26

Table 3.1: Differences and similarities in hydrological process responses of the KNP Supersites 38

Table 4.1: Catena Soil Hydropedological Response Units and Hillslope Classes 43

Table 5.1: Hydrometric monitoring points in the Southern Granite KNP Supersite 62
Table 5.2: Southern Granite Borehole in-situ hydraulic parameters following drilling (2012) 63
Table 5.3: vertical hydraulic gradients (VHG) monitored following the significant 19 January 2013 rainfall event 67
Table 5.4: Pearson's product moment correlation coefficient showing precipitation and runoff responses of three events at Southern Granites during the period from December 2012 to February 2013 68
Table 5.5: Southern Granites Runoff Coefficients for 1st to 3rd order reaches 68
Table 5.6: Rainfall and stream surface and subsurface isotopic signatures at Southern Granites for samples collected between September 2012 and March 2013 76
Table 5.7: Selected typical EC, silica and chloride concentration ranges at Southern Granites during December 2012 to February 2013 76
Table 5.8: Isotopic ($\delta^{18}O$) delta values and hydrochemical (Silica & Chloride) concentrations indicating connectivity points across scales at Southern Granites study site during October 2012 to January 2013. 78
Table 5.9: Estimated tributary runoff and corresponding percentage contributions to the main channel flows at Southern Granites on the 19th of January and 20th of February 2013. Discharges in brackets were observed at gauging stations. 86
Table 5.10: Soil classification per catena element on granite 1st order hillslope 92
Table 5.11: Soil classification per catena element on granite 2nd order hillslope 106
Table 5.12: Soil classification per catena element on granite 3rd order hillslope 117
Table 5.13: Catena element water budgets for 1st order granite hillslope 134
Table 5.14: Catena element water budgets for 2nd order granite hillslope 136
Table 5.15: Catena element water budgets for 3rd order granite hillslope 138
Table 5.16: Calibrated hydraulic conductivity property values for the Southern Granite model 146

Table 6.1: Hydrometric monitoring points in the Southern Basalt KNP Supersite 150
Table 6.2: Southern Basalt Borehole in-situ hydraulic parameters following drilling (2013) 151
Table 6.3: Pearson's product moment correlation coefficient for rainfall and runoff characteristics of three events at Southern Basalts monitored during December 2012 to February 2013. 157
Table 6.4: Southern Basalts Runoff Coefficients for incremental stream reaches. 158
Table 6.5: Rainfall and stream isotopic signatures for Southern Basalts site for samples collected between December 2012 and January 2014. 163

Table 6.6: Selected typical EC, silica and chloride concentration ranges at Southern Basalts during December 2012 to January 2014. 164
Table 6.7: Isotopic ($\delta^{18}O$) delta values and hydrochemical (Silica) concentrations indicating connectivity points at the 3rd order reach of Southern Basalts study site. 168
Table 6.8: Soil classification per catena element on basalt 1st order hillslope 179
Table 6.9: Soil classification per catena element on basalt 2nd order hillslope 189
Table 6.10: Soil classification per catena element on basalt 3rd order hillslope 199
Table 6.11: Catena element water budgets for 3rd order basalt hillslope 211
Table 6.12: Model layer elevations and thicknesses 216
Table 6.13: Calibrated hydraulic conductivity property values for the Southern Basalts model 218
Table 6.14: Calibrated values of effective recharge compared to monthly precipitation from October 2012 to March 2014. 221

GLOSSARY OF TERMS

Capillary Fringe Zone immediately above the water table in which all of the interstices are filled with water that is under pressure less than atmospheric. Saturated part of the vadose zone at negative pressure (tension)

Catena (or toposequence) is a series of soils and associated vegetation linked by their topographic relationship (Cullum & Rogers, 2011)

Catena Element Areas that have distinct hydrological regimes which are both cause and consequence of a particular combination of plant cover, soil, slope characteristics (e.g. gradient, curvature and aspect) and slope position (Cullum and Rogers, 2011)

Effective Recharge Infiltration in excess of actual evapotranspiration that reaches the groundwater store

Endorheic basin is a closed drainage basin that retains water and allows no outflow to other external bodies of water but converges instead into lakes, pans or swamps, permanent or seasonal, that equilibrate through evaporation

Groundwater Water held underground in the soil or in pores and crevices in rock, subsurface water occupying the saturated zone

Groundwater Discharge The removal of water from the saturated zone across the water table surface, together with the associated flow toward the water table within the saturated zone (Freeze and Cherry, 1979)

Groundwater Recharge The entry into the saturated zone of the water made available at the water table surface, together with the associated flow away from the water table within the saturated zone (Freeze and Cherry, 1979)

Hard Rock A continuously hard layer of rock that cannot be cut with a spade even when wet; most important members are igneous, metamorphic and indurated sedimentary rocks and silcrete (Soil Classification Working Group, 1991)

Hydraulic Conductivity Property of a saturated porous medium which determines the relationship, called Darcy's law, between the specific discharge and the hydraulic gradient causing it. The ease with which a fluid can move through an aquifer medium depending on the physical properties of the medium (grain size, grain shape, pore size, fracture arrangement and density) and the fluid (density, viscosity, gravitational acceleration) (Kresic, 2007)

Hydraulic Gradient (1) In a closed conduit: the slope of the hydraulic grade line. (2) In open channels: the slope of the water surface. (3) In porous media: measure of the decrease in head per unit distance in the direction of flow

Hydraulic Head (1) Elevation to which water will rise in a piezometer connected to a point in an aquifer. (2) Sum of the elevation and the pressure head in a liquid, expressed in units of height

Hyporheic Flow Flow of surface water or a mixture of groundwater and surface water through the bed sediments of a surface water course or wetland

Infiltration Flow of water through the soil surface into a porous medium

Intensity depth/time (mm/hr)

Interflow (A/B horizon) duplex soils where the textural discontinuity facilitates build-up of water in the topsoil. Duration of drainable water depends on rate of ET, position in the hillslope (lateral addition/release), and slope (discharge in a predominantly lateral direction) (Van Tol et al., 2013)

Interflow (groundwater) The rapid flow of water along essentially unsaturated flow paths, water that infiltrates the subsurface and moves both vertically and laterally before discharging into other water bodies

Interflow (soil/bedrock) Soils overlying relatively impermeable bedrock. Hydromorphic properties signify temporal build of water on the soil/bedrock interface and slow discharge in a predominantly lateral direction (Van Tol et al., 2013)

Overland Flow Flow of water over the ground before it enters a definite channel

Perched Water Table The existence of a low permeability medium or layer in a high permeable formation can lead to the formation of a discontinuous saturated lens, with unsaturated conditions existing both above and below the low permeable layer (Freeze and Cherry, 1979)

Percolation Flow of a liquid through an unsaturated porous medium, e.g. of water in soil, under the action of gravity (process of potential recharge becoming recharge)

Phreatic Surface Surface within the zone of saturation of an unconfined aquifer over which the pressure is atmospheric (0 pressure contour)

Piezometric Surface Surface within the zone of saturation of an unconfined aquifer over which the pressure is atmospheric

Potential Recharge Soil water movement which is vertical through the soil to groundwater and has left the root zone (after percolation and redistribution has happened)

Recharge Soil Soils without any morphological indication of saturation. Vertical flow through and out of the profile into the underlying bedrock is the dominant flow direction. These soils can either be shallow on fractured rock with limited contribution to evapotranspiration or deep freely drained soils with significant contribution to evapotranspiration (Van Tol et al., 2013)

Redistribution Movement up (capillary rise)/down (percolation) change in storage.
Lateral – lateral movement in soil horizons, fractured rock. (Upper and lower vadose zone)
(Composite of Interflow A/B and Soil/bedrock + fractured rock) – Usually saturated

Responsive Soil – Saturated Soils with morphological evidence of long periods of saturation. These soils are close to saturation during rainy seasons and promote the generation of overland flow due to saturation excess (Van Tol et al., 2013)

Responsive Soil – Shallow (Infiltration Excess) Shallow soils overlying relatively impermeable bedrock. Limited storage capacity results in the generation of overland flow after rain event where rainfall rate>infiltration rate (Van Tol et al., 2013)

Return Flow Any flow which returns to a stream channel or to the groundwater after use

Runoff That part of precipitation that appears as streamflow

Saprolite A horizon of weathering rock with general organization in respect of colour, structure or consistence, which still has distinct affinities with the parent rock (Soil Classification Working Group, 1991)

Seep Line Catena element at which subsurface water moving downslope from the sandy crests is often forced to the surface when it encounters the clay layer of midslope in the KNP landscape. Often saturated for much of the rainy season, when pools and wetlands may form along its length and characterised by *Terminalia sericea* which establish along a distinct line that follows the contour that separates the crest from grassy midslopes (Cullum & Rogers, 2011)

Sodic Site regions in arid and semiarid landscapes, where salts accumulate near the soil surface at predictable points along hydrologic pathways, giving rise to saline or sodic patches (Jacobs et al., 2007). Sodic soils tend to form along the upland edge of riparian zones in the African savanna (Khomo and Rogers, 2005). We add a distinction of **Return Water Sodic Sites**, the grassy midslope duplex soils below the seep line.

Soil The usually thin upper surface layer of the earth's crust comprising living organisms, organic matter, decomposed rock or unconsolidated sediments, water and gases with properties attributable to the interaction of its parent material, time, climate, fauna and flora

Stream Body of water, generally flowing in a natural surface channel

Supersite Areas within the KNP that are selected as examples of catchments characteristic of a certain physiographic zone. Research projects will be focused on these areas, aiming to construct a holistic, trans disciplinary description and understanding of the ecological processes and interactions that operate within each physiographic zone (Cullum and Rogers, 2011)

Terrain Morphological Units Crest, Scarp, Midslope, Footslope, Valley Bottom (Soil Classification Working Group, 1991)

Transmissivity It is the product of hydraulic conductivity of the aquifer material and the saturated thickness of the aquifer (Kresic, 2007)

Vadose Water Any water that occurs in the vadose (unsaturated) zone

Vadose Zone Zone between the land surface and water table which may include the capillary fringe. Water in this zone is generally under less than atmospheric pressure, and the voids may contain water, air or other gases. (Upper vadose [regolith to saprolites, head is >0, therefore potential for capillary forces]; Lower vadose [phreatic surface to bedrock surface does not have capillary forces i.e. head is 0])

Water Level Elevation of the free-water surface of a body of water relative to a datum level

Water Table Surface within the zone of saturation of an unconfined aquifer over which the pressure is atmospheric

Weathered Zone The subsurface region where chemical, physical and biological processes occur decaying rocks causing them to crumble to a material in which, unless transported, soil will form (Soil Classification Working Group, 1991)

LIST OF ACRONYMS

CRD	Cumulative Rainfall Departure
DEM	Digital Elevation Model
dH	Change in Hydraulic Head
DWA	Department of Water Affairs
FDC	Flow Duration Curve
FL	Fluid Logging
GDE	Groundwater Dependent Ecosystem
GMA	Groundwater Management Area
IWRM	Integrated Water Resources Management
K	Hydraulic Conductivity
KNP	Kruger National Park
KNPRRP	Kruger National Park Rivers Research Programme
MAP	Mean Annual Precipitation
Q	Discharge
SAM	Strategic Adaptive Management
SBAS	Southern Basalt Supersite
SBAS1	Southern Basalt Supersite 1st order
SBAS2	Southern Basalt Supersite 2nd order
SBAS3	Southern Basalt Supersite 3rd order
SC	Specific Conductance
SEBAL	Surface Energy Balance Algorithm for Land
SGR	Southern Granite Supersite
SGR1	Southern Granite Supersite 1st order
SGR2	Southern Granite Supersite 2nd order
SGR3	Southern Granite Supersite 3rd order
T	Transmissivity
TDI	Tension Disc Infiltrometer
TDS	Total Dissolved Solids
TPC	Thresholds of Potential Concern
VHG	Vertical Hydraulic Gradient

1. INTRODUCTION

1.1 Problem Statement (Context of the Study)

The rationale for this specific study is borne from a previous WRC project K5/1790: *A framework for the classification of drainage networks in savannah landscapes* by Cullum & Rogers (2011, University of the Witwatersrand). From research conducted within the Kruger National Park (KNP) a conceptual framework was developed for savanna landscape classification based on the premise that the spatial and temporal distribution of water at various scales is the key driver for geomorphological and ecological processes in these landscapes, and that these in turn have feedback effects on hydrological processes. Due to the tight coupling of hydro-geo-ecological processes, distinct landscape patterns have emerged over geological timescales within the lowveld savannas. These have resulted from the topographical redistribution of water and the highly organised nature of interdependent hillslope and channel morphologies which have established distinct patterns of soil and vegetation in the landscape. The crux being that there is a distinct hierarchy of ecological patches resulting from these different hydro-geo-ecological processes, which as a result then controls the ecological variability in the system. This project concluded with various conservation management recommendations for the custodians of the KNP, which included the recommendation that the optimal management unit ought to be that of the watershed or catchment, since ecological processes are largely intrinsic to the confines of such a unit.

The original zoning framework of the KNP developed by Venter (1990) was based on spatial grouping of soils, and also recognised a landscape hierarchy ranging from *catenal*[1] *elements* on the hillslopes to broad-scale zones based on differences in geology and climate. The proposed system builds on this by explicitly linking the pivotal role that fluvial systems have had on structuring the biophysical template, therefore facilitating the integration of riverine and terrestrial ecosystem processes into this framework. To this end Cullum & Rogers (2011) develop a classification system for the KNP based on *Physiographic zones* which display similar geology and patterns of landscape dissection, where these zones show repeating patterns of hillslope and channel morphology, including the distribution of catenal elements.

This is of course most interesting because water resource managers in South Africa and elsewhere have learnt from ecological principals such as Strategic Adaptive Management (SAM) in their Integrated Water Resource Management (IWRM) frameworks. SAM notes the importance of the river flow variability when meeting environmental water requirements. It would now seem to be a reciprocal affair where ecologists are increasingly attracted to viewing the importance of catchments as fundamental ecological units.

[1] Catenal Elements – are parts of a catchment that have a particular combination of plant cover, soil, slope characteristics and slope position that are proposed to be both cause and consequence of a relatively homogenous water budget (Cullum & Rogers 2011).

1.2 Research Aims and Objectives

Thus the *super research sites* (hereafter referred to as Supersites) concept was predicated on this ecological thinking, through which the KNP would select sites that have typical landscape characteristics within the classification system of Cullum & Rogers (2011). These sites may then attract an array of non-manipulative ecological research and become data rich multi-disciplinary sites, where all ecological process understanding could be integrated – and thus have the benefits of robust scientific understanding for extrapolation to other parts of the KNP, lowveld and other savanna systems. It is on this basis that project K5/2051 augments this supersite dataset as one of the first registered KNP projects on these sites to develop an abiotic template for landscape level ecohydrological understanding through the determination of surface water, groundwater and vadose zone interactions within the KNP's hierarchical drainage landscape.

Understanding of catchment hydro-connectivity within the KNP is in its infancy and presently relies on the conceptual models developed by Cullum & Rogers (2011) and this of course is a key aim of the research reported here.

This project has the following core objectives:

- Quantify the role of hydrological inter-connectedness between hydrological process domains; and

- Determine the spatio-temporal variability of this interconnectedness in order to understand the hydrological fluxes that drive these savannah systems.

1.3 State of Knowledge of Groundwater-Surface Water Interactions and Hydrological Connectivity the in KNP

Savannas form approximately one-fifth of the planet's surface and support a large proportion of the world's population and most of its biomass, a defining feature of these systems is the co-existence of trees and grasses. These systems are largely controlled by rainfall distribution, along with soil properties, herbivory and fire, where a figure of 650 mm per annum for African savannas was shown to be the threshold above which these ecosystems would become increasingly dominated by woody biomass (Sankaran et al., 2005). Moreover it has been shown that moisture regimes are in general highly variable and pulsed in savannas such as in the KNP, and are thus an important temporal control on nutrient cycling and export to the riparian zone, which is further controlled by landscape configuration (Jacobs et al., 2007). Savannas have been shown to have an important role in global carbon dynamics and those such as found in KNP are constrained by the annual drought and re-wetting cycle as suggested by Kutsch et al. (2008). Hence understanding the hydrological template of such systems is important for predicting ecosystem state changes as a result of long-term climatic uncertainty.

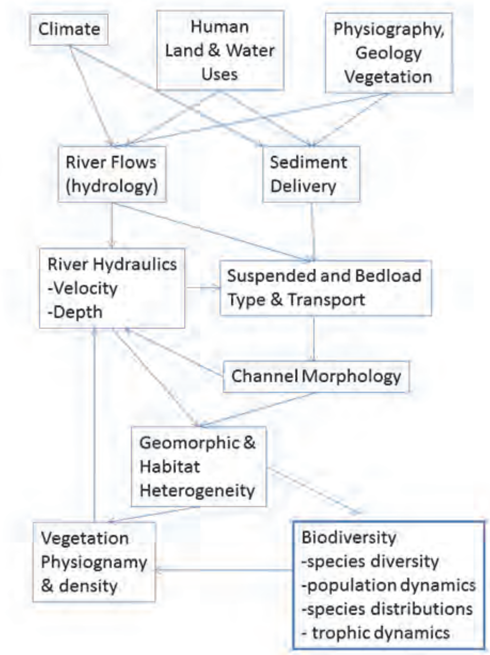

Figure 1.1: The central elements that guided 1990s research in the Kruger National Park Rivers Research Programme (KNPRRP). Adapted from Rogers & O'Keeffe (2003)

The KNP has a long history of research conducted on its rivers and water resources, the impetus being during the 1990s Kruger National Park Rivers Research Programme (KNPRRP) which took a multi-disciplinary approach to determine the hydrological and geomorphological drivers for river system heterogeneity, through the monitoring of biotic responses (see for example Rogers & O'Keeffe, 2003). This was in order to better understand the ecosystem dynamics of the KNP's large perennial rivers and use this information for policy and decision-making in both ecosystem and water resource management, as depicted in Figure 1.1. The success of this research can be assessed in the way that outcomes from this programme have recognised the dynamic, variable and complex processes that govern ecosystems and translated into policy via adaptive management principles within the KNP. For example the use of bio-indicators for river health, relating these to water flow and quality to inform Thresholds of Potential Concern (TPCs). Moreover this ecological understanding of the rivers hydrology has often translated into water resource management policy in the lowveld rivers, most notably in the Sabie, Crocodile and Letaba (See McGloughlin et al., 2011 for a review).

The focus on the large perennial rivers of the KNP has yielded a wide variety of hydro-ecological studies ranging from post-modelling of the 2000 floods which revealed the return interval of that event to be up to 200 years (Smithers et al., 2001) and the spatially variable biotic re-setting and restructuring of the rivers macro-channels following these floods (Parsons et al., 2006). To the focus on biotic-abiotic interactions such as the link of flooding regimes on reed bed patch dynamics and re-colonisation in the Letaba River (Kotschy & Rogers, 2008) or the temperature tracer study to distinguish thermal zones of the Sabie river and its tributaries (Rivers-Moore & Jewitt, 2004). In addition the Sabie had been the focus of riparian water use determination in order to inform low flow environmental water requirements for this river, this study by Everson et al. (2001) revealed through energy balance techniques that the reed beds in the Sabie consistently used more water than the adjacent riparian zone trees. This study followed that by Birkhead et al. (1995) which revealed a longitudinal piezometric groundwater gradient between the Sabie River and its channel bank that switched from discharging to recharging in relation to river stage at different times of the year.

Meanwhile very few studies have focused on meso-scale hydrology, which we here define as between the hillslope or catenal element up to the scale of a large perennial watershed. This gap had been noted to be a shortcoming of research efforts in the KNP where the aquatic-terrestrial linkages along seasonal and ephemeral streams has largely been ignored whilst attention has been paid to the larger perennial rivers (O'Keeffe & Rogers, 2003) which make up approximately 30,000km and 600km respectively.

1.4 Surface & Vadose Zone processes in the KNP

The KNP has received a large amount of scientific attention on a broad swathe of ecosystem functions and processes of which those that relate to hydrological processes have to date largely focused at the macro-scale such as the large perennial rivers

Similarly significant attention has been paid to the micro- or point scale on fundamental ecohydrological processes such as the traditional climate-soil-vegetation dynamics of Rodriguez-Iturbe (2000) largely in an attempt to explain why the KNP's savannas do not conform to Walter's (1971) niche-separation hypothesis to explain tree-grass co-existence. An early study by Ben-Shahar (1990) tried to explain vegetation patterns on the hillslope catena by linking soil moisture measurements on catenal elements in the neighbouring Sabie-Sand Game Reserve. Although during this study which focused on short rainfall periods, no explicit link could be made but rather that soil moisture regime was but one of a suite of controlling site factors.

Quantitative studies of this type in the KNP include those linking plant physiology with soil water availability, such as that by Kulmatiski et al. (2010) who showed that trees and grasses in the mesic Pretoriuskop area partitioned soil water resources but only to the extent that they took greater proportions from <20 cm deep for the former and <5 cm deep for the latter. This did not reflect as suggested by the two-layer niche hypothesis, the ability of trees to access deep soil water that was unavailable to grasses. Trees also did not take a greater proportion of water >50 cm deep suggesting that they do not have exclusive access to this water. A similar study also with the use of stable isotopes distinguished the groundwater source for *Philenoptera violacea* from the limited soil water store used by *Colophospermum mopane* along the riparian zone of the Phugwane river in the northern KNP (February et al., 2007).

There have been a variety of studies on both manipulated experimental sites and un-manipulated sites detailing vadose zone processes in the KNP. Three sites in the northern plains region, in the far north of KNP determined dominant hydrological processes across monitoring transects as part of the Northern Plain Research Programme (NPRP), assessing the potential response of water point withdrawal to the biota, specifically rare antelope.

The first of these studies aimed to explain significant spatial differences perceived in the vegetation guilds (grassland & apple leaf) along a transect in the N'warihlangari region as a causal explanation for perceived differences in the soil-water-plant dynamics. It was found through hydrometric observations (tensiometers) coupled with a soil-water-plant-atmosphere model (SWAP) that the limiting effect of plant transpiration, and hence their particular presence at a site was not so much the soil depth but rather the soil hydraulic properties, particularly the spatial variability in water retention, that is the limiting factor. The latter seemed to be the main determinant of the amount of water available for transpiration and hence crucial to plant survival at a certain spot. The study also acknowledged that the presence of impermeable calcrete layers fostered the presence of the apple leaf as lateral upslope contributions would accumulate on the calcrete and become available to the apple leaf which had a greater evaporative demand than other vegetation along the transect (van der Scheur, 2001, Lorentz et al., 2006). The fact that these basalt soils have high water retention means that they have the propensity to retain water from one season to the next and thus a cumulative rainfall surplus may signify the rate at which water is supplied to the grassy drainage lines in the northern plains (Dunham et al., 2004). This process was explained by observations at the N'washitshumbe Rare Antelope Enclosure in the northern plans, where sub-surface lateral hillslope contributions maintained the moisture levels in a valley bottom vlei (Lorentz et al., 2006). These vleis are considered key resource areas for these antelope during the dry season (Grant & de Buys, 2004).

As part of the same programme, hydrometric observations were made along the river terraces of the Phugwane River where it was noted that different ecotopes existed due to different sorting of alluvial and colluvial sediments. For instance where a hydric grass zone existed within a zone of coarse sediments that was fairly well saturated but water actually ponds on top of a sealing layer of finer sediments. It was also suspected from these observations that large riparian trees may tap into alluvial aquifers and continually use this water throughout the year (Lorentz et al., 2006).

At two long term monitoring sites, the Sabie-Nkhulhu experimental exclosures (on granite) and the dryer Letaba experimental exclosure (on granites) Lorentz et al. (2007) examined soil moisture behaviours within the sections of the large granitic hillslope catena along the Sabie & Letaba Rivers respectively. General observations were that the crest soils were dominated by the rapid vertical movement of water down to the weathered saprolitic zone where there was little propensity for lateral flows following large precipitation events and furthermore these sections of the catena completely dried out during winter. Whilst at the same time the midslope or 'sodic' soils only responded to extreme rainfall early in the wet season and thereafter remained wet with a slow drying out period during winter, where in essence there was a 'capillary break' such as a crust at the soils surface which limited evaporation. The coarse sandy material of the riparian zone at the bottom of these hillslopes meant that these responded to both rainfall inputs and lateral seepage from the rivers very quickly. In addition, overland flows were determined at the Sabie exclosures and here it was noted that the crest soils had a much higher propensity for runoff generation than riparian soils, but that the footslope soils below the seep line typical of the sodic areas had the greatest runoff rate and lowest rainfall depth threshold for runoff initiation.

1.5 Geohydrology of the KNP

Based on a study by (Fischer et al. 2009) the aquifers of the KNP mainly occur in crystalline hard rock lithologies; these crystalline rocks are usually fractured to various degrees and have relatively low hydraulic conductivities. Groundwater occurrence is mainly in water filled joints, fractures, faults, zones of weathering and structures such as dyke intrusions. The fractured aquifer systems of KNP mostly form anisotropic and heterogeneous groundwater bodies as the geometry and arrangement of fractures, joints and faults are influenced by various tectonic features. According to Wright (1992, as cited by Fischer et al., 2009) basement aquifers generally develop within the weathered residual overburden i.e. the regolith as well as in the fractured bedrock. Examples of groundwater exchanges commonly occur between saturated regolith and alluvium with adjacent underlying bedrock. As a result of this weathering profile and the relatively shallow depths to groundwater ranging mainly from 3 m to 11 m below the ground surface it is reasonably safe to expect mainly unconfined aquifers within KNP. Confined or at least semi-confined fractures are a possibility at greater depths, especially in areas with low hydraulic conductivity horizons. Sandy or primary aquifers do occur within the park, these aquifers are particularly found along river systems such as the Crocodile, Limpopo, Sabie and Sand Rivers. Furthermore, sandy aquifers can be found in the north-eastern part of the park where a relatively large area is covered by aeolian sand. There is strong possibility that this particular area may host a mixed aquifer of sandy and fractured basement rock properties (Fischer et al., 2009).

Artificial water provision for wildlife in the park resulted in the construction of dams and the drilling of boreholes with a present estimate 1000-2000 boreholes drilled across the park (Du Toit, 1998). Du Toit (1998) evaluated some 1011 of these boreholes of which 41% were drilled in the Letaba Formation (basalt) and 37% drilled in the Basement Complex (various gneisses). The depth to groundwater strikes varied from 1.2 m to 49.2 m below the ground surface with indications that groundwater level fluctuations are seasonal. However, there were some boreholes showing a continuous decline in groundwater levels which are the result of a combination of factors such as, localised over-abstraction from areas of limited storage and limited recharge due to below-average rainfall. This study also suggested that the regional groundwater flows in an easterly to south-easterly direction and regionally follows the topography of the surface-water drainage. Although there is no empirical scientific data, it appears that effluent flow conditions (groundwater discharge into rivers) prevail most of the time along the major rivers under normal climatic conditions. It is further believed that bank recharge occurs during flood events. The study further indicated that boreholes drilled in elevated areas (close to topographic water divides) between two rivers stood a good chance of drying up during periods of extended drought (Du Toit, 1998).

Groundwater chemical analysis revealed that quality within the KNP is generally good (TDS = <1000 mg/l) to poor (TDS vary from >1000 to < 10 000 mg/l- the latter in a few isolated localities). Groundwater types that commonly occur in the KNP are sodium-magnesium-bicarbonate, sodium-bicarbonate, sodium-chloride, sodium-magnesium-chloride-bicarbonate and sodium-chloride-bicarbonate (Du Toit, 1998, Leyland et al.,2008).

The natural fluctuations of groundwater levels as well as the groundwater chemistry strongly indicate that groundwater is directly recharged from local rainfall.

In 2007 the Department of Water Affairs (DWA) installed 34 electronic data loggers in unused boreholes across the KNP. Based on the water level data obtained from the 34 monitoring stations Du Toit et al. (2009) delineated representative areas based on the water levels response in terms of drainage, geology and water level horizons for the purpose of effective groundwater management. Using a digital terrain model a groundwater piezometric map was generated to establish the groundwater flow direction in the park. From a regional perspective the groundwater flows from west to east through the park, although on a more localised scale 14 distinctive drainage regions which coincide very closely with surface water drainage regions were identified. Du Toit et al. (2009) classified these drainage regions as groundwater management areas (GMA). Further, potential recharge areas were also identified from the generated piezometric map as shown in Figure 1.2.

Du Toit et al. (2009) attempted to quantify groundwater recharge by correlating the cumulative rainfall departure (CRD) for 25 rainfall stations across the park and the observed water level behaviour. In most cases a good correlation between the CRD and the groundwater level exist.

To this end a representative reflection of natural water level fluctuations in the KNP, are displayed in Figure 1.3. Two prominent low recharge periods and 3 prominent high recharge periods can be seen between 1954 and 2009. Indications are that the KNP is currently moving into another low recharge period which started around 2001/2002. These low and high recharge periods seem to vary in duration from 6 up to 14 years (Du Toit, 2009).

During above average rainfall years the water levels rise significantly. This was perfectly illustrated when the 2000 flood recharged the aquifers fully. During these major 1:100 year rainfall events the aquifers are fully recharged, thereafter they recede again. During below average rainfall years the water levels decline although there are small seasonal fluctuations the overall trend is declining due to outflow to streams and rivers. This is particularly apparent in the perennial rivers where groundwater maintains baseflow.

Petersen (2012) compared isotopic composition of surface water samples from rivers and streams to that of groundwater and concluded that the large perennial Sabie and its tributary the Sand River are consistently fed by groundwater, maintaining base flow during the dry season. These rivers act as basin sinks receiving groundwater discharge all year round. Seasonal and ephemeral rivers that flow along the basalts and rhyolite at the particular sites were interpreted as detached streams that do not interact with groundwater. Along the granites it was found that ephemeral streams act as groundwater sinks during the rainy season.

Based on CRD (after Bredenkamp et al., 1998) and isotope data (Petersen, 2012) the dominant recharge processes that occur in the southern region of the KNP are direct and focused recharge. Recharge occurs during the rainy summer months (December to March) and very little to none during the dry winter season. Recharge takes place during rainfall sequences of 100 mm or more, while rainfall sequences below 100 mm contribute little or zero to recharge. Along the eastern half of the KNP on the basalts and rhyolite direct recharge via piston flow and localised recharge as a result of surface runoff ponding in small depressions being dominant. Groundwater recharged via small streams and rivers on the basalts were regarded as minimal. Along the western granitic areas the dominant recharge process are indirect recharge, taking place via preferred pathways particularly from streams and rivers.

There have been other more localised studies within the KNP examining the role of groundwater in landscape processes. For example it has been described by Grootjans et al. (2010) that in the KNPs far north artesian groundwater processes have facilitated the development and relatively long term existence (up to 14,000 years) of thermal spring mires, in the form of small peat domes (cupolas) at Malahlapanga and Mfayeni. The sizes and state of degradation (through desiccation) of these cupolas suggest that they are not continuously maintained by emerging groundwater, and occur in phases over geological time. Moreover, these unique ecosystems lie in almost straight lines, supporting the hypothesis that water originates from deep aquifers that discharge along geological faults.

Another recent study investigated the riparian and terrestrial interactions in the use of groundwater along the Shingwedzi River in the north of KNP, specifically to determine the groundwater requirements of Groundwater-Dependent Ecosystems, or GDE’s (Colvin et al., 2011), where such systems require groundwater to maintain their ecological structure and function. The aim to determine how and why groundwater supply maintains primary productivity of riparian vegetation during the dry season, and to couple this with carbon and water uptake in both the riparian zone and surrounding Mopane veld, through in-situ evapotranspiration measurements and up-scaled through remote sensing. In order to link this with the KNP biodiversity management objectives the study also determined how groundwater contributes to hydrological heterogeneity in savanna landscapes.

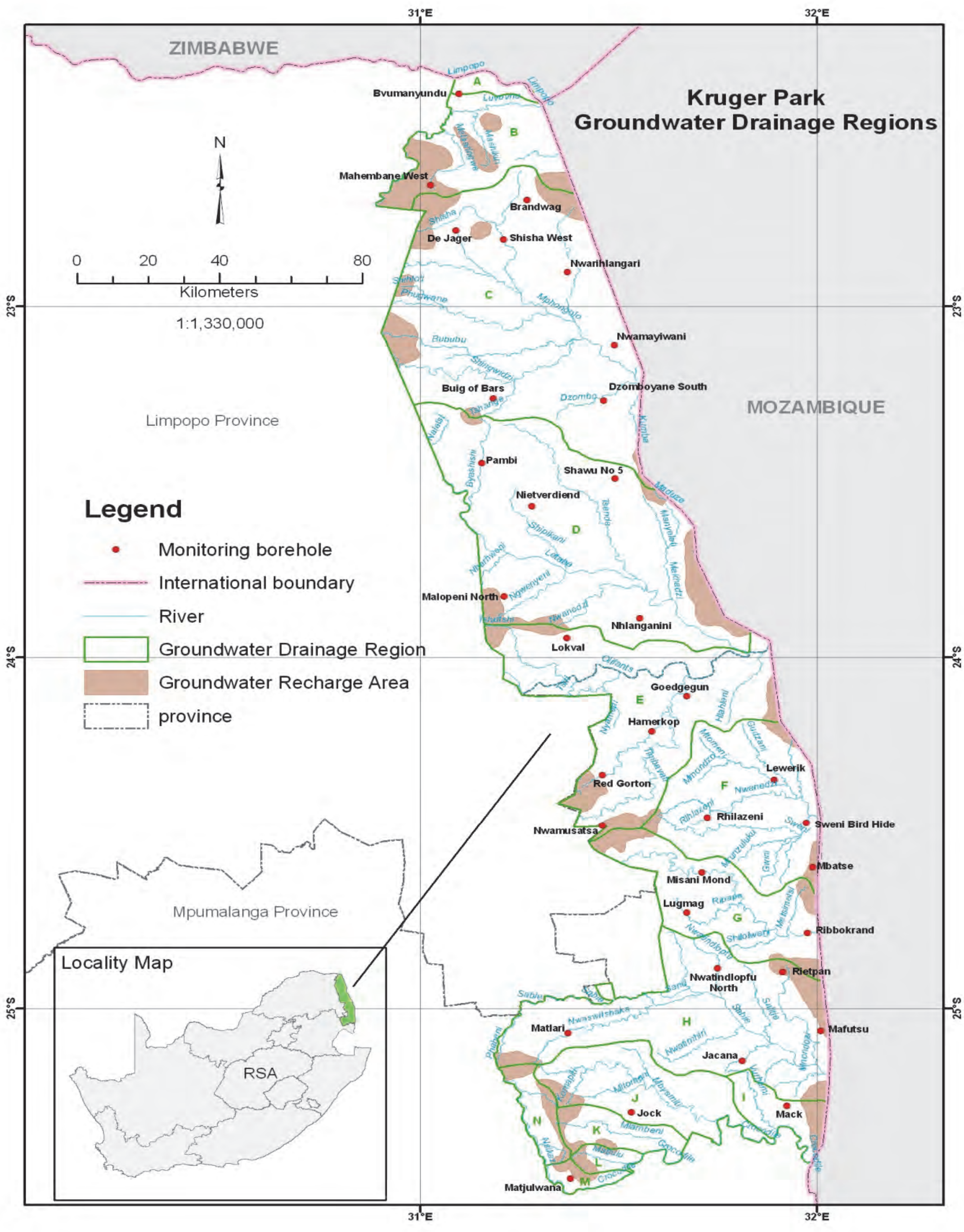

Figure 1.2: Groundwater Drainage Regions within the KNP (after Du Toit, Verster & Smit, 2009)

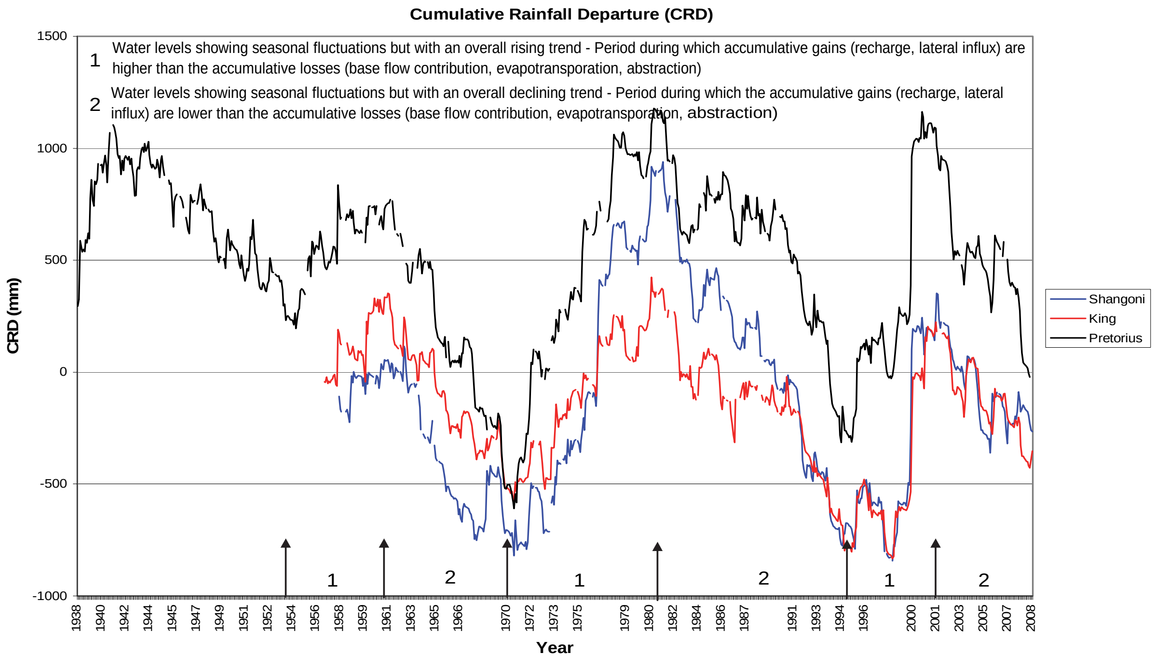

Figure 1.3: History of water level behaviour in the KNP reflected by the cumulative rainfall departure of three rainfall stations (taken from Du Toit, 2009)

1.6 Relevant soil and geomorphology information

To date there is also varying geomorphological data related to the KNP's catena sequences, building upon the work on soils and landscape characterisation detailed by Venter (1990). This geomorphic data is useful supporting information for this study, but particularly the vadose zone processes. Important findings include those by Khomo & Rogers (2005) for the evolution of sodic sites within the KNP catena's which they show for the northern KNP to be a result of both the lateral transmission of fine colluvium down a hillslope and due to the high evaporative demand in these landscape leading to sodium enrichment at the foot of the hillslopes.

Meanwhile, Levick et al. (2010) were able to link the distribution if termite mounds and below seep line grasslands along a catenal sequence to mean annual precipitation (MAP) in various landscapes in the KNP, using hyperspectral LiDAR data. It was suggested that hillslope redistribution of clay takes place under drier (400-500 mm MAP) conditions; hence, a dominant seep line is not present and there is little ecological differentiation across the entire hillslope. Whilst clay would be retained in valley bottoms areas under an intermediate MAP (500-600 mm), creating distinct and broad grassland with a prominent seep line, with termites limited to sandy crests. However under wetter MAP of 600-750 mm the hillslope crests are too sandy to support mound building by termites, but the deep soils still support tall broad-leafed woody vegetation. Clay is still present in the valley bottoms and lower slopes, where termite mounds are larger and more abundant. The seep lines are situated further downslope and with a much narrower grassland.

Hartshorn et al. (2007) suggested that long residence times of the cosmogenic isotopes allowed for the differentiation of soil properties along catenas, whereupon total erosion on the granites in the KNP were dominated by chemical denudation and especially so in the upper hillslope elements with high rates of infiltration. Whilst lateral hydrological processes such as overland flow immediately below seep lines leads to gullying in sodic zones.

1.7 Concepts of hydrological connectivity in groundwater and surface water and application to the study area

Multiple definitions of connectivity exist across and within disciplines. For the purpose of this study some working definitions of hydrologic connectivity were selected. Herron and Wilson (2001) define the term as the efficiency with which runoff moves from source areas to streams and then through the stream network. Michaelides and Chappell (2009) view hydrologic connectivity as a measure of the degree of coupling between different components of the hydrological cycle, specifically the coupling of surface and groundwater flows. According to Tetzlaff et al. (2010) this term refers to the presence of a continuous saturated zone that links different landscape elements to the catchment outlet. From Pringle's (2003) perspective this term is taken to mean the hydrologically mediated transfer of mass, momentum, energy, or organisms within or between compartments of the hydrological cycle. It is portrayed from these definitions that precipitation into catchments follows defined pathways dictated by the structure of catchments (topography, soils & vegetation), prevailing climatic conditions. The influence of anthropogenic activities cannot be ruled out since these alter catchment structure through different land use practices. It is also evident from these definitions that hydrologic connectivity as a state and/or process of interaction of fluxes between surface and groundwater domains conveying mass (water and solutes) and energy to a catchment outlet. Figure 1.4 summarises the concept of how interactions occur between the afore-mentioned process domains.

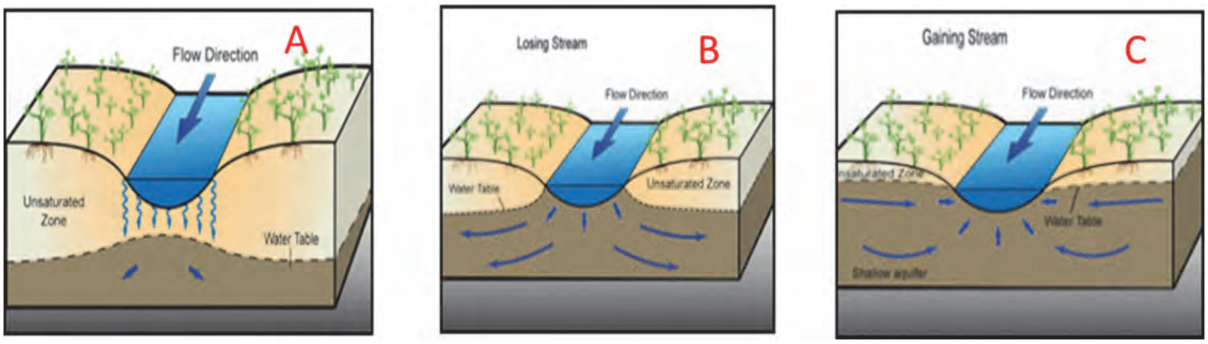

Figure 1.4: Recharge-discharge mechanisms (after Winter, 2007)

Groundwater-stream interaction is demonstrated by natural recharge and discharge processes, through the streambed and hillslope interface. Recharge occurring through channel leakage gives rise to losing or influent streams. Losing streams have water surface elevations that lie above aquifer water table which result in water seeping through streambeds to indirectly recharge groundwater aquifers. Stream A has an unsaturated zone under it while stream B overlies a saturated zone, but both streams are similarly losing. Stream A is typical of ephemeral streams (event-driven) while stream B epitomizes intermittent streams (only flowing seasonally). Conversely, groundwater discharge into channels results in gaining or effluent streams, as in stream C. Gaining streams are usually perennial with flows that typically occur all year round. While a gaining stream can be described as having a saturated connection to the aquifer a losing stream may either have a saturated or an unsaturated connection to the aquifer (Winter, 2007). The direction of fluxes between groundwater and streams commonly varies spatially and temporally along a stream reach and is influenced by the scale of analysis (Ivkovic, 2008).

The nature and extent of groundwater-stream interactions determine whether or not headwaters upstream of catchments are entirely transmitted through channels to downstream points. This phenomenon is what Nadeau and Rains (2007) describe as stream network connectivity or connectivity along streams. Longitudinal linkages are defined by upstream-downstream as well as tributary-trunk relationships (Fryirs et al., 2007). Notably streams can be gaining in one reach while experiencing transmission losses in another (Kalbus et al., 2006). When gaining, an increase in downstream discharge occurs whereas transmission losses result in a reduction of downstream flow (Beven and Hornberger, 1982).

1.7.1 Hydrologic Connectivity and Catchment Function

The term ‘function’ has plural meanings in environmental science denoting either processes, roles, services or the operation of whole systems (Schroder, 2006). With respect to catchments, ‘function’ can broadly be classified into hydrological, geomorphological, pedological and ecological functions which essentially, are interconnected functions. The collective response of a catchment as a result of the interaction of component processes is termed catchment functioning (Bloschl et al., 2013). A catchment’s component processes include the partitioning, transmission, storage and release of water, energy and matter into different pathways and storage areas (Bloschl et al., 2013). How these processes are connected within the catchment is controlled by thresholds and feedbacks over space and time scales. The controls and feedbacks governing hydrologic behaviour reflect inherent variability in catchment physiography and climate forcing across spatio-temporal scales (Wagener et al., 2008).

Inference of how connected hydrological processes are within catchments can be achieved by observing vegetation distribution patterns which tend to coincide with water distribution especially in water limited semi-arid environments. As such integrated studies between hydrology and ecology (vegetation structure & distribution) mutually assist either discipline in dealing with their respective research questions (Rodriguez-Iturbe, 2000; Schroder, 2006). The above observation concurs with Mackenzie et al. (2003), who noted that the fluvial geomorphology of the Sabie River in KNP is a critical component of the riparian vegetation distribution patterns. Thus hydrologic, geomorphic and ecological processes tend to undergo a process of co-evolution to produce patterns of self-organisation (Tetzlaff et al., 2010). For instance, riparian and wetland areas in semi-arid environments usually show concentrations of woody, evergreen vegetation more than any other part within catchment landscapes due to moisture and nutrients availability conveyed by the interaction of hydrological processes. Hillerislambers et al. (2001) further support this notion through their study which revealed the formation of patterns in semi-arid areas portrayed by positive feedback between plant densities, local water infiltration coupled with the spatial redistribution of runoff water.

Similarly the soils of a catchment have an interactive relationship with its hydrology. The partitioning, transfer and storage of water (i.e. catchment hydrologic function) can be traced by studying soil properties across space and time scales since soils are products of water-related physical and chemical processes (Van Tol et al., 2013). The distribution of particular soils with discernible properties gives an indication of a catchment’s hydrological response and it forms the basis of hydropedology (Lin et al., 2006). When correctly interpreted, the spatial variation of soil properties associated with the interaction of soils and water can serve as indicators of dominant hydrological processes (Van Tol et al., 2010). Pedologists, therefore, have the capacity to contribute valuable information to the science of hydrology by interpreting and relating soil properties to catchment hydrological behaviour

(Lin et al., 2006). Hydrologists agree that the spatial variety of soil properties significantly influences the connectivity of hydrological processes but their major challenge is the skill to gather and interpret soil information (Van Tol et al., 2010). The importance of integrating hydrology and soil science demonstrated in the above discussion can be achieved through interdisciplinary studies involving pedologists and hydrologists. Integrating hydrology and other science disciplines (e.g. ecology and pedology) as already described, will provide better understanding of hydrologic processes that characterise the catchment's hydrologic function. Nuttle (2002) agrees that coupling hydrologic and ecosystem science is vital for understanding catchment function which in turn is vital to inform sustainable water management decisions. This is schematically presented in Figure 1.5.

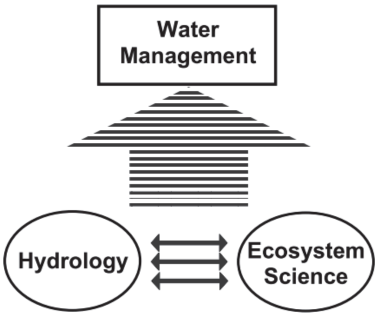

Figure 1.5: Integration of hydrology and ecosystem science (adapted from Nuttle, 2002)

In addition to interdisciplinary approaches, Tetzlaff et al. (2007) posit that a better understanding of catchment function can be obtained through use of tools and methodologies that present integrated perspectives of how catchments route water across spatio-temporal scales. This can be achieved through coupling multi-scale traditional techniques with integrated methods such as tracer analysis, geophysical surveys, remote sensing and modelling tools including Geographic Information Systems (GIS) and hydrologic models (Tetzlaff et al., 2010). For instance, hydrochemical tracers and geophysical surveys can provide integrated insights into emergent hydrological processes and how these are influenced by different landscape elements (Tetzlaff et al., 2007).

Analysing the chemistry of water from surface, subsurface and groundwater zones gives an indication of how flow paths are integrated within these process domains. Quantifying water transit time distributions from tracer data within catchments leads to better understanding of the functioning of catchments. According to McDonnell et al. (2010) the modelling of transit times provides new insight to catchment functioning since transit times portray how catchments retain and release water and solutes thereby setting up biogeochemical conditions. Transit time distributions enable inference into dominant processes and catchment function by relating catchment responses to catchment characteristics including soils, vegetation, topography and climate. Integrated insight for understanding emergent behaviour of complex mixing processes and flow paths within catchments can also be gained through quantifying transit times for water from rainfall input to the moment it reaches the stream (MacKinnon and Tetzlaff, 2009). Tracer determined transit times and flow paths can further be used to inform distributed, physically-based hydrologic models which integrate catchment characteristics and processes to better understand the functioning of catchments (MacKinnon and Tetzlaff, 2009; McDonnell et al., 2010).

1.7.2 Drivers and Controls of Hydrological Connectivity

Studies have shown that hydrologic connectivity depends on several factors such as rainfall intensity, catchment wetness, vegetation characteristics, soil properties, geology, surface and bedrock topography (e.g. Buttle et al., 2004; Jencso et al., 2009; McGuire and McDonnell, 2010). These controls cause hydrologic connectivity to vary spatially and temporally thus reflecting geographic differences in key forcing factors and catchment characteristics. Interpreting these differences requires an understanding of catchments as evolving systems where climate and landscape organisation interact in different ways in response to external forcing to influence hydrological processes (Tetzlaff et al., 2010). However, since catchments are enormously complex and heterogeneous concentration should initially be on dominant or first order controls that influence observed heterogeneity (Wagener et al., 2008).

Antecedent soil moisture prior to a rainfall event plays an important role in initiating runoff and in ensuring continuity of flow to the stream outlet. Catchments in semi-arid areas, which often experience clearly demarcated seasons, have low antecedent moisture during dry seasons and high in wet seasons. Consequently, hydrologic connectivity often fluctuates with these changes in seasons as well as episodically during and between rainfall events. As McGuire and McDonnell (2010) posit, a clear seasonality of a catchment accentuates connectivity presence and absence.

Soil properties in a catchment also determine hydrologic connectivity between constituent parts of the basin. These include soil macropores, soil layering and soil depth. Macropores are formed and developed by various mechanisms which include subsurface erosion, animal burrows, live and decayed plant roots as well as surface bedrock fractures. Noguchi et al. (1999) assert that connection of macropores can possibly occur over relatively long slope distances creating considerable waterflow pathways.

The influence of topography on water fluxes cannot be overemphasized. Having bearing on catchment slopes or gradients, topography poses as an important control on flow direction. Micro-topography also determines whether flow should occur or not, as some water should contribute to depression storage before it can flow to downslope areas. However, it has been noted in recent studies that surface and subsurface topography should be considered separately, since their effects on waterflows are distinctly different (Costa et al., 2012). While surface topography mainly influences surface flows, bedrock topography controls local hydrological gradients and has significant impacts on flows in the vadose zone.

Extraordinary high rainfall events resulting from short wet cycles were observed to drive groundwater-surface connectivity in semi-arid environments of South Africa (Van Wyk et al., 2011). The rainwater hydrochemistry of such events is very distinct such that it is easily traceable between process domains. Such events were observed to last from 3 to 8 days with a recurrence interval of 1:5 years with approximate volumes of 50 to 150 mm per day (Van Wyk et al., 2011). These rainfall depths are usually associated with groundwater recharge if they occur consecutively during these episodic rainfall cycles.

1.7.3 Connecting Mechanisms of Surface and Groundwater Resources

Various mechanisms facilitate the interaction of groundwater and surface water within and between nested catchments. These include subsurface lateral flow occurring either through soil/bedrock interfaces or through soil material underlain by a layer of low hydraulic conductivity. Surface water can be connected to groundwater aquifers by infiltrating the soil and weathered zone matrices or directly through fractures or macropores as preferential flow (Sophocleous, 2002). Stormflow can be distinguished from baseflow in that baseflow occurs due to the sole contribution of groundwater discharge from persistent, slowly varying sources (Sophocleous, 2002) into streams and this keeps streams flowing during dry periods. Subsurface flow that enters streams quick enough to contribute to event-response is known as subsurface stormflow or quickflow (Sophocleous, 2002). According to Beven (1989) interflow can be defined as near-surface flow occurring within the soil profile and enters a stream channel within the time frame of a storm hydrograph. Interflow has been isotopically observed to contribute to stormflow response through a displacement or translatory process in which event water displaces or shifts onto stored subsurface water pushing it towards stream channels (Beven and Germann, 1982; Sklash and Farvolden, 1979). If the rate of interflow entering a saturated area from upslope exceeds that of interflow leaving the area, excess interflow returns to the surface as return flow.

1.7.4 A Review of Existing Knowledge on Hydrological Connectivity

Several studies have been conducted on groundwater-surface water interaction with goals including (i) the understanding of hydrological processes (e.g. McCartney et al., 1998; Burns et al., 2001; Bohte et al., 2008; Wenninger et al., 2008; Riddell et al., 2013) (ii) water resources evaluation and management (e.g. Ogunkoya et al., 1993; McGlynn and McDonnell, 2003; Baskaran et al., 2009; Praamsma et al., 2009; Bohte et al., 2010), and (iii) monitoring hyporheic fluxes to identify ecological zones suitable for fish spawning (Malcolm et al., 2005). Although this subject has been investigated fairly widely, most of the studies have largely been descriptive rather than quantitative (McDonnell, et al., 2007; Jencso and McGlynn, 2011). This has resulted in research findings that are site-specific with no chance of being generalised to other catchments with similar environmental conditions. As a result, there has been partial understanding of linkages between catchment structure and function.

Research studies (e.g. Bracken and Croke, 2007; McGuire and McDonnell, 2010) have generally shown that subsurface flow is the dominant mechanism in forested or vegetated catchments, however, specific flowpaths, transit and residence times and sources of water are not well understood. Devising new approaches needed to determine and quantify hydrological process linkages remains the most pressing challenge in environmental hydrology (Ali and Roy, 2009).

Stream-aquifer interactions are characterised by spatio-temporal variability (Katz et al., 1998) which is understood at least at local/hillslope scales (Soulsby et al., 2008). Since management decisions are made at catchment scale, recent research has shifted towards upscaling from smaller research plots to larger mesoscale catchments. Due to process complexity and catchment heterogeneity upscaling often requires identification of dominant processes evident at catchment scale rather than attempting to capture all small scale variability and complexity (Tetzlaff et al., 2010). Tracers (e.g. Uchida et al., 2005) and geophysical surveys (Wenninger et al., 2008) were noted to be useful for conceptualising smaller scale catchment processes which can be used for upscaling studies. Applying these techniques at a multi-scale level in nested catchments yields useful results which inform hydrological model building and allows unanticipated or emergent responses to be identified (e.g. Soulsby et al., 2008).

The variability of hydrological responses within and between catchments is attributed to plural controls influenced by heterogeneous catchment characteristics such as geology, streambed permeability, surface and bedrock topography, antecedent moisture, vegetation characteristics, and soil properties (Jencso et al., 2011; Van Tol et al., 2013). Studies have investigated individual influence of these controls, for instance streambed topography (e.g. Harvey and Bencala, 1993) and local channel geomorphology (e.g. Malcolm et al., 2005). However, it is noted that very few studies have comparatively investigated the combined and hierarchical influence of these controls across space and time scales (Jencso et al., 2011). Despite existing inter-catchment variability, comparative studies make it possible to discern similar functional patterns between catchments which could be used to formulate and test generic hypotheses that are applicable to other catchments, especially ungauged basins (Wagener et al., 2008). Earlier approaches that characterised and catalogued enormous heterogeneity and complexity of catchment processes have produced findings that are not generic for prediction in ungauged basins (PUB) (McDonnell et al., 2007). As such contemporary approaches advocate the exploration of sets of organising principles (McDonnell et al., 2007) which relate catchment hydrology to vegetation distribution (e.g. (Nuttle, 2002; Bloschl et al., 2013) or to soil properties (e.g. Van Tol et al., 2013). The concept of identifying organizing principles is actually a paradigm shift from emphasizing reproduction of process complexity to that of simplifying complex systems by identifying patterns or dominant processes that explain the existence of those complexities (Sivapalan, 2005). Organizing or optimality principles form diagnostic generalization tools and analytical frameworks that act as a basis for cross-scale characterisation and prediction (MacKinnon and Tetzlaff, 2009).

Other studies advance the concept of providing a common hydrologically significant classification framework through assessing and mapping catchment form, climate and function (Wagener et al., 2008). When achieved such a framework provides insight into causal relationships between the afore-mentioned aspects (form, climate and function) thereby increasing predictive power through rational testing of hypotheses about similarity/dissimilarity of hydrological systems (Wagener et al., 2008). Tested hypotheses can lead to theories or models which when proven can be established as laws with wide applicability.

Integrated approaches involving various disciplines and methodologies (e.g. tracers, geophysical surveys, remote sensing and hydrological models in addition to hydrometry) are recommended in literature for better understanding of how catchments respond to rainfall events (Lorentz et al., 2008; Jencso et al., 2011). From a study in a semi-arid environment in South Africa, Wenninger et al. (2005) observed that use of different methods at the same site promotes acquisition of better results as disadvantages of one method are overshadowed by advantages of the other methods. If the use of different methods is coupled by the involvement of experts from various disciplines (e.g. geologists, ecologists and engineers) a better understanding of catchment functioning and underlying governing processes is enhanced (Rodriguez-Iturbe, 2000).

1.8 Structure of the report

Due to the large volume of monitoring data gathered during this study the remainder of the report has the following structure in order to aid the reader:

- chapter 2 overviews the site characteristics of the two Supersites
- chapter 3 provides a summary of key findings of ephemeral hydrology determined on the granite catchment (details referred to in Chapter 6)
- chapter 4 provides a summary of key findings of ephemeral hydrology determined on the basalt catchment (details referred to in Chapter 7)

- chapter 5 gives the detailed methodology use in the study
- chapter 6 provides detailed hydrological process descriptions of ephemeral hydrology on the granite catchment
- chapter 7 provides detailed hydrological process descriptions of ephemeral hydrology on the basalt catchment

2. KNP STUDY SITE DESCRIPTION

2.1 KNP Geology drainage and climate

The Kruger National Park (KNP) has a north-south longitudinal geologic alignment, consisting mainly of granites to the west (Figure 2.1) and basalts to the east with patches of shale and sandstone sandwiched between them (Cullum and Rogers, 2011; O'Keeffe and Rogers, 2003). This longitudinal stretch of geology is dissected by 5 main river systems (Luvuvhu, Letaba, Olifants, Sabie and Crocodile) with a west-east flow direction across it (O'Keeffe and Rogers, 2003). These major river systems have their origin outside the park in the Klein or Northern Drakensburg Escarpment and they pass through landscapes under diverse land use practices ranging from forestry, irrigated crop and citrus fruit agriculture to communal mixed farming. Conversely, smaller drainages originate in and end within the boundaries of the park in low rainfall areas resulting in them being ephemeral streams. O'Keeffe and Rogers (2003) further observe that the occurrence of intrusive dykes of dolerite, patches of gabbro and minor faults add heterogeneity and complexity to the geological template of the park.

KNP is generally semi-arid with a rainfall range falling between 6-400 mm per year (O'Keeffe and Rogers, 2003). A north-south rainfall gradient of 450-650 mm/year exists (O'Keeffe and Rogers, 2003) with an east-west gradient of between 400 and over 600 mm per year (Cullum and Rogers, 2011) in the KNP. Seasonal rainfall is experienced within KNP, with November to March being wetter months while April to October constitutes the drier period. KNP is situated in the savanna biome of South Africa which is a semi-arid system where water plays a pivotal role in many biotic and geomorphic processes.

The diversity of vegetation in KNP varies with underlying geology, rainfall amounts and faunal activity (particularly of large herbivores such as elephants). Some parts of the park are still under pristine conditions while others have been altered by human interference adding to the spatial variability in the occurrence and diversity of vegetation. Due to higher rainfall, deeper and more diverse soils, the southern parts of KNP have varied woody vegetation species which are also influenced by hillslope position and geology (Cullum and Rogers, 2011).

2.2 KNP Supersite Selection Process

The proposal for research 'Supersites' in the KNP began with Cullum & Rogers (2011) in agreement with SANParks personnel to establish multi-disciplinary research catchments in the two dominant and diametrically opposed geologies within the KNP (granite and basalt). Within these there are four landscape systems in which the Supersites should be located, these are the Skukuza (southern granites), Phalaborwa (northern granites), Satara (southern basalts) and Letaba (northern basalts) which are the largest of the land-systems in the KNP. These collectively represent 80% of the total park area (Venter et al., 2003) and thus the four land-systems also allow broad comparisons between geologies and rainfall.

Through collaborative processes between KNP managers and scientists the four final Supersites were selected based on the following (Smit et al., 2013):

- Between themselves include contrasts of the two main abiotic variables driving much of the larger scale variation in the park, namely, geology (granite and basalt) and rainfall (higher rainfall in the south versus lower rainfall in the north).

- Be large enough to contain at least one third-order catchment situated entirely within a single geology, allowing ecological patterns to be studied at the three scales associated with first-order, second-order and third-order catchments.

- Contain the hillslope vegetation and soil patterns (catenal sequences) that commonly occur in the local land system.

- Be easily accessible from as many sides as possible by all-weather roads.

- Be close to research camps and facilities.

- Be outside of areas demarcated as 'wilderness' or 'remote' in the KNP zoning plan, in order to allow installation of instrumentation.

Smit et al. (2013) also provide a detailed description of this site selection process, the philosophy of the supersites concept and detailed description of the areas, the reader is thus referred there for further information.

2.3 Study Site Details

A summary of the geologic, geomorphologic and morphometric characteristics of these sites as described by Venter (1990) land systems, land type classifications and hydrogeological characteristics are summarised in, Table 2.1 and
Table 2.2 respectively.

2.3.1 Southern Granites (SGR)

The southern granite supersite sits within the Renosterkoppies land type, which is a transitional zone between the land types associated with the perennial Sabie and Crocodile River catchments, as its sits on the watershed between these two. This supersite sits within the Msimuku sub-catchment. Dolerites dykes should be of lower frequency at this site than Ronesterkoppies land type catchments that sit closer to the Skukuza land type, where they are quite frequent. *Acacia nilotica* dominates the lower slopes and *Euclea divinorium* is associated with the duplex sodic soils, whilst the crest becomes frequented by *Terminalia sericea*.

2.3.2 Southern Basalts (SBAS)

The southern basalt supersite sits within the Satara land type which is characterized by its shallow to moderately deep red olivine-poor clays. It is very flat with open tree savanna dominated by *Sclerocarya birrea* and *Acacia nigrescens*.

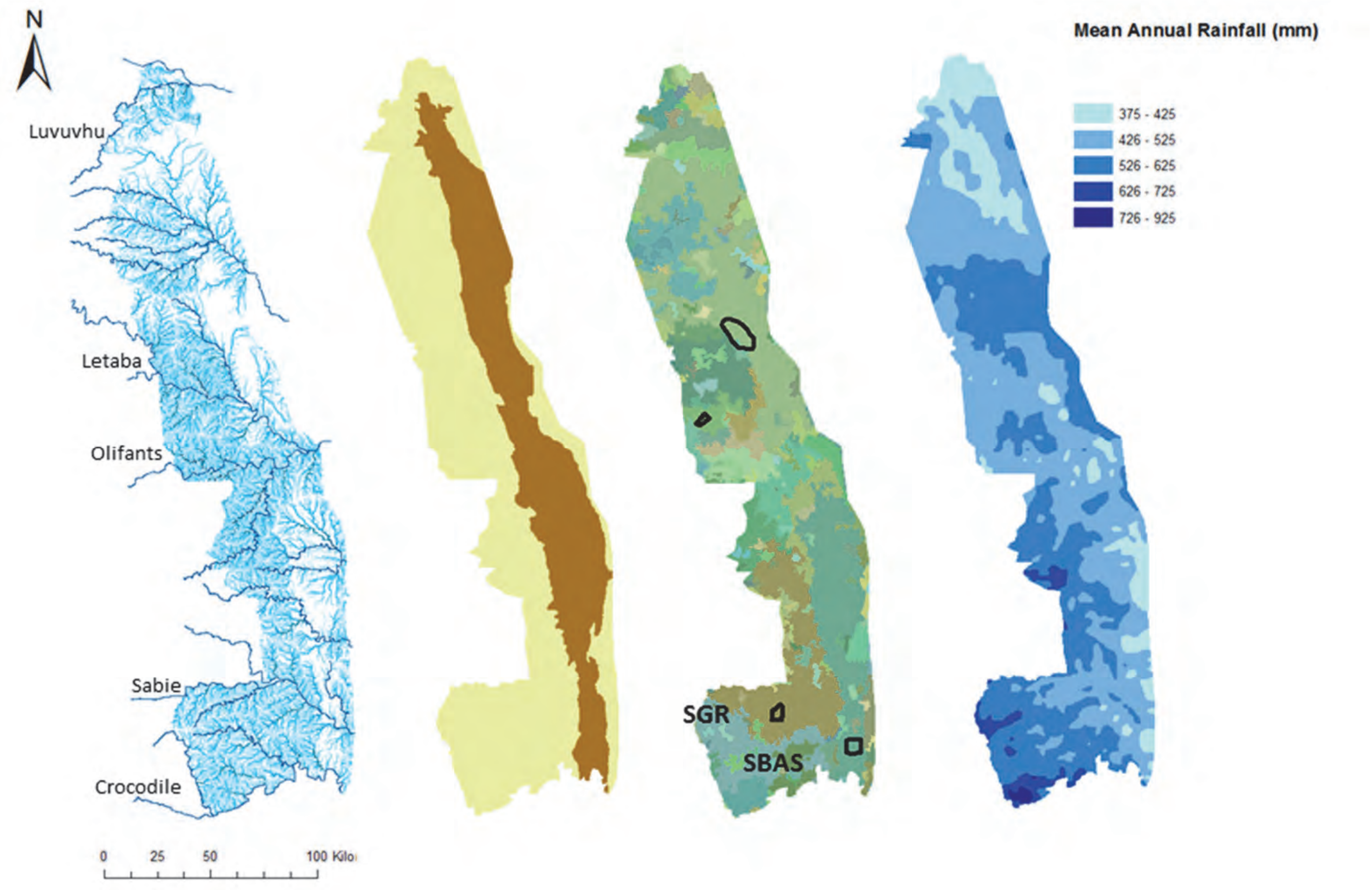

Figure 2.1: Location of final selected Supersites in KNP in relation to (from left to right): drainage network; dominant geology (yellow=granites, brown=basalts); physiographic zones of Cullum & Rogers, 2011; and mean annual precipitation.

Table 2.1: Land system and land type characteristics for the locations of the KNP Supersites (source Venter, 1990)

							Selected Morphometric Features				
								Slope classes (% of area)			
Supersite	**Land System**	**Land Type**	**Geology**	**Geomorphology**	**Rainfall (mm)**	**Altitude (m)**	**Stream Frequency (n/km^2)**	**0-2**	**2-6**	**6-15**	**>15**
Southern Granites	Skukuza	Renosterkoppies	Granite/Gneiss of the Nelspruit granite suite	Moderately undulating plains sloping down towards the Sabie River	500-750	250-350	2.3	7	86	6	1
Southern Basalts	Satara	Satara	Olivine-poor basalt of the Sabie River basalt formation intruded frequently by dolerite dykes	Flat to slightly undulating plains associated mainly with interfluvial areas and related to the LTIII erosion surface	500-650	140-310	0.39	97	3	0	0

LTIII* - Later Tertiary Phase 3

Table 2.2: Land forms and soil characteristics for the locations of the KNP Supersites (source Venter, 1990)

Supersite		**Crest**	**Midslope**	**Footslope**	**Valley Bottom**
Southern Granites		convex well drained interfluvial areas with slope angles seldom more than 10%	convex to concave moderately to poorly drained slopes with slope angles less than 1-13%	straight poorly to moderately drained slopes with slope angles of 1-9%	concave and irregular drainage channels
	Soils	moderately deep eutrophic yellow apedal coarse sand occassionally with plinthic subsoil horizons	shallow grey eutrophic coarse sand over weathered rock or greyish-brown clay	duplex soils with shallow (10-20cm) brown and grey loam abruptly overlying primatic clay which is frequently calcareous	complex association of deep brown sand to calcareous clay (occassionaly calcareous along drainage lines) and shallow to deep brown sand to clay with rock outcrops (small drainage lines)
Southern Basalts	**Soils**	moderately deep tp shallow red and brown structured and paraduplex clay	shallow red and brown orthic and melanic loam and clay	deep to moderately deep black and brown vertic and pedocutanic frequently calcareous clay	a complex association of black and brown calcareous alluvial clay and loam in various stages of profile development

Table 2.3: Hydrogeological characteristics for the regions of the KNP Supersites (source Du Toit, 1998)

Super Site	Formation	Typical borehole depths	Typical water strikes	Borehole yield	Occurrence of groundwater	Water Type
Southern Granite	Nelspriut Suite	Between 30m-80m, Average 51m	Between 10m-50m	54% - <1 l/s, 37% - 1-5 l/s	Broken/weathered gneiss	Na-HCO3
Southern Basalts	Letaba	58% - 50m, 35% - 50m-100m, Average - 49m	Within the first 20m	58% - <1l/s, 34% - 1-5l/s, Average - 1.48l/s	Broken Basalt	Na-Mg-HCO3

2.4 Development of Initial Conceptual Model of GW-SW Interactions for the two Southern KNP Supersites

This section details the initial conceptual development of hydrological processes understanding within the two southern KNP Supersites. This was conducted at the outset of the research through desktop analysis and field reconnaissance. This understanding has an explicit focus on four scales of hydrological connectivity across the stream orders at these sites, as depicted in the framework of Figure 2.2.

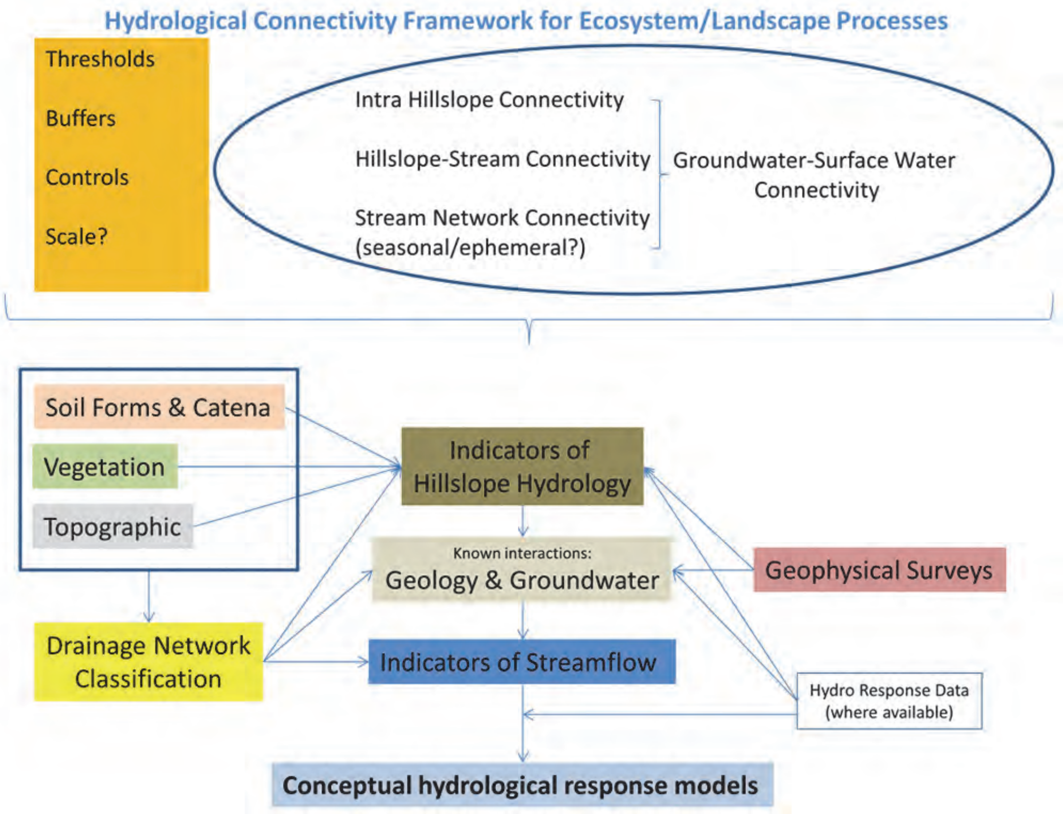

Figure 2.2: Framework for the development of conceptual models on hydrological connectivity of surface and groundwater processes in the KNP Supersites 2011-12.

2.4.1 Southern Granite (Stevenson-Hamilton) Supersite

The initial perceived hydro- and hydrogeological characteristics for the Southern Granite supersite are summarised in Table 2.4 and Figure 2.3. It was noted through observation as one moves up the catchment orders in this site that in general the lower order catchments appear to be steeper than the higher order catchments. Although the opposite trend was revealed through mean slopes derived via ArcGIS^{TM} on the modified 90 m STRM DEM (of Cullum & Rogers, 2011) for the specific 1st, 2nd and 3rd order catchments where hydrological observations took place where the mean slopes are 2.3%, 3.2% and 3.2% respectively.

Moreover, there appeared to be a concomitant increase in the proportion of footslope elements, while in general the average soil depth and consequent soil water storage potential increases with incremental catchment orders. The dominant soil forms described at the southern granite site are hydro-pedologically indicative of soil bedrock interflow at the crests and midslopes due to their propensity for free vertical infiltration of water, and this is the case in all three orders. Therefore dominant lateral flow process were hypothesised in these catchments through soil bedrock interflow, which was expected to increase proportionally with each incremental catchment order.

In addition the hydro-pedology of the footslopes was indicative of near surface macropore flow being the dominant connecting hydrological mechanism between the hillslopes and stream networks in all catchment orders. This was expected to be augmented by fractured rock interflows from the mid- and footslopes. In all catchment orders it was expected that these will be event driven contributions, particularly at the footslopes, and consequently these catchments are expected to yield low baseflow contributions from the hillslopes.

In terms of the linkages of these catchments with their aquifers, the hypothesis was of vertical infiltration properties of the heavily illuviated crest soils, with potential recharge to the groundwater store being largely limited to these hillslope positions. Meanwhile in these positions (crest soils) the actual recharge would largely be an event (large rainfall) driven process via cracks and fractures, with very little sustained contributions from hillslope storage over longer periods. Moreover, it was speculated that the aquifer connected to lower order catchments in particular will contribute to event streamflow as gaining reaches. However the 3rd order catchments were expected to be the threshold at which stream morphology switches to increasingly losing river reaches such that aquifers will be increasingly recharged by streams at these higher orders. This hypothesis was based on the observation that the 3rd order stream has a very broad shallow macro-channel encompassed by tall evergreen woody vegetation, in stark contrast to the lower order streams which are very deeply incised.

2.4.2 Southern Basalt (Nhlowa) Supersite

The initial perceived hydro- and hydrogeological characteristics for the southern basalt supersite are summarised in Table 2.5 and Figure 2.4. It was noted through observation moving up the catchment orders in this site that in general the lower order catchments appear to have a lower gradient on average and particularly so at the footslopes than the higher order catchments. However, mean slopes derived via ArcGIS^{TM} on the modified 90 m STRM DEM (of Cullum & Rogers, 2011) for the specific 1st, 2nd and 3rd order catchments where we focused our hydrological observations are 1.4% for all orders.

At this supersite there appeared also to be continuous representation of footslope regions almost all the way along the stream reaches, which is in contrast to the southern granites where this is patchy. Meanwhile at the southern basalts there was an apparent decrease in soil depth and thus soil water storage capacity with incremental catchment orders. In all cases crests are largely dominant with narrow mid- and footslopes.

Based on the representative soil forms in these catchments, the hydro-pedological interpretation was that crests and midslopes are dominated by vertical free infiltration, with the propensity for small scale overland flows under intense rainfall conditions. Furthermore, the hydro-pedology suggested that these catchments are largely disconnected from their stream networks, with only the footslope regions having intermittent event driven lateral transmissivity via fractured rock at the footslope stream interface.

As in the rest of the KNP aquifer recharge potential is low, but was again expected to occur via the crest areas (with some contributions from midslope) as diffuse piston flow. However this recharge was expected to only follow a sequence of large preceding rainfall years. In addition the potential for recharge via endorheic pools on the crests was expected. It was hypothesised that in these southern basalt catchments the aquifers are largely if not completely detached from the stream networks which often contain clay rich vertic soils that impede free drainage.

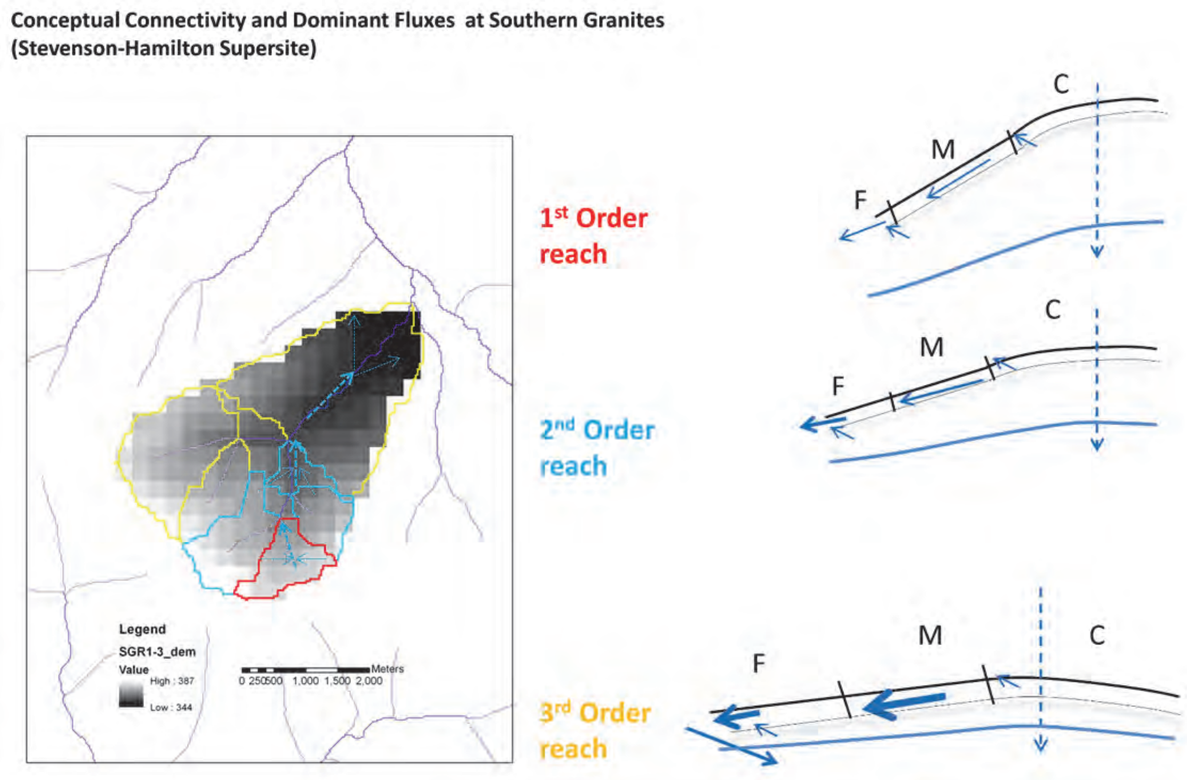

Figure 2.3: Schematic of conceptual dominant hydrological processes at the southern Granite (Stevenson-Hamilton) Supersite.

Table 2.4: Conceptual dominant hydrological process at the southern Granite (Stevenson-Hamilton) Supersite.

Catchment	1st Order			2nd Order			3rd Order		
Hillslope Element	Crest	Midslope	Footslope	Crest	Midslope	Footslope	Crest	Midslope	Footslope
Morphological Characteristics	Slope Gradient decrease ---->								
	<--- Footslope prominence decrease								
	Soil depth & storativity increase --->								
Soil Form	Cl/Ms/Gs/Cf	Cl/Ms/Gs/Cf	Ss/Mw/Bo/My	Cl/Ms/Gs/Cf	Cl/Ms/Gs/Cf	Ss/Mw/Bo/My	Cl/Ms/Gs/Cf	Cl/Ms/Gs/Cf	Ss/Mw/Bo/My
Hydropedology interpretation	Soil Bedrock Interflow	Soil Bedrock Interflow	Near Surface Macropore Flow	Soil Bedrock Interflow	Soil Bedrock Interflow	Near Surface Macropore Flow	Soil Bedrock Interflow	Soil Bedrock Interflow	Near Surface Macropore Flow
		Fractured rock interflow contributions to seeps	Fractured rock interflow contributions to footslopes		Fractured rock interflow contributions to seeps	Fractured rock interflow contributions to footslopes		Fractured rock interflow contributions to seeps	Fractured rock interflow contributions to footslopes
			Event driven Contributions			Event driven Contributions			Event driven Contributions
			low baseflow			low baseflow			low baseflow
		saturation excess responsive soils			saturation excess responsive soils				
	Interflow increase --->								
Hydrogeology	KNP Generally Low recharge potential 1.5-3% of MAP p.a.								
	event driven dominant recharge via crest			event driven dominant recharge via crest			event driven dominant recharge via crest		dominantly losing reaches
	preferential flow via cracks and fractures		gaining reaches	preferential flow via cracks and fractures		gaining reaches	preferential flow via cracks and fractures		
Streamflow Connectivity	Intermittent Event driven			Intermittent Event driven			Intermittent Event driven + seasonal baseflow		

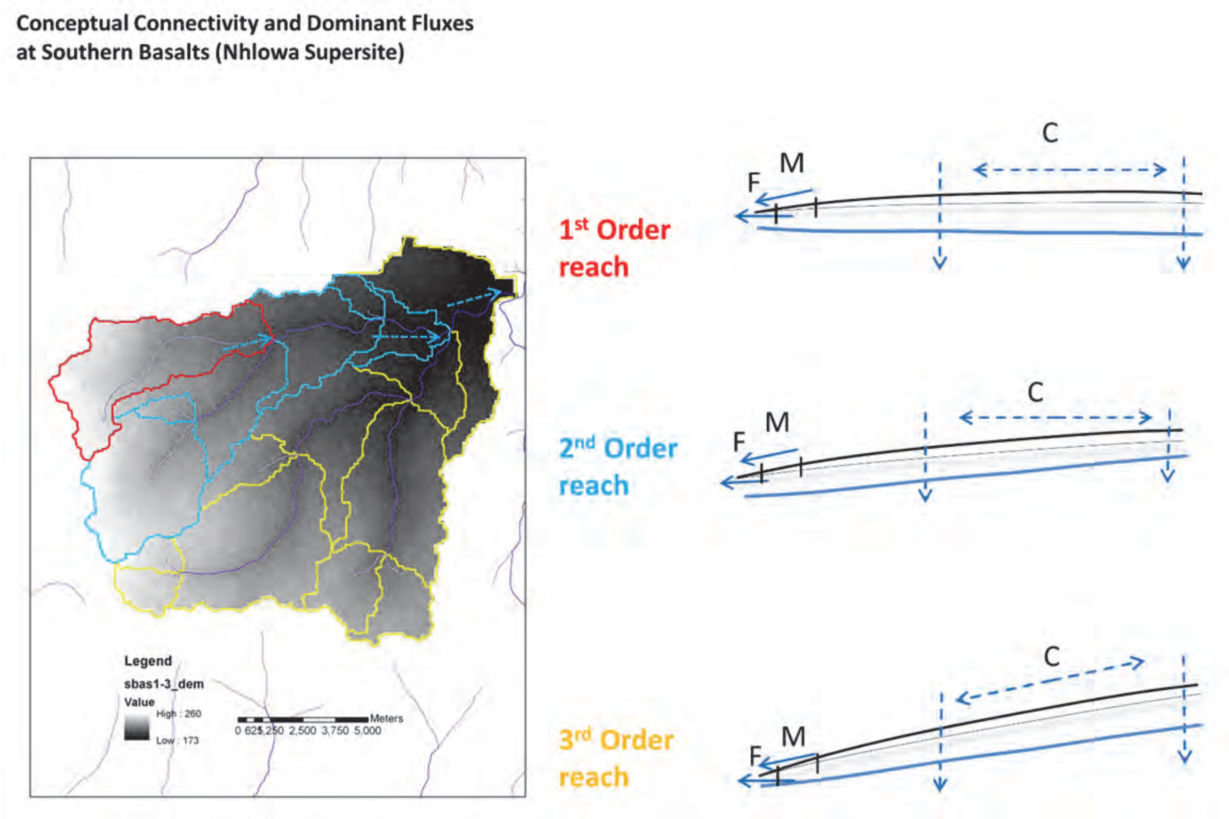

Figure 2.4: Schematic of conceptual dominant hydrological processes at the southern Basalt (Nhlowa) Supersite.

Table 2.5: Conceptual dominant hydrological process at the southern Basalt (Nhlowa) Supersite.

Catchment	1st Order			2nd Order			3rd Order		
Hillslope Element	Crest	Midslope	Footslope	Crest	Midslope	Footslope	Crest	Midslope	Footslope
Morphological Characteristics	Slope Gradient extremely low, but increases --->								
	Footslopes continuous (~5m wide)								
	Soil depth & storativity decrease --->								
Soil Form	Sd/Gs	Ms/Gs/Sd/Sw/Mw	Ms/Mw/Bo/Sd	Ms/Gs/Sd	Sd/Va/Sw/Ms/Gs/	Va/Se/Bo/Mw	Sd/Ms	Ms/Gs	Mw/Ms
Hydropedology interpretation	vertical infiltration/overland	vertical infiltration		vertical infiltration	vertical infiltration		vertical infiltration	vertical infiltration/overland	
	Fractured Rock storativity &	Fractured Rock storativity &		Fractured Rock storativity &	Fractured Rock storativity &		Fractured Rock storativity &	Fractured Rock storativity &	
			Fractured rock transmissivity			Fractured rock transmissivity			Fractured rock transmissivity
	high ET loss								
Hydrogeology	KNP Generally Low recharge potential 1.5-3% of MAP p.a.								
	sequence of preceeding seasonal rainfall event dominant at crest		detached from stream	sequence of preceeding seasonal rainfall event dominant at crest		detached from stream	sequence of preceeding seasonal rainfall event dominant at crest		detached from stream
	diffuse (piston)			diffuse (piston)			diffuse (piston)		
	potential recharge via surface runoff ponding (?)			potential recharge via surface runoff ponding (?)			potential recharge via surface runoff ponding (?)		
Streamflow Connectivity	Intermittent Event driven			Intermittent Event driven			Intermittent Event driven		

.

3. KEY RESPONSES & CONCEPTUAL UNDERSTANDING OF HYDROLOGICAL CONNECTIVITY OF KNPS SOUTHERN GRANITE AND BASALT SAVANNAS

This aim of this chapter is to give the reader a synthesis of key findings of the hydrological research undertaken on both the Southern Granite (Figure 5.1) and Southern Basalt (Figure 6.1) Supersites. This primarily between September 2012 and September 2013 for the former and September 2013 and March 2014 for the latter. The aim is to familiarise the reader with the conceptual overview of the sites upfront to which the reader is then referred to relevant sections in the following chapters of the report for more detailed description of the hydrological processes at each site. This chapter also explores the key similarities and differences in hydrological responses determined between the two contrasting geological templates that the Supersites represent, and there to use this information to offer recommendations for future management of these pristine areas.

3.1 Southern Granites

Streamflows at the southern granite supersite (Figure 3.1) were found to be extremely intermittent and directly linked to rainfall events as expected, and explained due to high runoff coefficients (Table 5.5), short flow duration curves (Figure 5.3) and hydrograph separation (Figure 5.13, Figure 5.16 and Figure 5.18). Typically runoff coefficients decreased with increasing catchment order for low intensity rainfall sequences, with antecedent precipitation index's (API) below 50 mm (Figure 5.2), thereafter runoff coefficients increased with catchment order. Event water dominated discharge on the southern granites typically 60-70% contributions implying that there is some displacement of antecedent water throughout the catchment to generate runoff.

However, the 1st order stream (SGR1) was observed to be a point of sustained streamflow. This was because at the 1st order headwater sub-catchment both borehole and stream data coupled with tracers ($\delta^{18}O$, EC and silica) demonstrated that this reach is gaining from groundwater (Table 5.7, Figure 5.9, Figure 5.10 and Figure 5.11). This occurs following the development of a perched water table within the weathered rock creating a hydraulic gradient to the stream triggering fluxes through the weathered zone as interflow towards the stream (Figure 3.2). Slope decline at the footslope causes interflow water to emerge into the un-channelled valley bottom seasonal wetland. This wetland then drains into a short stream channel at the catchment outlet primarily through saturation overland flow. Low resistivity values in ERT profiles are evidence of soil saturation at this point. This is consistent with field observations in the months of February and March 2013 (Figure 5.20) when the wetland was fully waterlogged.

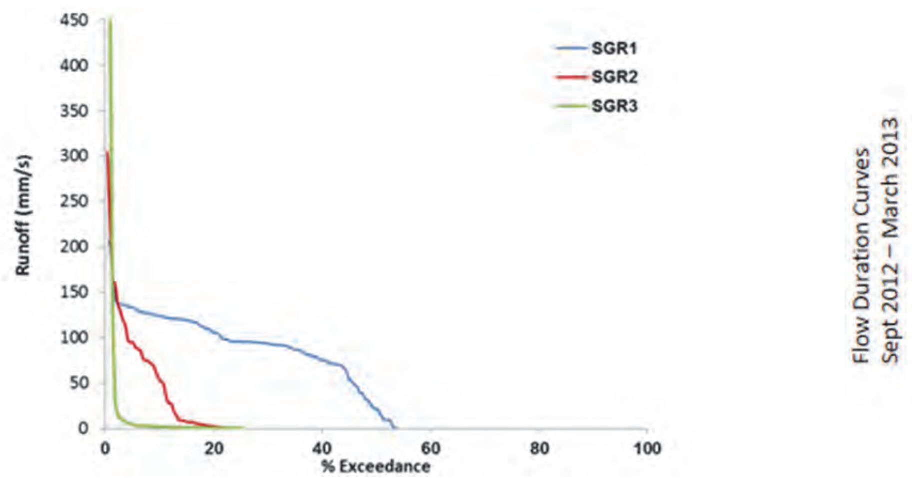

Figure 3.1: Southern Granites stream (SGRQ) flow duration curves September 2012 to April 2013.

Meanwhile the 2nd order (SGR2) was shown to be a losing reach and an indirect groundwater recharge point through hydrometry and tracers (Figure 3.3). This contrasted with the original hypothesis that SGR2 reach would be gaining. This reach experiences minimal subsurface gain during intense rainfall events that raise subsurface riparian hydraulic heads as observed in a riparian piezometer (Figure 5.7) which was always dry but had water after the high intensity event on the 19th of January 2013. Geophysical surveys revealed a geological base level control at the transition from second to third order stream in the form of a bedrock outcrop (Appendix I). This verified our own field observations of significant sediment trapping that had induced a localised discontinuity of sediment and surface water transfer to downstream reaches. This would be considered a key morphometric threshold that sees the catchment at this juncture switch from a high potential energy (erosive) system to a low energy (depositional) system. Furthermore, this is an important control point as trapped sediment barricades surface flows which coupled with high hydraulic conductivities (mean 1054 mm/h or 25 m/d) at this reach, induces deep percolation to recharge groundwater. It was found that the preceding rainfall events should exceed a recharge threshold of approximately 95-100 mm in order to facilitate this.

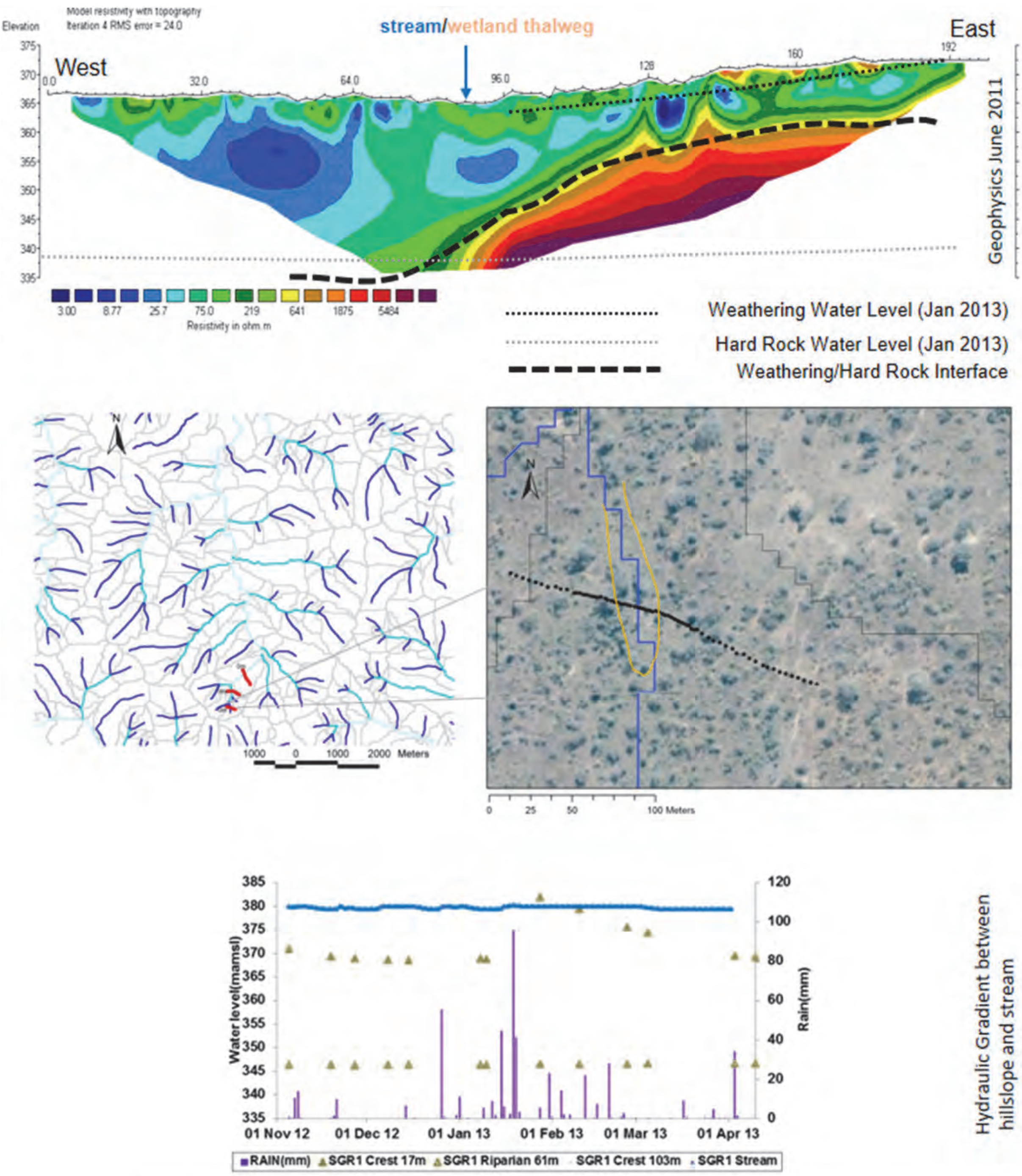

Date	Location	$\delta^{18}O$ (‰)
5/12/2012	SGR1 Riparian 61m (40m)	-2.96
21/1/2013	SGR1 Crest 17m borehole (sampled at 17m)	-3.2
	SGR1 Stream	-3.27
	SGR1 Riparian 61m borehole (sampled at 40m)	-3.35

Selected hydrochemistry

Figure 3.2: Key responses on Southern Granites first order (SGR1) September 2012 to April 2013.

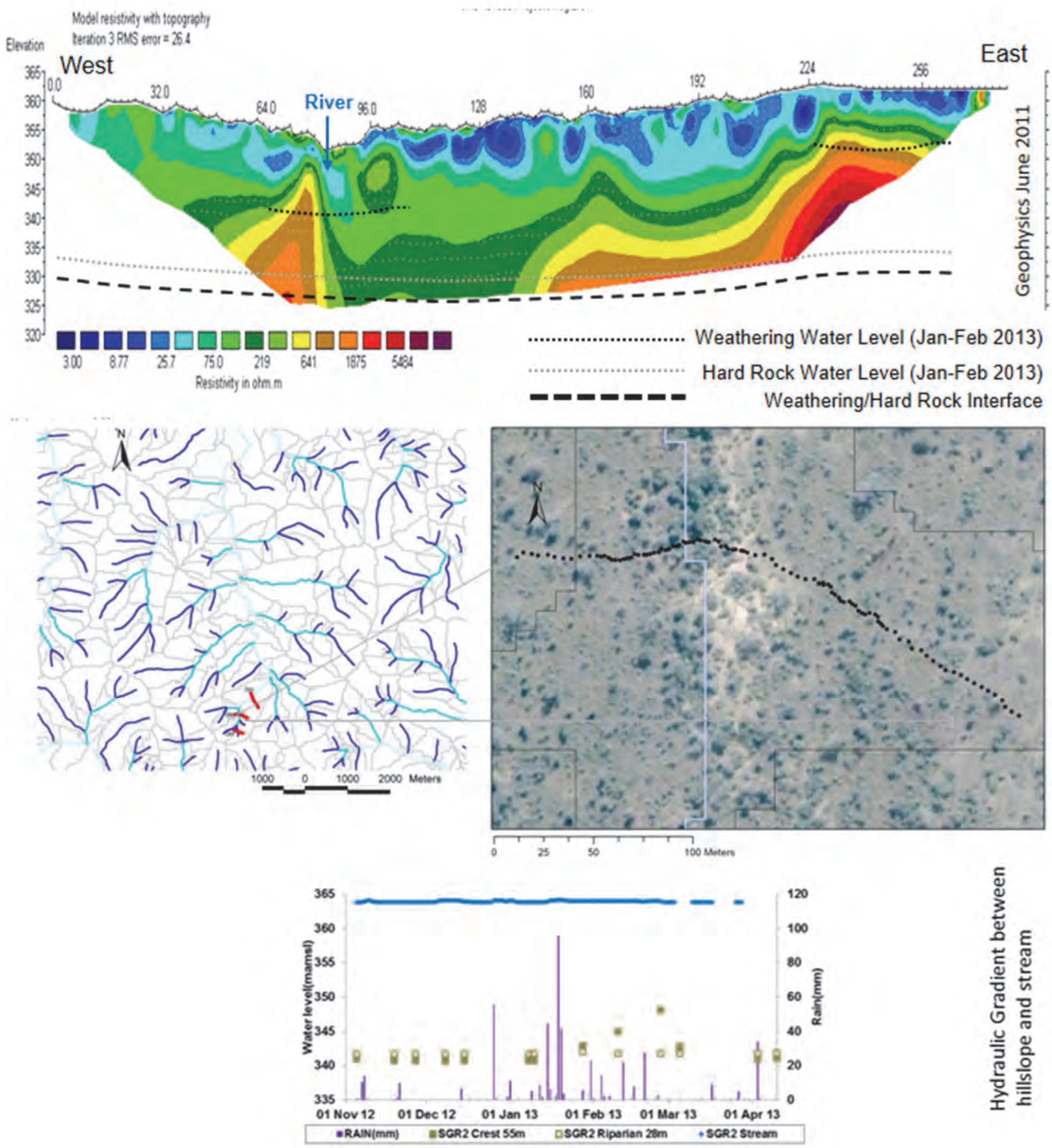

Date	Location	$\delta^{18}O$ (‰)
6/12/2012	SGR2 Stream	-0.95
21/1/2013	SGR2 Stream	-3.99
	SGR2 Riparian 28m borehole (sampled at 28m)	-3.68
	SGR2 Riparian 40m borehole (sampled at 30m)	-3.42

Selected hydrochemistry

Figure 3.3: Key responses on Southern Granites second order (SGR2) September 2012 to April 2013.

Moving to the depositional environment of the 3rd order (SGR3), the study showed this reach to be predominantly losing between rainfall events with evidence of continuous negative hydraulic gradients between riparian zone boreholes and stream water levels (Figure 5.7). At the lower orders the study showed responses in riparian zone groundwater. At the third order no such responses were seen. Furthermore, the lower orders also showed contact between the hillslope vadose zone through interflow soils along the footslope, however this was limited at the third order due to a low gradient floodplain which is largely decoupled from the hillslope.

In terms of vadose zone responses it was generally observed that all hillslopes transmit soil water as interflow whilst groundwater interflow occurs via a shallow perched (seasonal) groundwater wedge on at the 1st order scale to the stream (Figure 5.22, Figure 5.24, Figure 5.25 and Figure 5.28). At the scale of the 1st order the soils of the valley bottom wetland and footslope region cause saturation excess flows (responsive soils) leading to localised hillslope connectivity with the stream at surface. However this hillslope stream connection mechanism is absent at the 2nd and 3rd order, where interflow occurs but is reduced in its significance by the 3rd order.

Importantly there is a switch from predominantly gaining to predominantly losing reaches as one moves from the 1st to 2nd order, whilst this stream connects with the groundwater through direct mechanisms at this reach, observations suggest that by the 3rd order losses from the channel are more dominant through evapotranspiration. Therefore it is assumed that most water flowing along the stream is lost to diffuse flow in the alluvial sediments and thence returned to the atmosphere through the riparian vegetation as a transmission loss. Interestingly the 1st order catchment appears to have a greater ET overall than compared to the higher orders, which is could be explained by augmented flows to this zone from the perched seasonal shallow groundwater on that hillslope and the associated retention of water and consequent high evapotranspiration through the valley bottom wetland.

The study identified that in general two aquifer types exist namely, a weathered (average depth ranging 383-328 mamsl) and hard rock (average depth ranging 364-299 mamsl) granite/gneiss aquifer. The study characterization showed that the general groundwater flow direction in the weathered and hard rock aquifer extends from the 1st order hillslope towards the 3rd order hillslope, not mimicking the local topography, but rather following a regional flow gradient from the 1st to the 3rd order. The weathered aquifer flow system responds to localized processes such as localised preferential recharge, indirect surface water recharge and groundwater water discharge via interflow. This was due to the relatively rapid response time of 2-3 weeks in groundwater levels to the major sequence (Figure 5.2) of rainfall events over the hydrological year and the freshening out or decrease in specific conductance (SC) values during recharge, based on fluid logging results (Figure 5.28, Figure 5.29, Figure 5.37, Figure 5.47, Figure 5.48 and Appendix VI). The hard rock aquifer controls the regional groundwater flow system showing response lags of 2-3 months in deep borehole groundwater levels in response to the major rainfall sequences, suggesting an indirect delayed recharge mechanism. Furthermore, the SC fluids logs conducted over both wet and dry seasons did not vary significantly for the boreholes drilled into the hard rock aquifer, suggesting no active influx of localized fresh (low SC) groundwater or rainfall. Due to the generally low transmissivity (ranging 9.50E-08-11.2 m^2/day) inclining trend of groundwater levels after the wet season, suggest these ephemeral hillslope landscapes likely to act as groundwater storage areas. In that they contribute during the dry season to the regional groundwater flow which generates baseflow to the perennial rivers of the KNP. At the scale of the study area the crest areas of the 1st and 2nd order is a key point of direct recharge, where very high intensity rainfall sequences generate a shallow perched aquifer, contributing to (detached) river baseflow as well as recharge to the hard rock aquifer.

Based on the results obtained from the numerical model setup, calibration and sensitivity the following observations were made for the Southern Granite site:

- Regional groundwater gradient not directly linked to local processes. The numerical model boundaries of the sub-catchments are not represented by local rivers and topographical high areas. Aquifer drainage patterns not a function of the positions of the small ephemeral streams, but rather of some bigger regional drainage pattern cutting across the sub-catchments.
- Recharge of shallow aquifer fast with horizontal flow to rivers of short time frames. This interaction depends on the weathered aquifer properties, controlling the rate and position of the water discharge. The shallow perched aquifer in its turn recharges the deeper regional aquifer as an indirect recharge mechanism.
- The perched aquifer contributes to a slow downwards percolation of water to the disconnected regional aquifer. The 1st,2nd and 3rd order streams are disconnected from the regional water level with no baseflow contribution expected from the regional system. The shallow perched aquifer is however expected to contribute to surface water at the 1st order scale for a few weeks after rainfall events.

Figure 3.4 shows a perspective of the southern granite supersite dominant hydro- and hydrogeology distribution. This depicts the two aquifer types: the shallower weathered (orange) and deep hard rock granite/gneiss (grey) aquifer. Along the 1st, 2nd and 3rd hillslope weathering is generally deeper at the crest and shallower at the riparian zones. The general topographical slope is greatest at the 1st order hillslope and decreases towards the 3rd order hillslope. In general the hard rock aquifer (blue arrows 6, 7 and 8) and weathered aquifer (yellow arrows d, e, f and g) groundwater flow direction is from the 1st order towards the 3rd order running parallel to the streams. Furthermore, and critical to the issue of scale is the surface water and vadose zone hydrology follows to local intra-order catchment topography i.e. the hillslopes, whilst the deeper groundwater system does not follow this rule and rather runs parallel to the drainage network, likely sloping directly toward the regional larger drainage networks such as the Sabie River.

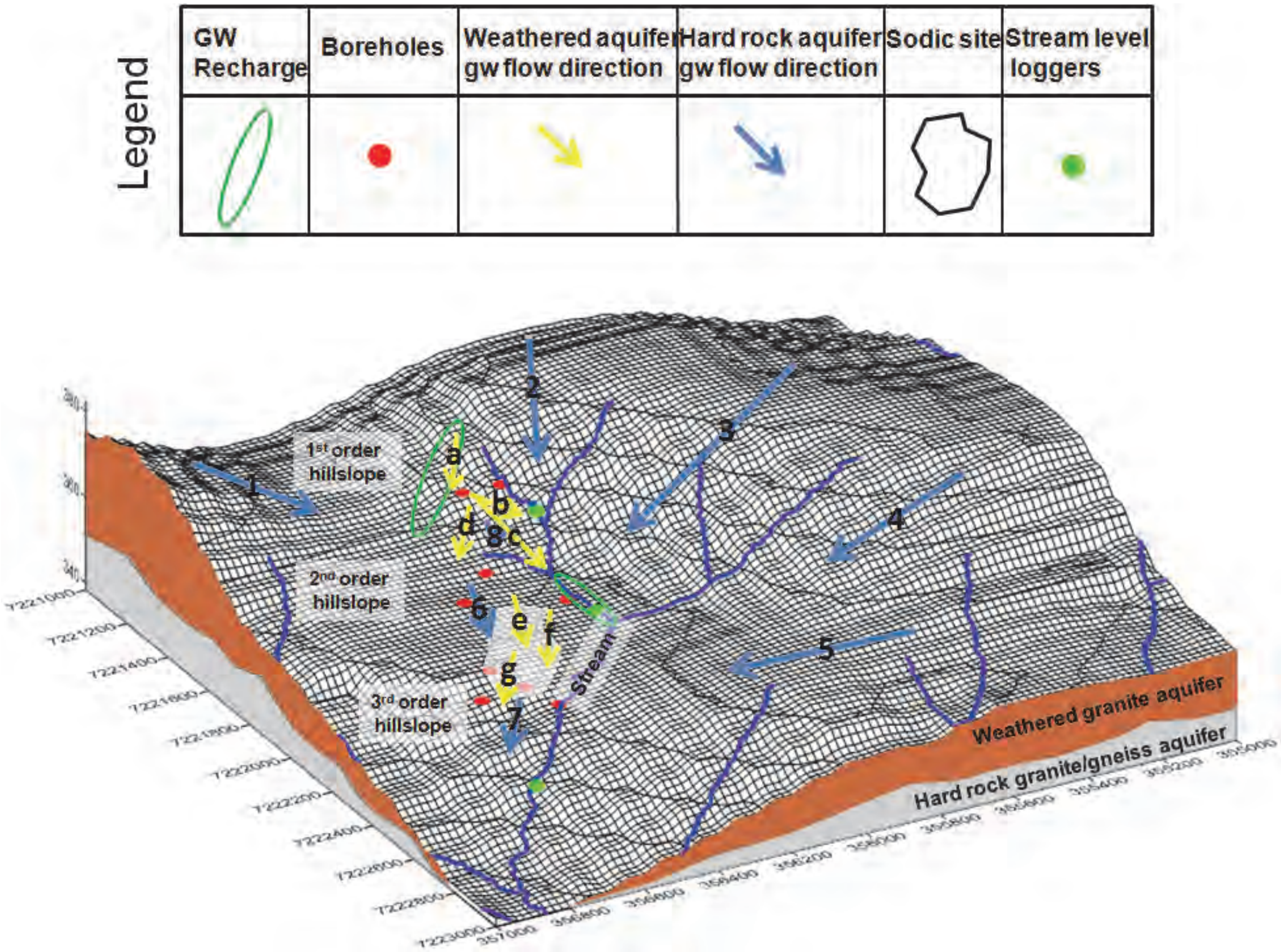

Figure 3.4: A hydrogeological conceptual site model of the southern granite supersite

3.2 Southern Basalts

The 3rd order reach on the southern basalts had the most persistent event-driven flows compared to lower order reaches during the monitoring period and this was revealed clearly in flow duration curves (Figure 6.4). As anticipated, high rainfall intensities resulted in short delay times and such high intensities positively correlated with short duration rainfall events in all stream orders. Whilst the 1st and 2nd orders typically did not show any signs of sustained streamflow responses. Typically runoff coefficients increased with catchment order when the API was > 35 mm. Event water dominated the discharge at the southern basalts, it was found that this was more pronounced along the 1st and 2nd order, whilst the 3rd order showed lower event water as a proportion of total flow, implying mixing with antecedent water (Figure 6.19, Figure 6.21 and Figure 6.22).

This mixing at the 3rd order is explained by intermittent contact with the shallow aquifer in that catchment, likely to be a point where the general catchment topography intersects the regional groundwater table. This was revealed through simple observation of evergreen vegetation along this reach (e.g. *Vachellia xanthophloea*), and end-member mixing analysis (Figure 6.18, Figure 6.20 and Figure 6.23) and other hydrochemical tracer data (Figure 6.16 and Figure 6.17). It was also apparent that piston flow mechanisms may contribute to perpendicular groundwater discharges to the stream at the 3rd order, whilst these typically being parallel to the stream network at lower orders. This was evident through both hydrometric analysis (Figure 6.11), hydrochemical (Figure 6.14 and Figure 6.15) and geophysics responses (Figure 6.48). Having said that, the 3rd order reach whilst it gains from the aquifer in places, does also appear to be a conduit for localised recharge, especially evident at the catchment outlet a triangulation borehole (Figure 6.54) in the piezometric network at that catchment order. It must be considered here that the contact zone between the basalt geology of the supersite and the rhyolites of the Lebombo Formation may be having a role to play here. Thus the lower end of the 3rd order reach may not be truly reflective of the ephemeral hydrogeology on a basalt setting. Nevertheless, in general terms it is recognised from the data that 1st and 2nd order streams are disconnected from the groundwater aquifer (Figure 3.5), while for the 3rd order there are seasonal points of contact.

On the basalts the weathered zone depth ranges from 210 mamsl at the 1st order (Figure 6.25) to approximately 170 mamsl at the 3rd order (Figure 6.47). Whilst groundwater is typically shallow across the catchment (<20 m from surface) it does not appear that two distinct aquifers exist between the weathered zone and hard rock. At all catchment orders it was found that the groundwater is recharged by direct infiltration through the overlying soils of the vadose zone, as shown by the vertical free drainage of soils in most parts of the catchment (Figure 6.28, Figure 6.39 and Figure 6.50). Where this does not occur is within the stream channel itself due to impeding vertic soils. Lateral flows within the basalt hillslopes whether at the surface or shallow sub-surface are almost entirely absent. However evapotranspiration plays a key role in the southern basalts and potential recharge of the aquifers is only likely to occur following significant rainfall sequences with an API greater than 130 (Figure 6.2). Evapotranspiration is clearly linked to the depth of the soil store, where for instance lower order catchments had deeper soils and consequently greater rates of ET (Figure 6.62. Figure 6.63 and Figure 6.64).

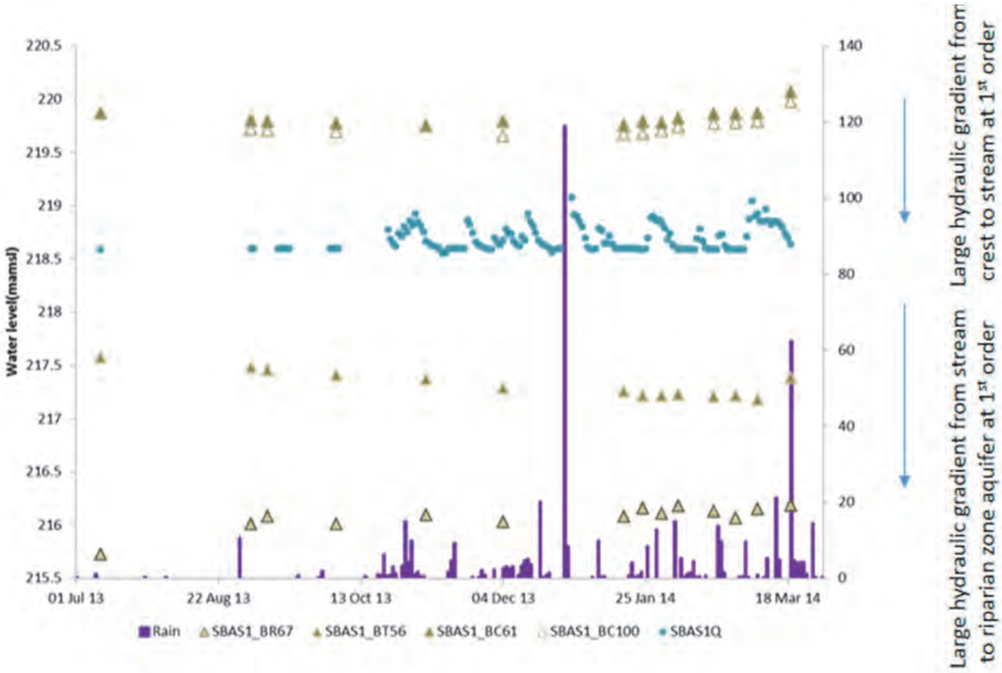

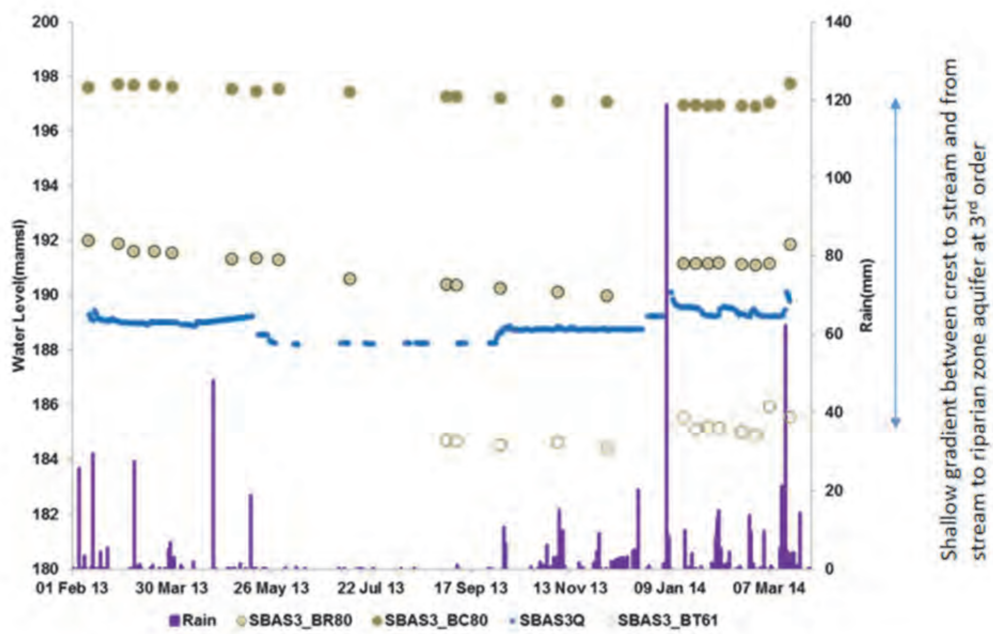

Date	Location	$\delta^{18}O$ (‰)
20/1/2014	SBAS1 Riparian 67m Borehole	-2.67
	SBAS1 Crest 61m Borehole	-2.52
	SBAS1 Stream	-3.71
	SBAS2 Riparian 80m Borehole	-2.58
	SBAS2 Crest 57m Borehole	-2.66
	SBAS2 Triangulation 80m Borehole	-2.33
	SBAS2 Stream	-3.70
	SBAS3 Riparian 80m Borehole	-2.23
	SBAS3 Crest 80m Borehole	-1.97
	SBAS3 Triangulation 61m Borehole	-2.44
	SBAS3 Stream	-3.46

Selected hydrochemistry

Figure 3.5: Key responses on Southern Basalts first order (SBAS1) and third order (SBAS3) September 2013 to April 2014 (Blue = streamflow, Q; sepia = groundwater levels crest, triangulation, riparian).

Based on the results obtained from the numerical model setup, calibration and sensitivity the following observations were made for the Southern Basalt:

- Regional groundwater flow direction is influenced by the 3rd order river reaches intersecting the groundwater table. The aquifer drainage patterns are not influenced by the 1st order streams.
- The shallow wethered zone seems to be in hydraulic connection with the deeper fractured rock aquifer, with no perched aquifers after rainfall events.

Similar to the granites there is deep hard rock aquifer linking all the orders but these water levels tend only to respond to high intensity rainfall sequences typically >100 mm. This is important to reflect on since, the lower order catchments are significantly larger (at least half an order of magnitude) than each higher catchment. So whilst there is a significant 'ET' trap in the geo-climatic setting of the southern basalts, these large inter-fluvial zones do play an important role for regional groundwater recharge, since they do not yield excess water to lateral flows and hence runoff.

A conceptual perspective of the southern basalt supersite dominant hydro- and hydrogeology processes is shown in (Figure 3.6). This demonstrates the two types of aquifers on this basalt catchment, a shallower weathered and a deep hard rock aquifer. Weathering in this catchment is typically deeper at both lower orders and at the crest regions than elsewhere in the catchment. These lower orders also have a lower slope and deeper soils, fostering recharge. Although as seen through field observation, rather than having been explicitly captured in the data, are areas in the 1st order catchment in particular that form endorheic pools with deep vertic soil, that impede drainage. The general topographical slope is lowest at the 1st order hillslope and increases towards the 3rd order hillslope. A morphological/geological switch may explain the apparent change in dominant hydrogeological processes moving from the 2nd to the 3rd order. However it would be somewhat speculative to suggest a causal mechanism for this, and hence this warrants more detailed study. It is interesting to note the general similarity to the granites however that the deep (regional) groundwater in the basalts also runs parallel to the stream network.

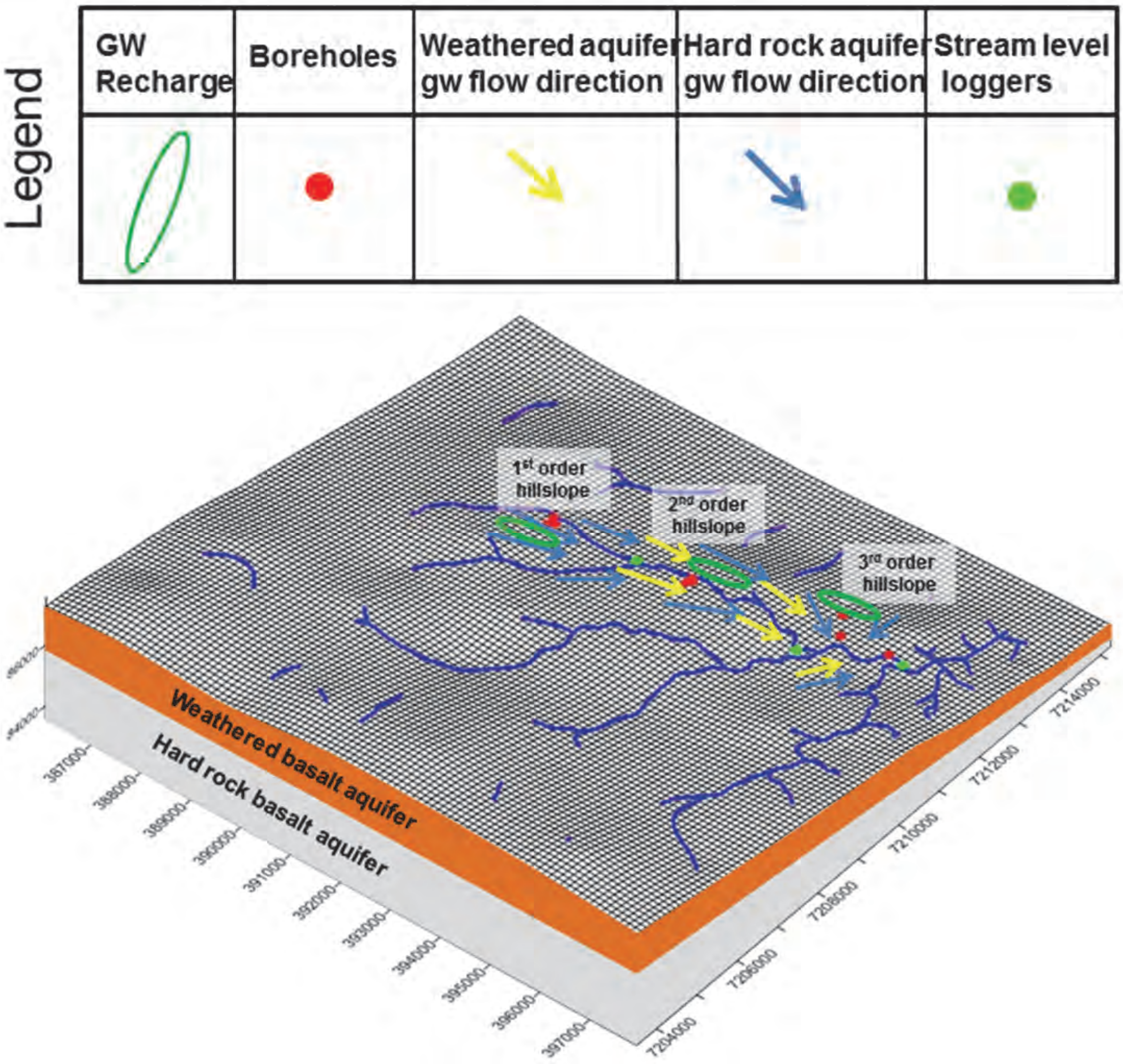

Figure 3.6: A hydrogeological conceptual site model of the southern basalt supersite.

3.3 Key Differences and Similarities in Hydrological Processes between the two Supersites

Based on the aforementioned summary, and detailed findings in proceeding chapters we present which compartmentalises those responses that were expected from initial field observations and desktop analysis. This is in order to present a summary of key differences and similarities between ephemeral hydrological processes on the granite and basalt catchments. Those with tick marks conform to original conceptual models, those with crosses did not, and those blocked in grey were un-anticipated results of the monitoring.

Table 3.1: Differences and similarities in hydrological process responses of the KNP Supersites

Granite geology	Original hypothesis	Basalt geology	Original hypothesis
2 distinct geo-zones		2 distinct geo-zones	
GW flows parallel to stream except at 1st order (thresholds of >90mm/day - weathered).	✓ Parallel flow was not originally conceptualized.	GW flows parallel to stream and connects to stream at 3rd order reach through fractured rock preferential flow.	✓ except 3rd order where GW connects to stream through fracture flow.
ET demand decreases from 1st to 3rd order scale. Greatest at riparian zones		ET demand is similar across scales being greatest at crest	
1st order reach has greater potential for sustained flow	✓	3rd order reach sustained streamflow through fracture & piston flow	✓
High intensity rainfall events result in stream network connectivity. Event water = 70%.	✓	High intensity rainfall events result in stream network connectivity. Event water = 90%	✓
Hydraulic gradient between deep boreholes and stream always away from stream except at 1st order (>90mm/day).	✓	Hydraulic gradient between deep boreholes and stream is away from stream except at 3rd order stream outlet during and between rainfall events. At the 1st order (lineament barrier)	✓ Lineament control observed from research findings.
The 2nd order reach plays an indirect recharge role through channel leakage (transmission loss).	✗	Similarly the 2nd order reach loses to groundwater and this sets up indirect recharge. (Paleo-channels)	✗
Soil forms vary across catenal elements for all incremental contributing areas. decrease from crest to riparian zone.	✓	Soil forms vary slightly but hydropedological function (recharge soils) remains the same across 1st to 3rd order spatial scales. K decreases from crest to riparian zone	✓
Potential recharge is greatest at 1st order than the higher order scales		Potential recharge is uniform across all 1st to 3rd order spatial scales.	

3.4 Findings: relevance to catchment management, savanna ecology and the KNP Supersites concept

This monitoring study has allowed further insights into improved opportunities for catchment management and savanna ecology, upon which certain principles can be used. The first of these principles is the realisation that similar process responses observed on the 1st order granite catchment have been encountered elsewhere in the lowveld region on a similar geological template. It was hereby noted that the perched groundwater contributions to a valley-bottom wetland led to sustained stream flows at that scale. This has similarly been observed in a wetland hydrological study in a first order tributary of the Sand River catchment (Riddell et al., 2013). The implication of this therefore is to emphasise the important role that these 1st order and low order systems have in catchment processes. The realisation through this study that the 2nd order channel reaches on both geologies are also key in-direct recharge points in these landscapes is also important. This speaks to similar findings of stream channel recharge informing emerging concepts in ephemeral river hydro-ecology (Larned et al., 2010) and emphasises the potential role that even these ephemeral catchments can play in regional groundwater recharge processes. In addition the generally low transmissivity of the southern granites in particular and the steady rise of both the weathered and hard rock aquifers following the wet season could be described as characteristic geo-hydraulic boundaries in these ephemeral landscapes. This is emphasised by similar observations made at Matlari in the Biyamiti sub-catchment of the Crocodile basin within KNP (Du Toit et al., 2014, *unpublished*). It is believed that the hydraulic conditions at these watershed areas create a hydraulic gradient through the dry season to lower altitude (high order) catchments. Given that the perennial rivers of the lowveld at their lower reaches are maintained by regional groundwater contributions (Petersen, 2011) this information of course becomes important for catchment planning purposes. This in order to identify and protect groundwater recharge zones and the ability to maintain the perennial nature of the water course given the context of integrated land and water resources management in the lowveld. To this end, it would be worthwhile to establish monitoring beyond the 3rd orders in order to identify the threshold scale at which deep groundwater in ephemeral catchments contributes to perennial river baseflow.

The study also revealed that on the southern basalt the 3rd order streams play a significant role as hydrological refugia for terrestrial biota during most of the dry season due to their intersection with the hard rock groundwater seasonal points of contact. Whether this phenomena only occurs during wetter climate cycles where groundwater levels are relatively higher than compared to the long term mean remains to be determined. Thus long term continued monitoring of this nature is justified on the basalts supersites, for both hydrological interest and to inform KNP of potential ameliorating effects in the artificial water provisioning post-closure period for wildlife.

Thoughts on the trade-off relationship between groundwater recharge and actual evapotranspiration data suggests that groundwater recharge processes are typically withheld until a threshold ‘episodic’ rainfall sequence occurs, as suggested by van Wyk (2011) and in the KNP case this is typically >100 mm. Should this type of rainfall not occur then potential groundwater is otherwise evaporated. Whilst this study was fortunate to have been conducted during above normal wet seasons, it is interesting to note that whilst intra-annual groundwater recharge occurred on both catchments, at the scale of the entire Kruger National Park, for the past 7-8 years there has typically been a steady regional groundwater decline (Du Toit et al., 2014 *unpublished*). This is based on Cumulative Rainfall Departure (CRD) analyses showing that KNP is presently in a low recharge cycle since 2001/2002, explaining the declining trend despite short term wet cycles in between (Du Toit, W *pers comm*). One hypothesis to test in future on the KNP supersites, in order to make explicit scale dependent relationship between the terrestrial flora and water availability (in a water-limited setting) is that woody and herbaceous biomass equilibrate with the available water supply. This in effect creates an *ET trap*, and to some extent therefore could be responsible for the observed groundwater declines at a park-wide scale where natural losses (contributions to base flow, evapotranspiration, etc.) during such cycles exceed the natural gains through recharge. Further questions then arise at to the role of fire and herbivory in limiting water availability and hydrological processes at a landscape scale.

4. METHODOLOGY

4.1 Approach

The conceptual framework to the study, as described in Section 2.4, required a multi-tiered approach to determine the processes in the four hydro-/hydrogeological domains. A variety of methods were utilised, some were used in all cases whilst some methods were unique to a specific hydrological domain. The overall approach and specific methods utilised are depicted in the framework of Figure 4.1 and described with more detail in subsequent sections.

The study commenced in October 2011 where baseline and preliminary catchment characterisation data was collected. However the majority of the data presented in this report are for hydrological seasons October 2012-September 2013 and October 2013-March 2014 for the southern granite and southern basalt supersite, respectively.

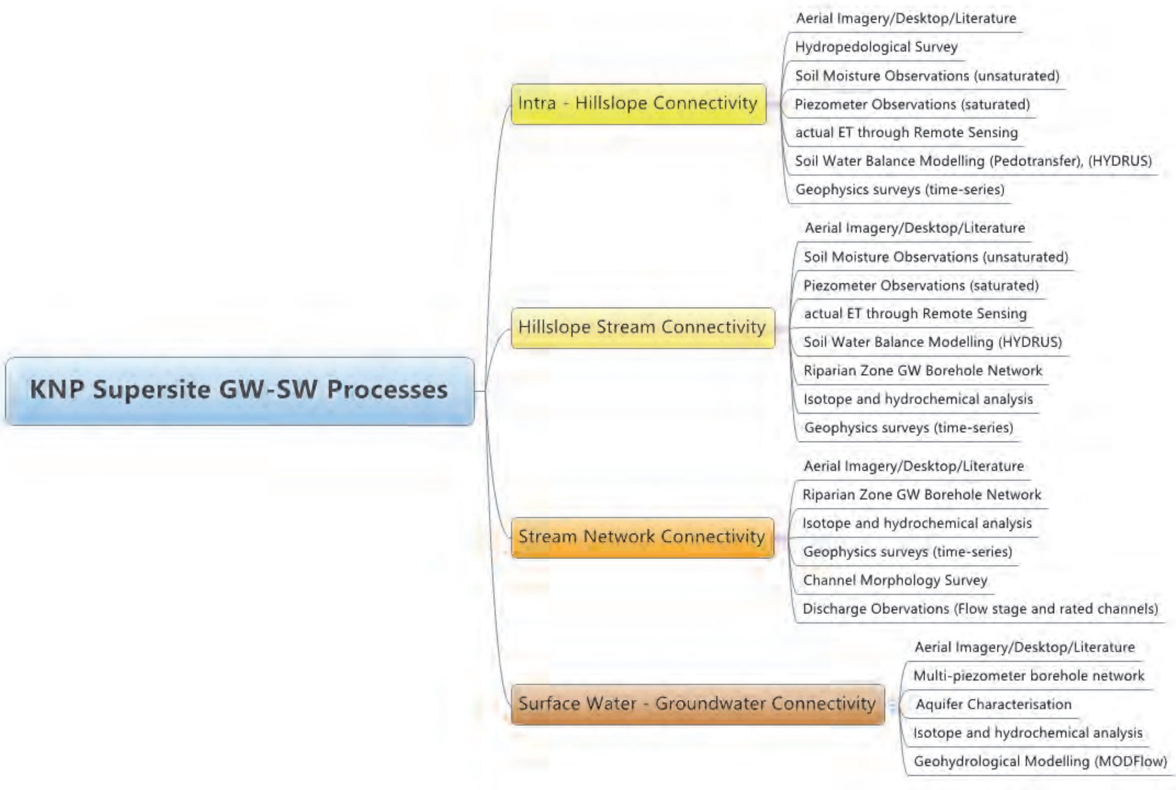

Figure 4.1: Methodological approach for quantifying groundwater-surface water interaction on the KNP Supersites

4.2 Characterisation datasets

The determination and quantification of hillslope and broader processes in contributing catchment areas to 1^{st}-3^{rd} order streams was achieved using a number of characterization techniques such as geophysical surveys (ERT), soil surveys, hydrometry, and numerical modelling. These typically followed the selection of hillslope hydrological monitoring transects selected in each catchment order (See Figure 5.1)

4.2.1 Geophysical surveys

An initial series of Electrical Resistivity Tomography (ERT) geophysical surveys were undertaken in the pre-selected 1st to 3rd order catchments within the KNP Supersites 4 June and 1 July 2011. The surveys determined sub-surface electrical resistivity distributions along two dimensional transects at pre-determined locations. These transects were pre-selected based on desktop analysis of evident geological features from aerial imagery using Google Earth© and relative ease of access from tourist and management roads within the KNP, for both geophysics equipment and groundwater-surface instrumentation installation and maintenance.

The resulting data were ultimately used to identify suitable points to install groundwater piezometric boreholes and provide information on the hillslope geomorphological template used for vadose zone hydrological monitoring and modelling, and in later surveys (2012-13) for spatial variations in catchment moisture (using fixed point time-series surveys).

The basis of the geophysical surveying is the induction of an electrical current by an array of current electrodes inserted into the ground surface, with a sequence of potential electrodes receiving the electrical signal. Hence the measurements of electrical potential at the surface are dependent on the electrical resistance of sub-surface materials, expressed in ohm metres (Ω.m), which vary according to sub-surface strata, as a result of their inherent pore size distribution, variations in water content and degree of salinity (Loke, 1999). The collation of this sub-surface resistivity distribution is facilitated by computerized devices known as switching units that control the sequence of pairs of current and potential electrodes, known as the quadripole. Variations in the position and sequence of current and potential electrodes along transects facilitate measurements with different degrees of horizontal and/or vertical resolution, these computer-generated sequences (protocols) are known as arrays. Inversion algorithms are used to create a model of measured and apparent (calculated) resistivity values. Using Jacobian matrix calculations and forward modelling procedures produces values of the true resistivity, which when plotted in 2D or 3D are known as pseudosections. The law governing apparent resistivity (pa) is written as follows:

$$pa = kR \qquad \text{Equation 4.1}$$

$$R = V/I \qquad \text{Equation 4.2}$$

where k is the geometric factor and varies according to the quadripole array, R is the resistance, V is the voltage and I is the current.

These plotted pseudosections are then used to examine sub-surface resistivity heterogeneities based on the differences of equipotential surfaces where they hit the ground surface at potential electrodes; the interpretation of this data is based on known resistivity ranges of geologic materials.

The surveys were conducted using a SAS1000 ABEM™ Terrameter and Switching unit. The locations of each probe in the survey were determined with differential GPS points of probe locations using a Trimble™ ProXRS Asset Surveyor GPS system. Data was differentially corrected against available TrigNET (http://www.trignet.co.za/) beacon data.

In the interests of the integrated study it was decided to use the combine Schlumberger Long and Short arrays to maximum resolution of resistivity readings near the surface, required for the vadose zone aspects, as well as obtain a good penetration depth required for the groundwater aspects of the study. The hillslope transects were surveyed perpendicular to the stream channel, along the hillslope interfluve in the 1^{st}-3^{rd} order catchments. Due to the considerable difference in distance of the interfluves between the basalts and granite catchments, a 5 m spacing was chosen for the former and a 2 m spacing for the latter. The resulting data was then checked for errors and optimised according to the methods of Loke (2004) and inverted using the software package RES2DINV (Loke, 2008).

The interpretation involved an informed estimation of at which depth the weathering/hard rock interface and groundwater level could be encountered. This consisted of assigning resistivity values to a specific subsurface material or mineral (refer to Figure 2.6 in chapter 2 for resistivity values for various materials or minerals) and at the same time taking into consideration at which depth these resistivity values are encountered. Based on previous relevant studies, ground truthing and the theory behind electrical resistivity surveys for these particular geologies, possible water levels would be associated with a continuation or sharp change in low resistivity values relatively close to the surface. The high resistivity values would be associated with hard rock. This information was then used to infer the development of an initial hydrogeological conceptual model consisting of estimated subsurface lithological descriptions i.e. depth to weathering and hard rock, depth to groundwater level and piezometric borehole positions targeting specific hillslope components i.e. crest, midslope or riparian zone.

Results of geophysics not presented in the main body of the report may be found in Appendix A1.1 to A1.6.

4.2.2 Soil and Hillslope Classification (hydropedology)

Since soils and hydrology are highly interactive. Soil properties such as morphology can serve as indicators of the hydrological regime. Soils have a governing influence on a number of hydrological processes therefore soil surveys and classification was conducted on the Supersites in collaboration with the team from the University of the Free State. In each catena element along the hydrological monitoring transect pits were dug from the surface down to saprolite where possible. Diagnostic horizons were identified and recorded. The structure, texture and the presence of concretions (if any) were also recorded for hydropedological classification purposes (See Appendix A2.1).

The hillslope were then classified according to hydropedological classification of South African hillslopes, (van Tol et al*.,* 2013). According to this classification system, there are six hillslope classes (Table 4.1). Soils at each catena element are first classified into one of the three soil types namely recharge, responsive and interflow then the whole hillslope will be classified into one of the six classes. In order to classify the hillslopes data from geophysical surveys, hydraulic conductivity tests, soil textural classes and hydrometric data was used.

Table 4.1: Catena Soil Hydropedological Response Units and Hillslope Classes

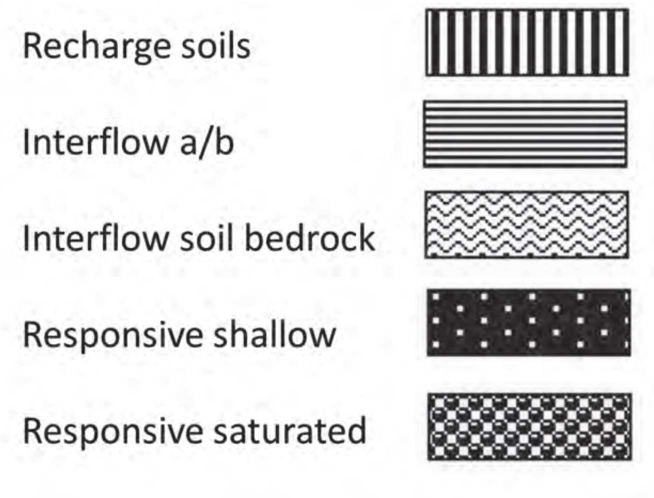

CLASS	NAME OF CLASS
1	Interflow (Soil/Bedrock Interface)
2	Shallow Responsive
3	Recharge to Groundwater (Not Connected)
4	Recharge to Wetland
5	Recharge to Midslope
6	Quick Interflow

4.2.3 Soil Hydraulic Properties Characterisation

The tension disk infiltrometer (TDI) was used to measure unsaturated hydraulic conductivity (k_{unsat}). This has an advantage of measuring the permeability of the soils at different capillary pressure heads whilst the permeameter and double ring infiltrometers were used to measure saturated hydraulic conductivity (k_{sat}) at zero head. Soil cores were collected in the field for particle size distribution and the determination of matric potential of the soil.

The K_{unsat} of soils determined through TDI was calculated according to the methods of Ankeny et al. (1991):

$$A = \frac{Q_{tA} - Q_{tB}}{Q_{tA} + Q_{tB}} \times \frac{2}{tB - tA} \qquad \text{Equation 4.3}$$

Where A is the parameter for hydraulic conductivity equation [cm^{-1}], Q is the steady state infiltration rate [$cm^3.min^{-1}$], tA is the 1st tension of [cm], and tB is the 2nd tension of [cm].

Calculation of K_{unsat} may then be formulated as:

$$K = \frac{AQ_{t6}}{(A\pi r^2)+4r} \qquad \text{Equation 4.4}$$

Where K is hydraulic conductivity [cm.min^{-1}], and r is infiltration radius of the disc [cm].

In the case of the permeameter the steady state infiltration (k_{sat}) is measured from an augered cylindrical hole. A constant head of water is maintained in the hole whilst water infiltrates from a 20 L container with two permeameters connected to one pipe. This method allows for minimally intrusive K_{sat} measurements in deep horizons with the need for a profile pit. The 3D flow water flow is governed by the Glover equation (Amoozegar, 2002):

$$K = CQ \qquad \text{Equation 4.5}$$

where: $K =$ Saturated hydraulic conductivity (mm h^{-1}), $Q =$ Steady-state rate of water flow (mm^3 h^{-1}), $C =$ Constant:

$$C = \left[\sinh{}^\wedge - 1\left(\frac{H}{r}\right) - \left(\frac{1+r^2}{H^2}\right)^{0.5} + \left(\frac{r}{H}\right)\right] / (2\pi H^2) \qquad \text{Equation 4.6}$$

where: $H =$ Height of water in the reservoir, $r =$ Radius of the cylindrical augered hole.

The K_{sat} from a double ring infiltrometer is calculated as:

$$V_{IR} = \Delta V_{IR} / (A_{IR} * \Delta t) \qquad \text{Equation 4.7}$$

where: $V_{IR} =$ Inner ring incremental velocity cm/hr, ΔV_{IR} =Volume of liquid used to maintain a constant head in the inner ring, $A_{IR} =$ Area of internal inner ring cm^2, $\Delta t =$ Time interval in hours, Space between rings:

$$V_A = \Delta V_A / (A_A * \Delta t) \qquad \text{Equation 4.8}$$

where: $V_A =$ Incremental velocity in annual space cm/hr, $\Delta V_A =$ Volume of liquid used to maintain constant head in outer ring in cm^3, $A_A =$ Area of space between rings in cm^2

4.2.4 Soil hydrodynamics

Soil moisture sensors (Water Marks™) were used to determine characteristic subsurface unsaturated soil-water dynamics within typical catena soils at the hillslope scale representing crest, midslope and riparian soils. Water Mark™ sensors measure di-electrical resistance of porous medium in kilo-ohms (kΩ). Where there is low water content, a high resistance is recorded and vice-versa. In order to convert the millivolt readings to capillary pressure head, a calibration function for 3 channels against a temperature reading was derived by Lorentz and Pretorius (2008 unpublished, University of KwaZulu-Natal). The sensitivity range for the sensors is from 0 to about 15 000 mm CPH. This is the range that measurements are considered realistic. At each station, two to three Water Mark sensors were installed alongside a temperature probe connected to a 4-channel U12 Hobo® logger. These were installed in a single profile with sensors in each diagnostic horizon identified during the soil classification surveys were conducted and soil hydraulic properties were characterised. Alongside the stations shallow PVC piezometers were installed to monitor and sample saturated soil water responses.

4.2.5 Surface Water

Sub-catchment outlets were identified and ground-truthed (GPS) using a combination of aerial imagery (recent Google™ Earth) overlaid with a stream-order network derived from 25 m disaggregated 90 m ASTER DEM data (provided by Cullum and Rogers, 2011). Solinist™ Levelogger Junior water level data loggers were installed at the outlet of each 1st to 3rd order catchments for real-time stream stage monitoring. These loggers were installed in a way that helped to prevent damage by animals by placing them inside perforated polyvinyl chloride (PVC) piezometers which were in turn placed inside perforated metal casings of larger diameter (Figure 4.2). The piezometer tops were then covered by plastic caps with holes that allow free water movement but concurrently concealing the loggers from animals. The loggers were set to log at 5 minute time steps which enabled acquisition of reasonably high temporal resolution stage data sets actual water levels were then obtained by compensating for barometric pressure using a Solinst™ Barologger which was placed at a weather station on site to obtain barometric pressure readings. The stages obtained from levelloggers were calibrated against a datum (stream bed surface) in each catchment and used to compute observed discharges (see Appendix A3.4) at the outlet of each catchment. Since this study was carried out in ephemeral streams, the measured stage had two components one for subsurface water (negative stage) and the other for surface water (positive stage). This was done in order to determine the significance of subsurface flows in these ephemerally drained catchments.

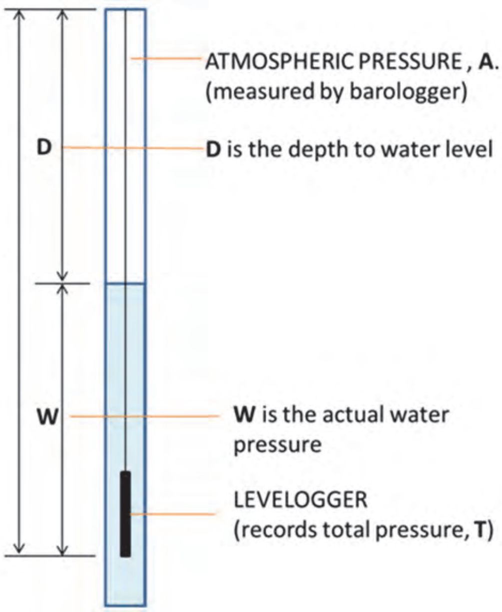

Figure 4.2: Solinst Levelogger installation and schematic on how water pressure (W) is calculated from total pressure (T) and atmospheric pressure (A) for determination of actual water level (W = T minus A).

4.2.5.1 Stream channel surveys

Longitudinal and cross sectional surveys were conducted for the three catchment outlets where streamflows were monitored. A DT5A SOKKIA surveyor's theodolite was used for this purpose. Elevations of surveyed transects were calibrated against a datum (metres above mean sea level, mamsl). The Concalcs HydroToolBox (Renshaw, 2010) was used to determine channel and flood plain cross sections and streambed slopes for surveyed reaches (see Appendix A3.1). Channel longitudinal profile elevations and horizontal distances were measured and recorded with subsequent plotting of streambed slope profiles for the reaches. The streambed slope for a rated reach was calculated as the change in elevation over known horizontal distances as follows:

Channel slope = $\frac{\Delta y}{\Delta x}$ Equation 4.9

Where Δy = change in elevation, and Δx is the change in horizontal distance of the reach.

The change in flow velocity in the channel reaches was observed to be gradual. Therefore, the energy slope was essentially equated to the water surface slope as well as to the slope of the streambed (Chow, 1959).

4.2.5.2 Streamflow ratings

The slope-area method which is widely used to estimate flows in natural channels (Herschy, 1985) was used to calculate discharges at the outlet of each sequential stream order (1^{st}-3^{rd} order). In order to use the slope-area method knowledge of the channel cross section area, channel energy slope and an estimate of the channel roughness coefficient for the reach was a pre-requisite. The first two hydraulic variables were determined as described in the preceding section, however Manning's channel roughness coefficients were determined as follows (Cowan, 1956):

$n = (n_b + n_1 + n_2 + n_3 + n_4)\, m$ Equation 4.10

where n_b is a base value of n for a straight, uniform, smooth natural channel; n_1 is a correction factor for the effect of surface irregularities; n_2 is a value depicting channel cross sectional area variations in shape and size; n_3 is a value for flow obstructions in the channel; n_4 is a value for vegetation and flow conditions; m is a correction factor for the meandering of the channel.

Having determined the channel class, base n values were then selected from values presented in Aldridge and Garret (1973). The base n values selected for this study and corresponding adjustment factors are presented in Appendix A3.3.

Since the selected base n values are for straight channels with relatively uniform flow conditions, they were adjusted for the roughness increasing factors (n_1 to n_4) including the meandering effect (m) as given in Eq 2. These factors physically define what is observed in field reconnaissance surveys done in the study catchments. Compound cross sections at the Southern Granite 3^{rd} order and Southern Basalt 1^{st} order reaches were each sub-divided into 3 subsections according to visible abrupt changes in roughness conditions. Compound channels are those consisting of channel and floodplain subsections marked by distinct roughness or geometric changes (USGS, 2008). Accordingly, identified subsections of the floodplain were assigned different n values as determined by prevalent physical characteristics influencing streamflow processes.

4.2.5.3 Stage-Discharge relationships

These data were incorporated into Manning's equation (using Concalcs HydroToolBox [Renshaw, 2010]) to calculate flow velocity as follows:

$$V = \frac{1}{n}R^{2/3}S^{1/2} \qquad \text{Equation 4.11}$$

where v is flow velocity; n is Manning's roughness coefficient; R is hydraulic radius and S is bed slope.

Computed velocities were then converted to estimated discharges using the continuity equation:

$$Q = AV \qquad \text{Equation 4.12}$$

Where Q is discharge in m^3/s; A is cross section area and V is flow velocity.

Rating curves were constructed from stage with increments of 0.0001 m up to maximum observed stages in each catchment plotted against estimated discharges. Polynomial rating equations fitted to these curves were subsequently programmed into a Microsoft Access database to compute actual observed discharges. Details of channel ratings are presented in Appendix A3.4.

4.2.5.4 Subsurface flow characterisation

Subsurface flows depend on the hydraulic conductivity of the porous medium, its cross sectional area as well as the hydraulic gradient between the points over which the flow occurs. The flow rate or specific discharge was calculated from Darcy formula as follows:

$$V=-K\frac{dh}{dl} \qquad \text{Equation 4.13}$$

where V is the flow rate or velocity; K is the hydraulic conductivity or permeability of the porous medium, and $\frac{dh}{dl}$ is the hydraulic gradient.

Hydraulic gradients were calculated by dividing observed head differences (dh) between nested piezometers installed within stream channels by the distance between the two piezometers (dl).

Subsurface discharge (Q) was then calculated from the continuity equation as follows:

$$Q = AV \text{ or } \quad Q = -KA\,\frac{dh}{dl} \qquad \text{Equation 4.14}$$

where Q is the subsurface discharge; A is the cross sectional area of streambed aquifer;
The continuity equation was applied across incremental subsurface depths obtained using the method of Mansell and Hussey (2011) where steel probes were driven into the streambed until resistance or refusal was experienced and the depth recorded. When plotted

against the channel width, these depths will produce total cross sectional areas from which theodolite surveyed channel areas are subtracted to obtain subsurface areas only. Rating curves were plotted from the relationship between logged water levels and discharge or channel runoff.

Streambed hydraulic conductivities were estimated from falling head slug tests data obtained from installed streambed piezometers. The slug tests were done by quickly adding known volumes of water to dry monitoring piezometers and then using the rate at which water level falls to calculate K. Where piezometers had some water, a known volume of water was removed from the piezometer and the rate of water rise or recovery was recorded. K was calculated using the Bouwer and Rice (1976) equation as follows:

$$K = \frac{rc^2 \ln(\frac{Re}{rw})}{2L} \frac{1}{t} \, \boldsymbol{ln} \frac{y0}{yt} \qquad \text{Equation 4.15}$$

where K is the hydraulic conductivity; r_c is inside radius of piezometer if water level is above perforated area; R_e is the effective radius over which y is dissipated; r_w is the horizontal distance from well centre to original aquifer (radius of casing plus thickness of gravel pack); the term $\frac{1}{t} \, \boldsymbol{ln} \frac{y0}{yt}$ is obtained from the best fitting straight line in a plot of ln y against t.

4.2.6 Rainfall-Runoff Analysis

The relationships between rainfall and runoff characteristics were statistically examined. Pearson's product moment correlation coefficient (r) was used to determine linear dependencies between various facets of the aforementioned parameters. Identified dependencies were tested using the *t*-test in order to ascertain the level of significance (*p*) at which these relationships were valid.

Runoff coefficients were calculated using total runoff volumes for selected events to further understand the general reaction of study sites to rainfall events. The following equation was used (Blume et al., 2010):

$$\text{Runoff Coefficients } (R_c) = \frac{\textbf{runoff volume(mm)}}{\textbf{rainfall depth(mm)}} \qquad \text{Equation 4.16}$$

4.2.7 Stream and Riparian Zone Hydraulic Head Monitoring

Monitoring of hydraulic head in boreholes, piezometers and stream was conducted in order to determine places of potential lateral connectivity between deep groundwater, hillslope vadose zone and the stream.

Vertical hydraulic gradient (VHG) and streambed hydraulic conductivity (K_h) helped to quantify hyporheic exchange between streambed alluvium and stream. Vertical hydraulic gradient is a dimensionless quantity that is positive under upwelling conditions and negative under downwelling conditions according to the following equation (Baxter et al., 2003):

$$\mathbf{VHG} = \frac{\Delta \mathbf{h}}{\Delta \boldsymbol{l}} \qquad \text{Equation 4.17}$$

where Δh is head difference between water level in piezometer and water level in the stream surface; Δl is the piezometer depth from streambed surface to the first opening of piezometer screen.

4.2.8 Sampling and laboratory analyses

Surface water from streams, groundwater from boreholes and subsurface water from riparian and streambed piezometers were routinely sampled fortnightly at first and then weekly during the peak rainfall period from January to February 2013. In addition to the routine sampling, samples were also collected after every rainfall event. This was done to get the signature of processes between rainfall events as well as during stormflow periods. Sampling before and after rainfall events was crucial to determine time-variant water sources contributing to total runoff, commonly denoted as event and pre-event components in two component hydrograph separations using tracers. Piezometers were purged first before a sample could be collected in order to ensure fresh subsurface samples which are free from direct rain or enriched ponded water. Surface water samples were grabbed from streams. Groundwater was sampled at 10 m specific depth intervals using a sampler with a calibrated extension. This was done in order to capture signatures at different depths which could be influenced by changes in aquifer properties such as presence of a fracture.

At the 3rd order outlet of both Supersites an ALCO automatic streamflow sampler was installed (manufactured by the Centre for Water Resources Research at the University of KwaZulu-Natal (Figure 4.3). This sampler is controlled by a CR200 Campbell Scientific™ datalogger which measures stage, calculated as a pressure via a CS450 sensor after every 10s. The data logger was programmed to trigger the sampler to collect a sample when the stage surpasses a threshold change of 5 cm head. The rationale for the 5 cm threshold was to allow all the 20 bottles in the sampler to be used in an average event (determined from streamflow data collected during 2011-12) where head change in the stream would be ±50 cm.

Figure 4.3: ALCO 20-bottle sequential sampler built by the Centre for Water Resources Research at the University of KwaZulu-Natal.

Physico-chemical parameters which included electrical conductivity (EC), temperature and pH were measured using a calibrated PC5 Testr 35 Multi-Parameter instrument as soon as the sample was collected in the field. These samples were analysed for stable isotopes (^{2}H and ^{18}O) and for major cations and anions (K^{+}, Mg^{2+}, Na^{+}, Cl^{-}, Ca^{2+}) and dissolved silica (SiO_2) which shall be referred to hence forth as silicon (Si). The analyses were done at the Chemistry and Hydrology laboratories of the University of KwaZulu-Natal. The above-mentioned hydrochemical parameters were selected for analysis because they are major cations and anions which usually exist in abundance (greater than 1 mg/L) in many environments (Younger, 2006). Silicon and chloride in particular, are commended for being less reactive in natural catchment conditions and because of that they have been used effectively as tracers in several earlier studies with considerable success (Shanley et al., 2002; Kirchner et al., 2001).

Stable isotope analysis was conducted using a Los Gatos Research (LGR) DT-100 Liquid Water Laser Isotope Analyser following International Atomic Energy Agency (IAEA) guidelines. This equipment is capable of analysing a maximum of 30 prepared samples at a time and completes analysing within a total of 21 hours. Analytical errors using this equipment are +/-0.3‰ for oxygen and +/-1.0‰ for hydrogen. Standard solutions were run concurrently with the prepared samples for the analysis of $\delta^{2}H$ and $\delta^{18}O$ isotopes.

The mixing of components or sources of streamflow was distinguished by analysing the assortment of isotope concentrations from various sources including rainfall and the stream on an $\delta^{18}O/\delta^{2}H$ plot. These concentrations are plotted as differences (delta values) between sample values and the Vienna Standard Mean Ocean Water (VSMOW).

Cation analysis was done using Inductively Coupled Plasma-Optical Energy Spectrometry (ICP OES) whose analytic precision is +/-0.3 mg/L. Chloride was analysed using HACH DR/2000 Spectrophotometer which measures concentrations with a precision of ±0.3 mg/L. Both were conducted at the University of KwaZulu-Natal.

4.2.8.1 Tracer Analysis

Tracer analysis was done through time series hydrochemical and isotopic plots to capture and interpret trends in chemical parameter and isotopic signatures. Lumped plots of $\delta^{18}O$ and $\delta^{2}H$ values on x and y axes respectively, were done relative to the GMWL to identify possible mixing of different water sources. Quantification of component contributions to total runoff was accomplished through hydrograph separations using $\delta^{2}H$, $\delta^{18}O$, Cl, EC and Si.

4.2.8.2 Hydrograph separation

Hydrochemical and isotopic tracers were used to quantify components of streamflow based on the following assumptions (Liebundgut, 2009; Uhlenbrook & Hoeg, 2003):

- that there are significant differences between tracer concentrations of different components
- that tracer concentrations do not change in space and time, and any changes that occur can be explained that contributions of an additional component must be negligible or that its concentration must be similar to that of another component in the sample that tracers must mix well and conservatively, without readily reacting with other chemicals.

These assumptions were met in that isotopic delta values and the concentrations of EC and Si were distinct for different water sources which included surface water from streams, subsurface and groundwater from piezometers and boreholes respectively, and that their ranges were not significantly variable for each source (standard deviation of ±0.01).

To determine whether two or three component hydrograph separations were valid, $\delta^{18}O$ values were plotted against discharge and collinear trends were observed which validate two component separations for studied reaches (Cey et al., 1998).

Given complete mixing of two components, pre-event (QP) and event water (QE) with CP and CE respective concentrations in a total streamflow, QT, with a concentration, CT, mass balance equations for water and tracer were solved as follows (Uhlenbrook and Hoeg, 2003):

$$QT = QP + QE \qquad \text{Equation 4.18}$$

and,

$$CT*QT = CP*QP + CE*QE \qquad \text{Equation 4.19}$$

These relationships enabled percentage contributions of components to be calculated thus:

$$QP = QT* \left[\frac{CT-CE}{CP-CE}\right] \qquad \text{Equation 4.20}$$

and

$$QE = QT * \left[\frac{CT-CP}{CE-CP}\right]. \qquad \text{Equation 4.21}$$

The pre-event concentration was taken from a subsurface sample collected a day before the rainfall event being investigated.

A three component hydrograph separation model was used to partition total runoff into three components with two conservative tracers, EC and $\delta^{18}O$ using Ogunkoya and Jenkins (1993) model. Full chemical-isotopic mass balance equations were solved as follows:

$$CT_{\delta 18O} = QR.CR_{\delta 18O} + QSS.CSS_{\delta 18O} + QG.CG_{\delta 18O} \qquad \text{Equation 4.22}$$

$$QT.CT_{EC} = QR.CR_{EC} + QSS.CSS_{EC} + QG.CG_{EC} \qquad \text{Equation 4.23}$$

where, QR is the proportion of incident precipitation; QSS is the proportion of soil water; QG is the proportion of groundwater; CT, CR, CSS and CG are concentrations of total runoff, incident rain, soil water and groundwater respectively. Given the above, the proportions QR, QSS and QG were calculated as follows:

$$QR = \frac{-\ (CT_{d18O} - CG_{d18O})(CSS_{EC} - CG_{EC}) + (CT_{EC} - CSS_{EC}) - (CSS_{d18O} - CG_{d18O})}{(CSS_{d18O} - CG_{d18O})(CR_{EC} - CG_{EC}) - (CSS_{EC} - CG_{EC})\ (CR_{d18O} - CG_{d18O})}$$

Equation 4.24

$$QSS = \frac{(CT_{d18O} - CG_{d18O})(CR_{EC} - CG_{EC}) - (CT_{EC} - CG_{EC}) - (CR_{d18O} - CG_{d18O})}{(CSS_{d18O} - CG_{d18O})(CR_{EC} - CG_{EC}) - (CSS_{EC} - CG_{EC})\ (CR_{d18O} - CG_{d18O})}$$

Equation 4.25

$QG = 1 - QR - QSS$ Equation 4.26

4.2.9 Multi-piezometer groundwater monitoring network

Borehole positions were drilled by The Department of Water Affairs (DWA) Polokwane drilling division, along the geophysics traverses which were initially used to explore the lithology and prospective drilling positions in the shallow (weathered) and deep (hard rock) subsurface of the riparian, mid-slope, crest regions of the hillslope of each order. At each hillslope region (or catenal element) boreholes were drilled piezometrically such that one or two boreholes would be in contact with the shallow weathered material and the deeper borehole in the consolidated hard rock. In addition piezometric boreholes were drilled in a triangulation position to each hillslope to determine the three dimensional groundwater slope. Given the environmental setting of hard rock terrain air percussion drilling was favourable in that it permitted the collection of detailed information on subsurface material where penetrated, providing information such as depth to weathering, hard rock, water strikes.

To understand the lithological description of percussion boreholes drilled, a classification of the subsurface material was required. The subsurface material brought to the surface by means of compressed air were placed in rows for geological logging. Sub-samples were collected and transported to the Geology Department laboratory at the University of Pretoria for identification analysis. The analysis involved using the Guidelines for Soil and Rock Logging in South Africa which apply methodology set out in the South African National Standard (SANS) 633 profiling and percussion and core borehole logging in South Africa for engineering purposes (Brink and Bruin, 2002). These guidelines took into account properties such as texture, colour, mineral composition of the lithology log samples in order to categorize weathered and hard rock material.

4.2.9.1 Monitoring Groundwater level trends

In order to determine hydraulic gradients, differentially corrected groundwater elevations were measured using a Solinst waterlevel meter. Intervals were at least monthly, but more regularly following large rainfall events (typically bi-weekly). Selected boreholes were also fitted with Solinst levelloggers for continuous time series data. The water levels were then used to calculate spatial hydraulic gradients using the Kriging geo-statistical method within Surfer v9. These gradients were then used to infer potential recharge (generally shallower water levels) and discharge/surface water interaction processes.

4.2.9.2 Borehole Fluid logging

Borehole fluid logging (FL) was used to provide undisturbed in-situ borehole parameters of specific conductance (SC), temperature and pH with depth serving as spatial baseline data across the catchment. A secondary objective of the FL was to log the boreholes over different seasons to observe possible changes in these parameters. A YSI (Yellow Spring Incorporated) sonde multi-parameter in-situ monitoring device was used for this purpose at 2 second intervals in order to record these parameters at ~0.25 m depth intervals. YSI profiles of the boreholes were conducted on a quarterly basis.

4.2.9.3 Borehole Specific Depth Sampling

Boreholes in all catchments were subject to routine specific depth sampling (name of sampler) on a monthly basis, but more frequently following significant rainfall events and in tandem with streamflow grab sampling. In the southern granites samples were taken in each borehole at 10 m depth intervals and on the basalts 20 m. Samples were analysed in-situ for Temperature, EC and pH. Samples were also analysed for stable isotopes.

4.2.9.4 Aquifer properties characterisation

Aquifer tests were performed to determine the hydraulic properties transmissivity (T) and hydraulic conductivity (K) of an aquifer. Single-borehole aquifer tests were conducted for this purpose these included pump and slug tests as described by Kruseman and De Ridder (1994).

The Cooper-Jacob (1946) equation (Equation) was applied for the determination of T values using a pump test. These pump test were restricted to the boreholes drilled into the hard rock aquifer to satisfy the assumptions of the Cooper-Jacob solution. If the assumptions were not met for a pump test, for example a minimum pump drawdown test of >2 hours, and/or a constant pump rate achieved then slug tests would be performed. If boreholes drilled into the weathered aquifer subjected to a wedge-shaped aquifer the Huntush solution (Eq 3.20) would be performed. Slug tests data was analysed using the Bouwer & Rice (1976, Equation 4.15) method to determine T or K.

$$Sc(r,t) = S(r,t) - \frac{S^2\,(r,t)}{2D} \qquad \text{Equation 4.27}$$

where Sc(r,t) is corrected drawdown (m); S(r,t) is observed drawdown (m); and 2D is the saturated thickness (m) prior to pumping.

if the thickness of a confined aquifer varies exponentially in the flow direction (x-direction) while remaining constant in the y-direction the drawdown equation for unsteady-state flow takes the form and is written as follows (Huntush):

$$s = \left[\frac{Q}{4\pi K D_w t} exp(\frac{r}{a} cos\theta)\right] W\left(u, \left|\frac{r}{a}\right|\right)$$ Equation 4.28

Where D_w is the thickness of the aquifer (m) at the location of the borehole

4.2.10 Meteorologic Data

Texas ™ and Davis™ tipping bucket rain gauges were installed at Stevenson Hamilton (granites) and Nhlowa (basalts) respectively, to measure event-based rainfall assumed to be representative of the rainfall received by all 1st to 3rd order catchments. The rain collectors have funnels of size 0.254 mm and are set to log at event increments of 0.1 mm at Stevenson Hamilton and 0.2 mm at Nhlowa study sites. Tipping bucket rain gauges were essential since they enabled the calculation of rainfall intensities which are crucial in comparative connectivity studies. Bulk rain gauges were also installed on study sites for the collection of rain samples for use in isotopic and hydrochemical tracer analyses.

This data was collected by an in-situ Davis weather station during the hydrological year of September 2012-September 2013. This station stored variables in the following SI units:

Rainfall (mm): using a Davis vantage pro2 tipping bucket rain gauge calibrated to 0.1 mm
Temperature (^oC) and Relative Humidity (%): using a Davis vantage pro2 temperature sensor (PN Junction Silicon Diode) and relative humidity sensor (Film capacitor element).

Wind Speed (m/s): using a Davis vantage pro2 solid state magnetic sensor.

Solar Radiation (W/m^2): was also collected with an integrated pyranometer, all data were recorded on a 15 min time step.

The Integrated Sensor Suite (ISS) houses these sensors and communicates with a console which provides a display of the logging variables. The console is interfaced with an Asus laptop using Weatherlink™ software to download the logging variables.

The rainfall data was used to derive a 7 day Antecedent Precipitation Index (API[7]), based on the method of Kohler and Linsley (1951) in order distinguish particular rainfall sequences during the monitoring season.

4.2.11 Actual Evapotranspiration

This project utilised a residual method to determine actual evapotranspiration in the KNP Supersites namely the SEBAL – Surface Energy Balance Algorithm for Land model (Bastiaanssen et al., 1998), which uses surface energy equations combined with remote sensing images to directly estimate evapotranspiration (Courault et al., 2005).

The SEBAL model computes evapotranspiration from remote sensing images and weather data using the surface energy balance (Equation). The satellite can only capture an instantaneous image of the area of interest (AOI) as it passes over. Daily evapotranspiration is estimated by linearly interpolating the reference evapotranspiration fraction over periods between two consecutive images and multiplying this value by the cumulative 24 hour reference evapotranspiration for that day. Generally, however, the SEBAL model calculates an evapotranspiration flux for immediate images. The evapotranspiration flux is determined for each pixel of the satellite image as a “residual” of the surface energy budget equation:

$$\lambda ET = R_n - G - H \qquad \text{Equation 4.29}$$

where λET is the latent heat flux (W/m^2), R_n is the net radiation flux at the surface (W/m^2), G is the soil heat flux (W/m^2), and H is the sensible heat flux to the air (W/m^2).

The remote sensing satellites have sensors that receive spectral bands (or wavelengths of electromagnetic energy) emitted from objects on the earth's surface. Healthy vegetation reflects very strongly in the near-infrared part of the electromagnetic spectrum. The amount of infrared reflected by vegetation is used in an equation to calculate the normalised difference vegetation index (NDVI). In simple terms the SEBAL model then estimates an actual evapotranspiration amount using various parameters and calculations based on the amount of reflectance, at different wavelengths or electromagnetic bands, from the vegetation in each pixel, or area of interest (Waters et al., 2002).

SEBAL 30 m pixel satellite data was obtained from the Inkomati Catchment Management Area (ICMA) and eLeaf through the European Union WATPlan Project. The data is for the period from November 2011 to October 2013. This data is presented as weekly values of actual ET (mm/week). For the purposes of daily hydrological modelling these weekly values were disaggregated by fitting them to a relationship derived from the Penman-Monteith equation for potential evaporation (using weather station data), in the form:

$$\frac{\mathrm{aET}}{\mathrm{hr}} = \frac{\mathrm{pET(hr)}}{\mathrm{Total\ pET(week)}} \times \ \mathrm{Total\ aET\ (week)} \qquad \text{Equation 4.30}$$

where aET = Actual ET and pET = Potential ET.

Selected Raster images of the SEBAL data over the supersites through the hydrological monitoring period are displayed for interest in Appendix IV.

<u>4.2.12 Modelling</u>

4.2.12.1 Catena Water Balances (HYDRUS)

HYDRUS-1D (Šimůnek et al., 2013) was used to simulate flow and calculate model catena element soil water budgets. HYDRUS can simulate water flow, solute and heat transport in saturated, unsaturated and partially saturated porous media even on non-uniform soils which is crucial in this study considering the non-homogenous soils on the study sites. HYDRUS 1D numerically solves the Richards equation for variably-saturated water flow. Water flow through the unsaturated porous medium is highly variable and is controlled by a number of soil physical properties such a texture and pore configuration. Antecedent moisture conditions in the soil also play a part in controlling water movement through the medium. A modified form of the Richard's equation is used to describe the one dimensional water movement in porous media. An assumption is made that the air phase is insignificant in the water flow process and thermal gradients can be ignored (Šimůnek et al., 2013).

$$\frac{\partial\theta}{\partial t} = \frac{\partial}{\partial x}\left[K\left(\frac{\partial h}{\partial x} + \cos\alpha\right)\right] - S$$ Equation 4.31

Where
h = water pressure head (L)
θ = volumetric water content (L^3L^3)
t = time (T)
x = spatial coordinate (L)
S = sink term ($L^3L^{-3}T^1$)
α = angle between flow direction and axis (vertical)
K = unsaturated hydraulic conductivity function (LT^{-1}) which is given by the following equation:

$$K(h,x) = K_s(x)K_r(h,x)$$ Equation 4.32

Where:
K_r = relative hydraulic conductivity (-)
K_s = saturated hydraulic conductivity (LT^{-1})

The user specifies the type of domain, boundary conditions, initial conditions and the distribution of materials in the soil profile (Figure 4.4: Schematic illustration of diagnostic horizons and boundary conditions applied in this study using Hydrus 1D). Simulated results from the model are then used to calculate catena element water balances using the equation by Zhang et al. (2002).

$$\Delta S = P - ET - R - FD$$ Equation 4.33

Where: ΔS = change in water storage,
P = precipitation,
ET = evapotranspiration,
R = surface runoff,
FD = free drainage or groundwater recharge.

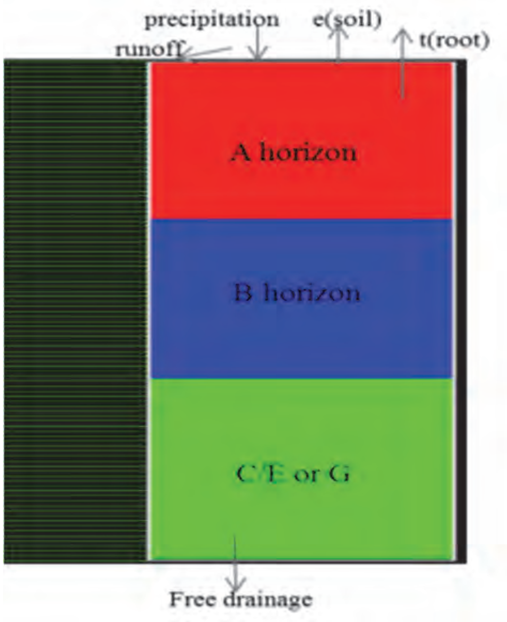

Figure 4.4: Schematic illustration of diagnostic horizons and boundary conditions applied in this study using Hydrus 1D

4.2.12.1.1 Model Set-up

The following protocol was used in setting up Hydrus-1D in order to simulate water balances at each catena element:

The modelling period was set from the 3rd of October 2012 to the 30th of April 2013 (i.e. 210 days during the wet season). The model was run in hourly time steps (Total 5040 hours) and model output yielded every 24 hours.

The model domain was designed according to material distribution depths identified during field surveys. An atmospheric boundary condition with surface runoff was applied at the surface and free drainage at the base (i.e. vertical flow from the soil column and the potential recharge to aquifer). Initial conditions for the model run were set in terms pressure head, related to observed values from the soil moisture sensors (However in a number of cases soils were very dry before the beginning of the rainy season therefore a CPH of -15 000 mm [wilting point] was used as the absolute minimum, where necessary).

Quantified soil textural classes were determined and HYDRUS-1D default values for these classes were used in terms of: θ_r (residual soil water content) and θ_s (saturated soil water content). The α and *n* soil water retention curve fitting parameters were obtained using RETC (Van Genuchten et al., 1991) using observed K_{unsat} data.

On-site observed precipitation was used as hourly atmospheric boundary layer input along with the derived hourly-aET determined from the SEBAL: Penman-Monteith disaggregation (Appendix A4.1). Where surface runoff was simulated in a catena element, this was added to the rainfall input at the next downslope element.

Actual evapotranspiration was then partitioned into two components: evaporation and transpiration. In order to achieve this, a simple dimensionless partitioning model was used in the form of the following equation (Smithers and Schulze, 1995):

$$ft = \frac{\lambda(t) - 0.2}{0.8} \qquad \text{Equation 4.34}$$

Where t= time (days)
λ= site specific crop factor

To partition the evapotranspiration, (*ft*) is then used as follows:

$$pT = p\,ET_O ft \qquad \text{Equation 4.35}$$

And

$$p\,E_{soil} = p\,ET_O - p\,T \qquad \text{Equation 4.36}$$

A simple sensitivity analysis of model performance was derived using the method of Hamby (1994), using the principle that one parameters values are varied whilst all the other parameters remain fixed. The parameters tested include rainfall, soil properties and evapotranspiration. A 50% increase and decrease in rainfall and ET was tested. A relative increase (>80 mm/hr) and decrease (<10 mm/hr) in soil hydraulic properties (K_{sat}) was also tested. The percent change in model output from original is then calculated using the following equation:

$$Change\ from\ original\ (\%) = \frac{Output\ value\ after\ change - original\ output\ value}{Original\ output\ value} * 100$$

Equation 4.37

The total percent change was calculated by adding all percent output variables of the water balance (all as positive values to get total percentage change) using the following equation.

$$Total\ (\%) change = \%\Delta FD + \%\Delta R + \%\Delta ET + \%\Delta S + \%\Delta P \qquad \text{Equation 4.38}$$

When calculating the total percent change, if it is for ET then the change in ET is omitted since it is the value that has been manipulated and the same applies for the calculation of the other parameters under analysis. The difference between the maximum and minimum values of the total change is then calculated to see which parameter the model is showing a much large variability for the same percent increments.

4.2.12.2 Geohydrological Processes (MODFlow)

The main objective of the groundwater flow modelling was to gain more insight into the groundwater flow system within nested catchments of the Southern Granite and Southern Basalt study sites.

4.2.12.2.1 Pre-Modelling Process and Modelling Procedure

The pre-modelling process involved analyses of geophysical profiles, borehole and stream hydraulic heads as well as physico-chemical and isotopic data. These analyses provided necessary conceptual model, input data and insight that informed the groundwater modelling process. This was then followed by setting up and running of steady-state models for the two sites in order to set initial starting heads. The steady-state models provided the platform for transient models which were needed to examine the behaviour of the aquifer over time.

4.2.12.2.2 Model construction & Governing Equations

The numerical model for the project was constructed using Groundwater Vistas (GV6), a pre- and post- processing package for the modelling code MODFLOW. MODFLOW is a modular three dimensional groundwater flow model developed by the United States Geological Survey (Harbaugh et al., 2000). MODFLOW uses 3D finite difference discretisation and flow codes to solve the governing equations of groundwater flow. MODFLOW NWT (Niswonger et al., 2011) was used in the simulation of the WE&M groundwater flow model. Both are widely used simulation codes and are well documented. The numerical model was based on the conceptual model developed from the findings of the desktop and the baseline investigations.

The simulation model used in this modelling study simulates groundwater flow based on a three-dimensional cell-centred grid and may be described by the following partial differential equation:

$$\frac{\partial}{\partial x}\left(K_{xx}\frac{\partial h}{\partial x}\right)+\frac{\partial}{\partial y}\left(K_{yy}\frac{\partial h}{\partial y}\right)+\frac{\partial}{\partial z}\left(K_{zz}\frac{\partial h}{\partial z}\right)\pm W = S_s\frac{\partial h}{\partial t}$$

Equation 4.39

where:

K_x, K_y, and K_z are values of hydraulic conductivity along the x, y, and z coordinate axes, which are assumed to be parallel to the major axes of hydraulic conductivity (L/T); h is the potentiometric head (L); W is a volumetric flux per unit volume representing sources and/or sinks of water, with $W < 0.0$ for flow out of the ground-water system, and $W>0.0$ for flow in (T^{-1});vS_s is the specific storage of the porous material (L^{-1}); and t is time (T).

Equation 1, when combined with boundary and initial conditions, describes transient three-dimensional ground-water flow in a heterogeneous and anisotropic medium, provided that the principal axes of hydraulic conductivity are aligned with the coordinate directions (Harbaugh et al., 2000).

4.2.12.2.3 Boundary conditions

Boundary conditions express the way in which the considered domain interacts with its environment. In other words, they express the conditions of known water flux, or known variables, such as the hydraulic head. Different boundary conditions result in different solutions, hence the importance of stating the correct boundary conditions. Boundary condition options in MODFLOW can be specified either as:

- specified head or Dirichlet; or
- specified flux or Neumann; or
- mixed or Cauchy boundary conditions.

From the conceptual point of view, it was essential to meet two criteria to the maximum extent possible:

1. The modelled area should be defined by natural geological and hydrogeological boundary conditions, i.e. the model domain should preferably encompass entire hydrogeological structure; and
2. The mesh size of model grid has to correspond to the nature of the problem being addressed with the model.

Where possible hydraulic boundaries were identified for model boundaries. The hydraulic boundaries were in many cases in one of the neighbouring sub-catchments, represented by watershed boundaries and delineated the entire model domain. These hydraulic boundaries were selected far enough from the area of investigation to not influence the numerical model behaviour in an artificial manner. The initial conditions used in the transient models are the values obtained from the steady-state calibration.

Outflows from the model domain were represented by drains. The MODFLOW Drain package was used instead of rivers because of the ephemeral nature of streamflows in the study sites. Flows are event driven and are of limited duration. Drain cells were assigned lengths and widths in such a way that they could totally fill the entire surface area of the cell. No-flow boundaries were specified in areas outside the model domain since these are a special kind of constant flux boundary where the flow is set to zero indicating their exclusion from the flow system.

4.2.12.2.4 Model Calibration

The aim of the Steady State calibration is to simulate the undisturbed state of the groundwater system (baseline conditions). Undertaking a steady state simulation has the dual benefit of testing the conceptual model without the complication of time variant behaviour, and of providing numerically stable starting conditions for time variant simulations. Water level data collected from the hydro-census was imported as groundwater elevation targets and used to calibrate the models. The steady state models were calibrated using recharge and hydraulic conductivity data.

The numerical model calculated head-distribution ($h_{x,y,z}$) is dependent upon the recharge from rainfall, hydraulic conductivity and boundary conditions. For a given set of boundary conditions the head distribution across the aquifer can be obtained for a given set of hydraulic conductivity values (or transmissivity value) and specified recharge values. This simulated head distribution can then be compared to the measured head distribution and the hydraulic conductivity or recharge values can be altered until an acceptable correspondence between measured and simulated heads is obtained.

To assess the accuracy of the steady state simulation the model results are compared to monitored water level data. The degree of error, or residual, is calculated as the observed water level minus the modelled:

Residual = Observed – Modelled Equation 4.40

The calibration for the two models (Southern Granites & Southern Basalts) was done using a combination of manual and inverse calibration using aquifer zone properties for all model layers. PEST (Parameter ESTimation) was also used to assist in model calibration. PEST, a nonlinear parameter estimator, automatically adjusts model parameters until the residual between model output values and field observation data are optimised.

The success rate of the calibration process is usually assessed by the following statistical quantities: Mean Error, Mean Absolute Error, Root Mean Square and Normalized RMS.

5. RESULTS – SOUTHERN GRANITES

Instrumentation of the southern granite (SGR) began in October 2011 with catena element soil moisture sensors and stream stage level loggers. This site was completely instrumented following the completion of groundwater monitoring boreholes by September 2012. Site names, descriptions and localities are given in Table 5.1 and Figure 5.1.

Table 5.1: Hydrometric monitoring points in the Southern Granite KNP Supersite (Site SGR_Q3 included and ALCO 20 bottle sequential streamflow sampler)

Site Name	Site Description	Easting	Northing
SGR1_C	Southern Granite Transect 1/Crest Soil Moisture Watermark Station	31.57480	-25.11488
SGR1_M	Southern Granite Transect 1/Midslope Soil Moisture Watermark Station	31.57430	-25.11473
SGR1_R	Southern Granite Transect 1/Riparian Footslope Soil Moisture Watermark Station	31.57407	-25.11452
SGR2_C	Southern Granite Transect 2/Crest Soil Moisture Watermark Station	31.57698	-25.11207
SGR2_M	Southern Granite Transect 2/Midslope Soil Moisture Watermark Station	31.57531	-25.11150
SGR2_R	Southern Granite Transect 2/Riparian Footslope Soil Moisture Watermark Station	31.57419	-25.11093
SGR3_C	Southern Granite Transect 3/Crest Soil Moisture Watermark Station	31.57843	-25.11030
SGR3_M1	Southern Granite Transect 3/Upper Midslope Soil Moisture Watermark Station	31.57802	-25.10938
SGR3_M2	Southern Granite Transect 3/Lower Midslope Soil Moisture Watermark Station	31.57744	-25.10844
SGR3_R	Southern Granite Transect 3/Riparian Footslope Soil Moisture Watermark Station	31.57701	-25.10760
SGR_Baro	Southern Granite Barologger	31.57476	-25.11520
SGR_Rain	Southern Granite Rain	31.57700	-25.11012
SGR_Q1	Southern Granite 1st order Streamflow levellogger	31.57336	-25.11352
SGR_Q2	Southern Granite 2nd order Streamflow levellogger	31.57391	-25.10975
SGR_Q3	Southern Granite 3rd order Streamflow levellogger	31.58041	-25.10310
SGR3_BR_43	MP190001 Southern Granite 3rd order riparian borehole 43m	31.57680	-25.10734
SGR3_BR_20	MP190002 Southern Granite 3rd order riparian borehole 20m	31.57682	-25.10736
SGR3_BM_49	MP190003 Southern Granite 3rd order midslope borehole 49m	31.57725	-25.10810
SGR3_BM_26	MP190004 Southern Granite 3rd order midslope borehole 26m	31.57727	-25.10811
SGR3_BM_23	MP190005 Southern Granite 3rd order midslope borehole 23m	31.57728	-25.10813
SGR3_BT_61	MP190006 Southern Granite 3rd order triangulation borehole 61m	31.57840	-25.10812
SGR3_BT_34	MP190007 Southern Granite 3rd order triangulation borehole 34m	31.57843	-25.10812
SGR3_BC_55	MP190008 Southern Granite 3rd order crest borehole 55m	31.57772	-25.10882
SGR3_BC_34	MP190009 Southern Granite 3rd order crest borehole 34m	31.57773	-25.10883
SGR2_BR_49	MP190010 Southern Granite 2nd order riparian borehole 49m	31.57435	-25.11092
SGR2_BR_28	MP190011 Southern Granite 2nd order riparian borehole 28m	31.57437	-25.11092
SGR2_BC_55	MP190012 Southern Granite 2nd order crest borehole 55m	31.57671	-25.11159
SGR2_BC_40	MP190013 Southern Granite 2nd order crest borehole 40m	31.57673	-25.11160
SGR1_BR_61	MP190014 Southern Granite 1st order riparian borehole 61m	31.57392	-25.11452
SGR1_BR_22	MP190015 Southern Granite 1st order riparian borehole 22m	31.57393	-25.11452
SGR1_BC_103	MP190016 Southern Granite 1st order crest borehole 103m	31.57472	-25.11484
SGR1_BC_17	MP190017 Southern Granite 1st order crest borehole 17m	31.57474	-25.11485
SGR1-2_BT_61	MP190018 Southern Granite 1st and 2nd order triangulation borehole 61m	31.57552	-25.11257
SGR1-2_BT_36	MP190019 Southern Granite 1st and 2nd order triangulation borehole 36m	31.57553	-25.11256
SGRMet	Southern Granite Weather Station	31.57476	-25.11520

Table 5.2: Southern Granite Borehole in-situ hydraulic parameters following drilling (2012)

Borehole	Temperature (°C)	Specific Conductance (mS/cm)	pH	Static water level (m)	Blow out yield (l/s)	Transmissivity (m^2/d)	Test Type
SGR3_BR_43	24.58	4	6.94	17.71	0.011	4.80E-03	BR
SGR3_BR_20	24.38	3.84	6.87	17.97	none	1.80E-04	BR
SGR3_BM_49	25.19	3.19	7.08	22.67	0.16	3.3	CJ
SGR3_BM_26	25.03	3.14	6.74	22.85	0.29	2.5	CJ
SGR3_BM_23	24.94	3.52	6.87	22.89	none	none	
SGR3_BT_61	25.79	6.87	7.3	27.69	none	1.10E-05	BR
SGR3_BT_34	25.67	6.78	6.81	27.73	none	5.00E-05	BR
SGR3_BC_55	25.95	2.2	7.2	26.83	0.33	9	CJ
SGR3_BC_34	25.96	4.06	6.99	26.8	none	1.20E-04	BR
SGR2_BC_40	25.16	4.87	6.73	34.92	none	1.90E-05	BR
SGR2_BC_55	25.23	3.02	7.2	34.69	none	5.90E-08	BR
SGR2_BR_28	25.16	4.87	6.3	24.21	none	0.02	BR
SGR2_BR_49	25.25	3.01	7.2	24.18	none	1.40E-03	BR
SGR1_BR_61	25.5	2.08	7.04	33.48	0.07	0.5	CJ
SGR1_BR_22				dry			
SGR1_BC_103	25.9	2.33	7.05	38.82	1.25	11.2	CJ
SGR1_BC_17				10.89			
SGR1-2_BT_61				31.85	none		
SGR1-2_BT_36	29.4	1.7	7.8	31.92	none	3.00E-03	BR
SBAS3_BR_80	25.51	1.41	7.06	10.64	0.39	13.1	CJ
SBAS3_BC_80	24.99	1.32	7.03	10.28	0.16	0.1	CJ

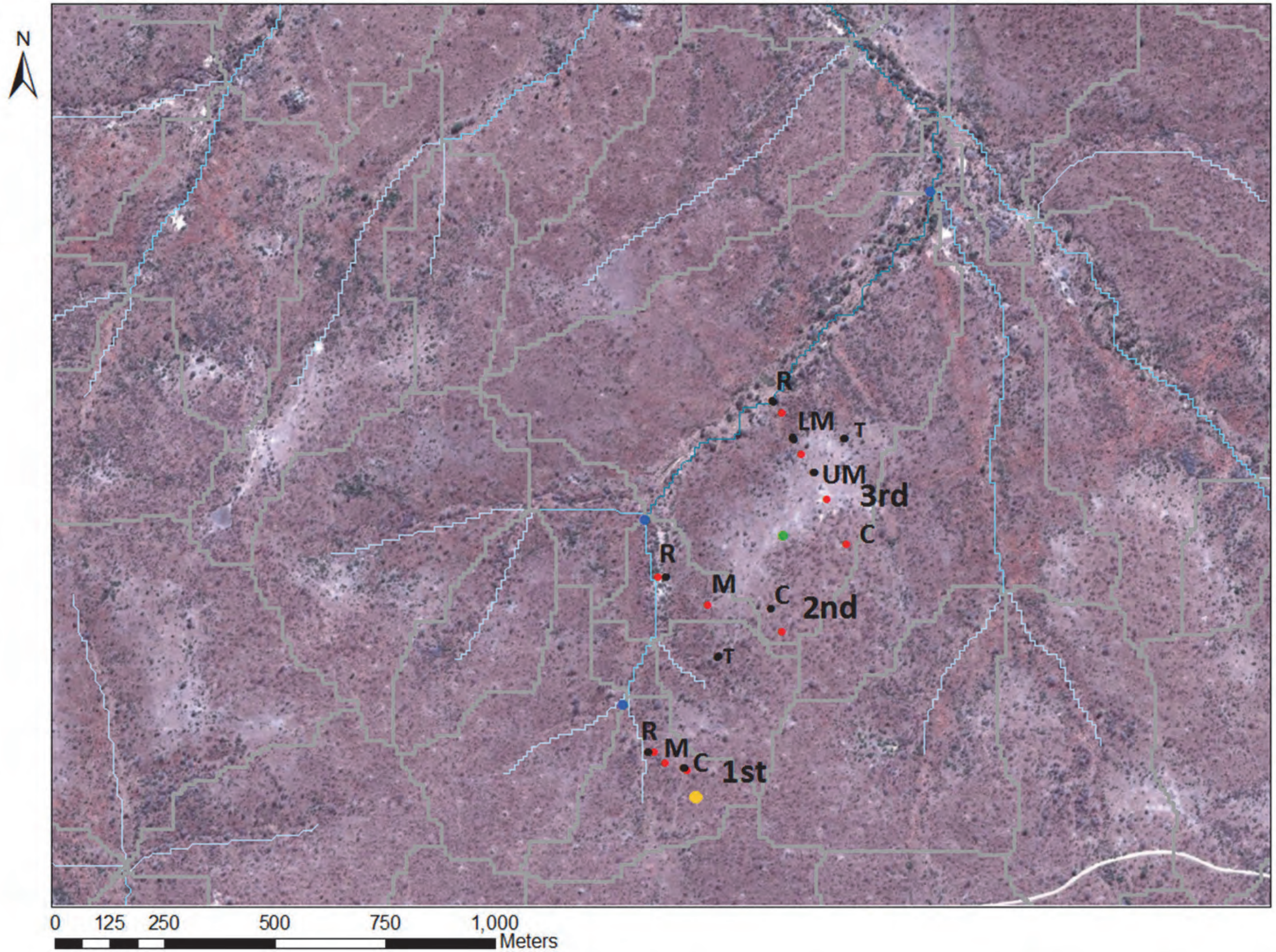

Figure 5.1: Map of installed instrumentation at the Southern Granite (Stevenson-Hamilton) Supersite (red = soil moisture station, blue = streamflow gauge, black = boreholes, green = rainfall station, orange = Davis^{TM} Weather Station, R = riparian, M = midslope, C = crest, T = triangulation, L = lower, U = upper).

5.1 Precipitation

The hydrological season for the southern granite supersite commenced on 4th September 2012 and thus we report data in this chapter to September 2013. The total precipitation for this period is 774 mm as depicted in Figure 5.2. Through the API[7] 3 major precipitation sequences occur namely, September 2012 (sequence 1), October-December 2012 (sequence 2) and December 2012 - February 2013 (sequence 3). Sequence 1 consisted of moderate rainfall ranging 5-31 mm/day for 2 weeks, sequence 2 consisted of moderate rainfall ranging 5-35 mm/day for 3 weeks, and sequence 3 comprised moderate to high rainfall ranging 5-95 mm/day for 4 weeks. Sequence 3 also included significant rainfall associated with a tropical cyclone over the Mozambique channel between 19-20 January 2013 with a total of 139.6 mm falling on the southern granite supersite.

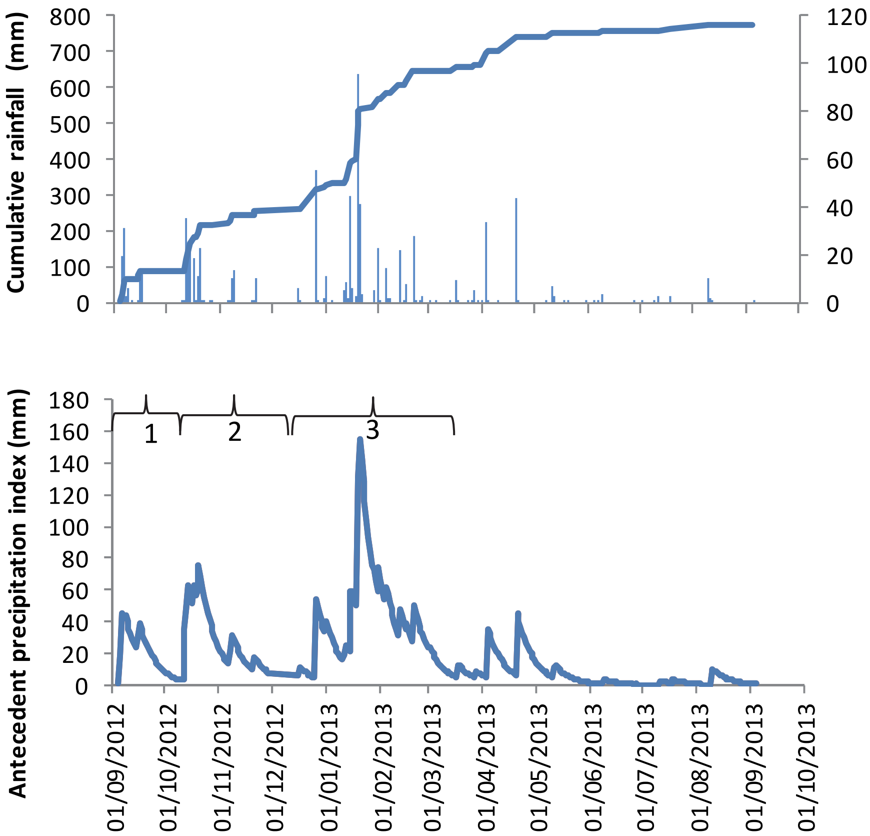

Figure 5.2: Southern Granite Rainfall September 2012-September 2013

5.2 Southern Granite Streamflows

5.2.1 Total Discharge at Southern Granites

The flashy, ephemeral nature of streamflow at the southern granite supersite is portrayed in Figure 4.3 as flow duration curves (FDCs) and as time-series in Figure 5.3, for the period the period September 2012 - March 2013.

The FDCs show extremely concave shapes that are cut off at lower tails (Yooko and Sivapalan, 2011). On this granitic geology, the first order subcatchment (SGR1) had persistent >0 mm/s runoff depths 45% of the time in. Conversely, at the second order (SGR2) and third order (SGR3) reaches respectively, surface flows were absent (</= 0 mm/s) between 85% and 75% of the time. This suggests that the SGR1 reach is gaining from a sustained subsurface water source. The vertical hydraulic gradient values calculated from streambed piezometer water levels following the significant 19th of January 2013 rainfall event (Table 5.3) reveal that at SGR1 shows upwelling with a positive VHG (+2.3408). Meanwhile SGR2 showed no channel surface flow 85% of the time suggests that this reach experiences transmission losses between rainfall events. At SGR3 flows only occurred 25% of the time indicating that this reach is also subject to losses between rainfall events. Whilst SGR2 and SGR3 reaches had negative VHGs indicating down-welling or infiltration losses. This suggests, as expected in this ephemeral landscape that there is a high degree of lateral disconnect along the stream network for the majority of the time.

Nevertheless high rainfall intensity events do allow all reaches to be connected as indicated by extremely concave shapes of the FDCs, although this connectivity rarely occurs more than 5% of the time between September 2012 - March 2013.

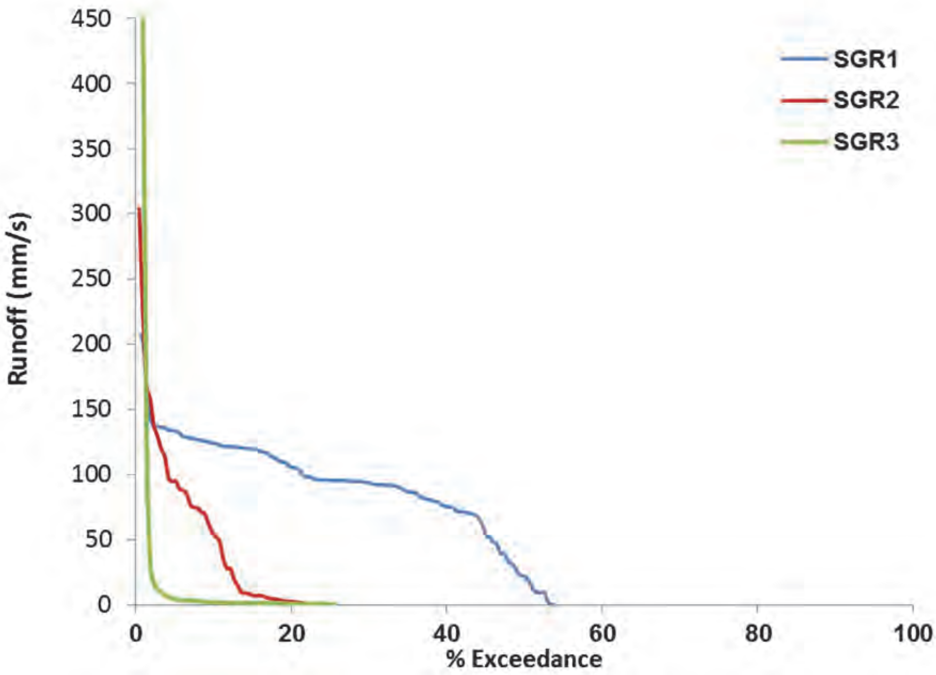

Figure 5.3: Southern Granites (SGR) Flow Duration Curves for the period from September 2012 to March 2013.

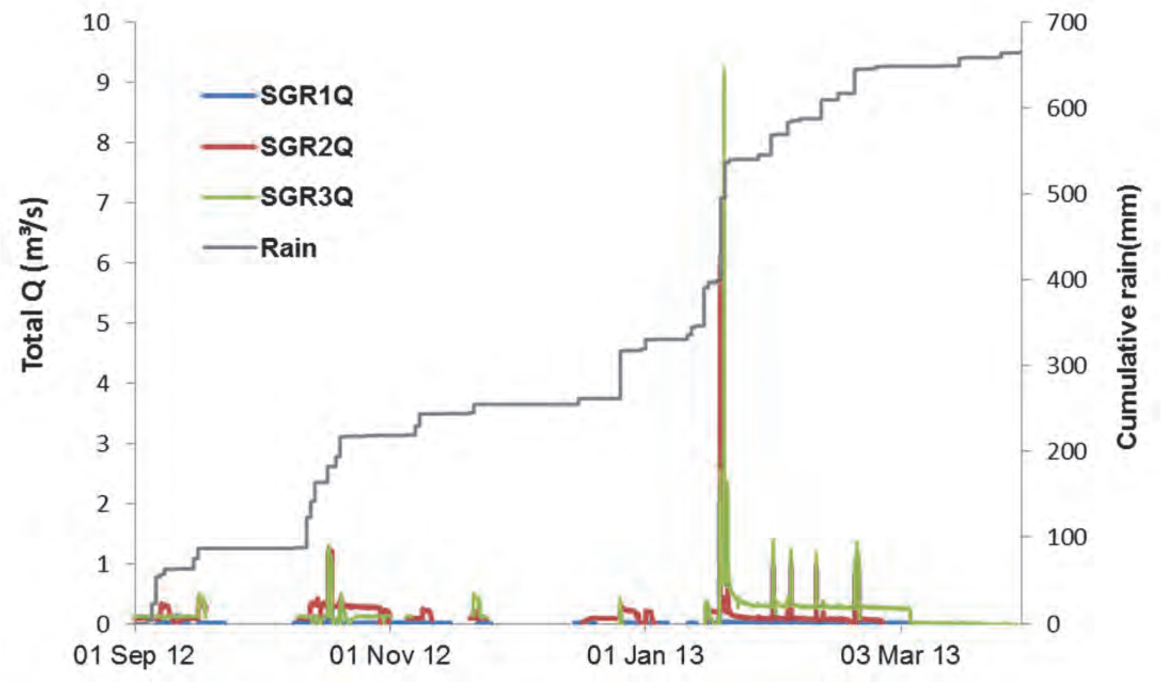

Figure 5.4: Total discharge (combined surface and subsurface) hydrographs at Southern Granites during the period, September 2012 to March 2013.

Table 5.3: vertical hydraulic gradients (VHG) monitored following the significant 19 January 2013 rainfall event

Stream reach	SGR1	SGR2	SGR3
VHG	2.341	-0.758	-0.283

5.2.2 Rainfall-Runoff Analysis Statistical Analysis

In order to get a better understanding of linkages between rainfall, runoff responses and soil moisture dynamics, an analysis of three events which occurred on 2012/12/26, 2013/01/19 and 2013/02/20 respectively, was conducted. This analysis helped to establish relationships between rainfall and runoff using Pearson's product moment correlation coefficient (r) with the level of significance (p) as presented in Table 5.4.

The occurrence of high precipitation depths has been identified to cause high runoff volumes and subsequently moderate peak runoff discharges ($r = 0.913$; $p = 0.05$ and $r = 0.915$; $p = 0.297$, respectively). High antecedent precipitation index (API[7]), a proxy for catchment antecedent soil moisture conditions was found to cause short rising times between the start of runoff response and peakflow ($r = -0.999$; $p = 0.001$). The volume of generated runoff also showed a strong dependency on API[7] ($r = 0.999$; $p = 0.003$). Since volume of generated runoff positively correlates with API[7], it indicates the important role played by pre-event water for the generation of runoff at Southern Granites study site. The significance of high rainfall intensity for runoff generation was revealed through causing short runoff lag times following rainfall events ($r = -0.988$; $p = 0.013$). Peakflow discharges were also observed to vary incrementally with increasing catchment scale ($r = 0.999$; $p = 0.003$).

Table 5.4: Pearson's product moment correlation coefficient (r) with level of significance (p, in parenthesis) showing precipitation and runoff responses of three events at Southern Granites during the period from December 2012 to February 2013

	Precip. Duration	Precip. Amount	Precip. Int_{mean}	Precip. Int_{max}	Precip API_{-7}	Runoff Delay time	Runoff Rising Time	Catchment Area	Runoff Peak Discharge
Precip. Amount	0.805 (0.153)								
Precip. Int_{mean}	-0.474 (0.322)	0.139 (0.450)							
Precip. Int_{max}	-0.668 (0.232)	-0.097 (0.465)							
Precip. API_{-7}	0.517 (0.303)	0.924 (0.068)	0.508 (0.307)	0.291 (0.395)					
Runoff Delay time	0.547 (0.186)	-0.055 (0.211)	-0.174 (0.438)	-0.988** (0.013)	-0.434 (0.339)				
Runoff Rising Time	0.500 (0.320)	-0.206 (0.322)	-0.474 (0.322)	-0.253 (0.409)	-0.999** (0.001)				
Runoff Peak Discharge	0.498 (0.430)	0.915 (0.297)	0.527 (0.180)	0.312 (0.346)	0.999** (0.001)			0.999** (0.003)	
Runoff Volume	0.482 (0.319)	0.913* (0.05)	0.543 (0.292)	0.331 (0.380)	0.999** (0.003)	-0.457 (0.329)	-0.587 (0.272)		0.999** (0.000)

** Significant to the 0.01 level
* Significant to the 0.05 level

Runoff Coefficients

Having identified the linear relationship between rainfall and runoff depths in this catchment runoff coefficients (Rc) were calculated using total runoff volumes as a proportion of total rainfall depths for the same events (Blume et al., 2010). The results are presented in Table 5.5. As shown runoff coefficients increase with increasing precipitation depths for the analysed events which upholds the positive correlation determined using Pearson's correlation coefficient (r). For the moderate rainfall events (27.9 mm to 55.3 mm) during low antecedent soil moisture conditions (API = 52.3 and 50.44, respectively) Rc values decreased from SGR1 to SGR3 suggestive of transmission losses at these higher order reaches (Blume et al., 2010).

Table 5.5: Southern Granites Runoff Coefficients for 1st to 3rd order reaches

DATE	SGR1Q(Rc)	SGR2Q(Rc)	SGR3Q(Rc)	Rain (mm)	API^7
26/12/2012	6.66	2.70	0.06	55.3	52.3
19/01/2013	18.19	27.52	40.74	95.7	130.96
20/02/2013	2.39	0.17	1.04	27.9	50.44

5.2.3 Hydrometric Analysis of Stream network and Stream-Catchment Connectivity

A closer look at the two latter events is presented here to single out these relationships and how they influence hydrologic connectivity at Southern Granites site. Observed discharges for this supersite show short-lived, event driven responses. This is indicated by sharp peaks and steep recession curves on the hydrographs (Figure 5.5 and Figure 5.6). Peakflow discharges for the three scales from 1st to 3rd order contributing areas on the granitic geology show an incremental change in magnitude for the events of 19 January and 20 February 2013.

The incremental changes in peakflows at the Southern Granites uphold the hydrological principle that discharge increases downstream due to subsequent increases of flow velocity and channel width-to-depth ratio for connected stream networks (Chow, 1959). This apparent increase in magnitude of streamflow responses with scale shows that larger contributing areas play a pivotal role in influencing event-based streamflow processes at this site. Streamflow recession after the January 19 2013 event was very rapid at SGR2 followed by SGR3. This further implies increasing losses at these reaches and in particular at SGR2 where an almost complete cessation of surface flow occurred rapidly and prior to the other reaches. Persistent flows at SGR1 as seen in Figure 5.6 suggest an additional water source apart from event contribution, indicating that this reach is gaining from groundwater or via shallow sub-surface hillslope processes at least during rainfall events. This assertion is supported by a one metre hydraulic head difference between the stream and a shallower (17 m) groundwater borehole at the hillslope crest of the SGR1 transect following a 95.7 mm rainfall event on the 19th of January, 2013 (See Figure 5.7). Events with exceptionally large precipitation depths as the one in question should be veiwed as key thresholds that determine interaction between groundwater and streams, since smaller events or even moderate ones (e.g. a 55.3 mm event on the 26th of December 2012) did not result in similar groundwater responses. In addition to being a large rainfall event, the 19th of January event had a high peak rainfall intensity of 16.3 mm/15 min. A rapid runoff response followed this high intensity rainfall event with a lag time of only 12 minutes. As such the role of rainfall intensity in runoff generation as well as in triggering connectivity between groundwater and the stream cannot be overemphasized. The fact that only the SGR1 crest shallow 17 m borehole responded suggests that groundwater contribution is through interflow via the weathered rock aquifer overlying a consolidated hardrock. The deeper SGR1 Crest 103 m borehole that penetrate the hard rock aquifer always had lower hydraulic heads than the stream for this period (Figure 5.7).

Lower borehole hydraulic heads compared to the stream support the idea that SGR2 and SGR3 reaches are potentially losing to groundwater (Figure 5.7). A 32 cm increase in water level in the 28 m riparian borehole following this large rainfall event supports the notion that SGR2 losses contribute to groundwater recharge. Although an SGR2 crest borehole also experienced a 7 m rise in head, this did not set up a hydraulic gradient towards the stream[2]. The fact that SGR3 reach does not gain from groundwater is also shown by lower borehole hydraulic heads relative to the stream at this scale (Figure 5.7).

Riparian zone water levels recorded in shallow PVC piezometers at the SGR3 hillslope monitoring transect (Figure 5.8) show hydraulic gradients inclined away from the stream towards the hillslope. Even after a sizable rainfall event in March 2013 (35 mm) the reach is still portrayed as losing through the stream bank interface. However, further down the same

[2] installation errors involving improperly sealed steel casing were noted for the SGR2 Crest boreholes such that the observed 7 m response is viewed with scepticism.

reach at the catchment outlet (SGR3Q), hydraulic head differences suggest possibility of alternate gaining and losing stream behaviour (Figures 4.8). Between rainfall events the in-stream piezometer had lower water levels than the riparian one, suggesting lateral flow towards the stream, hence potentially gaining. This was also the case during periods of moderate rainfall (e.g. 40-45 mm in early January, 2013) where water levels increased in both piezometers but still with a lower elevation in the in-stream piezometer. The assertion that the stream possibly gains from the hillslope at some point along this reach was initially suggested by hydropedological surveys (Le Roux et al., 2011) that identified certain soils on this section as interflow soils. Large, high intensity rainfall events typical of the 19 January 2013 95.7 mm event were observed to promote gaining trends as hillslope hydraulic heads were maintained above those of the stream. Such trends persisted until water levels equilibrated following which the stream switched to a losing status in response to potential increases in the soil water deficit of adjacent hillslope soils.

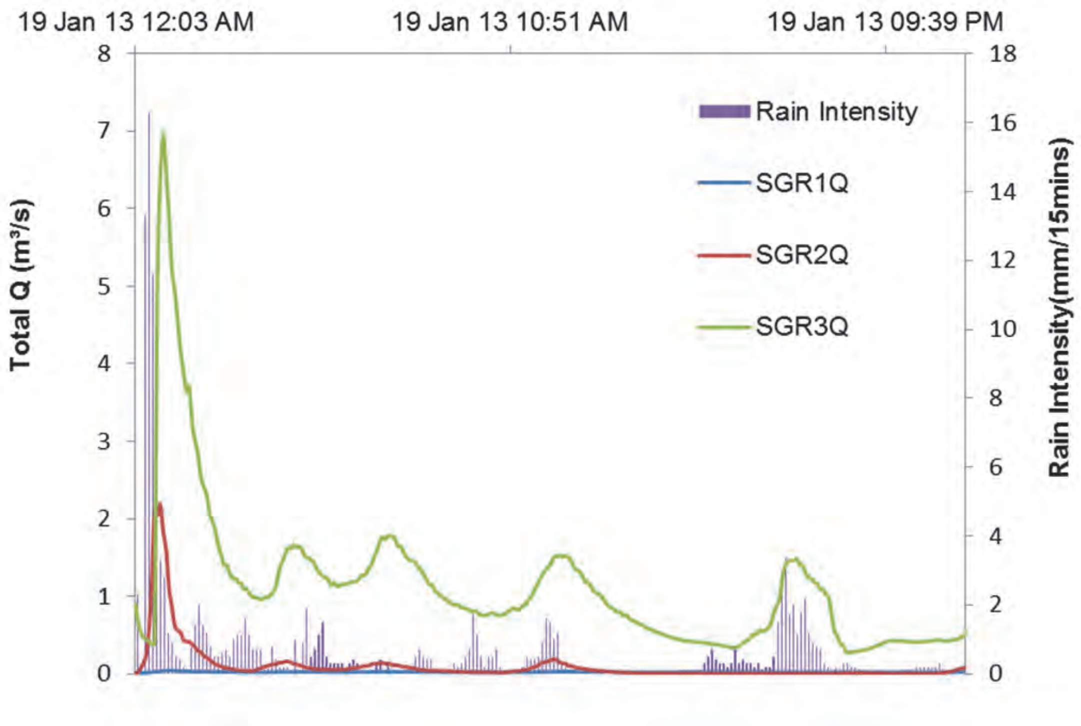

Figure 5.5: Southern Granites streamflow responses following the rainfall event on the 19th of January 2013.

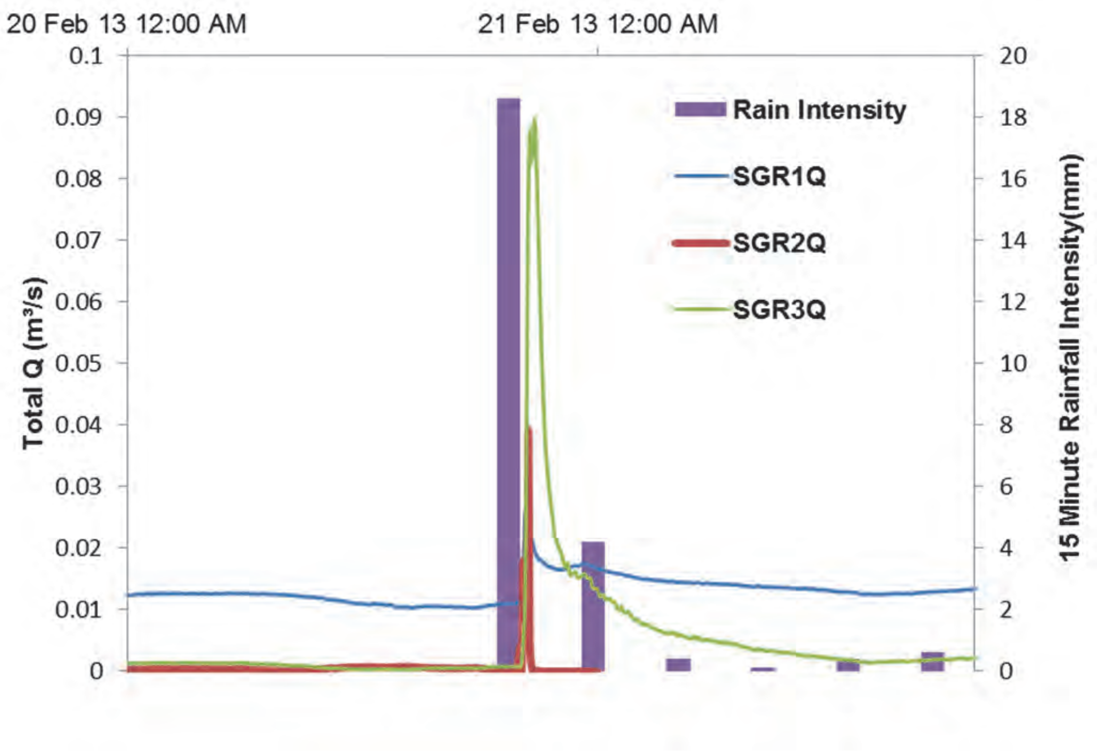

Figure 5.6: Southern Granites streamflow responses following the rainfall event on the 20th of February 2013.

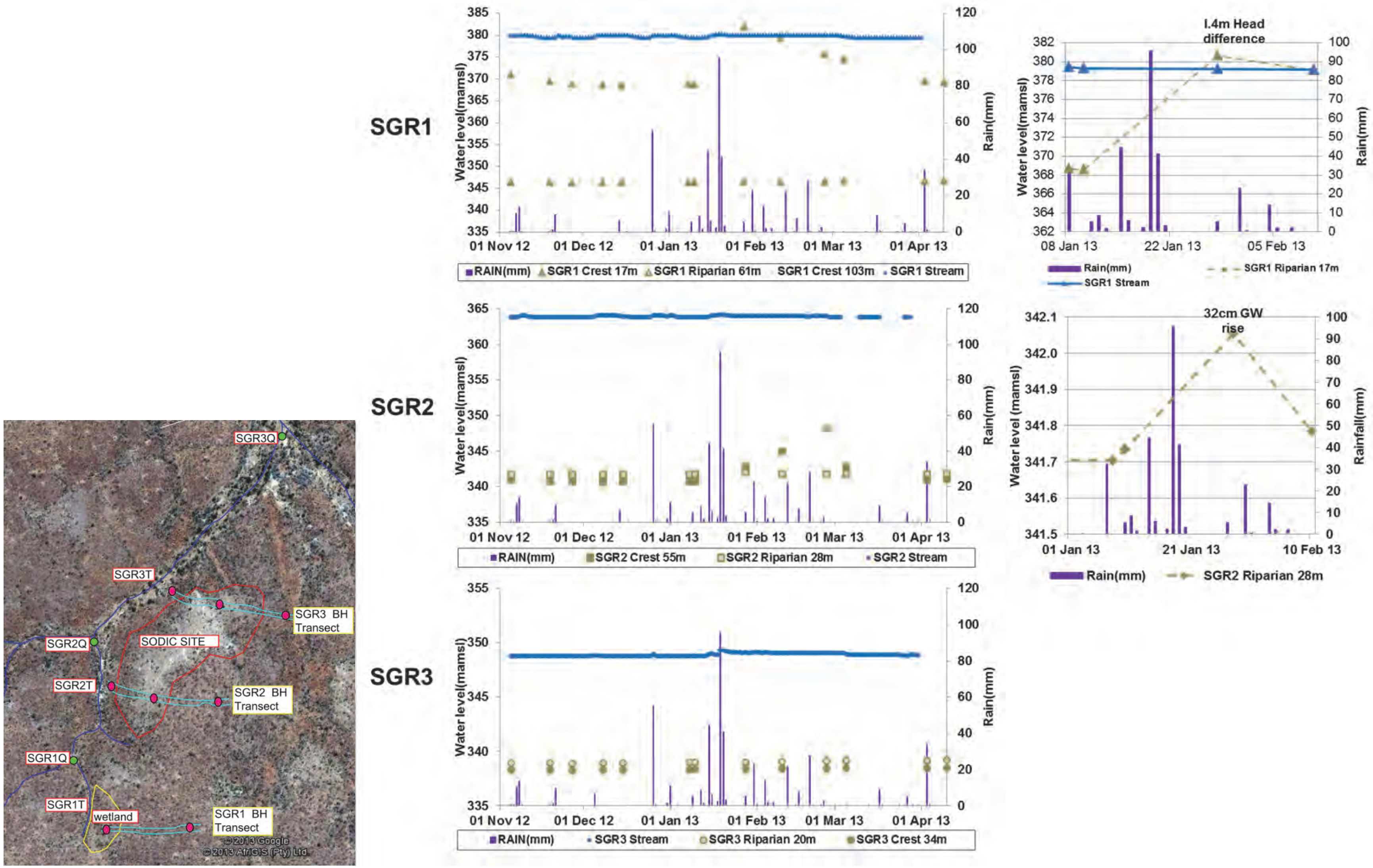

Figure 5.7: Southern Granites monitoring points map (extreme left), groundwater and stream water levels (middle) monitored from November 2012 to April 2013. Plots at the extreme right show enlarged points where responses were observed at SGR1 and SGR2 reaches (BH = groundwater; blue = stream water level; green = groundwater levels)

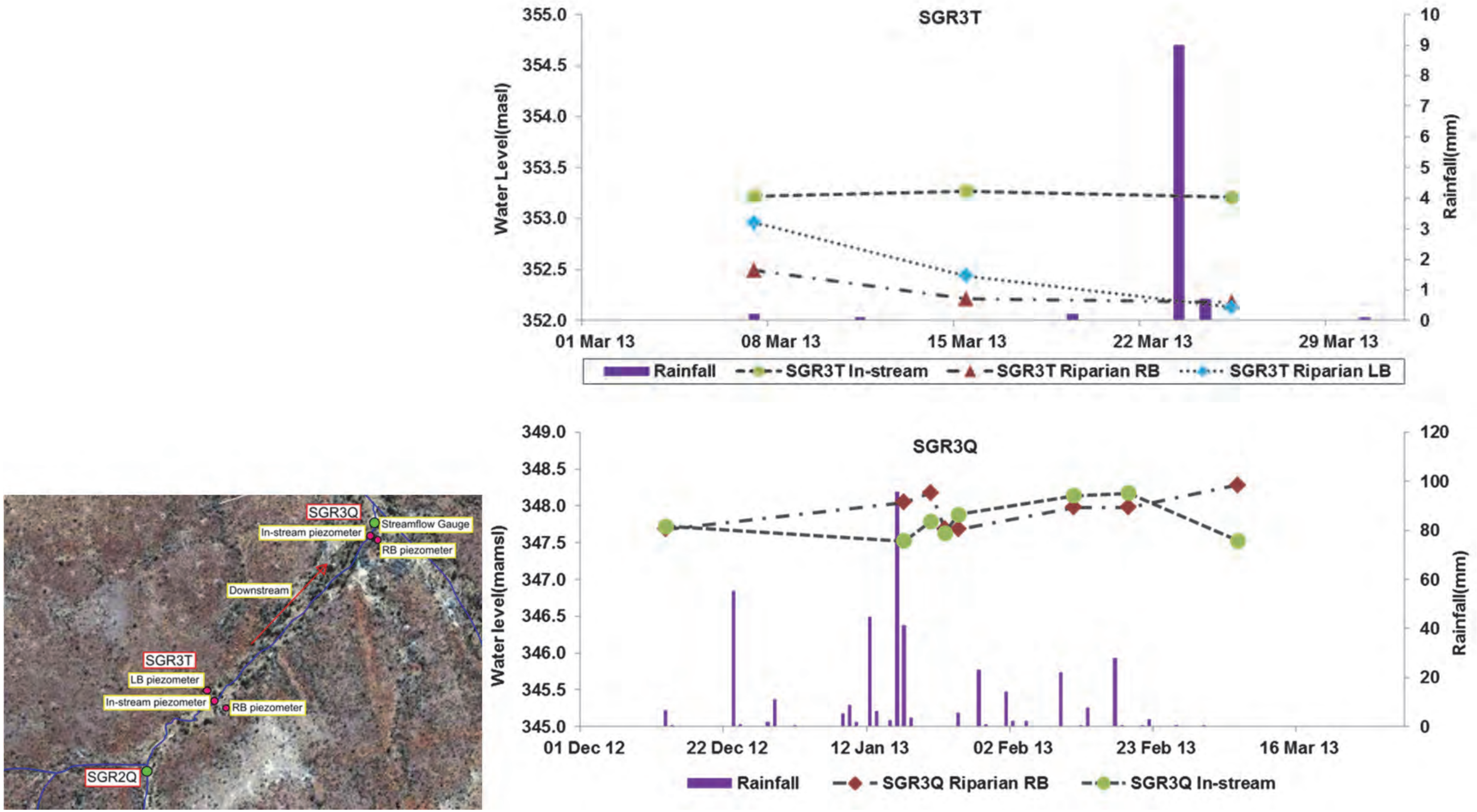

Figure 5.8: In-stream and riparian zone piezometer water levels at SGR3T during the month of March 2013 and at SGR3Q (from December 2012 to March 2013) at Southern Granites. (SGR3T refers to the hillslope hydrology monitoring transect at the 3rd order reach; SGR3Q is the catchment outlet of the same 3rd order reach; RB =right stream bank and LB = Left stream bank).

5.3 Streamflow Hydrochemistry

5.3.1 Isotopic trends in rainfall, subsurface and surface water samples

Rainfall isotopic trends were generally mimicked in most stream samples for the period from September 2012 to March 2013 at Southern Granites study site (Figure 5.9). This is an indication that event water has a significant contribution to total runoff in this catchment. For instance, samples collected on the 19th of January and 19 of February 2013 respectively, had -4.71 ‰ ; -4.77 ‰ and -3.47 ‰ ; -3.47 ‰ $\delta^{18}O$ delta values for the stream and rain respectively. Some subsurface samples across all stream scales also had close concentrations to that of rainfall (Table 5.6) indicating rapid responses from the subsurface domain. Generally the dominant influence of rainfall to runoff responses is revealed in subsequent depletion of stream samples following large rainfall events, such as the event on the 19th of January 2013 (Figure 5.9).

Physico-chemical (EC) trends in rainfall, stream and borehole water samples ranged between 50.4 µS/cm to 3640 µS/cm at Southern Granites. The highest values were recorded from groundwater, followed by stream and the lowest were from rainfall samples. Table 5.7 presents selected typical EC values for these catchments. Stream EC values dropped momentarily following large rainfall events (e.g. 95.7 mm on 19 January, 2013) showing pronounced dilution of solutes in the catchments during such wet conditions. No defined trend was observable for borehole EC values.

Hydrochemical (silica and chloride) trends in rainfall, stream and borehole water samples
Silica (SiO_2) ranged between 0.0 mg/L and 202 mg/L with streams having highest concentrations while rainfall samples had the lowest. Distinct differences in the silica concentrations were observed between boreholes, streams and rain samples. Chloride (Cl) concentrations ranged from 0.9 to 114.5 mg/L. Chloride concentrations between the three domains (groundwater, stream and rain) were also distinctly different. Since the sample concentrations in the three water sources were very distinct, it was feasible to use silica and chloride tracers for hydrograph separation. No clear cut trends within domains were observed for silica and chloride. On the 6th of December 2012, silica values were lower than they were on the 19th of January and 20th of February 2013. This is possibly due to lower moisture during early December than in the months of January and February where higher soil moisture promoted greater dissolution of silica from silicate compounds.

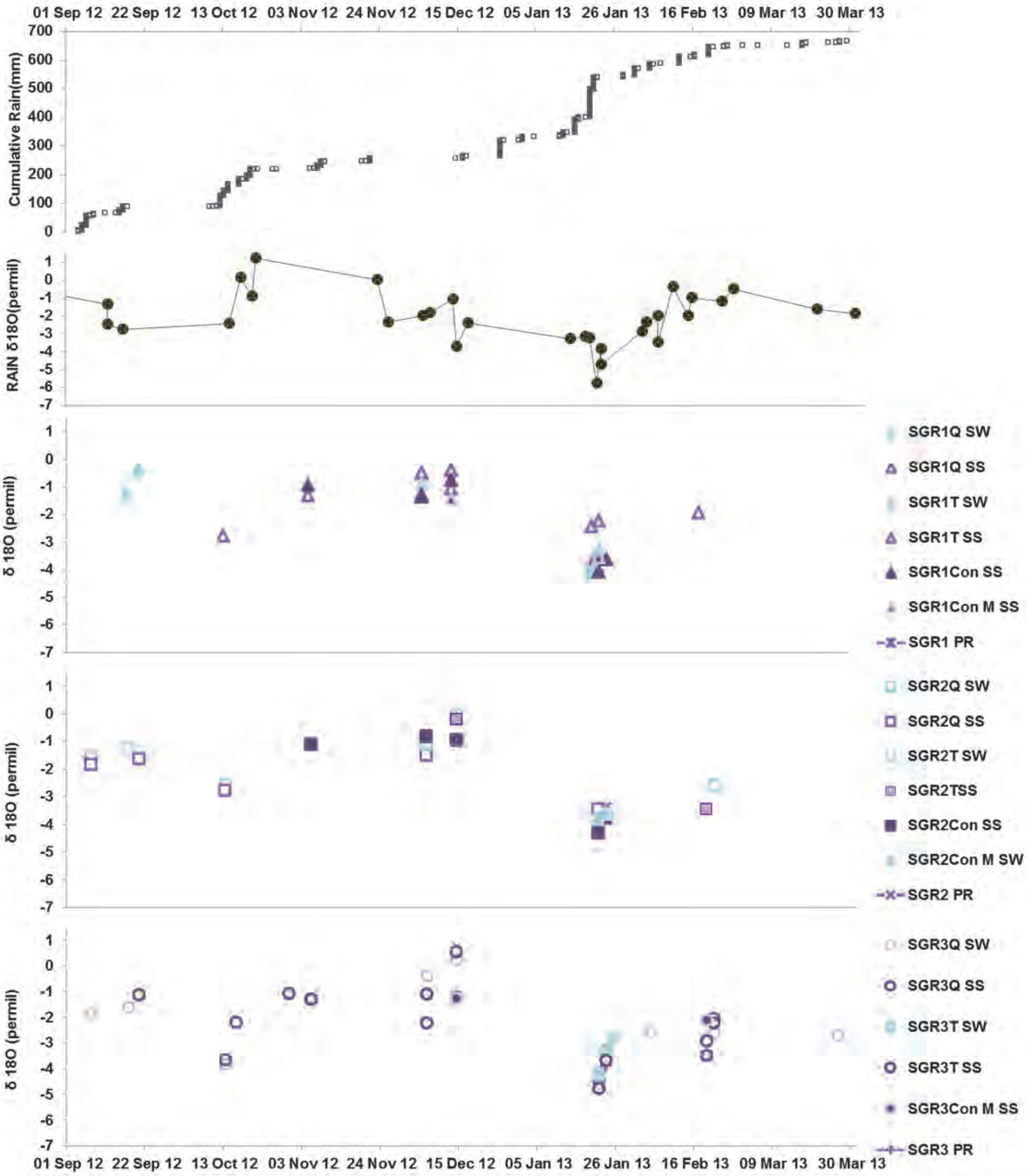

Figure 5.9: δO^{18} Isotopic trends in rainfall and stream samples at Southern Granites from September 2012 to March 2013 (Blue = surface water samples [SW}; Purple = subsurface samples [SS]; Black = rain samples).

Table 5.6: Rainfall and stream (surface[SW] and subsurface [SS]) isotopic signatures at Southern Granites for samples collected between September 2012 and March 2013

DATE	Location	Stream (permil)	Rain (permil)
17/09/2012	SGR2SS	-1.19	-1,35
13/10/2012	SGR2SW	-2.55	-2.44
25/11/2012	SGR3SS	-2.22	-2.36
13/12/2013	SGR1SS	-1.07	-1.27
19/01/2013	SGR3TSW	-4.71	-4.77
20/01/2013	SGR1SW	-3.66	-3.82
19/02/2013	SGR3SW	-3.47	-3.47

Analytical error for $\delta^{18}O$ is +/-0.3 ‰

Table 5.7: Selected typical EC (µS/cm), silica (mg/l) and chloride (mg/l) concentration ranges at Southern Granites during December 2012 to February 2013

	Borehole			Stream		Rain			
DATE	EC	Silica	Cl	EC	Silica	Cl	EC	Silica	Cl
06/12/2012	3640	9.93		103	6.98		73.8		
19/01/2013	2850	18.03	114.5	52.5	15.73	5.3	50.4	0	0.9
20/02/2013	3340	19.47		141.4	63.9		65		

5.3.2 Tracer Analysis at Southern Granites

Stable isotopes supported the hypothesis that all 1st to 3rd order reaches gain water from riparian zones at least during or immediately following rainfall events. Similar $\delta^{18}O$ values for stream and riparian zone piezometers on the 21st of January 2013 attest to this assertion. Considering an analytical error of +/-0.3 ‰ $\delta^{18}O$ values in the stream and riparian zone piezometers respectively, at SGR1 (-3.87 ‰ and -3.89 ‰), SGR2 (-3.44 ‰ and -3.41 ‰) and SGR3 (-3.66 ‰ and -3.90 ‰) support that the stream interacts with the shallow subsurface water source in adjacent footslopes (Figure 5.10 and Table 5.8). Silica and chloride concentrations in the riparian piezometers and the stream provide further support of stream-subsurface connectivity during rainfall events. For instance, on the 21st of January 2013 a sample collected from the riparian zone piezometer at SGR1 had a concentration of 9.12 mg/L which was similar (analytical error of +/-0.3 mg/L) to the stream concentration of 9.10 mg/L (Table 5.8). On the same date, chloride provided further support of stream-subsurface connectivity at the SGR2 reach where the concentrations were 4.80 mg/L and 4.29 mg/L for riparian zone piezometer and the stream, respectively. Near-surface lateral flow is the connecting mechanism as suggested by water levels in shallow piezometers (less than 3 m) that never overflowed onto the ground surface.

Interaction between groundwater and streams is isotopically supported by $\delta^{18}O$ signatures at SGR1 following the large and intense rainfall event on the 19th of January, 2013. Similar $\delta^{18}O$ signatures (-3.2 ‰, -3.27 ‰ and -3.35 ‰) for the 17 m crest borehole, the stream and the 61 m riparian borehole respectively, indicate the occurrence of groundwater-surface water interaction (Figure 5.10). Samples collected two days later, also had similar signatures (-3.52 ‰ and -3.53 ‰ for stream and borehole, respectively) confirming mixing of riparian borehole and downstream sections of the SGR1 reach. This observation tallies with the observed 1 m positive hydraulic gradient towards the stream from the 17 m crest borehole (Figure 5.7) which supports the hypothesis that this headwater reach is gaining. This shallow crest borehole does not extend beyond the weathered rock aquifer, which suggests a perched interflow pathway in weathered material overlying a consolidated hard rock of low transmissivity.

Groundwater and stream interaction at the SGR2 reach is evidenced by isotopic delta values (-3.68 ‰ and -3.66 ‰) for the 28 m riparian borehole and the stream, respectively. The similar isotopic signatures further support the combination of negative hydraulic gradients, with rapid recessions and the 30 cm riparian zone borehole water level rise (Figure 5.7) in affirming the SGR2 reach as increasingly losing to groundwater aquifers. Since water levels in boreholes on this reach have never exceeded stream water levels, the stream's hydraulic head seems to always be below groundwater levels even during rainfall events. Under such conditions, this reach can be described as having an unsaturated connection to the aquifer (Winter, 2007).

Similar tracer signatures on the 21st of January 2013, for $\delta^{18}O$ and silica in riparian zone piezometers and the stream at SGR3 support the existence of subsurface and stream water interaction. Isotopic delta values of -3.90 ‰ and -3.66 ‰ for riparian and stream samples respectively, indicate mixing of these water sources given an analytical error of +/-0.3 ‰ (Table 5.8). Silica concentrations for the same samples as above stood at 9.44 mg/L and 9.45 mg/L providing further support that the subsurface and the stream domains are hydrologically connected at this 3rd order reach (Figure 5.11).

Table 5.8: Isotopic ($\delta^{18}O$) delta values and hydrochemical (Silica & Chloride) concentrations indicating connectivity points across scales at Southern Granites study site during October 2012 to January 2013.

TRACER	DATE	LOCATION	CONCENTRATION
$\delta^{18}O$	14/10/2012	SGR2QSS	-2.76‰
		SGR2 Riparian49(49m)	-2.77‰
Silica (Si02)	14/10/2012	SGR1 Crest 17(17m)	19.38mg/L
		SGR1QSS	19.37mg/L
$\delta^{18}O$	05/11/2012	SGR2 Riparian28(28m)	-1.04‰
		SGR2Con	-1.11‰
	21/01/2013	SGR1PR	-3.89‰
		SGR1QSW	-3.87‰
	21/01/2013	SGR2PR	-3.42‰
		SGR2QSS	-3.44‰
	21/01/2013	SGR3PR	-3.90‰
		SGR3T	-3.66‰
	21/01/2013	SGR1 Crest 17(17m)	-3.2‰
		SGR1QSW	-3.27‰
		SGR1 Riparian 61(40m)	-3.35‰
Silica (Si02)	21/01/2013	SGR1PR	9.12mg/L
		SGR1T	9.10mg/L
		SGR3PR	9.44mg/L
		SGR3T	9.45mg/L
Chloride (Cl)	21/01/2013	SGR2PR	4.80mg/L
		SGR2ConMSW	4.49mg/L
Silica (Si02)	21/02/2013	SGR1	24.93mg/L
		SGR1 Crest 17(17m)	26.23mg/L
$\delta^{18}O$	23/01/2013	SGR1ConMSS	-3.53‰
		SGR1ConSS	-3.63‰
		SGR1 Riparian61(40m)	-3.52‰
	25/01/2013	SGR2ConMSW	-3.66‰
		SGR2 Riparian 28(28m)	-3.68‰

Analytical error for $\delta^{18}O$ is +/-0.3‰; for Silica is +/-0.3 mg/L and for Chloride is +/-0.3 mg/L)

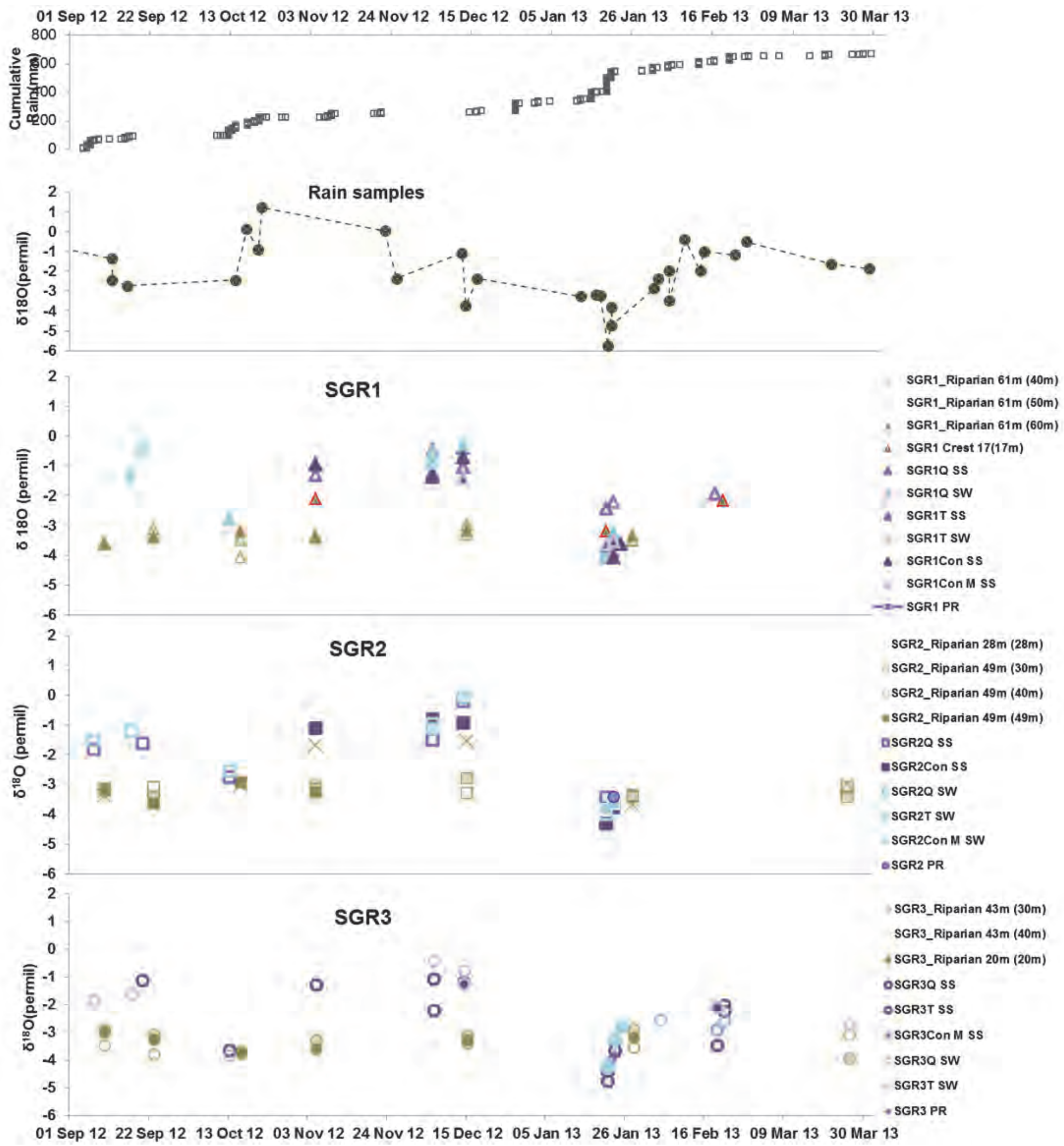

Figure 5.10: Isotopic ($\delta^{18}O$) delta values for three incremental spatial scales at the Southern Granites study site from September 2012 to March 2013 (Blue = surface water samples; Purple = subsurface samples; Green = groundwater samples).

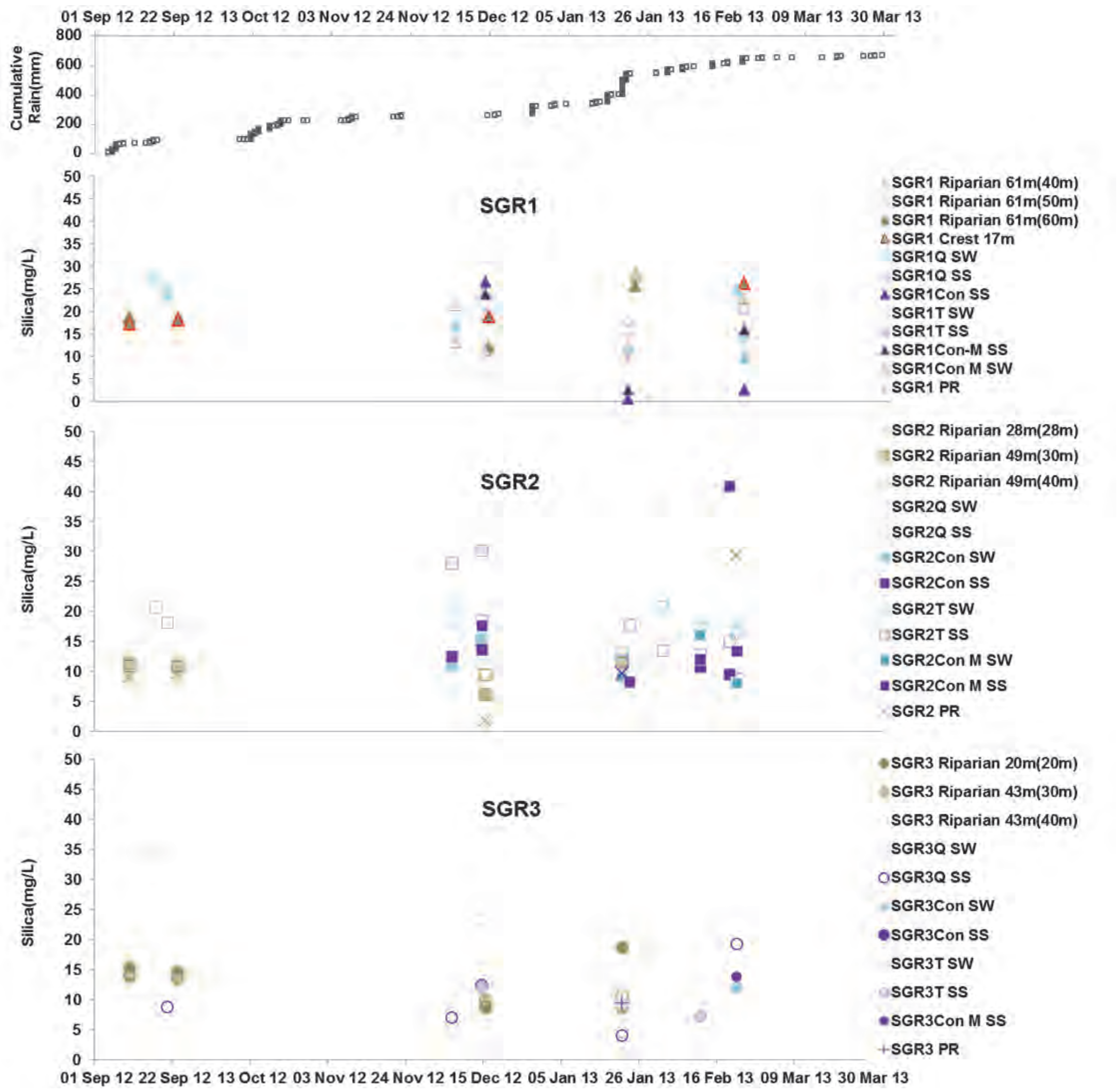

Figure 5.11: Southern Granites time series presentation of silica concentrations for three incremental spatial scales from September 2012 to March 2013 (Blue = surface water samples; Purple = subsurface samples; Green = groundwater samples).

5.3.3 Quantifying contribution of different water sources to streamflow

5.3.3.1 2 Stage Hydrograph Separation 19 January 2013

Hydrograph separation at Southern Granites relied on automatic sampling at the 3rd order reach and on grab samples for 1st and 2nd order reaches. Two high-intensity rainfall events were selected for hydrograph separation to check whether findings in one event would be similar in the other, thus increasing credibility of results. The 19 January 2013 event had 15-minute peak and mean intensities of 16.3 mm and 1.9 mm, respectively, whilst 20 February 2013 had 18.6 mm and 1.85 mm as peak and mean 15-minute intensity values. For 19 January 2013 almost 60% (56.2 mm) of this total (95.7 mm) was received in two hours. Stream discharge at the third order (SGR3Q) gauging station increased from 0.4 m^3/s to

6.5 m^3/s which marked the peakflow for this event. 20 February 2013 had a duration of 4 hours which totalled 27.9 mm, 84% of which fell in only one hour. Subsequent discharge at SGR3Q increased from 0.001 m^3/s at start of event to 0.136 m^3/s at peakflow.

Component contributions of different sources were first estimated by lumping sample concentrations from each source to give typical end member values (Lorentz et al. 2008). The end members calculated as volume averaged delta values for rainfall, runoff and the groundwater source were set at -5.40‰, -4.96‰ and -3.38‰, respectively. On an $\delta^{18}O$ and δD plot the runoff end member lies very close to rainfall and further away from the groundwater end member signifying more event water contribution to total runoff (Figure 5.12). A linear interpolation between the end members showed event water contribution of 84% while the pre-event estimate stands at 16% (See Appendix V). It is perceived that the SGR3 riparian zone contributes this 16% by soil interflow, being augmented by near-surface macropore flow as connecting mechanisms.

To verify interpolated estimations, two-component hydrograph separations were also done by solving mass balance equations for water and tracers (Uhlenbrook and Hoeg, 2003; Sklash and Farvolden, 1979). The analysis was done using $\delta^{18}O$, EC and Si as tracers. Isotopic ($\delta^{18}O$) results for 19 January 2013 showed an overall event water contribution of 84% while pre-event contribution was estimated at 16% (Figure 5.13). The progression of the rising limb of the hydrograph showed domination of event water contribution reaching 93% at peakflow. Thirty minutes into recession the storm runoff comprised 100% event water which thereafter gradually dropped to 75% before flows subsided. Conversely pre-event contribution decreased from 51% to 7% at peakflow and then further dropped to 0% thirty minutes into the recession limb. Thereafter, a gradual increase was noticed until it got to 25% before flow subsidence. The fact that the onset of streamflow was marked by a significant 51% of pre-event water emphasizes the importance of antecedent soil moisture conditions for runoff generation in this catchment. Overall results with silica as a tracer tallied with isotopes at 84% (event water) and 16% (pre-event water), while EC values for the same water sources were 86% and 14%, respectively. Result details for silica and EC are presented in Appendix V.

As was observed at the third order catchment scale, event water also dominated lower order streamflow hydrographs (Figure 5.14). At SGR1 event water contribution was estimated at 71% and 67% using EC and $\delta^{18}O$, respectively. Respective estimations of the contribution of event water using EC and $\delta^{18}O$ at SGR2 were 76% and 70%. It is noteworthy that the percentage contribution of event water is incremental with increasing catchment size. The estimated event water contributions are higher across scales thereby supporting and verifying hydrometric findings which showed that streamflows at the Southern Granite supersite are purely intermittent and event-driven. On the other hand, an inverse trend exists for pre-event water whose contribution decreases towards higher order reaches (SGR1: EC = 29%, $\delta^{18}O$ = 33%; SGR2 EC = 24%, $\delta^{18}O$ = 30%; SGR3 EC= 14, $\delta^{18}O$= 16). The highest pre-event water contribution at SGR1 relative to higher order reaches further supports that this reach is gaining from groundwater.

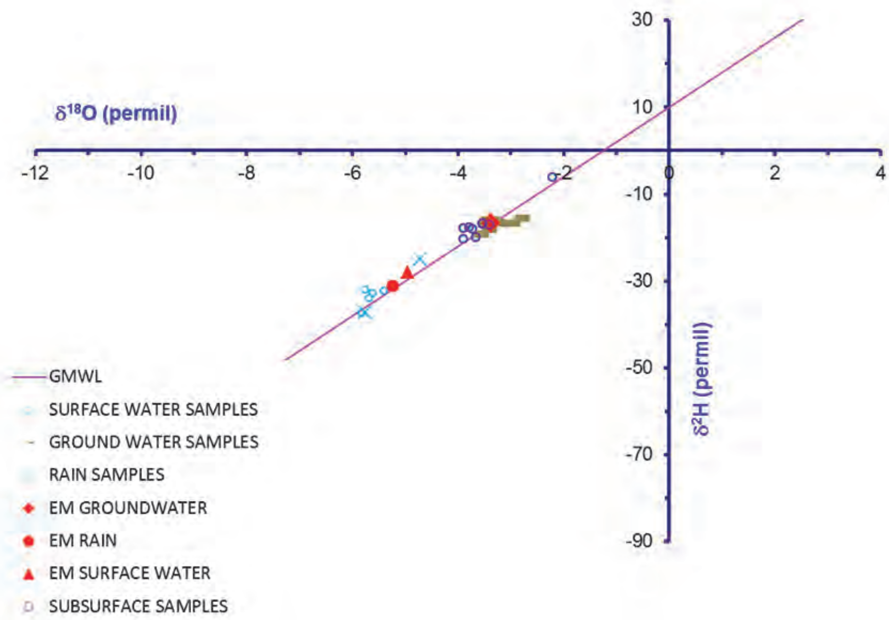

Figure 5.12: Isotope data for samples collected following the January 19, 2013 rainfall event at the 3rd order catchment of Southern Granites Supersites.

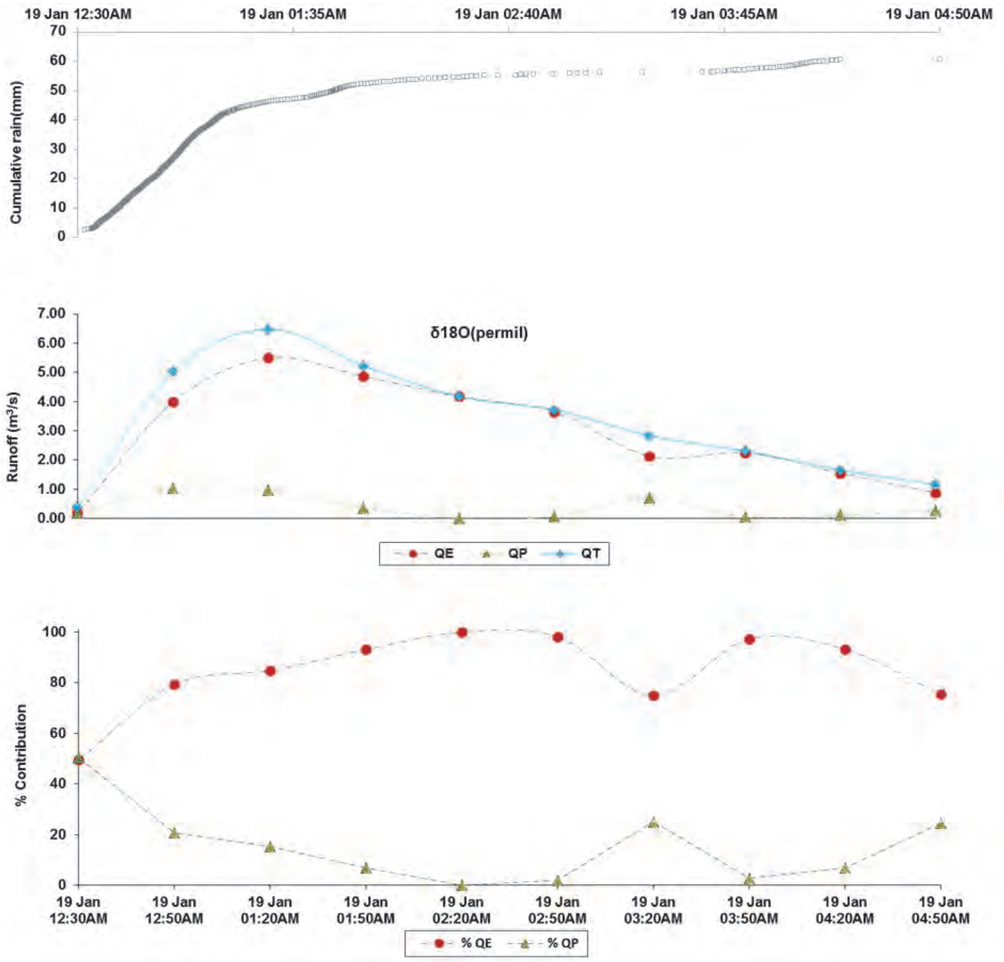

Figure 5.13: Two component hydrograph separation for 19 January 2013 at the 3rd order of Southern Granites showing rainfall, component and total stream runoff, and percentage contributions of event and pre-event water to total runoff. QT = total runoff; QE = Event water contribution; QP = Pre-event water contribution; %QE and %QP = percentage contributions of event and pre-event water, respectively.

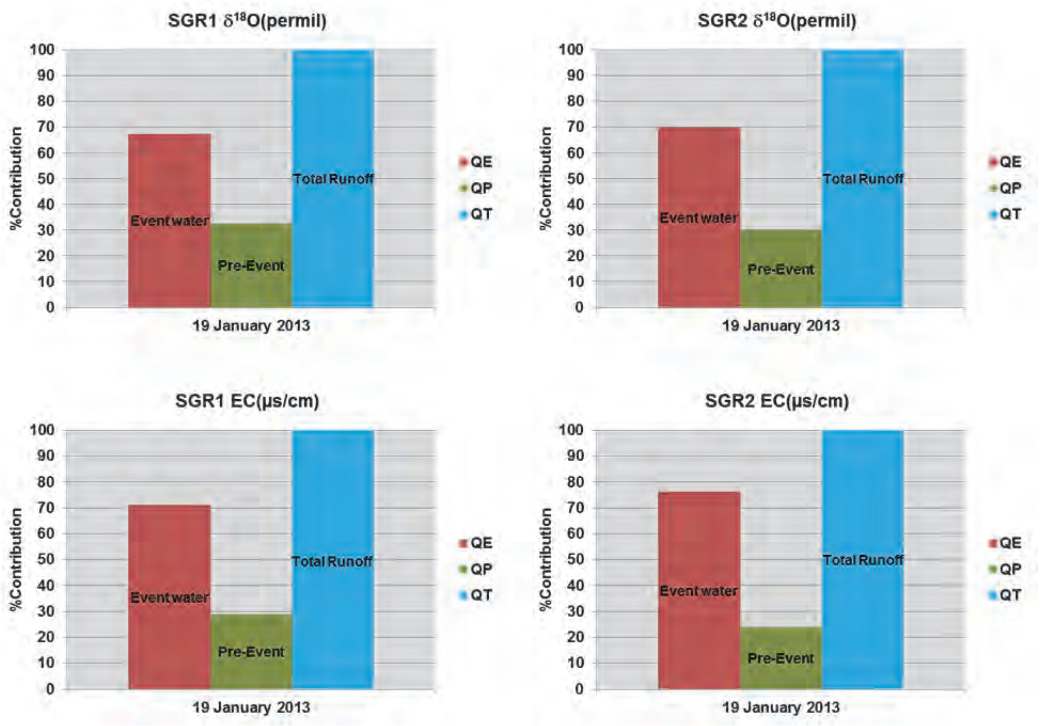

Figure 5.14: Contribution of event and pre-event water to total runoff at SGR1 & SGR2 reaches at Southern Granites using δ18O and EC as tracers for the event of 19 January 2013

5.3.3.2 2 Stage Hydrograph Separation 20 February 2013

The volume averaged end members for 20 February 2013 were set at -1.53, -2.14 and -3.10 for rain, runoff and groundwater samples, respectively (Figure 5.15). Respective interpolated estimates for event water and pre-event water contributions to total runoff were 64% and 36%. The significance of event water contribution to streamflow was further supported.

To further verify the above observations, a two component hydrograph separation using mass balance calculations for water $\delta^{18}O$ as tracer were conducted (Figure 6.16). Overall event water contribution was estimated at 75%, while pre-event contribution constituted 25%.

Two-component hydrograph separations for this event similarly confirm the dominance of event water in total streamflow at this study site. Using $\delta^{18}O$ as tracer, event water contributions at SGR1and SGR2 were estimated at 64% and 60%, respectively, with corresponding 36% and 40% for pre-event water (Figure 5.17). The increasing trend of event water contributions noted during 19 January is not repeated in 20 February. The size of the event seems a probable explanation to the contrasting observations. In terms of magnitude, the 19 January event (95.7 mm) was more than three times the size of that of 20 February (27.9 mm), although the latter was more intense than the former. Looking at these figures suggests that though rainfall intensity is necessary for stream network connectivity, it is the size of the event that determines the extent of pre-event water contribution to total runoff. Larger and more intense rainfall events result in higher event-water percentage contribution to streamflow than smaller events.

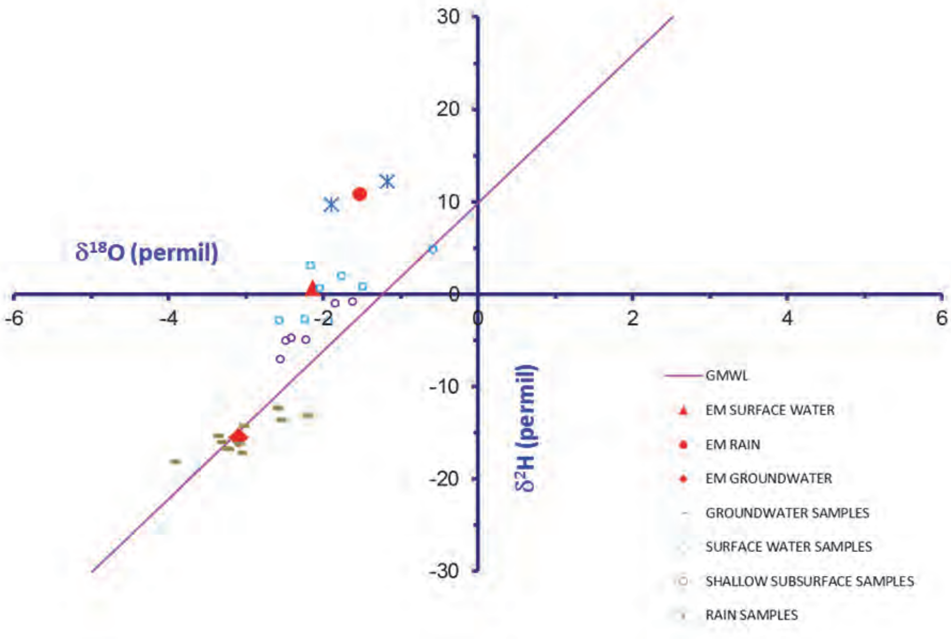

Figure 5.15: Isotope data for samples collected following the February 20, 2013 rainfall event at the 3rd order reach of Southern Granites study site. EM =End Member; GMWL = Global Meteoric Water Line.

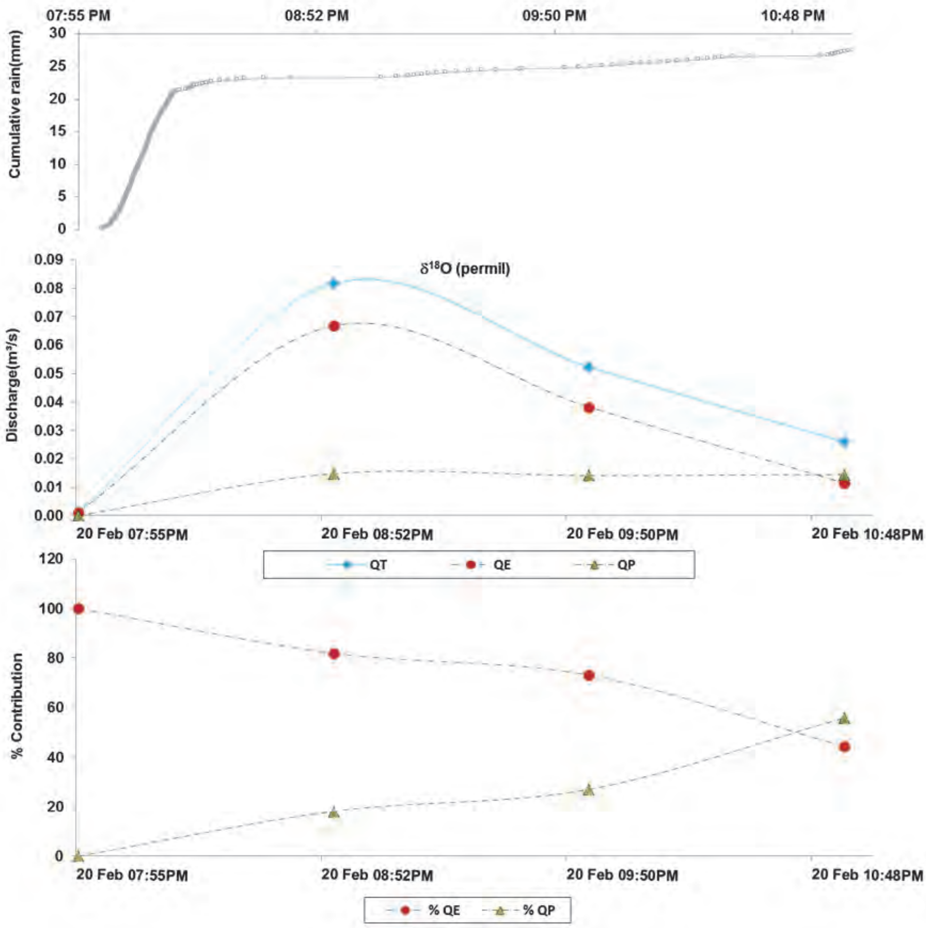

Figure 5.16: Two component hydrograph separation for 20 February 2013 at the 3rd order of Southern Granites showing rainfall, component and total stream discharge, and percentage contributions of event and pre-event water to the stream. QT = Total streamflow; QE = Event discharge; QP = Pre-event discharge; %QE and %QP = percentage contributions of event and pre-event water respectively.

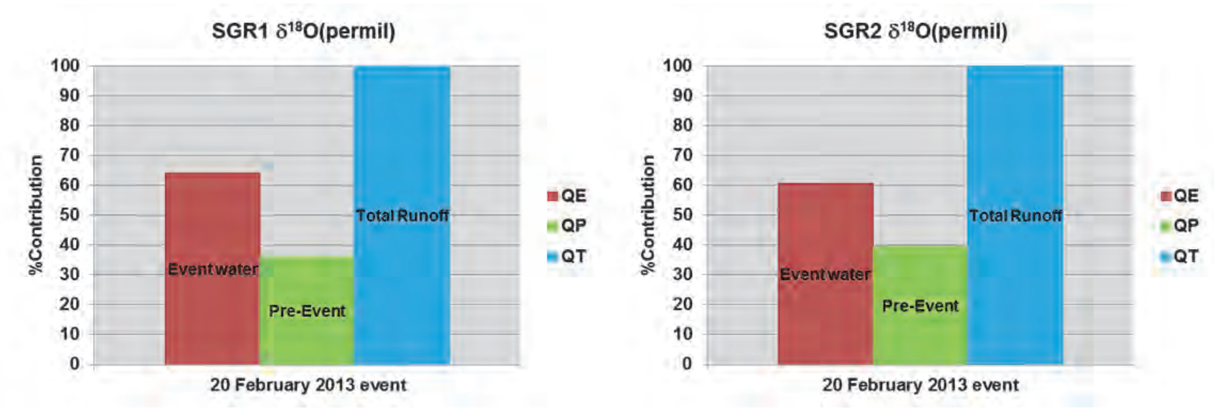

Figure 5.17: Contribution of event and pre-event water to total runoff using $\delta^{18}O$ as tracer for the event of 20 February 2013 for SGR1 and SGR2 at Southern Granites site.

5.3.3.3 3 Stage Hydrograph Separation 19 January 2013

After the contribution of groundwater at SGR1 was tested through hydrometry and tracers the partitioning of stream runoff into three components was conducted. Mass balance equations for two tracers (EC and $\delta^{18}O$) and water were solved for incident rain, groundwater and subsurface water as components to total runoff (Figure 6.18). Incident rain was estimated at 34% while subsurface and groundwater, were estimated at 40% and 26% respectively. The three component hydrograph separation revealed that the high event water contribution (67% with $\delta^{18}O$ as tracer) obtained in the two component separation for this reach and event comprised a significant amount of rapid response subsurface flow in addition to the 34% direct channel precipitation. The connecting mechanism for the rapid response subsurface flow to the stream was clearly through near-surface macropores created for instance, by tree roots and animal burrows in this mixed savannah woodland catchment. These macropores allowed the subsurface water to quickly reach the stream while still retaining similar or very close chemistry to that of the incident rainfall.

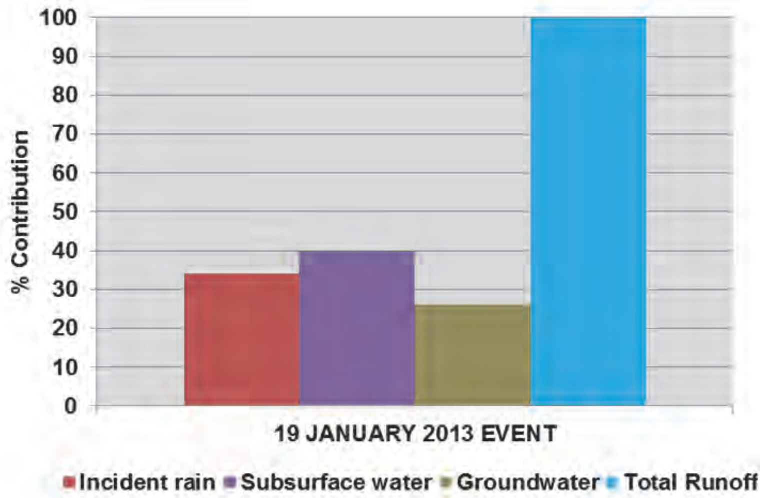

Figure 5.18: Three component hydrograph separation at the 1st order reach (SGR1) of Southern Granites study site for the 19 January 2013 rainfall event.

5.3.4 Stream Network Connectivity at Southern Granites

The fact that stream network connectivity is event-driven was revealed by time series plots of rainfall and discharge across spatial scales that are based on stream orders. However, contributions of tributaries draining into the main channel at incremental sub-catchments during events were not known. End member mixing analysis (EMMA) using mass balances for water and tracer were calculated to quantify these contributions. The results are presented in Table 4.9 while calculation details are presented in Appendix A5.3.

The presence of flows at all scales in tributaries and the main channel supports that stream network connectivity occurs during rainfall events. Runoff at gauging stations show incremental change with increasing contributing areas on the 19th of January 2013. However, on 20 February 2013, a reduction of runoff (0.6%) is recorded at SGR2 relative to SGR1. This is attributed to transmission losses at SGR2 details of which have already been presented in earlier sections. The large size of the 19 January event (95.7 mm) initially masked transmission losses at SGR2 at least during the event itself which however, manifest through rapid recession as already explained. The third order reach (SGR3) shows a 1.39% increase in discharge possibly due to its larger contributing area with more tributary inflows and less transmission losses relative to SGR2

Table 5.9: Estimated tributary runoff and corresponding percentage contributions to the main channel flows at Southern Granites on the 19th of January and 20th of February 2013. Discharges in brackets were observed at gauging stations.

Subcatchment	Reach	19 JANUARY 2013		20 FEBRUARY 2013	
		Mean Runoff (m^3/s)	Contribution (%)	Mean Runoff (m^3/s)	Contribution (%)
SGR1	SGR1Q (main channel)	(0.0218)	10	(0.0126)	11
	SGR1 Tributary	0.1963	90	2.8146	89
	SGR1 Confluence	0.2182	(Total) 100	3.1624	(Total) 100
SGR2	SGR2Q (main channel)	(0.1302)	97	(0.00078)	78
	SGR2 Tributary	0.0040	3	0.00022	22
	SGR2 Confluence	0.1342	(Total) 100	0.00012	(Total) 100
SGR3	SGR3Q (main channel)	(0.6688)	40	(0.0562)	30
	SGR3 Tributary	1.0000	60	0.0856	70
	SGR3 Confluence	1.6700	(Total) 100	0.1223	(Total) 100

5.4 Southern Granite 1st order hillslope

5.4.1 1st order Geophysics

Figure 5.19 shows the initial and revised (following borehole drilling) interpretation of the 1st order geophysics traverse, where the unsaturated zone across the profile had an interpreted depth of 8 m with variable moisture contents due to the changes in low resistivity (3-75 Ω/m) values across the profile at shallow depths. The estimated groundwater level was expected to be approximately 8-10 m across the profile. The riparian zone was estimated to have deep weathering which then decreases in depth towards the crest due to shallower depths of high (1875-5484 Ω/m) resistivity material there. Two boreholes were drilled at the riparian zone as saturated condition were expected to occur at two distinctive depths namely the weathered/unsaturated zone and hard rock/saturated zone given the difference in resistivity in the shallow (3-75 Ω/m) and deep (1875-5484 Ω/m) subsurface. The close banding of resistivity 219-641 Ω/m at 20-25 m depth across the hillslope suggests a possible interface zone between the weathered and hard rock granite. The crest also had two boreholes as it was estimated that two zones occur such as the high resistivity values (1875-5484 Ω/m) of hard rock/saturated zone and low resistivity values (7-75 Ω/m) of weathered/unsaturated zone annotated on the profile.

The final interpretation following drilling revealed that the 1st order hillslope exhibits a low permeability weathered granite aquifer and relatively high permeability hard granite rock aquifer at the crest. This is due to the shallow 17 m borehole being drilled dry and the deep 103 m borehole having a blow-out yield of 1.25 L/s (see Appendix VI). This suggests that the hard rock aquifer is more permeable and is likely to be an active groundwater flow system at this point. The T values discussed later in this section will verify a more active groundwater flow system in the crest position 103 m borehole. The weathered aquifer/perched water table at this point is likely to be an inactive groundwater flow system as it was drilled dry and owed to the low T values discussed later. Therefore the weathered aquifer can be seen as an ‘unsaturated reservoir’ owing to its low permeability and this would temporary store groundwater.

The borehole logs for the 1st order boreholes confirm the initial ERT interpretations that deeper weathering occurs at a depth of 25 m at the riparian zone and shallower weathering of a depth of 21 m at the crest (see Figure 5.19). The two water strikes encountered at the 1st order crest position 103 m borehole indicate a high yielding borehole which concurred with the final blow out yield of 1.25 L/s, whereas the one water strike at the 1st order riparian position 61 m borehole yielded a final blow out yield of 0.07 L/s (see Appendix A6.3). These water strike depths are consistent with fluid log profiles indicating the presence of fractured or flow zones (Appendix VI). These blow out yields indicate that the crest hard rock groundwater flow system is likely to be more active than the riparian groundwater system.

Figure 4.20 shows a time-series geophysics analysis of 1st order hillslope, where two key aspects may be observed. First a geological control (A) appears between the midslope and crest, this is signified by a vertical band of high resistivity material emerging to the surface. This is an important observation and could be used to explain the apparent perched groundwater responses seen in the 17 m borehole at the 1st order crest (refer to sections). Second, is the observed reduction in resistivity, particularly in the riparian zone (B) as well as the footslope region between January and March 2013. Here it is interesting to note that the region below 350 masl does not immediately see a drop in resistance as a result of the significant rains of mid-January. Neither does there appear to be ponding as a result of this event. This suggests that vertical movement between the vadose zone and groundwater is dominantly a slow matrix driven process rather than a direct contribution through fractures.

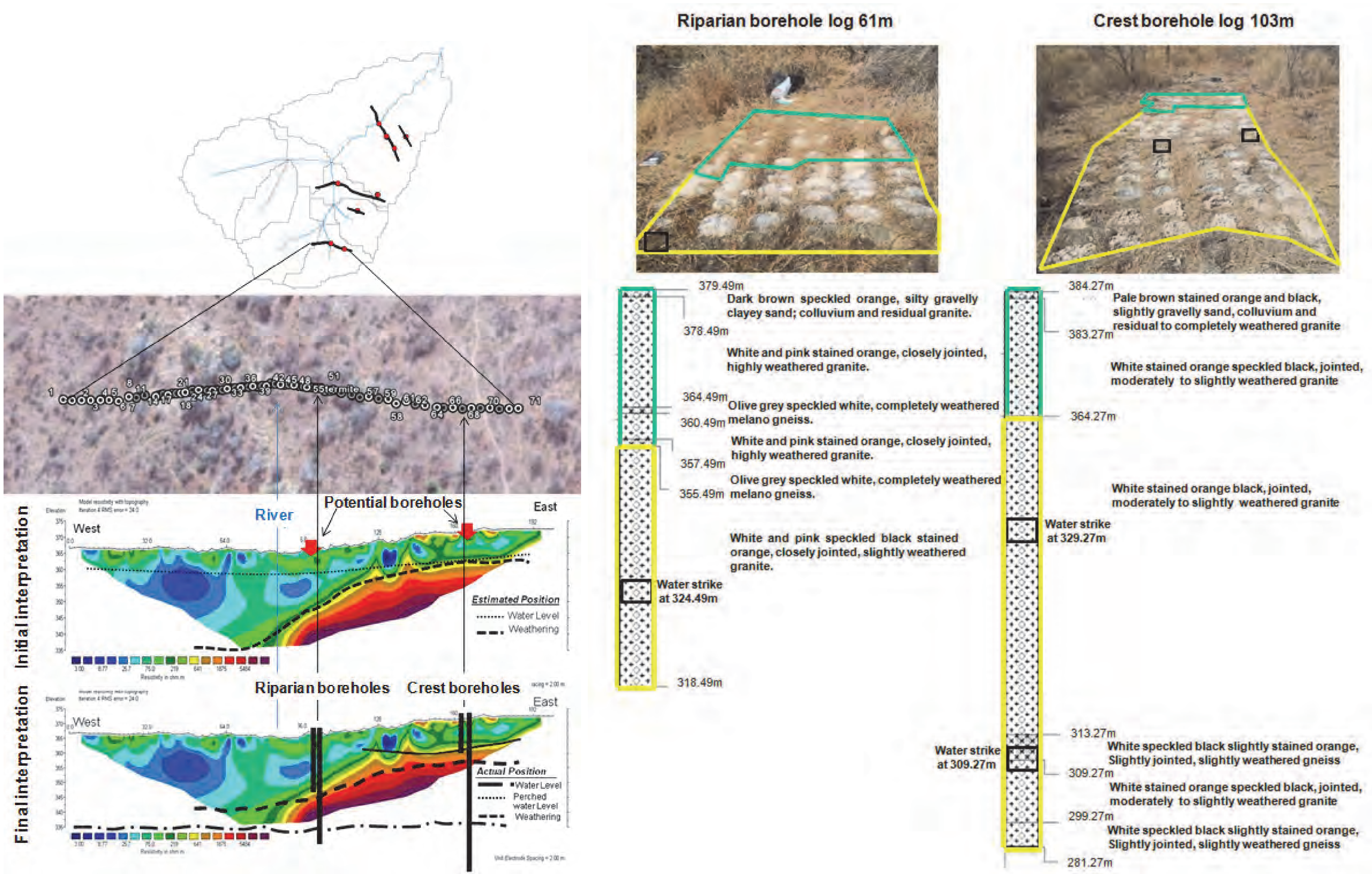

Figure 5.19: Initial and final interpretation of 2D ERT traverses coupled with topography data, satellite imagery and estimated and actual positions of groundwater level and weathering (left), Borehole lithology log of the southern granite 1st order riparian 61 m and crest 103 m boreholes, the green highlighted section indicates weathered material, the yellow highlighted section indicates hard rock material and the black blocks indicate water strike positions (right).

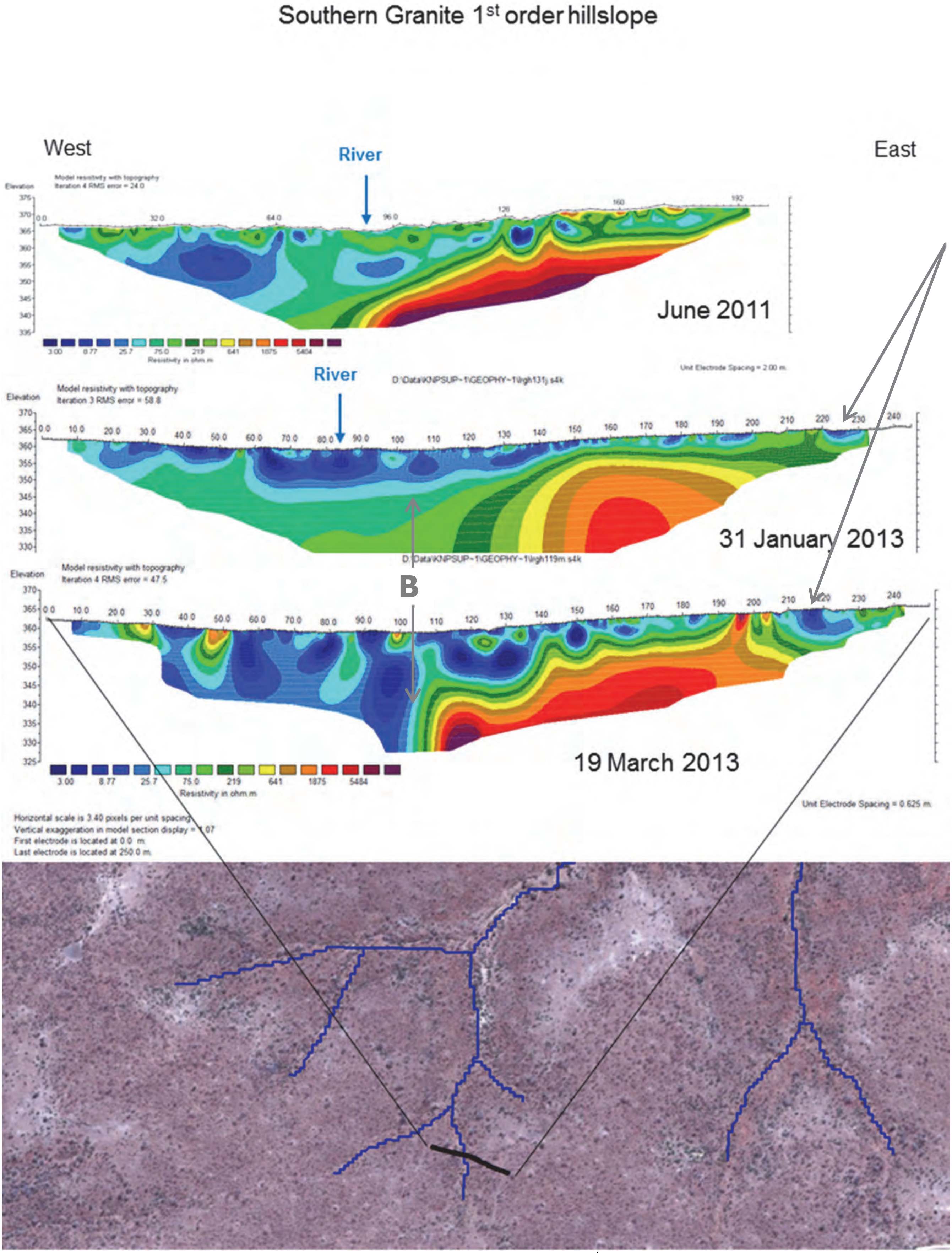

Figure 5.20: Time-series geophysics transect southern granite 1st order hillslope

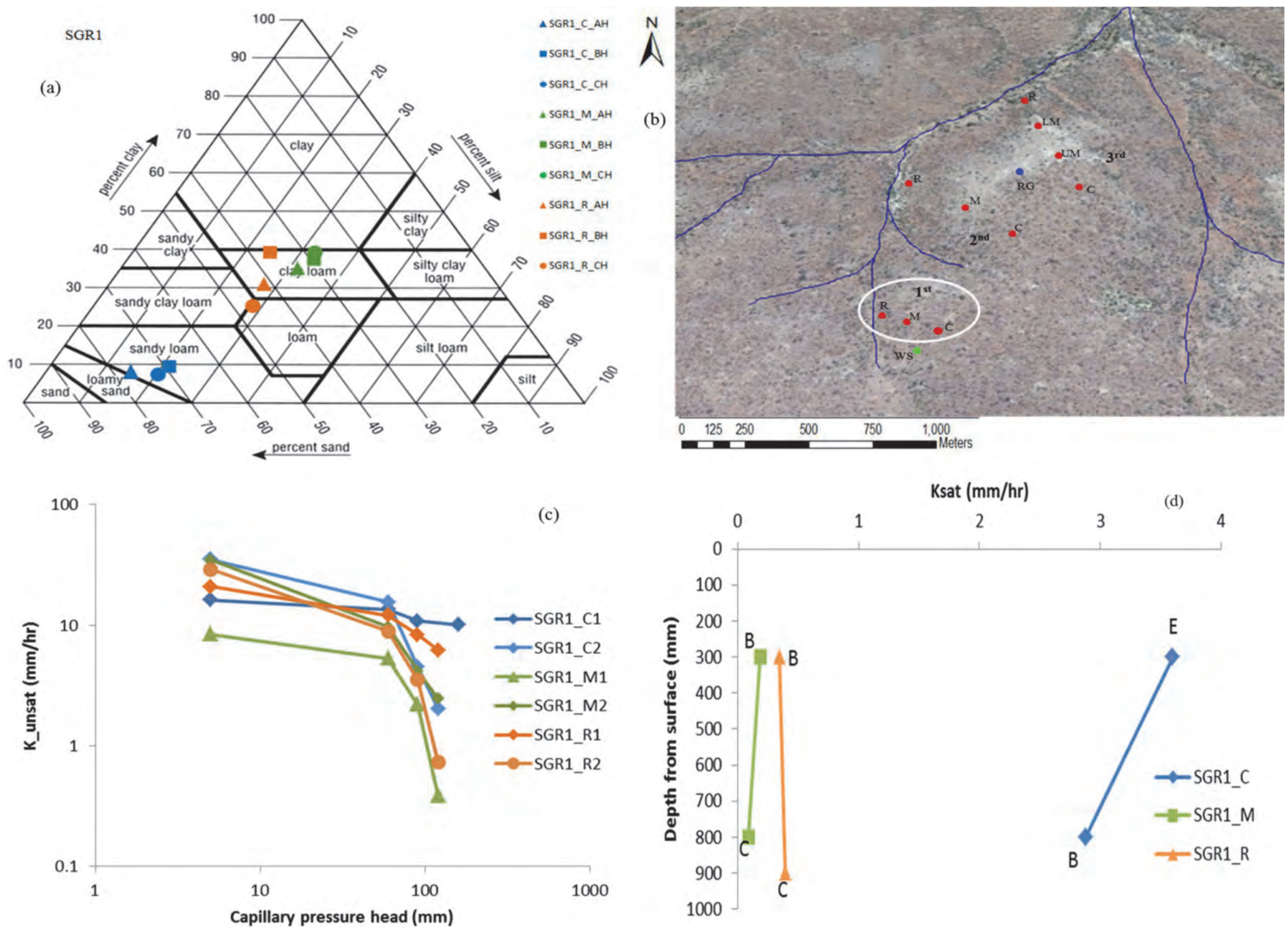

Figure 5.21: (a) Soil texture triangle (b) site map (c) K_{unsat} at soil surface (d) K_{sat} per soil horizon on southern granite 1st order hillslope

Table 5.10: Soil classification per catena element on granite 1st order hillslope

Catena Element	Taxonomical class	Diagnostic Horizons	Hydrological soil type
SGR1_Crest	Cartref	Orthic A	Interflow
		E	
		Lithocutanic B	
SGR1_Mid	Bonheim	Melanic A	Interflow
		Pedocutanic B	
		Unspecified	
SGR1_Rip	Bonheim	Melanic A	Interflow
		Pedocutanic B	
		Unspecified	

5.4.2 1st order shallow unsaturated zone characterization and responses

Soil texture, Kunsat and Ksat measured on the 1st order hillslope is shown in Figure 5.21. This hillslope comprises crest soils with high Kunsat at low pressure head (34 mm/hr at φ=5 mm) on the surface compared to the lower slopes (midslope and riparian catena elements). This element comprises sandy loams therefore high Kunsat was anticipated. The midslope and riparian catena elements show low Kunsat on the surface especially at high pressure heads (0.4 mm/hr and 0.7 mm/hr at φ =120 mm respectively). This is attributed to the clay loams encountered at both these catena elements. Clay particles are washed downslope through colluviation hence the low Kunsat measurements on these catena elements.

The crest element also has high Ksat compared to the catena elements down slope. The midslope has the lowest Ksat on this hillslope (0.08 mm/hr) due to the clay loams encountered on this catena element throughout the whole profile.

The 1st order crest is classified as a Cartref soil form (Table 5.10). The presence of an illuviated E horizon over a fine textured B horizon in this soil form implies the possibility of a perched water table forming (van Tol, 2008). This is supported by the low Ksat on the B horizon (2.8 mm/hr) underlying the E horizon on this element. This implies interflow at the AE/B interface. Therefore lateral contributions to downslope elements are expected and thus potential hydrological connectivity through lateral subsurface flow between the crest and the midslope.

The Midslope and riparian catena elements are classified as a Bonheim soil forms (Table 5.10) and they both show low Ksat (0.08-0.4 mm/hr) on the B and C horizon. They both have the same hydrological soil type (interflow soils) based on hydropedological field surveys (this does not necessarily mean all Bonheim soils are interflow soils). The presence of interflow soils from the crest down to the riparian implies potential connectivity between catena elements through subsurface lateral flow. Potential connectivity is therefore anticipated between the hillslope and the stream network.

The 1st order crest profile responds to all the rainfall events (Figure 5.22). Responses in all horizons show a more or less similar trend throughout the season showing no significant differences in wetting and drying cycles. The profile was close to saturation (<1000 mm) as a result of most of the rainfall events although the % ED data shows that these soils were dry (>1000 mm) for more than 60% of the time. Important to note is that there is no sensor in the C horizon. These quick responses shown at this catena element implies vertical subsurface flow but hydropedology and Ksat data show some flow restriction in the C horizon therefore interflow is anticipated.

The midslope full profile responded to the first rains (September 2012). The deep soil layers (depth= 450 mm) and the shallow soils (100 mm) show a quicker drying cycle. The intermediate layer (depth=300 mm) dries out last for most of the events and this is due to the presence of fine textured soils. The shallow soils dried out for the greater part of November and March probably due to a high evaporative demand from the soil surface during those periods whilst the other soil layers retained some moisture. % ED shows that for about 50% of the time, this profile remained relatively close to saturation (at <1000 mm). From field observations, whilst this data is suggesting moisture storage for approximately 50%of the time on the crest and midslope, the absence of ponded conditions suggests subsurface flow. These responses therefore show that it is quick interflow and this supports the hydropedological classification (Table 5.10) for this hillslope.

The riparian catena element on this first order hillslope shows a response to the early rains from the shallow and intermediate soils (rapid wetting cycle) whilst the deeper soil layers in the C horizon (depth=1000 mm) show a lag of two months then finally responds at the beginning of December season. This is due to either soils having low hydraulic conductivity deep in the profile evident in Figure 5.21 and/or the water being lost to ET before it could get deep into the profile. Overall, the riparian catena element retains moisture (<1000 mm) for about 40% of the entire season mostly in the shallow and intermediate layers whilst the deep layers were relatively dry (>1000 mm) for the greater part of the season. This therefore shows that the upper horizons are wet areas compared to the deep soil layers that are hydrologically disconnected most of the time.

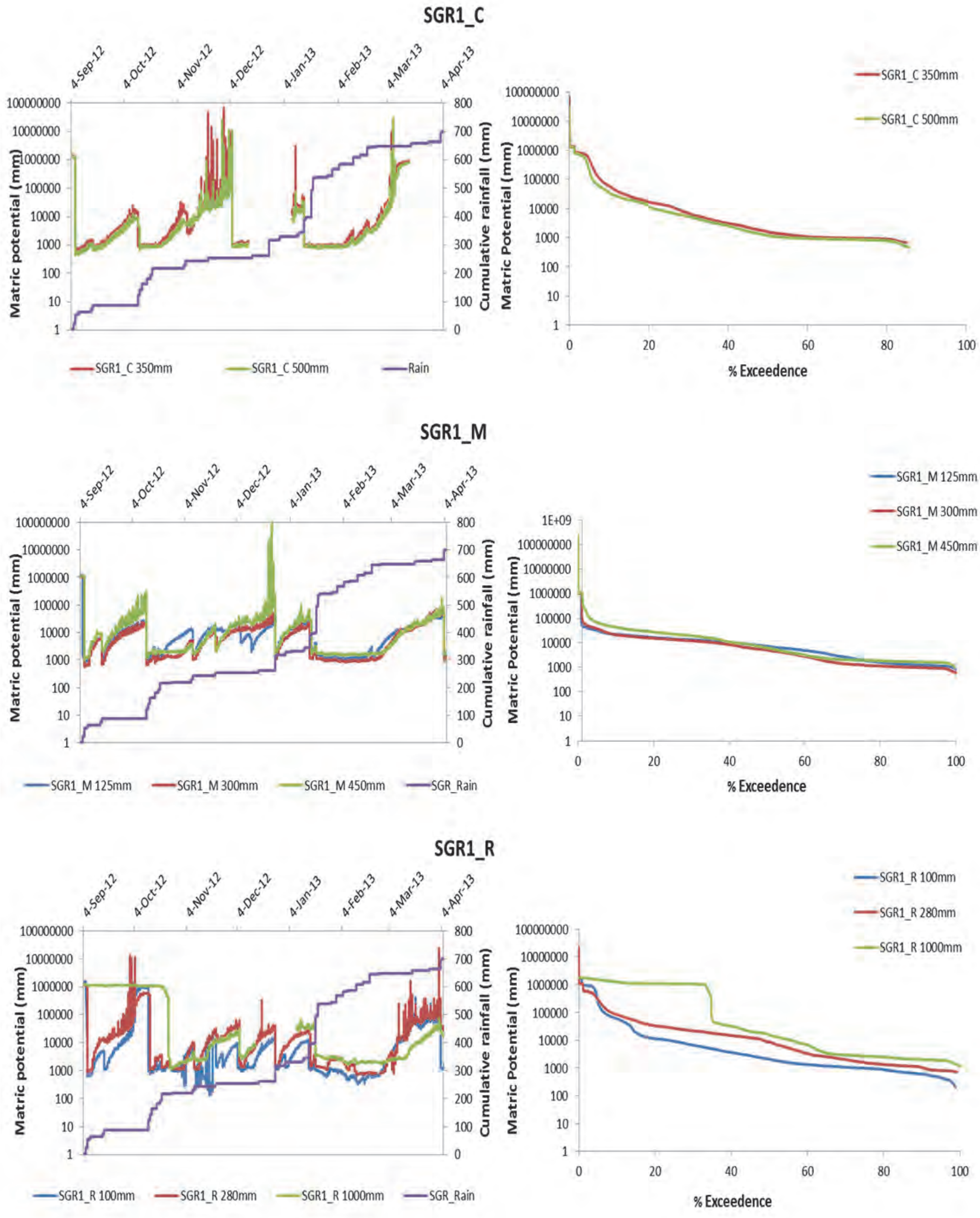

Figure 5.22: Soil matric potential responses and % ED curves along the southern granite supersite first order hillslope between September 2012 and April 2013

Hillslope Class 6: Quick Interflow

This hillslope is characterized by quick interflow soils (Figure 5.23). The majority of soils on the catena elements that make up this hillslope show indications of lateral flow at the A/B interface i.e. at the crest, the absence of ponding water suggests infiltration of water into the subsurface but flow is restricted in the lithocutanic B horizon underlain by an E horizon (Table 5.10) therefore interflow at the A/B interface results. Although some potential recharge is expected here during exceptional events. As this water moves downslope into the midslope, it continues to flow laterally. Judging from field observations, the riparian soils sometimes become responsive due to infiltration excess from direct precipitation but only after exceptional events. According the van Tol et al. (2013), the rate of lateral flow mainly depends on the gradient of the slope and this means therefore this 1st order hillslope has quick interflow compared to the 2nd and 3rd order hillslopes since it has a steeper slope than the higher orders. There is a high probability of lateral subsurface connectivity with the adjacent stream network but less hillslope storage is expected due to the quick interflow.

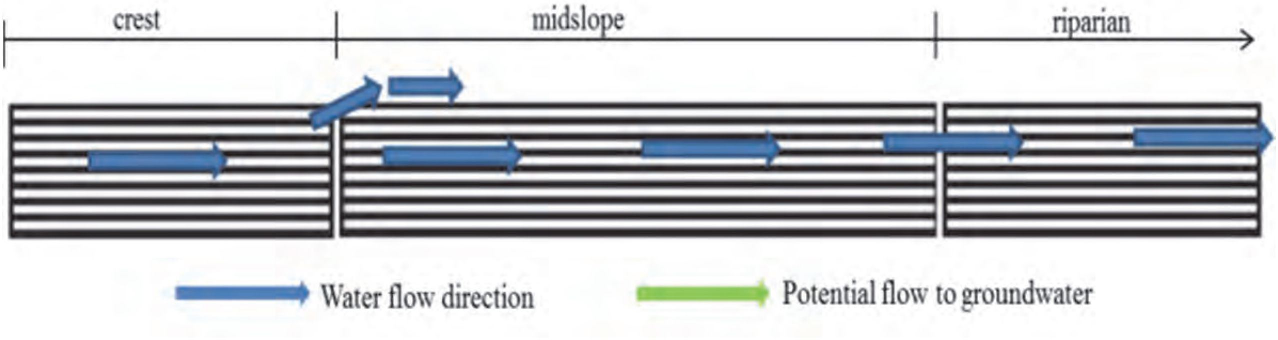

Figure 5.23: Hydrological soil types and conceptual flow paths for granite 1st order hillslope

5.4.3 1st order Hydrogeology: Hydraulic Responses and Parameters

To gain understanding of the trend in groundwater levels in response to rainfall, each nested piezometric (shallow and deep) borehole water level within a particular catenal element was plotted against rainfall. From this one is able to infer flow gradients and possible processes identified such as groundwater recharge, discharge and interflow.

The hard rock deep groundwater level can be seen in Figure 5.24 and the weathered shallow groundwater level can be seen in Figure 5.25. These two water levels have more than 20 m difference in depth to water level suggesting the presence of a perched water level in the shallow weather zone as observed at the crest 17 m borehole. Whilst crest 103 m borehole, in the hard rock has a 2 month lag in response to rainfall sequence 1 (see Figure 5.2) of 5-31 mm/day of rainfall over 2 weeks in September 2012. The change in hydraulic head (dH) was 0.08 m as a result of these sequences of rainfall. The dH had a lag of 2 months and increased by 0.09 m for sequence 2 of 5-35 mm/day of rainfall over 3 weeks during October 2012-December 2012 with a slight decrease in dH/dT. The dH increased by 0.32 m over the rainfall period of December 2012-August 2013. The dH/dT tends to increase more after the high intense rainfall that occurred during December 2012-February 2013 whereby sequence 3 of 5-95 mm/day of rainfall for 4 weeks occurred. The rise in dH to the sequence 3 rainfall events in has a response time of 2 months and then starts to follow a more gradual trend. These trends in water level indicate a direct piston recharge mechanism as a sequence of rainfall events is required for the water levels to rise.

This lag in response also suggests the recharge area for groundwater at the 1st order hillslope is much broader than the local catchment but rather connected to a regional groundwater scale process.

The 1st order riparian position 61 m borehole (Figure 5.26) responses to the major sequence of rainfall events are similar to the 1st order crest position 103 m borehole. The only differenc3 is that the riparian borehole has a higher hydraulic head. Therefore a slight upward gradient exists from the riparian zone to the crest.

The 1st order crest 17 m borehole provides an indication of shallow weather zone groundwater responses in that dH increased by 6.13 m as a result of the moderate sequence 2 rainfall events in October 2012 and then recedes after three months. The dH increases by 12.10 m with the high intensity sequence 3 of 200 mm of rainfall over 6 days in January 2013. The lag time for these responses are 2-3 weeks and given the required sequence 2 and 3 of rainfall events an increase in dH can be associated with a direct piston recharge process. The recharge appears to be localized to hillslope scale owing to the relatively shorter time lag in response to rainfall events than with the deep groundwater level

The 1st/2nd order triangulation boreholes (36 m and 61 m) follow a very similar trend and the depth to water level is similar (Figure 5.27). The water level record only starts in October 2012 and the dH has increased by 0.09 m in both the 1st/2nd order triangulation boreholes as a result of the moderate sequence 2 rainfall events. The dH/dT increases as a result of the 3rd sequence of rainfall. The dH rises with a lag of roughly 2.5 months after which it follows a more gradual gradient. In both boreholes the dH increased by 0.33 m subsequent to the December 2012-August 2013 rainfall events. The time lag in water level response to rainfall events are again indicative of possible recharge occurring from distant areas. The water levels at the triangulation points also dominantly responded to sequence 2 and 3 rainfall events inferring a possible direct piston recharge mechanism.

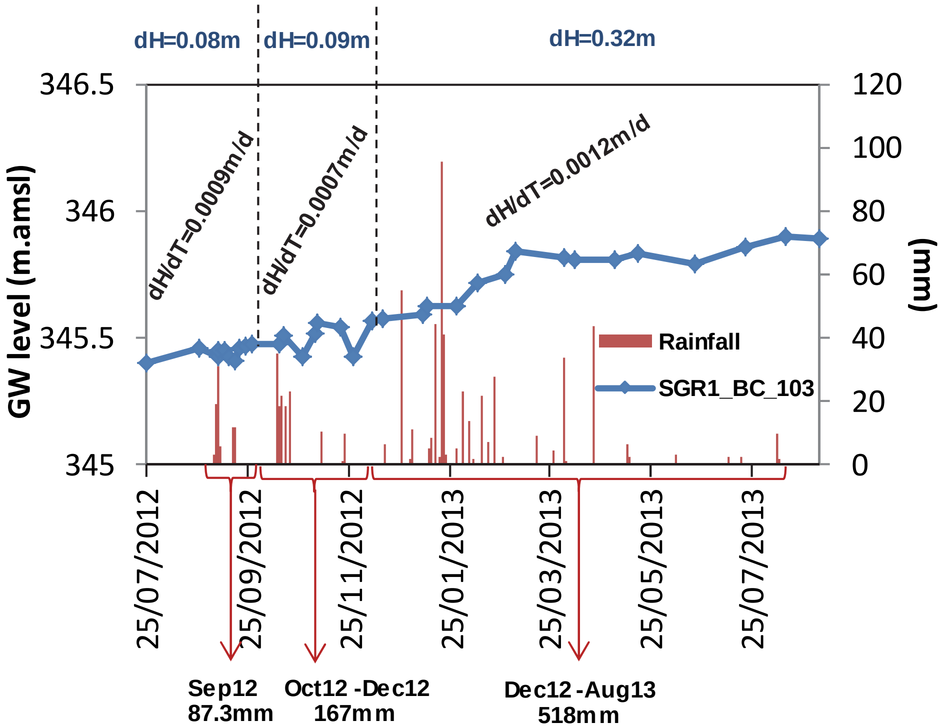

Figure 5.24: 1st order crest position 103 m borehole water level response to rainfall over the hydrological season September 2012to September 2013

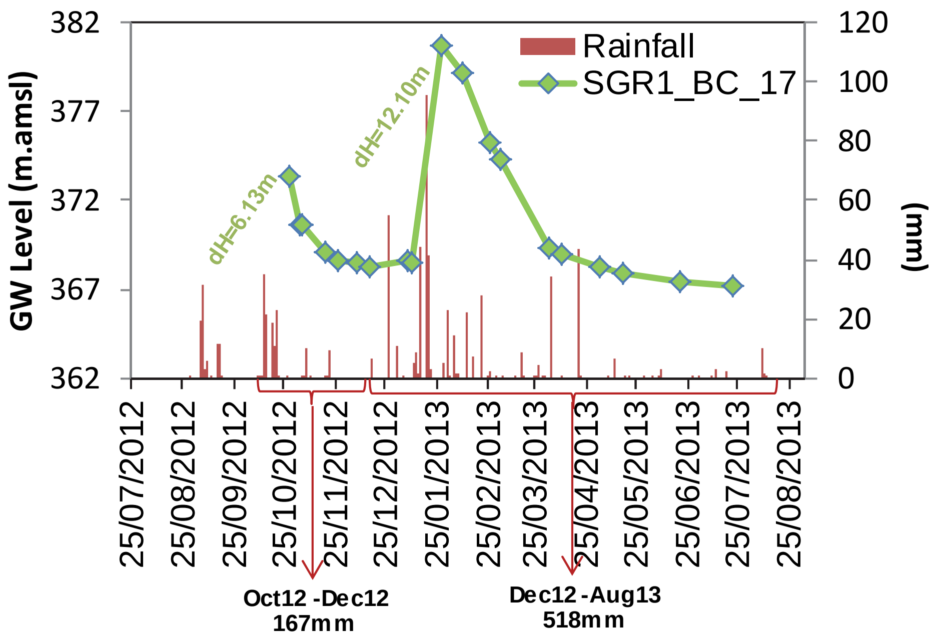

Figure 5.25: 1st order crest position 17 m borehole water level response to rainfall over the hydrological season September 2012 to September 2013

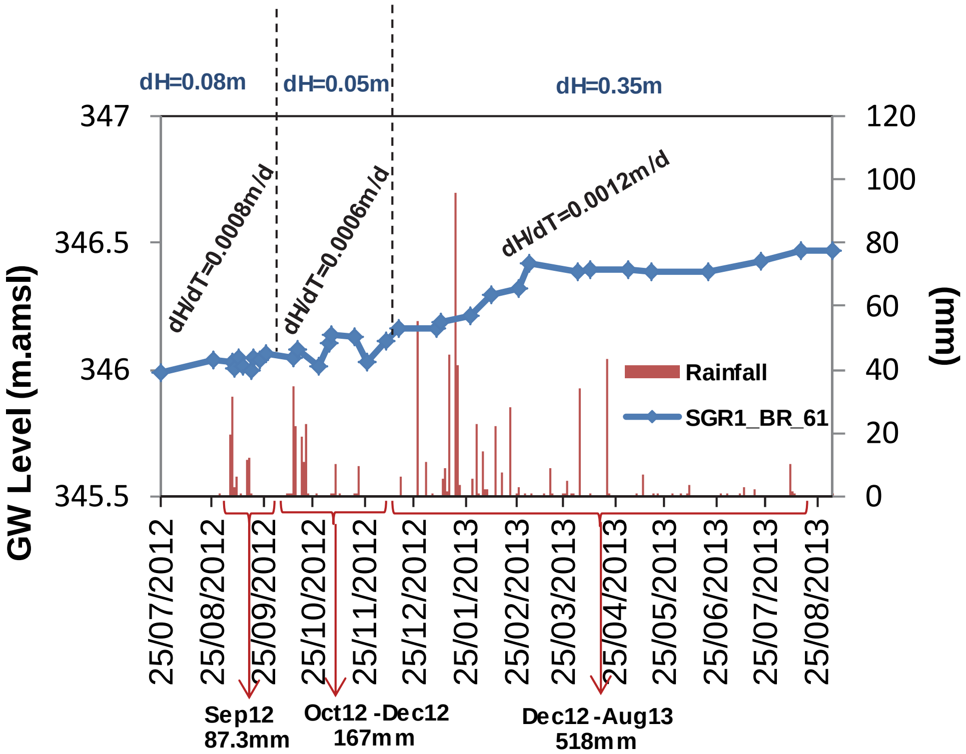

Figure 5.26: 1st order riparian position 61 m borehole water level response to rainfall over the hydrological season September 2012 to September 2013

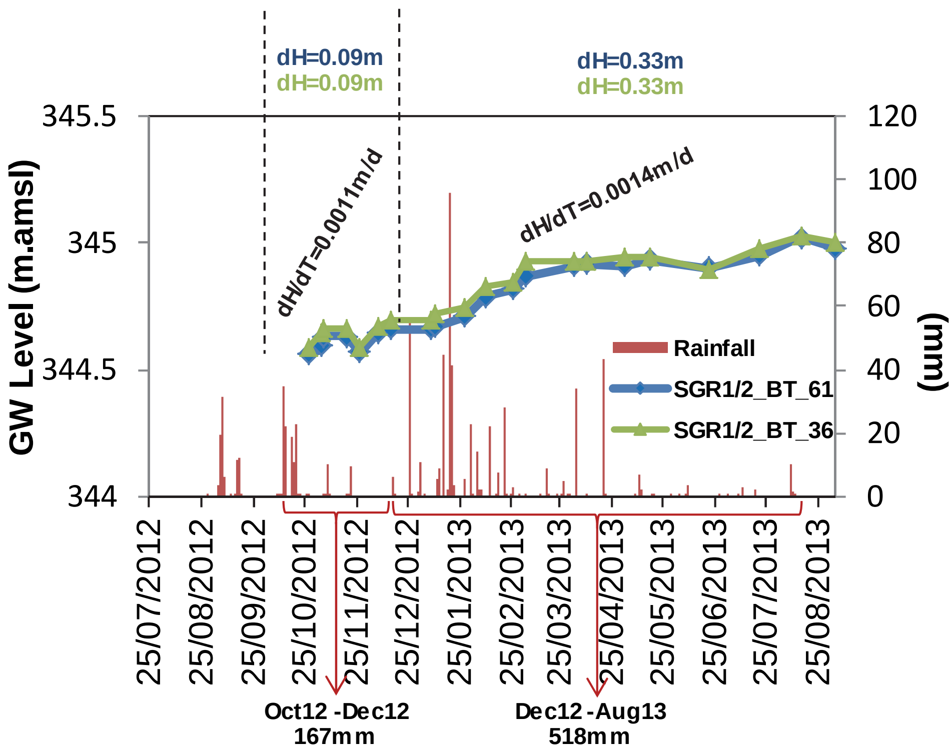

Figure 5.27: 1st/2nd order triangulation position 36 m and 61 m borehole water level response to rainfall over the hydrological season September 2012 to September 2013

To gain an improved understanding of the spatial temporal distribution of groundwater at the hillslope scale and within the catchment, in-situ measurements of specific conductance (mS/cm) in groundwater at the first order scale are plotted in Figure 5.28 and Figure 5.29 (see Appendix VI for Temperature and pH). In the case of the crest 103 m borehole specific conductance values do not change significantly over the successive monthly fluid logs. This indicates that there is no active influx or mixing of fresh (low specific conductance) groundwater. Hence, there is also no rapid response in water level to the moderate and high intensity sequence of rainfall events occurring in October 2012 and January 2013 respectively (see Figure 5.24). The 1st order crest 17 m borehole shows low specific conductance (SC) values throughout the logs which suggest direct rainfall permeating into the weathered aquifer which is then slowly released into the hard rock aquifer during high intensity (45-95 mm/day) sequence of rainfall events. This can be seen by the drop in SC values in the first 10 m of the February 2013 fluid log in the 1st order crest position 103 m borehole. The SC values do not show significant changes during the fluid logs of the 1st order riparian position 61 m borehole which indicates that the stream is not likely to contribute to recharge of the deep groundwater system at this point. This occurrence points again to the connection of the deep hard rock aquifer to a regional groundwater flow system. The step seen at the depth of roughly 329,322, 309 and 298 mamsl is likely due to fractured zones as some of these changes in the vertical profile coincide with water strikes see Figure 5.28.

The 1st/2nd order triangulation 61 m borehole SC does not change significantly during the successive fluid logs (see Figure 5.29). This suggests no active influx of fresh groundwater (low SC) or rainfall into the deep groundwater system at this point. Hence, there is no rapid response in water level to the moderate and high intensity sequence of rainfall events occurring in October 2012 and January 2013 respectively (see Figure 5.27). This again supports a regional groundwater flow process. The step seen at the depth of roughly 334 mamsl is likely to be due to the casing causing stagnant conditions within the borehole. (However the 1st/2nd order triangulation position 36 m borehole specific conductance does change significantly as seen in the February 2013 log. Although the drop in SC cannot be correlated with a recharge event due to the delayed responses in water level seen in Figure 4.28, it is however likely that an interflow contribution from the 1st order hillslope weathered aquifer produces the decrease in SC.

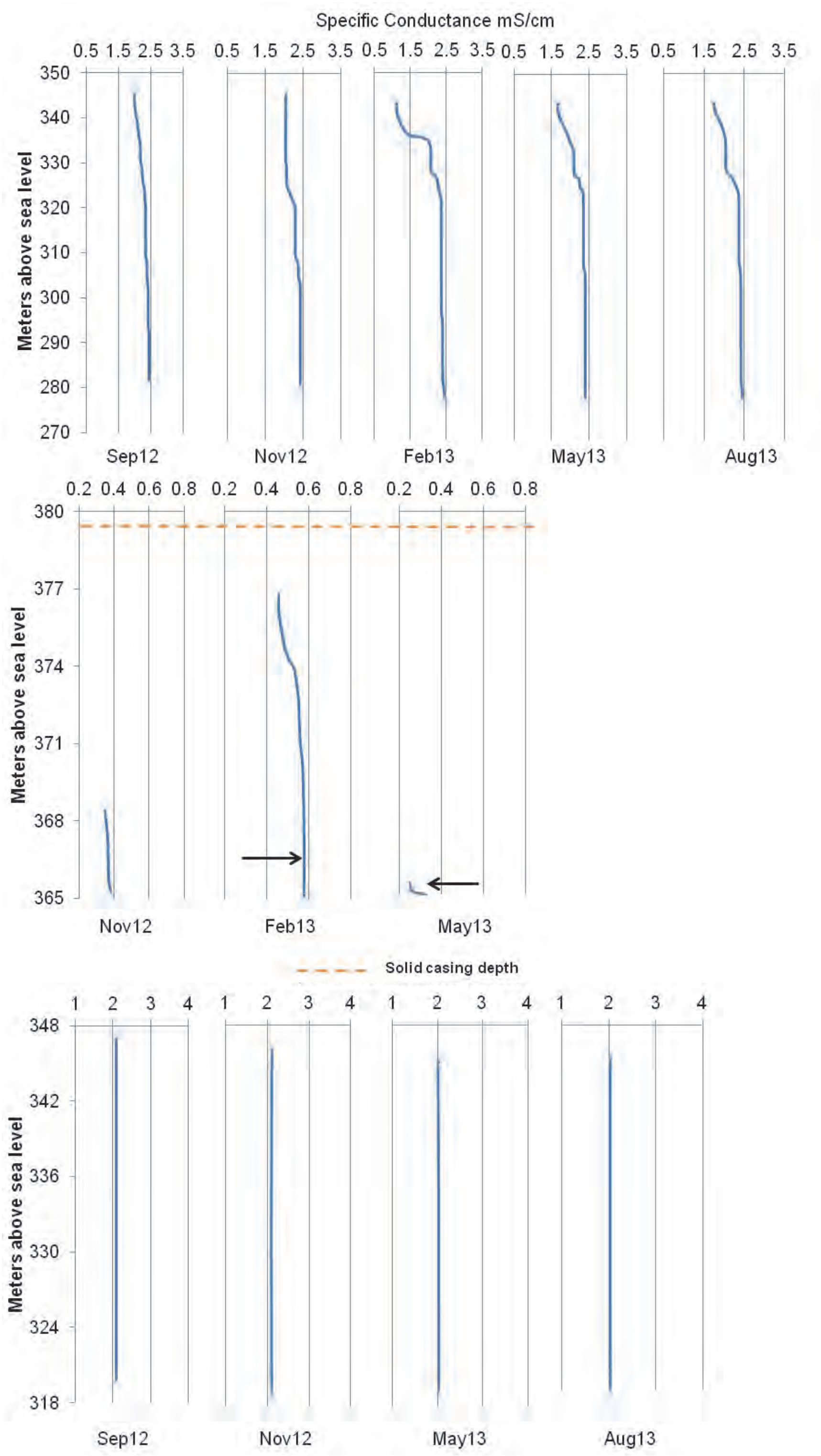

Figure 5.28: Specific conductance quarterly fluid log for the 1st order crest position 103 m borehole (top), crest 17 m borehole (middle), and riparian position 61 m borehole (bottom).

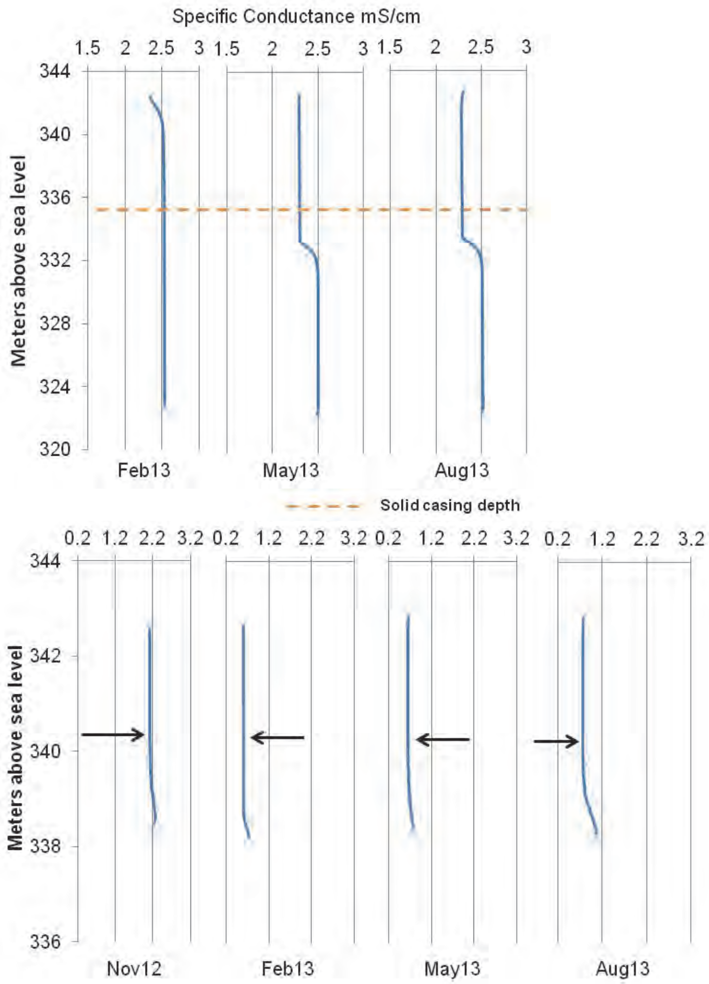

Figure 5.29: Specific conductance quarterly fluid log for the 1st/2nd order triangulation position 61 m borehole (top), and 36 m borehole (bottom).

5.5 Southern Granite 2nd order hillslope

5.5.1 2nd order Geophysics

Figure 5.30 shows the initial interpretation of the 2nd order hillslope sub-surface where it was estimated that the riparian zone exhibited an 8 meter unsaturated zone with shallow groundwater levels at 10 m due to the low resistivity values (3-75 Ω/m within 8-10 m) below the subsurface. The riparian zone was expected to have deep weathering which decreased toward the crest due to the higher (1875-5484 Ω/m) resistivity values occurring at a shallower depth at the crest. Two boreholes were drilled at the riparian zone to capture the expected saturated conditions two distinctive depths namely the weathered/unsaturated zone and hard rock/saturated zone. Across the profile the groundwater level was expected to be relatively flat due to a consistency with depth in low resistivity values (3-75 Ω/m) across the profile. The clumping together of resistivity values 219-641 Ω/m suggests an interface zone. The resistivity values suggest a low (3-75 Ω/m) and high (1875-5484 Ω/m) resistivity zone which could be interpreted as weathered and hard rock zones respectively. The crest also had two boreholes drilled to monitor the two zones of saturation.

Meanwhile following the drilling the final interpretation is as follows: The riparian boreholes of the 2^{nd} order hillslope have a shallower weathering profile of 29 m compared to the crests weathering depth of 43 m. At the 2^{nd} order hillslope two zones were indeed identified namely, weathered and hard rock zones. The shallow and deep boreholes of the 2^{nd} order hillslope riparian zone and crest produced no blow out yields which suggest a low permeable shallow and deep groundwater system at these points. The borehole logs for the 2^{nd} order hillslope counter the initial ERT interpretation of deeper weathering at the riparian zone than at the crest, with deeper weathering at the crest of 43 m and 29 m at the riparian zone. Since no blow out yields could be tested for it suggests a rather stagnant groundwater flow system at these boreholes.

The time-series plots for the same hillslope shown in Figure 5.31 show two key aspects. First the reduction in resistivity with depth in the riparian zone (C) over time signifies a steady vertically driven process there. This perhaps augments the interpretation of EC responses seen there (refer to section). Second, the riparian-midslope section (D) which sees a switch to a uniform resistivity distribution occurring towards March 2013. Again this suggests a steady vertical redistribution of significant event water through matrix flow, rather than fractured rick in to deeper material below 355 masl.

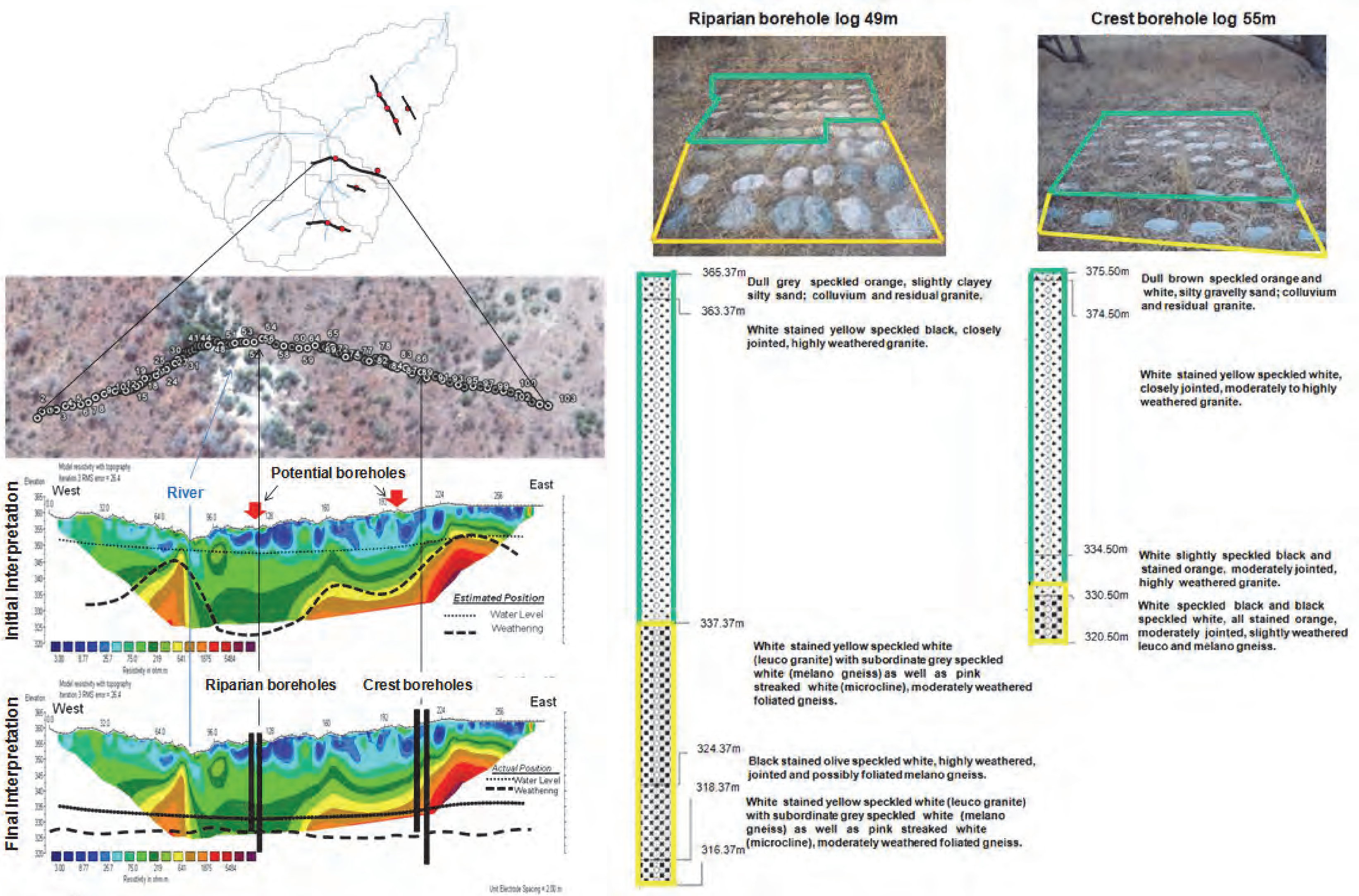

Figure 5.30: Initial and final interpretation of 2D ERT traverses coupled with topography data, satellite imagery and estimated and actual positions of groundwater level and weathering (left), Borehole lithology logs of the southern granite 2nd order riparian 49 m and crest 55 m borehole, the green highlighted section indicates weathered material and the yellow highlighted section indicates hard rock material (right).

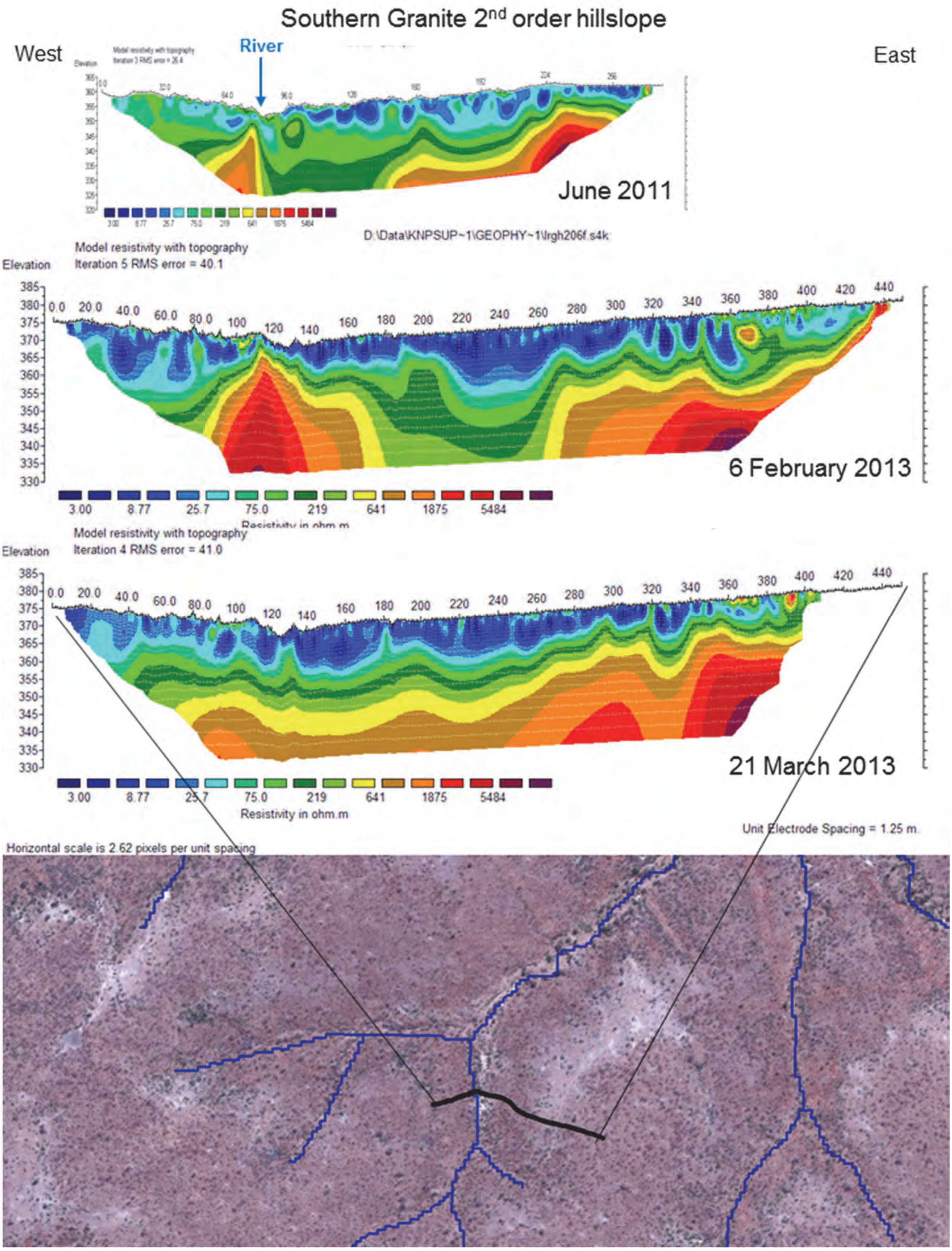

Figure 5.31: Time-series geophysics transect southern granite 2nd order hillslope

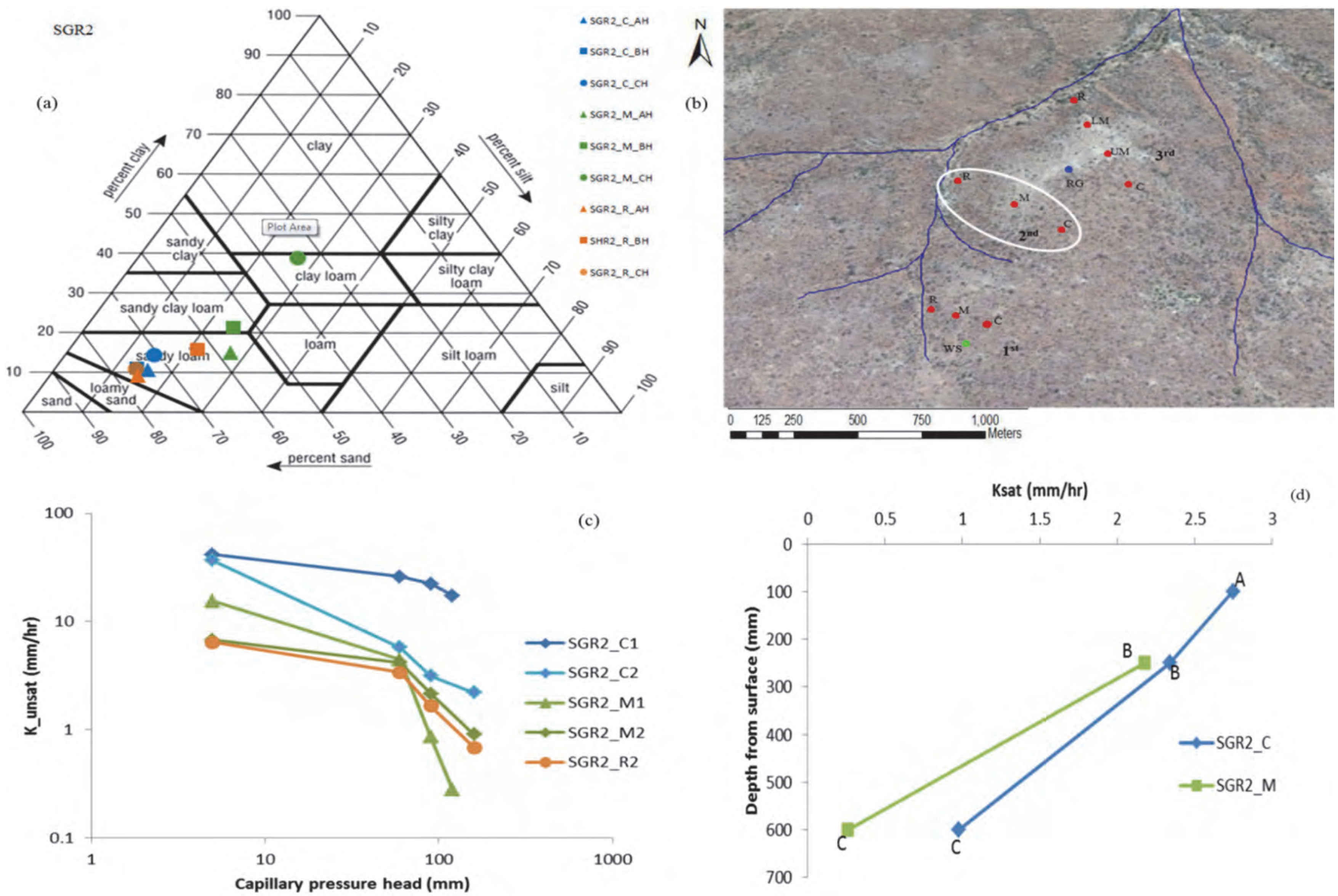

Figure 5.32: (a) Soil texture triangle (b) site map (c) K_{unsat} at soil surface (d) K_{sat} per soil horizon on granite 2nd order hillslope

Table 5.11: Soil classification per catena element on granite 2^{nd} order hillslope

Catena Element	Taxonomical class	Diagnostic Horizons	Hydropedological soil type
SGR2_Crest	Pinedene	Orthic A	Interflow
		Yellow Brown Apedal B	
		Unspecified with signs of wetness	
SGR2_Mid	Sterkspruit	Orthic A	Responsive
		prismacutanic B	
		-	
SGR2_Rip	Cartref	Orthic A	Interflow
		E	
		Lithocutanic B	

5.5.2 2^{nd} order shallow unsaturated zone characterization and responses

The 2^{nd} order hillslope shows high K_{unsat} at the crest at low capillary pressure head (41 mm/hr at φ =5 mm) on the surface (Figure 5.32). Sandy loams are characteristic of this catena element. Although values are low, the crest also shows high K_{sat} down the profile compared to the midslope catena element. The crest of the 2^{nd} order comprises a Pinedene soil form (Table 5.11). The K_{sat} data for the crest shows that the B horizon has a higher K_{sat} than the underlying unspecified horizon (with signs of wetness). Since K_{sat} is lower at the unspecified horizon this implies restricted flow on that horizon hence interflow in the overlying A and B horizons is anticipated.

The Midslope catena element shows the lowest K_{unsat} (0.02 mm/hr at φ =5 mm) compared to other catena elements. The 2^{nd} replicate for the midslope shows values more or less similar to those for the crest element. This large variation in K_{unsat} at the midslope is likely to be evidence of soil heterogeneity in the form of macro-porosity and soil pipes. Meanwhile K_{sat} in the subsurface on this catena element is low especially at the C horizon (0.2 mm/hr). This means flow is generally restricted in this region. This 2^{nd} order midslope comprises a duplex Sterkspruit soil form where clays particles are washed downslope through colluviation from the crest and accumulate at the midslope. Thus when water is moving from the crest downslope, a seepline develops between the crest and midslope due to textural discontinuities when the water gets to the clay layer. Interflow and/or overland flow is anticipated with this soil form, since the prismacutanic B horizon (clay variant) limits water movement. This means during rainfall events there is interflow at the A/B interface and/or infiltration excess flow (shallow responsive) at the soil surface, depending on rainfall intensity. Since lateral contributions are expected from the crest, this implies potential hydrological connectivity through to the riparian.

The riparian catena element at the 2^{nd} order is classified as a Cartref soil form; interflow at the AE/B interface is therefore anticipated. Since the K_{unsat} is lower than that at the crest element (6 mm/hr at φ =5 mm), flow is expected to be slow. Subsurface connectivity through lateral flow on this 2^{nd} order hillslope is expected but could be highly temporal and intensity driven.

The 2nd order hillslope (Figure 5.33), between September 2012 and April 2013 show that the shallow soils (depth=100 mm on A horizon) have quicker drying cycles compared to the intermediate soils (depth= 250 mm on B horizon). They both seem to follow a similar wetting and drying pattern only that the intermediate soils show a slight lag when drying. Since this is a Pinedene soil form, interflow is still anticipated between the B horizon and the unspecified (with signs of wetness) region. Although this crest has quick wetting and drying cycles, %ED shows that this is generally a dry area showing high potentials (>1000 mm) for the greater part of the season.

The midslope shows a quick full profile response to the first rainfall events with soils getting close to saturation (<1000 mm). Whilst the shallow and intermediate soils dried out, the deeper soil retained moisture for the greater part of the wet season (Taking note that the 1st two sensors are in the diagnostic orthic A horizon of the duplex Sterkspruit form). The B horizon is a prismacutanic horizon (clay variant); it is therefore characterized by soils with low hydraulic conductivity. The clay particles in that horizon help to retain moisture hence the low potentials. Potential movement of water on this catena element is interflow (A/B interface) but infiltration excess flow is anticipated during high intensity rainfall events. This is generally a dry region (>1000 mm) as illustrated by the %ED data which shows the intermediate and deeper soils getting close to saturation (<1000 mm) only about 35-40% of the time.

The riparian soils also show a full profile response to the first rains (sensors only in A and B horizon). The intermediate sensor (depth=250 mm) was faulty at some point so the data is not consistent but nevertheless it shows that the soils were responding to some but not all of the events. The intermediate soil layers show a slow drying cycle compared to the overlying soils. Since there is a Cartref soil form at this element (Table 4.2), the E horizon is an indication of a potential perched water table therefore some flow restriction in the underlying lithocutanic B horizon hence the low potential on the intermediate soils for a considerable amount of time. %ED data shows that this is a relatively dry area (values> 1000 mm) suggesting temporal or no connectivity with upslope catena elements through lateral or overland flow. Due to the impeding layer (B horizon), infiltration excess is anticipated during high intensity events.

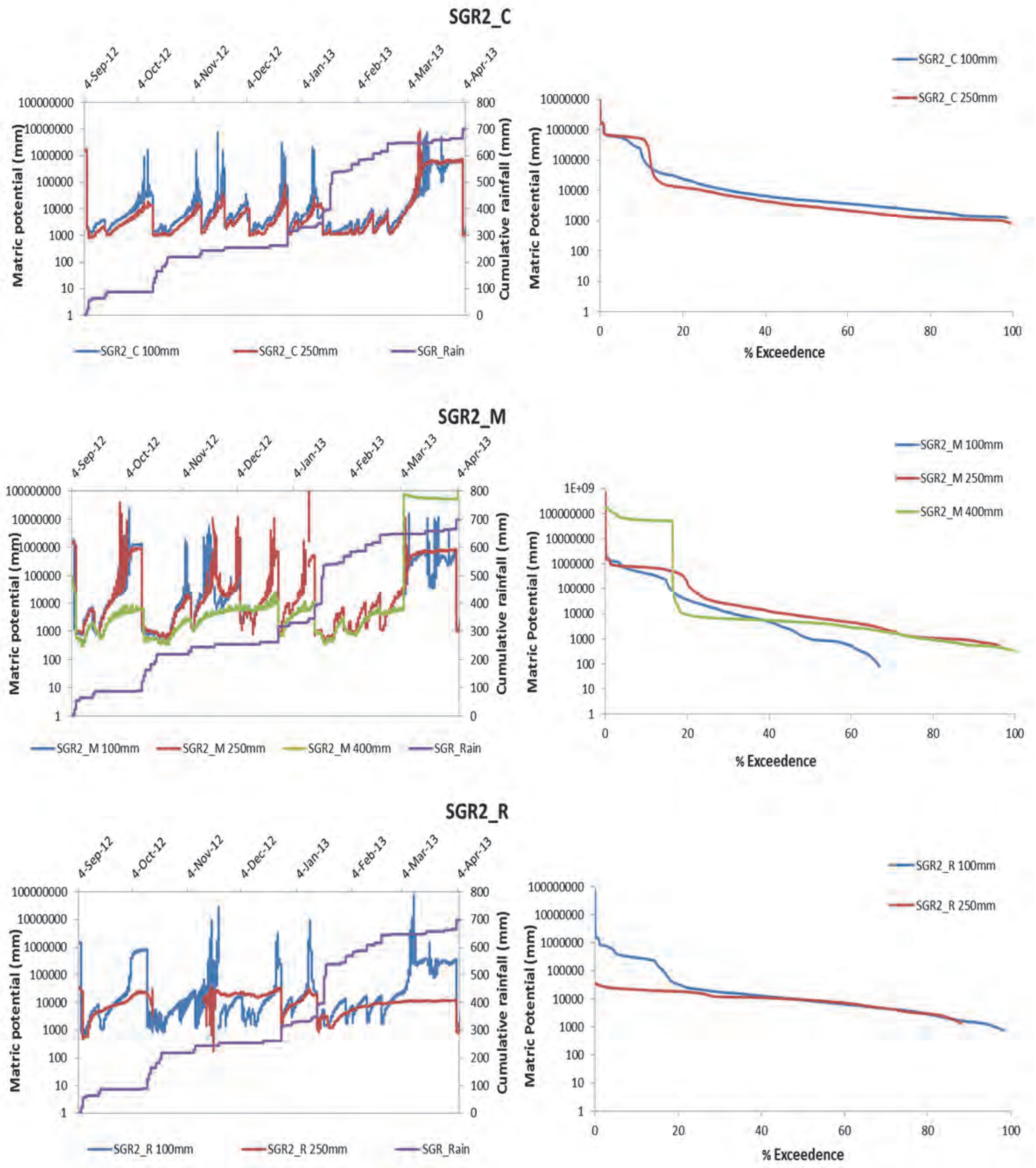

Figure 5.33: Soil matric potential responses and % ED curves along the southern granite supersite second order hillslope between September 2012 and April 2013

Hillslope Class 2: Shallow responsive

Figure 5.34 shows the perceptual flow paths of the 2nd order hillslope. There is interflow at the crest and a seepline between the crest and the midslope due to textural discontinuities (Pinedene soil form at the crest and Sterkspruit form characterized by duplex soils at the midslope). Some of the water continues to flow laterally into the midslope. The prismacutacic B horizon (clay variant) at this catena element impedes the vertical subsurface flow of water thereby resulting in lateral flows and during rainfall events, infiltration excess is anticipated. According van Tol et al. (2013), in drier climates characteristic of savannas, gypsum, lime and salt precipitates maybe washed downslope and the impermeable underlying rock in the riparian zone promotes limited contributions to the stream because of actual ET. Contributions to the stream may be from infiltration excess only after high intensity and or exceptional events. In terms of storage, this hillslope is expected to have limited storage due to the presence of impeding layers and low conducting material mostly in the B horizons of the catena elements hence water will be lost through ET and/or overland flow.

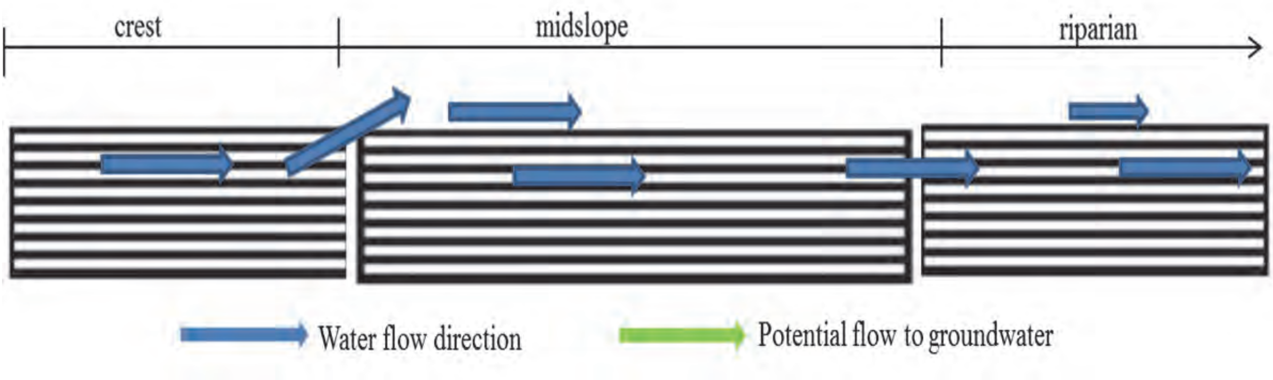

Figure 5.34: Hydrological soil types and flow paths for granite 2nd order hillslope

5.5.3 2nd order Hydrogeology: Hydraulic Responses and Parameters

The 2nd order crest 40 m and 55 m boreholes generally follow the same trend as each other with similar water level depth[3] (Figure 5.35). The 2nd order crest position 55 m borehole dH raises by 0.20 m during the moderate sequence 2 rainfall (See Figure 5.2) with a response time lag of 2 months. A steep dH/dT of 0.0041 m/d exists during the period of October 2012-December 2012 which is explained by the water levels equilibrating as a result of aquifer tests. As a result of the moderate sequence of rainfall events (10-35 mm/day over 3 weeks) during October 2012 caused the dH to increase by 4.38 m and receded back to a static deep groundwater level roughly a month later. A rise in dH by 7.39 m occurred as a result of the high intensity sequence 3 of rainfall events (200 mm over 6 days) during January 2013 and receded approximately 2 months later back to the static deep groundwater level. These abrupt changes in water level likely resulted from a borehole construction error whereby the gravel used to line the perforated section of the casing was filled to the ground surface creating a conduit for rainfall water. The general dH is 0.38 m for the 40 m borehole and 0.32 m for the 55 m borehole. The general rise in water level was a consequence of the 2 and 3 rainfall sequences. This infers a direct piston recharge mechanism possibly on a regional scale due to the time lag response in water levels.

The 2nd order riparian position 28 m and 49 m boreholes generally follow the same trends as each other with similar water level depth (see Figure 5.36). The dH/dT during sequence 1

[3] The dH and dH/dT for the water levels as a result of the September 2012 sequence of rainfall events has not been included. This was due to the water levels equilibrating consequent to aquifer tests being performed and would generate a negative gradient. The lengthy time taken for water levels to reach static would be a consequence of the low transmissivity (Table 5.2) values encountered in both the shallow and deep boreholes.

rainfall was relatively steep compared to the December 2012-September 2013 dH/dT due to the water levels reaching static as a result of aquifer tests. Therefore the rise in dH for the 28 m and 49 m borehole do not occur under ambient conditions. During the October 2012-December 2012 sequence 2 of moderate (5-35 mm/day) intensity rainfall events, dH increased by 0.12 m and 0.14 m for the 49 m and 28 m borehole respectively with a response time lag of 2 months. The deep and shallow water levels tend to follow a more gradual gradient during the December 2012- August 2013 rainfall events. However the shallow borehole dH increased by 0.35 m as a result of the high intensity (200 mm over 6 days) sequence of rainfall events that occurred during January 2013. The lag in water level response was 2 weeks. Due to the relatively rapid response and recession in water level suggests a possible indirect preferential recharge mechanism from the 2nd order stream, concurring with those observations revealed in 5.2.3.

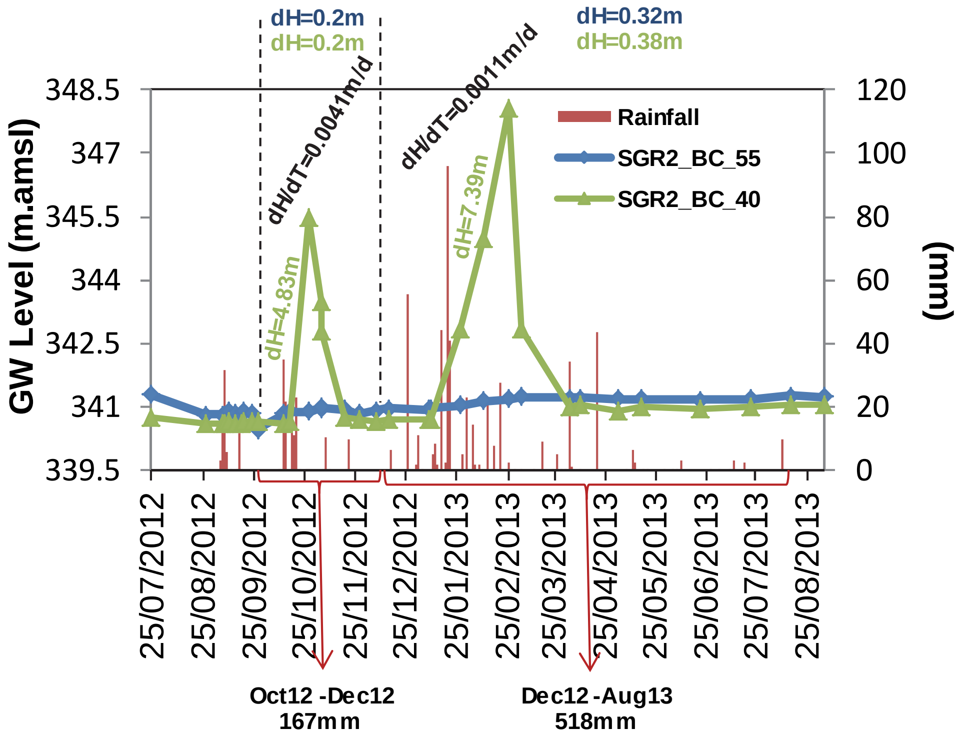

Figure 5.35: 2nd order crest position 40 m and 55 m borehole water level response to rainfall over the hydrological season September 2012 to September 2013

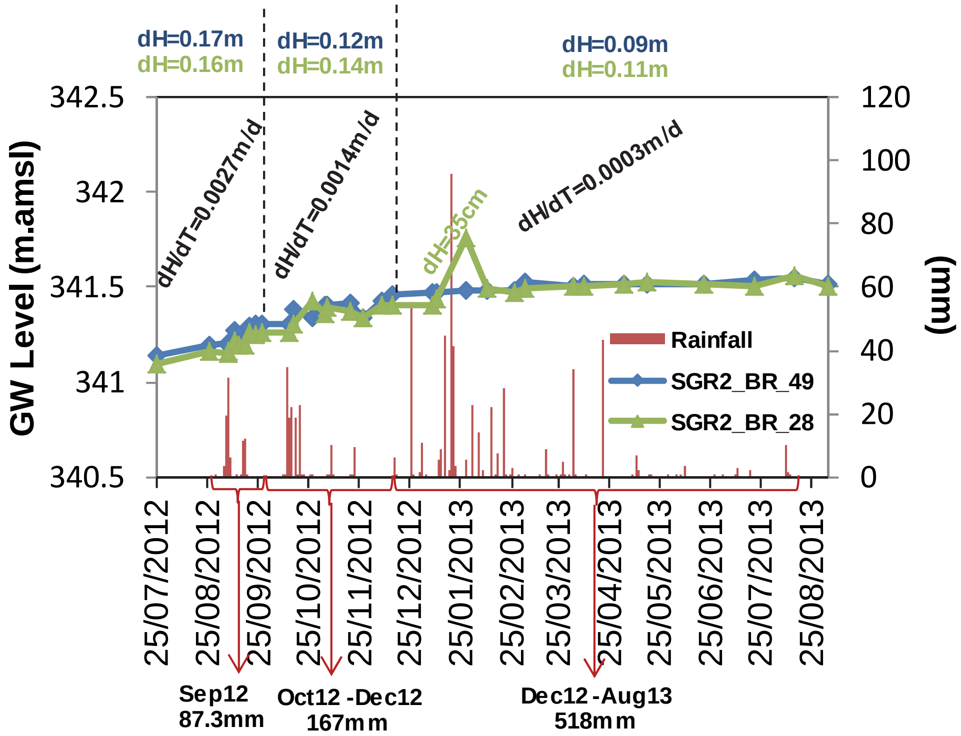

Figure 5.36: 2nd order riparian position 28 m and 49 m borehole water level response to rainfall over the hydrological season September 2012 to September 2013

Fluid logging of the 2nd order crest 55 m and 40 m boreholes showed SC decreases significantly during November 2012 (Figure 5.37). This was during the moderate (5-35 mm/day) intensity rainfall events during October 2012-December 2012 that caused the 40 m borehole water level to rise by 4.83 m. A 7.39 m rise in the 40 m borehole water level can be seen in Figure 5.35 as a result of the high (45-95 mm/day) intensity sequence of rainfall events during January 2013. Therefore the decrease in SC is likely due to a flush of rainfall that infiltrated through the preferential conduit as a result of the 40 m borehole installation error. The step seen at the depth of roughly 332 mamsl in the 55 m borehole fluid log is due to the casing causing stagnant conditions within the borehole. The SC of the 2nd order riparian position 49 m borehole does not change significantly, an indication of no active influx of fresh groundwater into the hard rock groundwater system at this point (see Figure 4.39). Hence, there is no rapid response in water level to the moderate and high intensity sequence of rainfall events occurring in October 2012 and January 2013 respectively. This again supports the notion of a regional groundwater flow process. The 2nd order riparian 28 m borehole SC decreased quite significantly during the November 2012 and consequent fluid logs. This decrease in SC for the 28 m borehole can be correlated with the rise in water level due to the October 2012 moderate (10-35 mm) and January 2013 high (45-95 mm) intensity sequence of rainfall events in Figure 5.2. This further supports the theory that the 2nd order stream recharged the weathered aquifer due to the rapid response in the water level rise and recession of the 28 m borehole. The drop in SC infers the contribution of fresh (low SC) water in the vicinity of the 2nd order riparian stream.

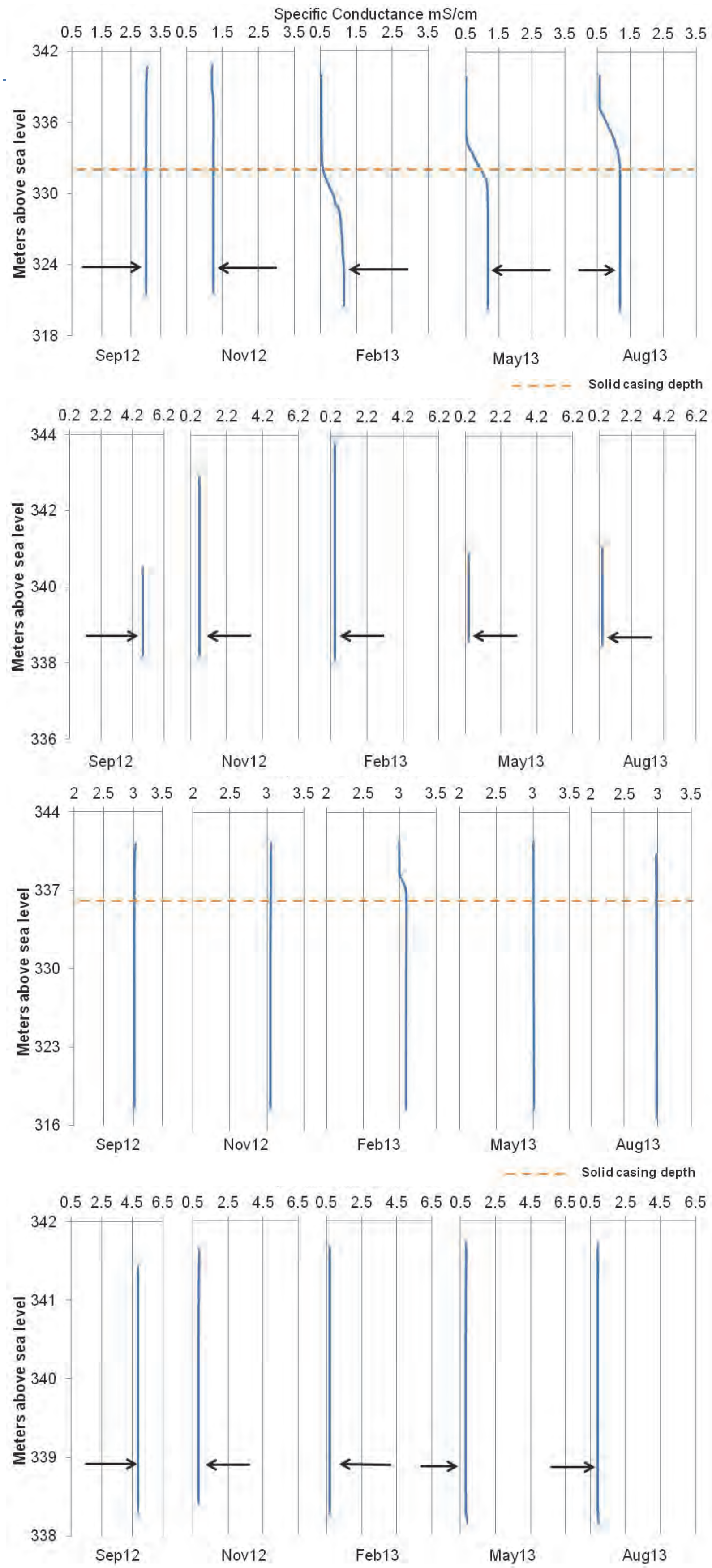

Figure 5.37: Specific conductance quarterly fluid log for the 2nd order crest position 55 m borehole (top), crest 40 m borehole (upper-mid), 2nd order riparian position 49 m boreholes (lower-mid), and riparian 28 m boreholes (bottom).

5.6 Southern Granite 3rd order hillslope

5.6.1 3rd order Geophysics

The initial geophysical interpretation of the 3rd order granite hillslope (Figure 5.38) suggested that the unsaturated zone was estimated at 8-12 m deep. Additionally a relatively flat groundwater level across the profile was expected due to the consistency of low resistivity values (3-75 Ω/m) at a shallow depth across the profile. High resistivity values (1875-5484 Ω/m) occur at a depth of approximately 25 m within the riparian zone, 26 m at the mid-slope and 30-35 m at the crest. The mid-slope has sodic site which could be explained by the low resistivity values (3-75 Ω/m) occurring at the mid-slope towards the crest.

Meanwhile following borehole drilling the final interpretation was as follows: The weathering occurs at a depth of 25 m, 26 m and 38 m at the riparian zone, mid-slope and crests respectively. Across the profile there are distinct weathered and hard rock zones. The riparian boreholes produced a very low blow out yield (see Appendix A6.3) which geologically suggests a low permeable shallow and deep groundwater system. The mid-slope and crest position boreholes produced blow out yields (see Appendix A6.3) which suggest permeable and active shallow and deep groundwater flow systems. The borehole logs for the 3rd order hillslope illustrate similar weathering depths at the riparian and mid-slope boreholes with 25 m and 26 m, respectively. The logs also confirm deeper weathering to 38 m at the crest which was expected. The water strikes encountered at the mid-slope and crest boreholes suggest active groundwater flow systems with final blow out yields of 0.16 and 0.33 L/s respectively (see Appendix A6.3). The intensely fractured and highly weathered lithology description of the mid-slope position 49 m borehole at a depth of 330-320 mamsl is likely to be a fractured or flow zone. This description concurs with the fluid log profile indicating the presence of a fracture or flow zone in the mid-slope borehole at a depth of 323 mamsl (see Appendix A6.3). The riparian zone has no water strikes but a very low blow out yield of 0.01 L/s, which suggests an in-active groundwater flow system at this point.

The time-series surveys of the 3rd order hillslope (Figure 5.39) reveals a midslope geological control (E) that appears unaffected by vertical processes although the region around it (G) shows a lowering of resistivity over time, again suggestive of deep matrix percolation. The crest (F) is underlain also by resistant material which may be an impediment to vertical percolation. This may also explain the very low resistant material seen between 360-380 m, at 355 masl, coinciding with the hillslope seep line and submergence of hillslope water underneath the clay wedge of the sodic site on that hillslope.

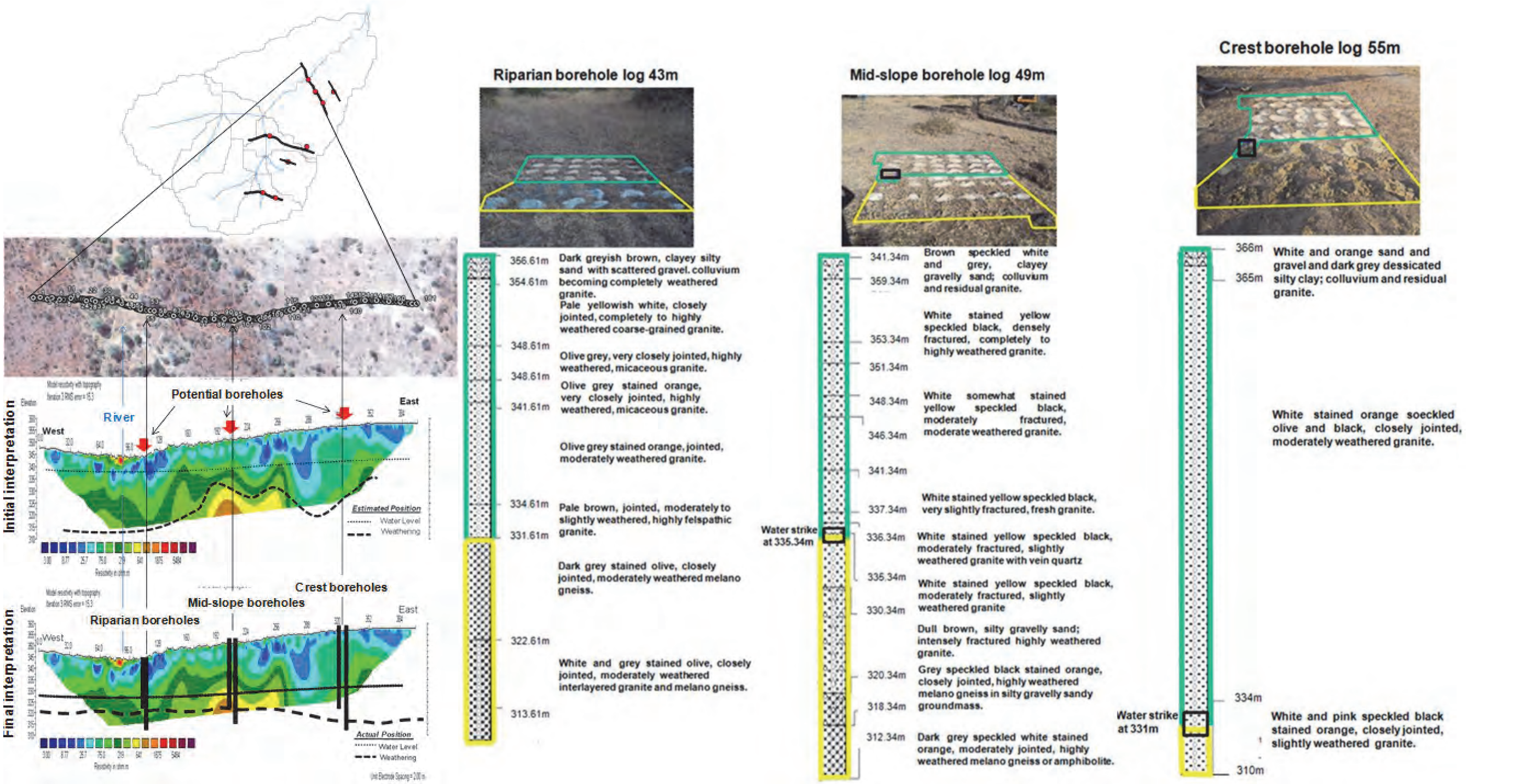

Figure 5.38: Initial and final interpretation of 2D ERT traverses coupled with topography data, satellite imagery and estimated and actual positions of groundwater level and weathering (left), Borehole lithology log of the southern granite 3rd order riparian 43 m, mid-slope 49 m and 3rd order crest 55 m borehole boreholes, the green highlighted section indicates weathered material, the yellow highlighted section indicates hard rock material and the black block indicates the water strike position (right).

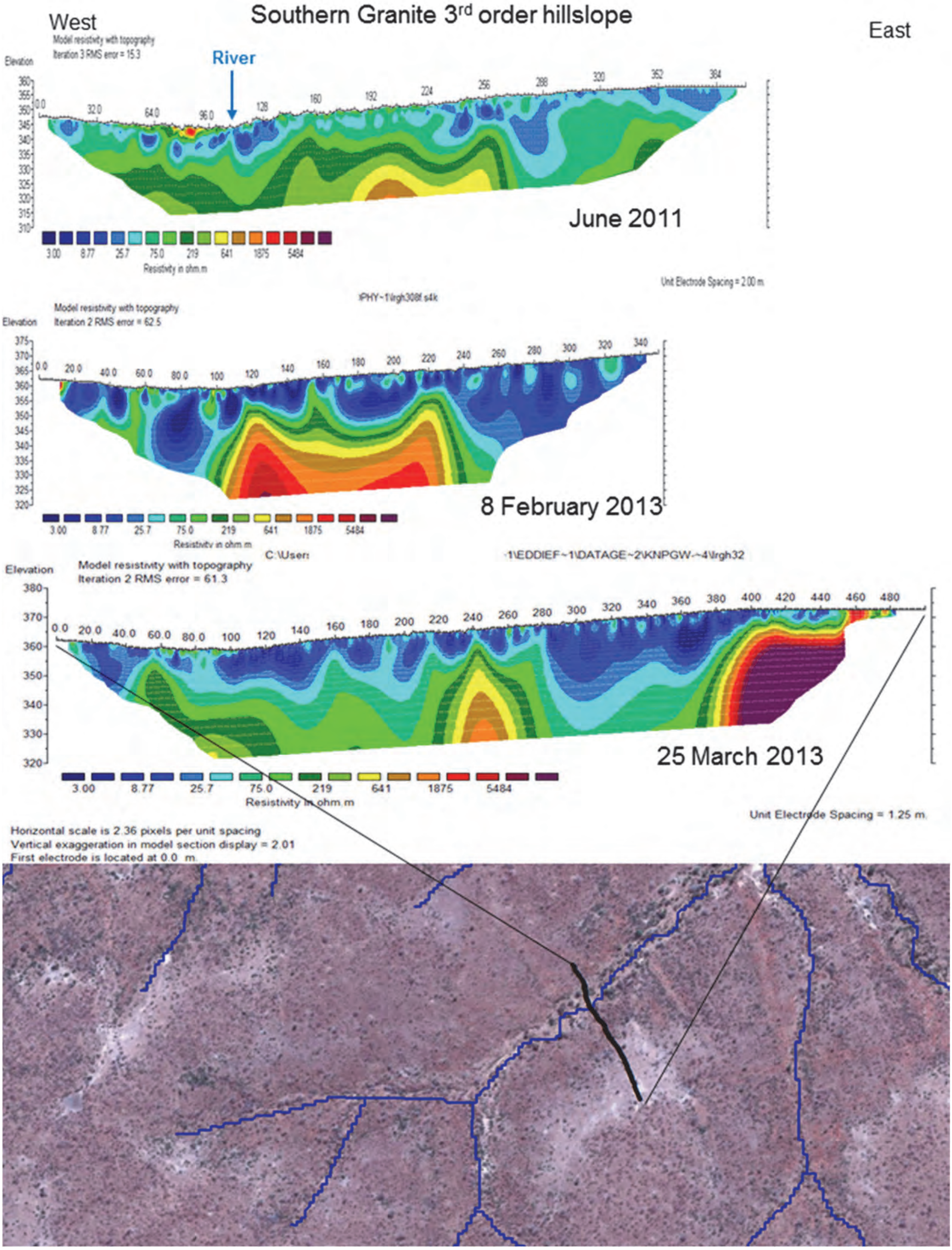

Figure 5.39: Time-series geophysics transect southern granite 2nd order stream

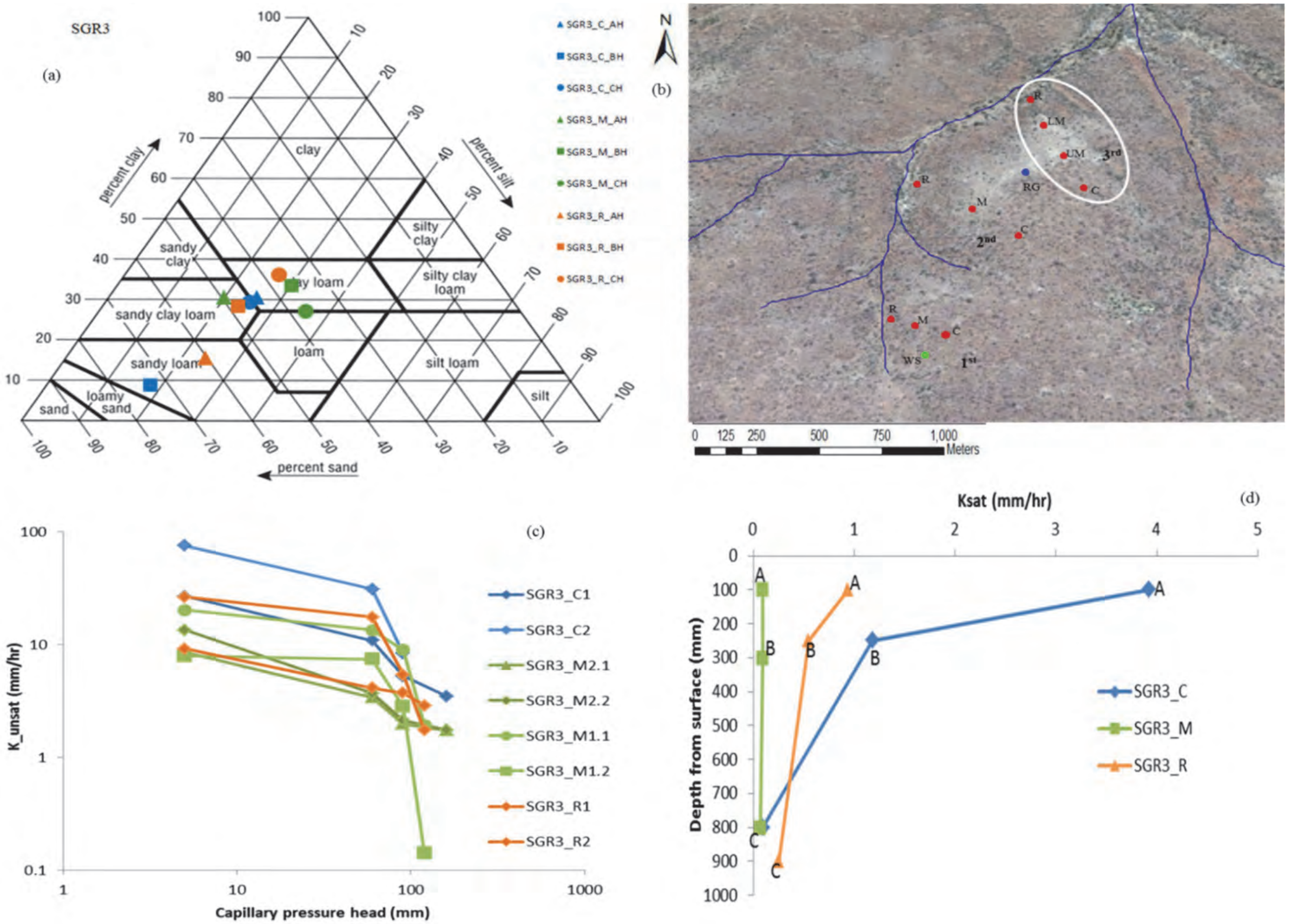

Figure 5.40: (a) Soil texture triangle (b) site map (c) K_{unsat} at soil surface (d) K_{sat} per soil horizon on granite 3rd order hillslope

Table 5.12: Soil classification per catena element on granite 3rd order hillslope

<table>
<tr><td>Catena element</td><td>Taxonomical class</td><td>Diagnostic Horizons</td><td>Hydropedological soil type</td></tr>
<tr><td rowspan="3">SGR3_Crest</td><td rowspan="3">Pinedene</td><td>Orthic A</td><td rowspan="3">Interflow</td></tr>
<tr><td>Yellow Brown Apedal B</td></tr>
<tr><td>Unspecified with signs of wetness</td></tr>
<tr><td rowspan="3">SGR3_Mid</td><td rowspan="3">Sterkspruit</td><td>Orthic A</td><td rowspan="3">Responsive(shallow)</td></tr>
<tr><td>prismacutanic B</td></tr>
<tr><td>-</td></tr>
<tr><td rowspan="3">SGR3_Rip</td><td rowspan="3">Bonheim</td><td>Melanic A</td><td rowspan="3">Slow Recharge</td></tr>
<tr><td>Pedocutanic B</td></tr>
<tr><td>Unspecified</td></tr>
</table>

5.6.2 3rd order shallow unsaturated zone characterization and responses

The 3rd order crest catena element (Figure 5.40), shows high K_{unsat} on the surface (26 mm/hr and 76 mm/hr at φ =5 mm). Values were expected to be low due to the clay loams close to the surface at this location. K_{sat} on the A horizon was also expected to be lower (clay loams), then high in the B horizon where there are sandy loams. Nevertheless, interflow is expected on this catena element since K_{sat} in the A horizon is higher than the underlying horizons which is also expected for a Pinedene soil form characteristic of this catena element. This suggests potential subsurface lateral connectivity with the downslope elements.

The 3rd order midslope shows low K_{unsat} especially at low pressure heads (0.14 mm/hr-1.7 mm/hr at φ =5 mm). This is also the case with the K_{sat} data here it has the lowest conductivity on the whole hillslope (0.7-0.9 mm/hr), attributed to the clay loams. Since there is not much variation in the very low K_{sat} values this would be a potential responsive soil. Similar to the 2nd order a seepline is also anticipated to develop between the crest and midslope due to textural discontinuities.

The riparian soils show intermediate K_{unsat} and K_{sat} compared to the crest and riparian catena element soils (Figure 4.4c and 4.4d respectively). K_{sat} data for this element is showing a decrease with depth. This means rate of water movement will be high in the A but gradually decreasing with an increase in depth which augments the hydropedological classification (Table 5.12: Soil classification per catena element on granite 3rd order hillslope) of slow potential recharge.

Similar to the 2nd order hillslope, hydrological connectivity between catena elements on this hillslope could be highly temporal and intensity driven. Since there is a potential recharge soil at the riparian, this hillslope is expected to be disconnected from the adjacent 3rd order stream network.

The 3rd order crest (Figure 5.41) show low potentials for both shallow and intermediate soils but showing quick wetting-drying cycles for most of the rainfall events similar to crest soils in the lower orders (the deepest sensor at 350 mm was faulty therefore data was omitted). The shallow and intermediate soils got close to saturation for most of the events (<1000 mm). Significant water retention occurred ~40% of the time which was a contribution mainly from the large January-February rains. Depending on the amount and intensity of rainfall received, contributions to the lower slopes are anticipated since these are interflow soils due to flow restriction in the unspecified region of the Pinedene soil form.

The 3rd order upper midslope shows relatively low potentials for the shallow soils and intermediate soils whilst the deeper layers (depth=>300 mm) show a lag of more than one month before they respond to rainfall events. They only get close to saturation in response to the January event and beginning of March but for more than 90% of the time, they remain relatively dry (> 1000 mm). Important to note is that even after the significant event in January 2013 a piezometer at this location remained dry. This suggests absence or limited subsurface flow therefore infiltration excess (shallow responsive) is anticipated during exceptional events and this is typical of duplex soils characteristic of this catena element. Importantly, this figure shows a reasonably prolonged saturation of shallow and intermediate soils (~50%). Hydrologically, this catena element is disconnected from the downslope elements and connectivity may be temporal following high intensity rainfall events through infiltration excess flow.

Meanwhile, the lower midslope shows a full profile response to the early rains (September 2012). The shallow soils have a quick drying cycle compared to soils in the underlying horizons. Similar to the upper midslope, due to the presence of duplex soils, water retention is expected to be high in the underlying horizons where there are finer soil particles. Interesting to note on this catena element is how the intermediate soils (depth=300 mm) retained moisture for the greater part of the season whilst the deep and shallow soils dried out. A possible interpretation is that the soils are in a region less affected by both evaporation from the soil surface and transpiration from the deep root zone. Since the upper midslope catena element is showing a disconnection with this lower midslope, this means water retained on this site is probably due to direct infiltration or to a lesser extent, contributions through overland flow from upslope catena elements after high intensity events.

The riparian zone show full profile responses to most rainfall events for the greater part of the season. The responses show more or less similar wetting and drying cycles. The rapid drying cycles are an indication of high evapotranspiration and/or free drainage. %ED data is similar for the full profile implying a well-drained profile but a relatively dry one (>1000 mm) for more than 90% of the time. This catena element may be connected to the lower midslope element but this data suggests a disconnection from the adjacent 3rd order stream network. This augments the hydropedological classification for this profile which suggests recharge (potential).

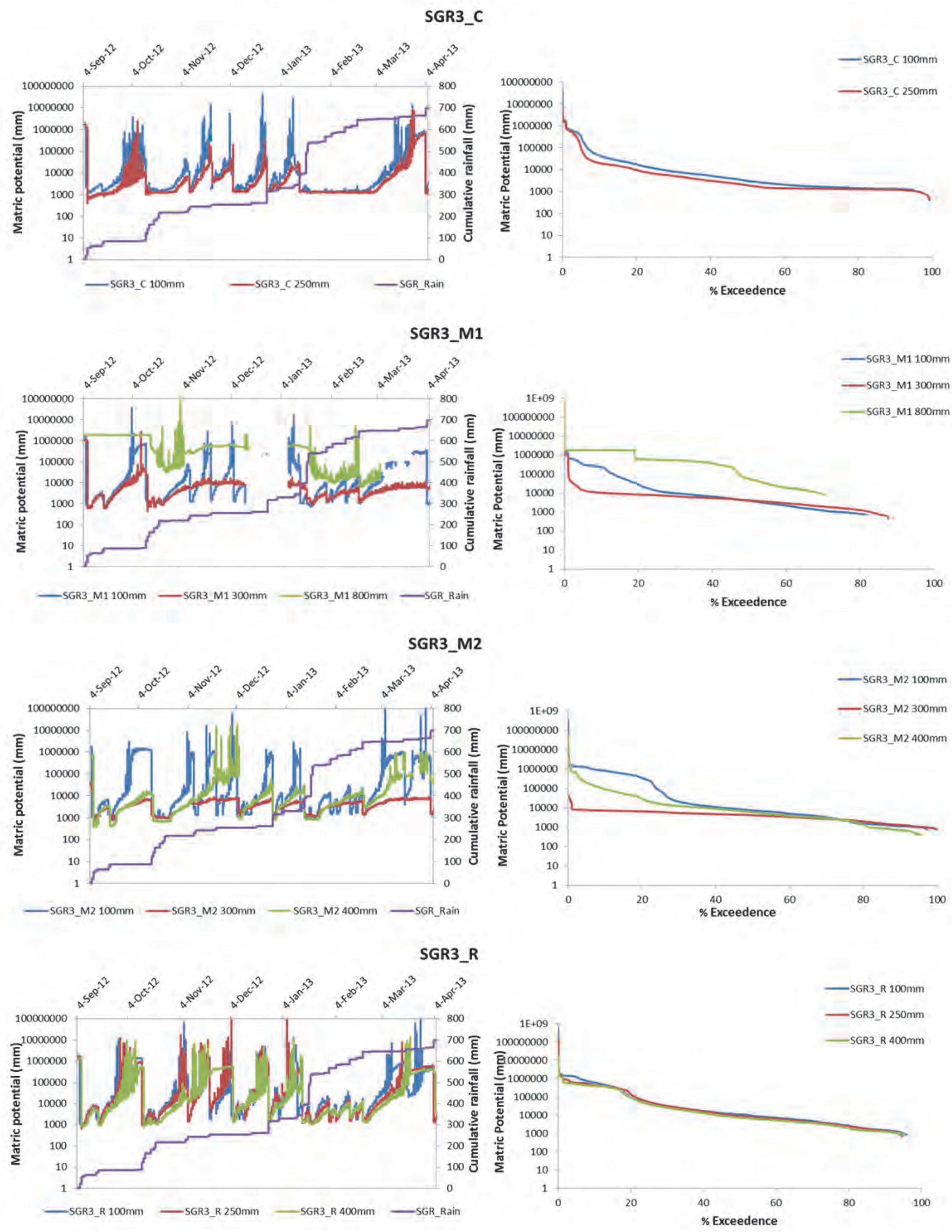

Figure 5.41: Soil matric potential responses and % ED curves along the southern granite supersite third order hillslope between September 2012 and April 2013

Hillslope Class 2: Shallow Responsive

The 3rd order hillslope (Figure 5.42) is dominated by shallow responsive soils. This hillslope has a large highly developed grassy midslope that comprises a duplex Sterkspruit soil form on both the upper and the lower midslope. This therefore implies responsive soils at this catena element. Meanwhile, lateral contributions from the crest result in the development of a seepline due to discontinuities in soil texture between the crest and the midslope. On the other hand, the riparian has a potential recharge soil therefore whilst there might be temporal connectivity through overland flow, the free draining soils at this element disconnects this hillslope from the adjacent 3rd order stream network. In terms of storage, this hillslope is expected to also have less storage because the crest and midslope have shallow soils due to underlying shallow rocks. The riparian has deep soils hence more storage is anticipated but due to its free draining nature water loss is anticipated through ET and free drainage.

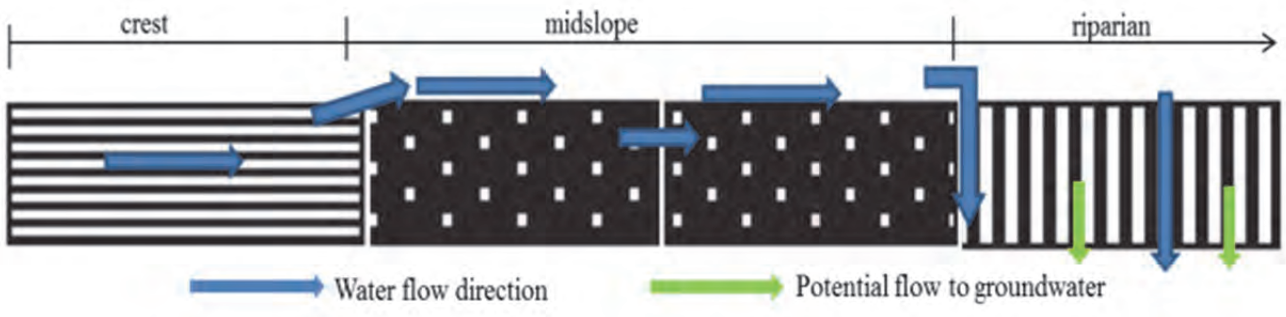

Figure 5.42: Hydrological soil types and flow paths for granite 3rd order hillslope

5.6.3 3rd order Hydrogeology: Hydraulic Responses and Parameters

The 3rd order crest position 34 m and 55 m boreholes generally follow the same trend as each other and are at a similar pressure (see Figure 5.43). The general gradient is relatively steep during the September 2012 rainfall events as a result of the water levels equilibrating after the completion of borehole installation. The dH increased by 0.16 m and 0.06 m for the 55 m and 34 m borehole respectively during the September 2012 sequence 1 rainfall events (See Section 4.1), these changes in hydraulic head are not representative of ambient conditions. The 55 m and 34 m borehole dH increased by 0.07 m and 0.08 m respectively during the October 2012-December 2012 sequence 2 rainfall events with moderate intensity rainfall of 5-35 mm/day over 3 weeks. The gradient is quite gradual during this period. The 55 m and 34 m borehole dH increased by 0.28 m and 0.29 m respectively with a rather gradual gradient during the December 2012-August 2013 rainfall events. Both water levels tend to have an increased gradient after the high intensity January 2013 events (200 mm over 6 days) for roughly 2 months after which it follows a more gradual gradient. These response lags to the different sequences of rainfall events during the hydrological year suggest that the boreholes at this point respond to a regional rather than local groundwater flow system.

The 3rd order mid-slope position boreholes generally follow the same trend as each other (Figure 5.44), however the 49 m borehole has a higher pressure than the 23 m and 26 m boreholes which suggest the 43 m borehole is flowing towards or contributing to the 23 m and 26 m boreholes. This distinction of groundwater head pressures at the 3rd order hillslope possibly indicates that the deeper groundwater system eventually intersects or contributes to higher order streams outside of this 3rd order study area. The dH increased by

0.12 m, 0.13 m and 0.11 m in the 49 m and 26 m and 23 m boreholes respectively during the sequence 1 sequence rainfall which consisted of moderate intensity rainfall (5-31 mm/day for 2 weeks). The gradient during this period was relatively steep due to the water levels equilibrating following borehole installation. These responses are thus not as a result of ambient conditions. The dH increased by 0.06 m for the 55 m and 0.02 m for the 26 m and 23 m boreholes during the sequence 2 rainfall with a decrease in gradient. The dH increased by 0.31 m, 0.28 m and 0.23 m for the 55 m, 26 m and 23 m boreholes respectively with an increase in gradient during the December 2012-August 2013 sequences of rainfall events.

The 3rd order riparian position boreholes(Figure 5.45) generally follow the same trend as each other, however the 43 m borehole has a higher pressure than the 20 m borehole which suggests the 43 m borehole is flowing towards or contributing to the 20 m borehole. This separation of pressures at the 3rd order hillslope possibly indicates that the deeper groundwater system eventually intersects or contributes to higher order streams. The dH increased by 0.12 m and 0.09 m for the 43 m and 20 m borehole respectively with a relatively steep gradient of 0.0016 m/d during the September 2012 sequence 1 rainfall events. The steep gradient was likely due to the water levels equilibrating as a result of the borehole installation. The increase in dH is therefore not under ambient conditions. The dH increased by 0.08 m and 0.05 m for the 43 m and 20 m boreholes respectively with a decrease in gradient during the sequence 2 rainfall. These rainfall events consisted of moderate intensities (5-35 mm/day for 3 weeks). The dH increased by 0.39 m and 0.41 m for the 43 m and 20 m boreholes respectively with an increase in gradient during the December 2012-August 2013 sequences of rainfall events. The 43 m and 20 m borehole water level tends to comprise of an increase in gradient for 2 months as a result of the high intensity rainfall during January 2013 after which it follows a more gradual gradient.

The 3rd order triangulation boreholes (Figure 5.46) generally follow the same trend as each other; however the 61 m borehole has a higher pressure than the 34 m borehole. This suggests the 61 m borehole is flowing towards or contributing to the 34 m borehole. Again this indicates that the deeper groundwater system at the 3rd order eventually intersects or contributes to higher order streams. The dH increased 0.78 m and 0.37 m for the 61 m and 34 m borehole respectively with a relatively steep gradient of 0.0091 m/d during the October 2012-December 2012 rainfall period. These increases in dH and gradients are likely to occur as a result of the water levels recovering from the borehole installation phase. The low transmissivity (Table 5.2) also contributes to the prolonged recovery of water levels at this point. These increases in dH are therefore not occurring as a result of ambient conditions. The dH increased to 0.37 m and 0.32 m for the 61 m and 34 m borehole respectively with a gradual gradient present during the December 2012-August 2013 rainfall sequences. The 61 m and 34 m borehole water level gradient increased as a result of the high intensity sequence of rainfall events during January 2013 for 2 months after which it followed a gradual gradient. The drop in dH for the 34 m borehole at 2013/04/25 was due to specific depth sampling.

Specific conductance analysis for the 3rd order crest 55 m borehole SC does not change significantly during the fluid logs (Figure 5.47). This suggests no active influx of fresh groundwater (low SC) or rainfall into the deep groundwater system at this point. The response in water level to the moderate and high intensity sequence of rainfall events occurring in October 2012 and January 2013 respectively has quite lengthy lag times of roughly 2 months. Supporting again that a regional groundwater flow process is likely to be associated at this point. The 3rd order crest position 34 m borehole SC slowly decreases at the November 2012 fluid log and continues to decrease with the consequent logs. The water level response at this point does not correlate with a decrease in SC inferring a possible recharge event. However possible interflows from the lower order weathered aquifer hillslopes are likely to contribute active and therefore fresh (low SC) groundwater flow.

The 3^{rd} order mid-slope 49 m borehole does not change significantly during the fluid logs. This also suggests no active influx of fresh groundwater (low SC) or rainfall into the deep groundwater system at this point. The response in water level at this point has a lag of 2 months. Change in SC in the 49 m borehole fluid log profile at 323 mamsl is likely to be a fractured zone as the lithology log describes highly weathered and fractured granite at this depth in Figure 4.47. The 3^{rd} order mid-slope position 26 m borehole SC decreases quite significantly during the February 2013 fluid log. The water level response at this point does not correlate with the decrease in SC which is inferred as a recharge event. It's speculated again that interflows from the lower order weathered aquifer hillslopes are actively contributing fresh (low SC) groundwater flow to this point.

The 3^{rd} order riparian 43 m borehole (Figure 5.48) SC does not change significantly during the fluid logs. This suggests no in-flux of fresh groundwater (low SC) or rainfall into the deep groundwater system at this point. The water level response at this point does not respond rapidly to the moderate and high intensity rainfall events seen in sequences 2 and 3. This supports a regional groundwater flow process. The 3^{rd} order riparian position 20 m borehole SC has a very slight decrease at the February 2013 and consequent fluid logs. The in-active groundwater flow system at the 43 m and 20 m boreholes suggests that the 3^{rd} order stream does not contribute to the shallow and deep groundwater flow system at this point. This flow system is likely to respond on a regional scale when considering the lag in water level responses following 3 major events of rainfall sequences monitored in this study.

The 3^{rd} order triangulation 61 m borehole SC (Figure 5.48) does not change significantly during the fluid logs, suggestive of no entry of fresh groundwater (low SC) or rainfall into the deep groundwater flow system at this point. The water level response at this point has a lengthy lag of about 3 months to the moderate to high intensity rainfall events of December 2012-February 2013. Therefore a regional groundwater flow process is likely to be associated at this point. The 3^{rd} order triangulation position 34 m borehole SC slowly decreases at the November 2012 fluid log and continues to decrease with the consequent logs which suggests that possible interflows from the lower order weathered aquifer hillslopes are contributing active and therefore fresh (low SC) groundwater flow to the 34 m borehole.

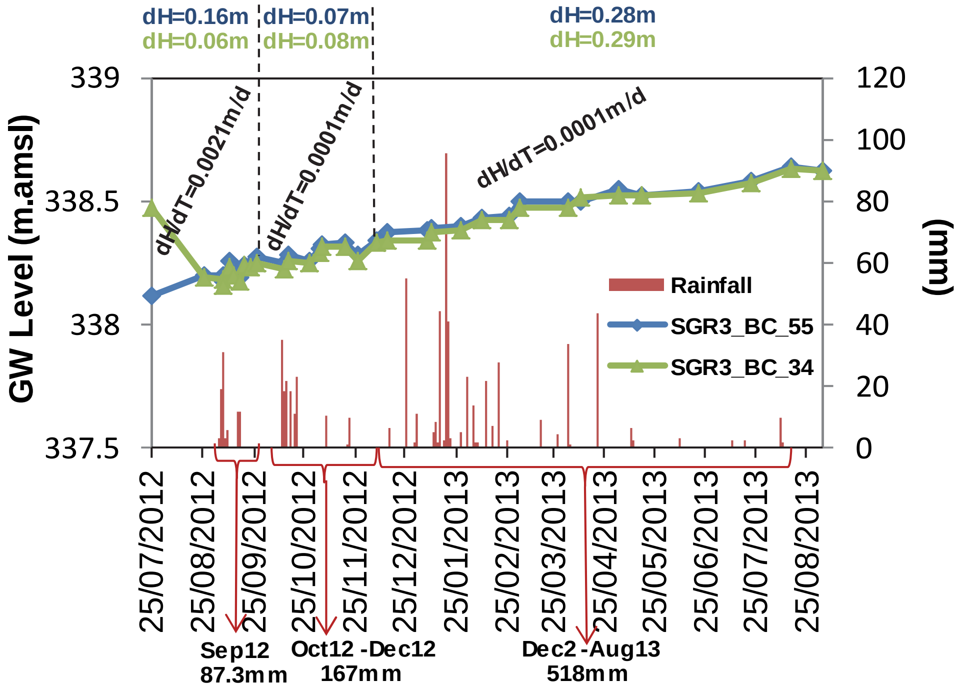

Figure 5.43: 3rd order crest position 34 m and 55 m borehole water level response to rainfall over the hydrological season September 2012 to September 2013

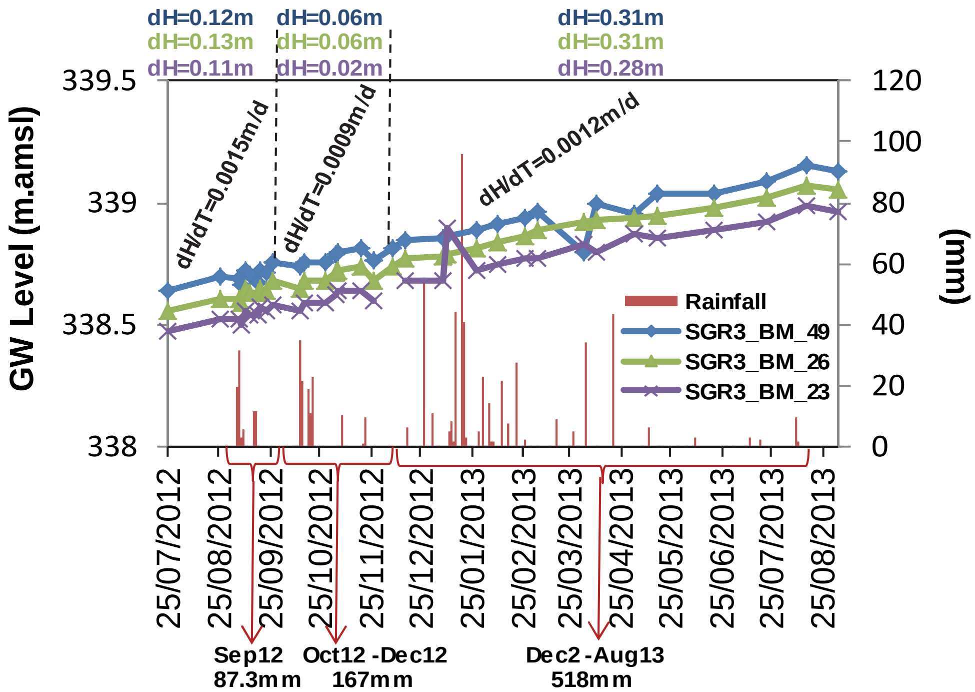

Figure 5.44: 3rd order mid-slope positionb23 m, 26 m and 49 m borehole water level response to rainfall over the hydrological season September 2102 to September 2013

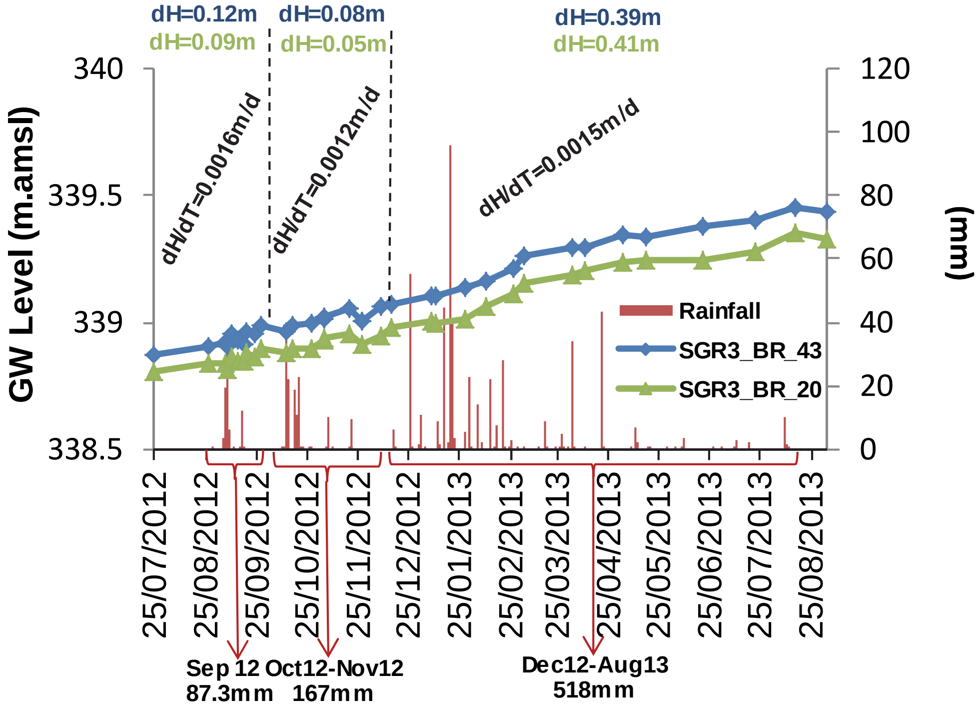

Figure 5.45: 3rd order riparian position 20 m and 43 m borehole water level response to rainfall over the hydrological season September 2012 to September 2013

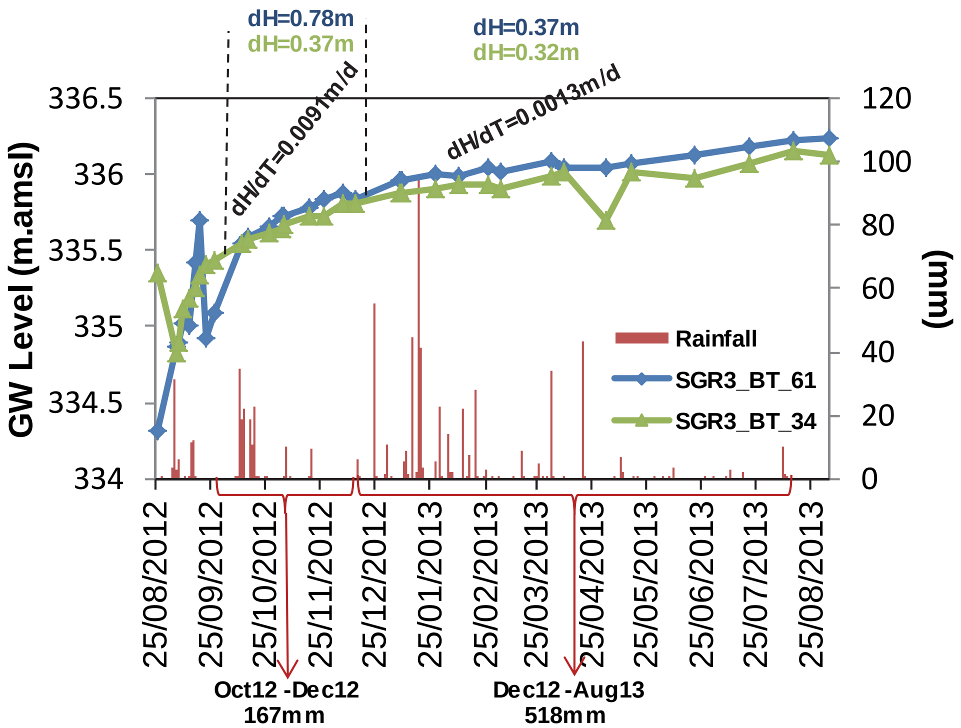

Figure 5.46: 3rd order triangulation position 34 m and 61 m borehole water level response to rainfall over the hydrological season September 2012 to September 2013

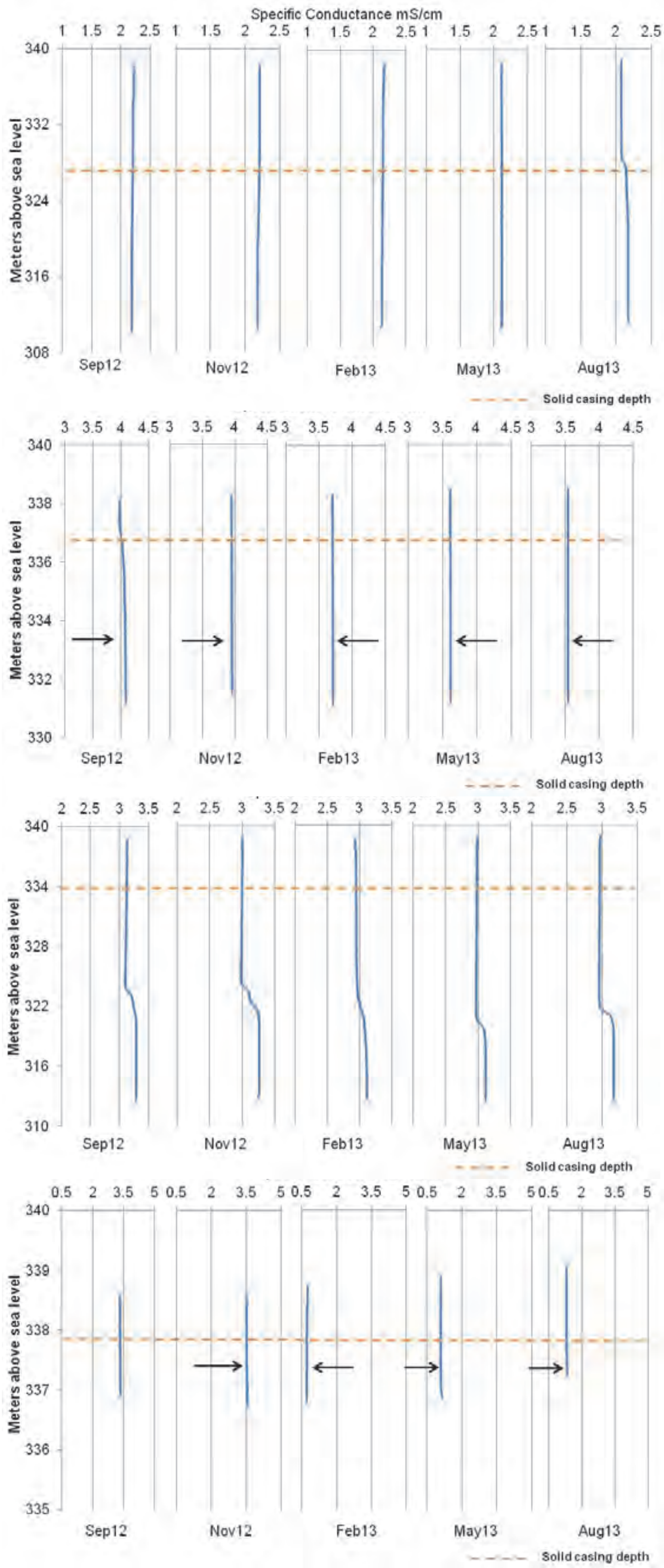

Figure 5.47: Specific conductance quarterly fluid log for the 3rd order crest position 55 m borehole (top), crest 34 m borehole (upper-mid), 3rd order mid-slope position 49 m borehole (lower-mid), and mid-slope position 26 m borehole (bottom).

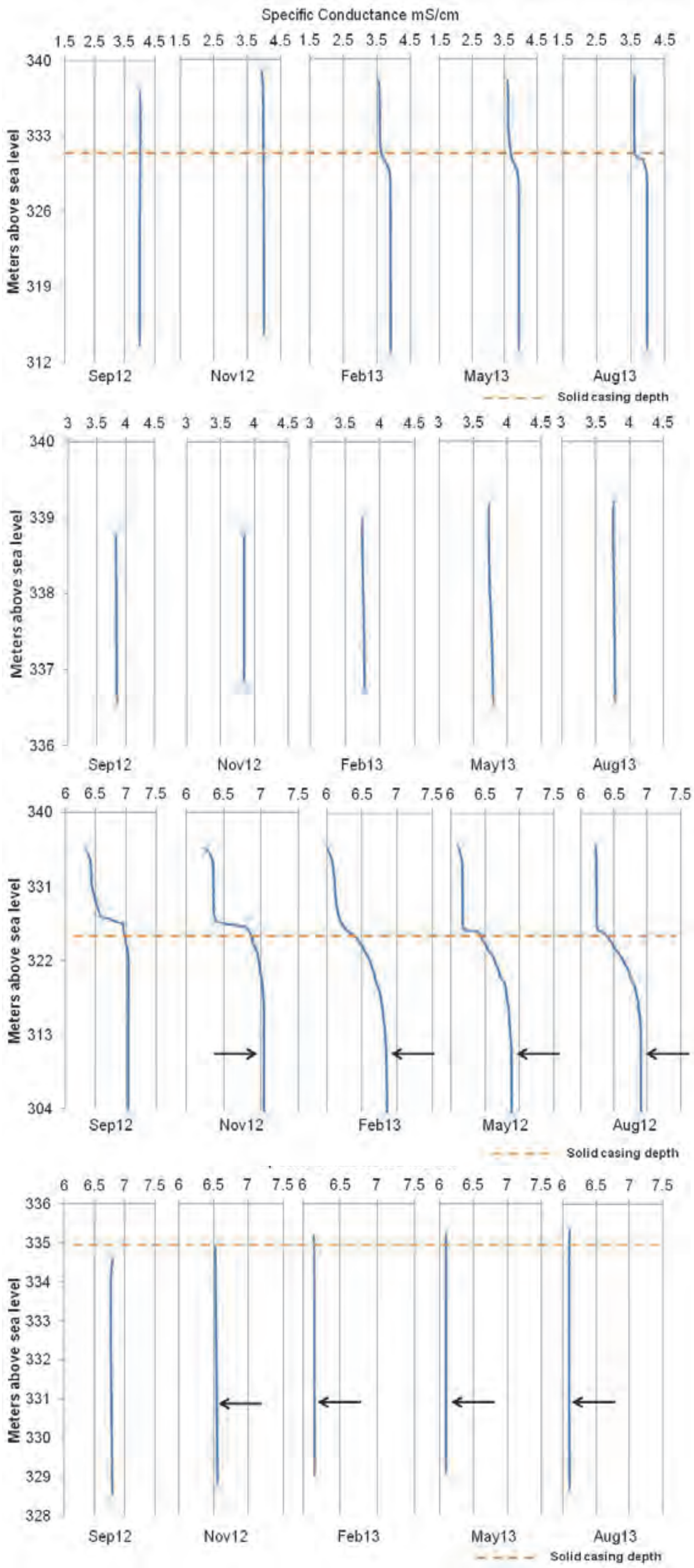

Figure 5.48: Specific conductance quarterly fluid log for the 3rd order riparian position 43 m borehole (top), riparian 20 m borehole (upper mid), 3rd order triangulation position 61 m borehole (lower-mid), and 3rd order triangulation position 34 m borehole (bottom).

5.7 Spatial Integration of Groundwater Data

5.7.1 Spatial distribution of groundwater head within the southern granite Supersite

The spatial diagram (Figure 5.49) illustrates the general flow contours of the deep boreholes. The water levels are quite deep and the gradient is from the 1st order hillslope towards the 3rd order hillslope and roughly parallel to the stream. This suggests that the deep fractured rock groundwater water is probably disconnected from these 3 stream orders. Figure 5.50 illustrates the general groundwater flow direction of the shallow boreholes. The water levels are quite shallow at the 1st order and deepen further and lower down the catchment. The gradient is in the direction from the 1st order crest toward the 1st order stream where there is extensive rise in water levels, suggesting a possible shallow aquifer contribution to stream flow for short periods after large rainfall events.

5.7.2 Spatial distribution of average specific conductance for the southern granite supersite boreholes

The average specific conductance or SC for the dry (May 2013 and August 2013) and wet (November 2012 and February 2013) season fluid logs have been plotted to enable the spatial observation of the change in SC for the shallow and deep boreholes across the catchment. These spatial SC plots (Figure 5.51-5.54) correlate with the groundwater flow direction seen in figure 5.49 and Figure 5.50 which moves from the 1st order hillslope boreholes with low SC towards the 3rd order hillslope boreholes with higher SC. Across the catchment the SC during the dry season fluid logs was slightly lower that the wet season fluid logs. This suggests that the generally low T values (Table 5.2) across the catchment resulted in the slow movement of fresh or low SC water through the shallow and deep groundwater flow system.

5.7.3 Spatial distribution of average temperatures for the southern granite supersite boreholes

The average temperatures for the dry (May 2013 and August 2013) and wet (November 2012 and February 2013) season fluid logs have been plotted to enable the spatial observation of the change in temperature for the shallow and deep boreholes across the catchment (Figure 5.55 and Figure 5.56). The general temperature gradient correlates with the groundwater flow direction moving from the high temperatures at the 1st order hillslope boreholes towards the low temperatures on 3rd order hillslope boreholes. However there appears to be a temperature gradient along each hillslope. The gradient extends from the crest towards the riparian zones.

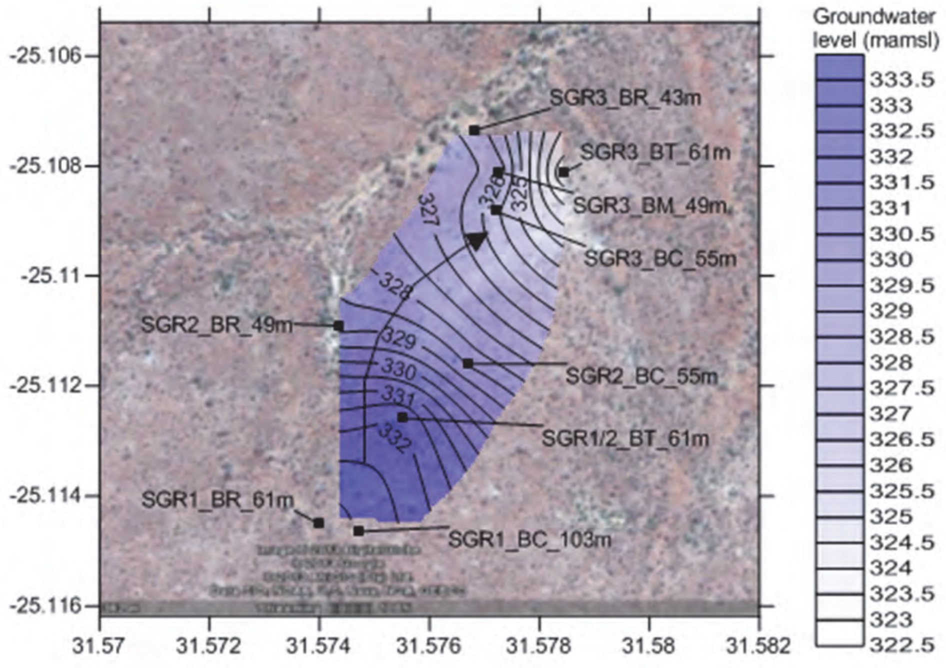

Figure 5.49: General groundwater contours of the deep boreholes within the southern granite Supersite.

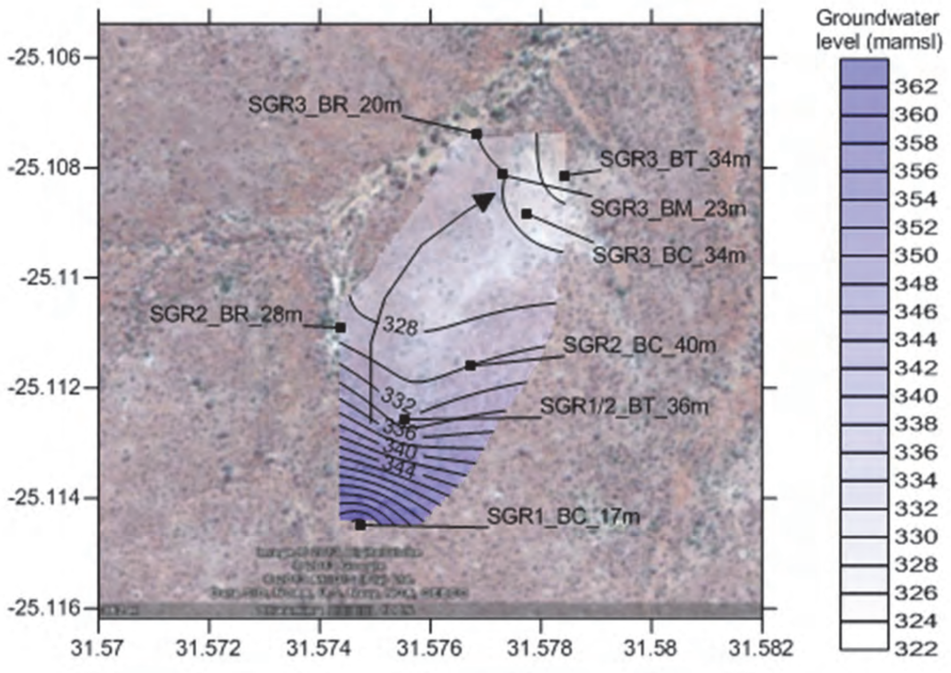

Figure 5.50: The general groundwater flow direction of the shallow boreholes within the southern granite Supersite.

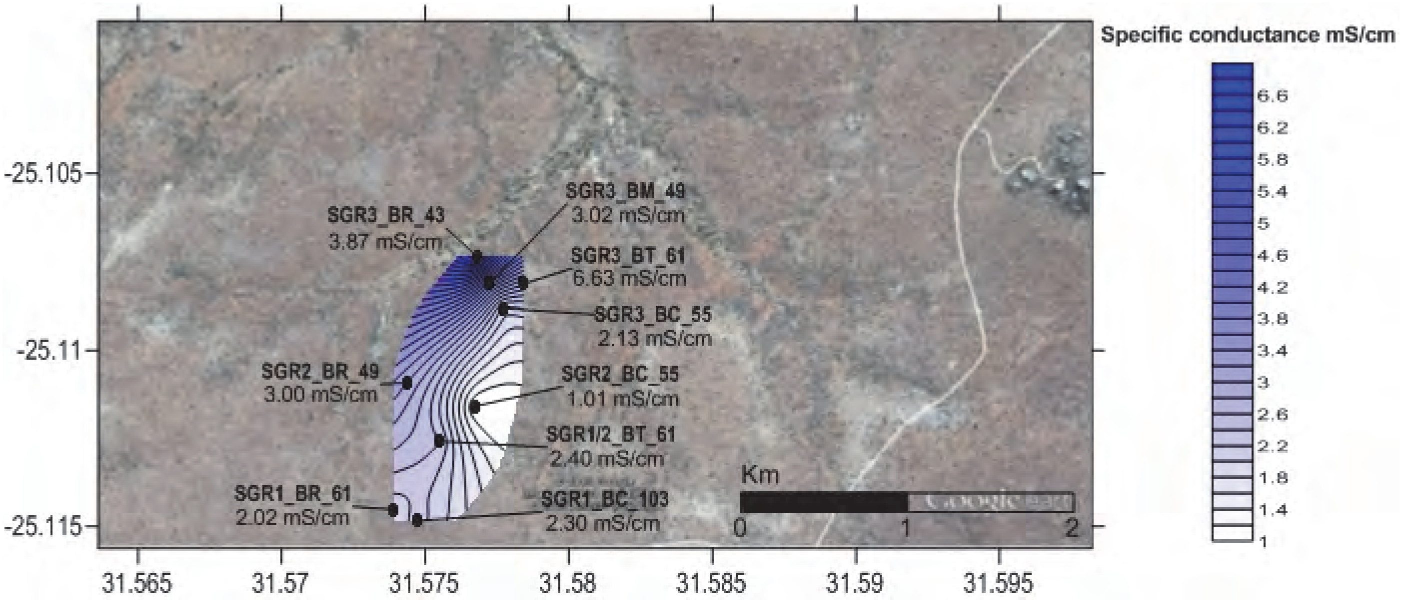

Figure 5.51: Spatial distribution of specific conductance for the southern granite supersite deep boreholes during the dry season combined averaged value fluid logs of May 2013 and August 2013.

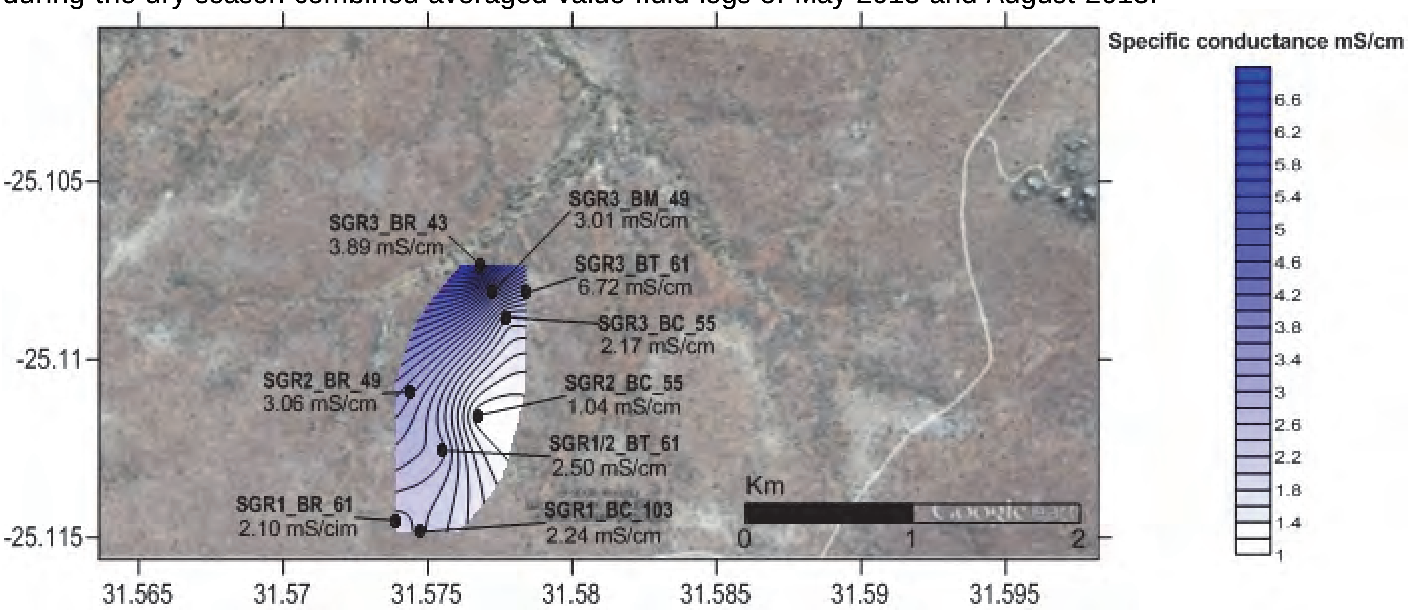

Figure 5.52: Spatial distribution of specific conductance for the southern granite supersite deep boreholes during the wet season combined averaged value fluid logs of November 2012 and February 2013.

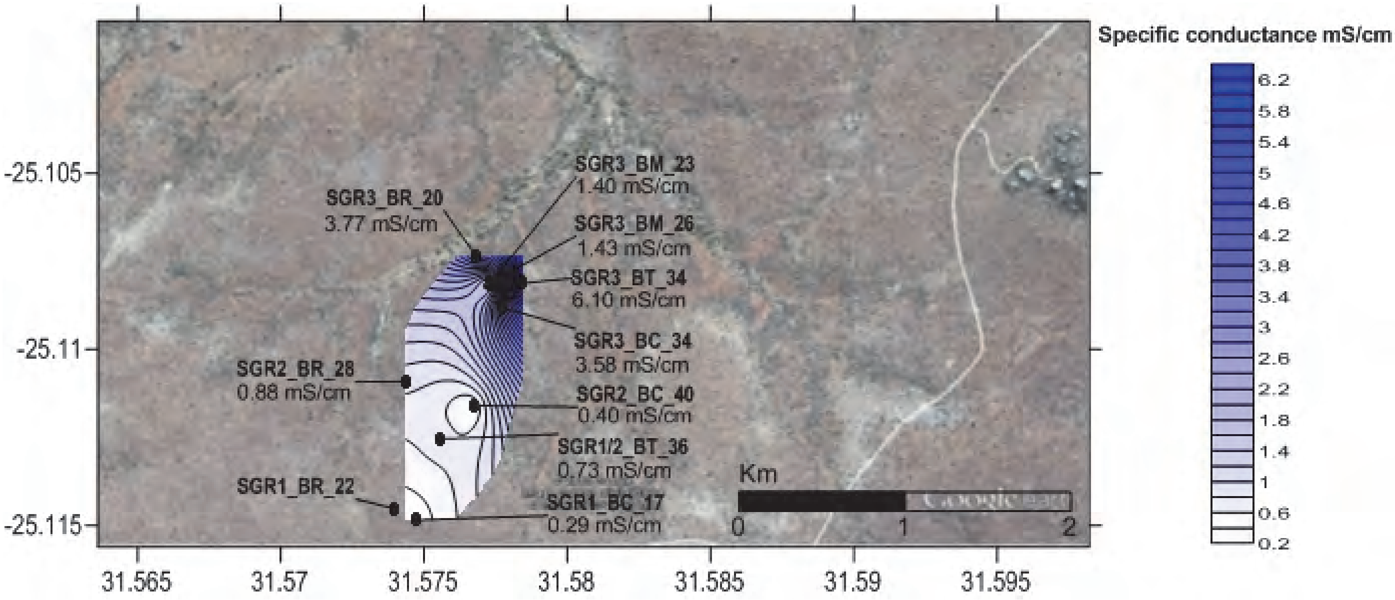

Figure 5.53: Spatial distribution of specific conductance for the southern granite supersite shallow boreholes during the dry season combined averaged value fluid logs of May 2013 and August 2013.

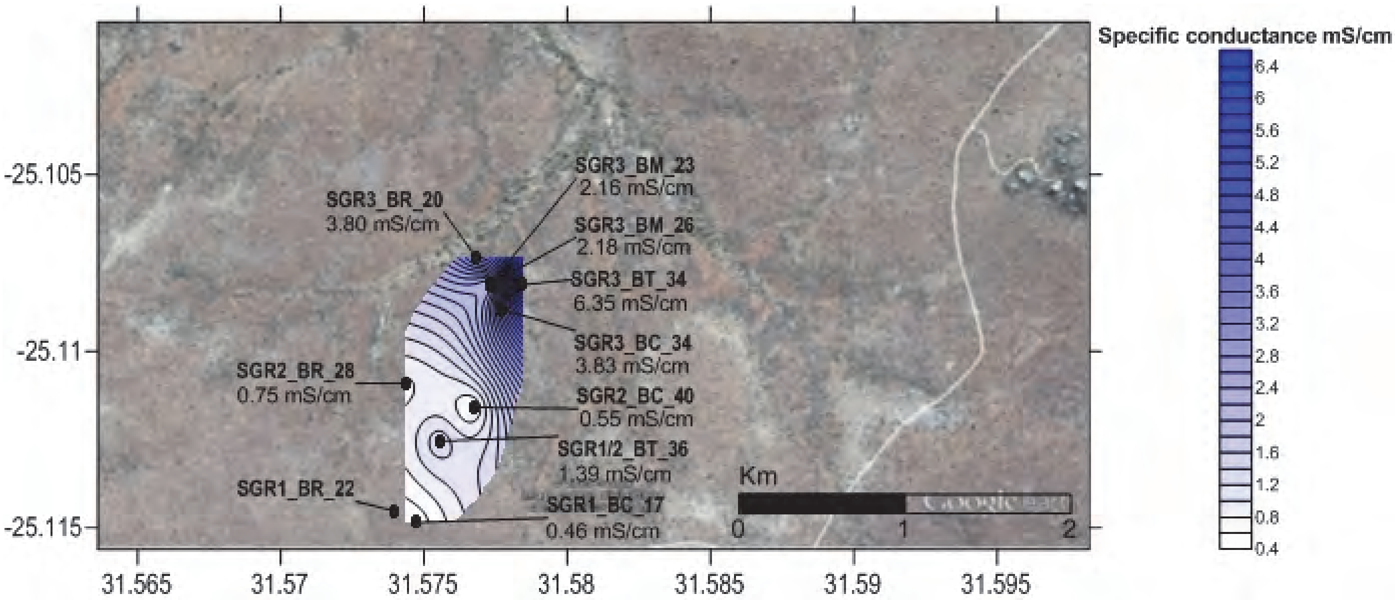

Figure 5.54: Spatial distribution of specific conductance for the southern granite supersite shallow boreholes during the wet season combined averaged value fluid logs of November 2012 and February 2013.

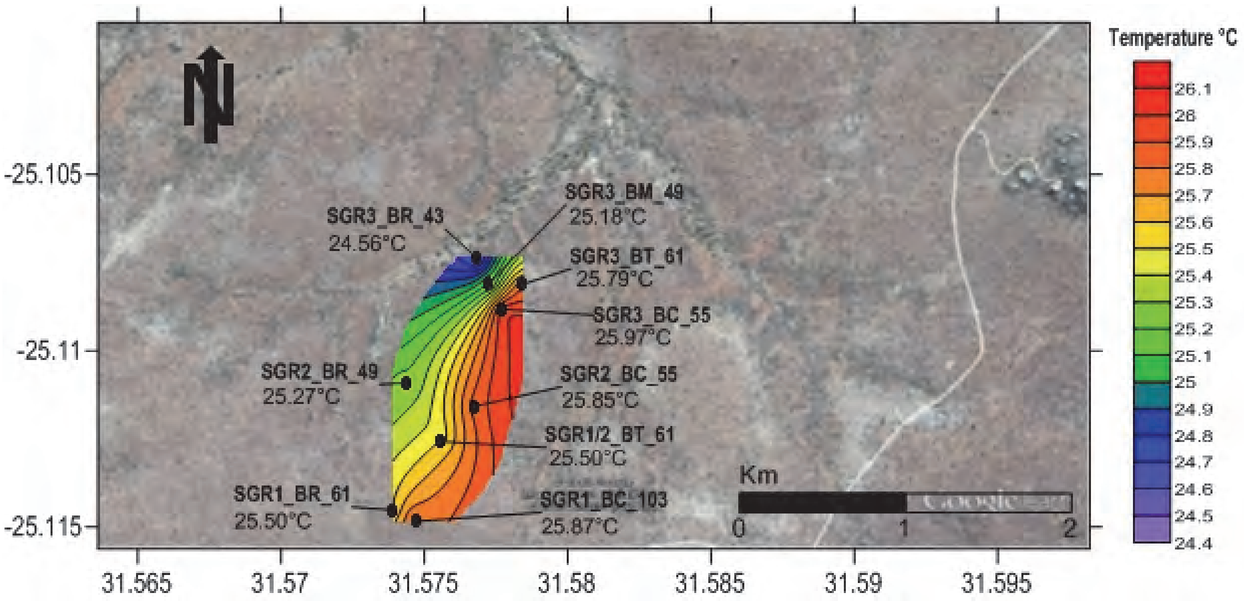

Figure 5.55: Spatial temperature distribution for the southern granite supersite deep boreholes during the hydrological season fluid logs of November 2012 to August 2013.

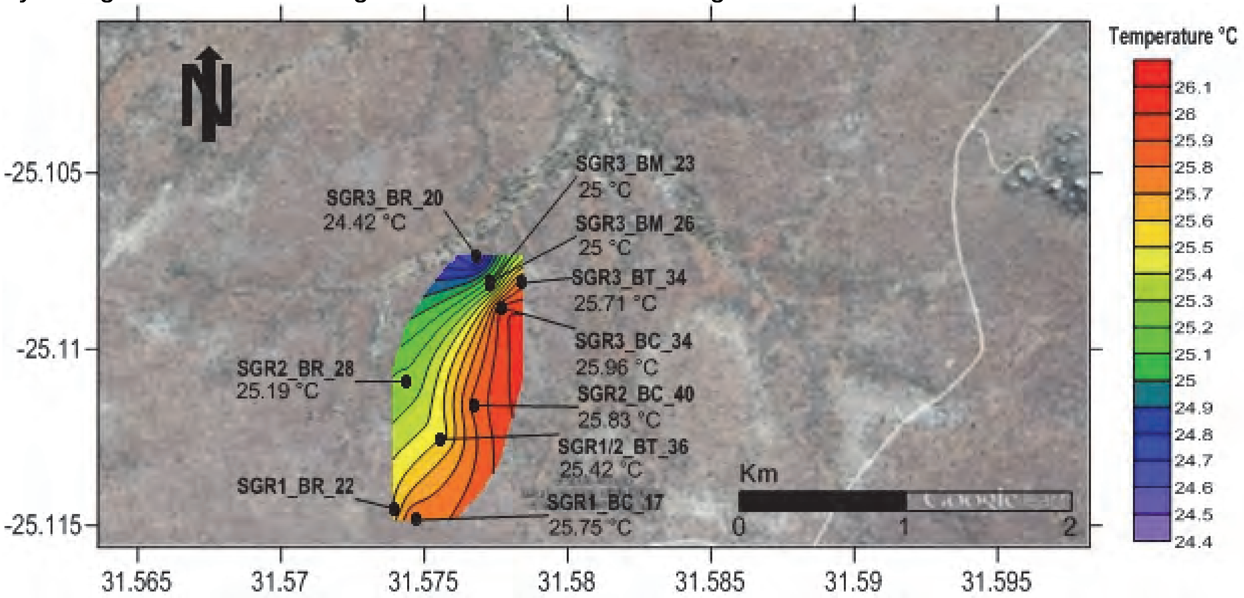

Figure 5.56: Spatial temperature distribution for the southern granite supersite shallow boreholes during the hydrological season fluid logs of November 2012 to August 2013.

5.8 Hydrological Modelling

5.8.1 Catena Water Balances (HYDRUS)

5.8.1.1 Atmospheric Input Variables

Rainfall on the southern granite supersite is described in section 5.1. Meanwhile in terms of aET the 1st order hillslope Figutr 5.57 showed distinct differences in water use between the three catena elements with highest demand at the riparian zone (809 mm) whilst the crest and midslope had 765 mm and 784 mm respectively. At the beginning of the season between the 10th of October and 10th of November, it shows that the midslope and the riparian did not have much variation in water use compared to the crest which had low water use from the onset.

The 2nd order hillslope (Figure 5.58) does not show much variation in water use between each catena element until the 10th of December 2012. However, from December to the end of the dataset, the crest and riparian zone showed similar water use with 782.5 mm and 779 mm respectively. Meanwhile, the midslope had a lower water use (755 mm).

The 3rd order hillslope as shown in Figure 5.59, show no significant differences in water use between catena elements. The crest has the highest water use (767 mm) followed by the riparian (765 mm) then the midslope (762 mm). Due to a large highly developed grassy area on the midslope of this catena, characterized by many bare patches and a very sparse woody cover, actual ET was anticipated to be lower than the woody crest and riparian zones.

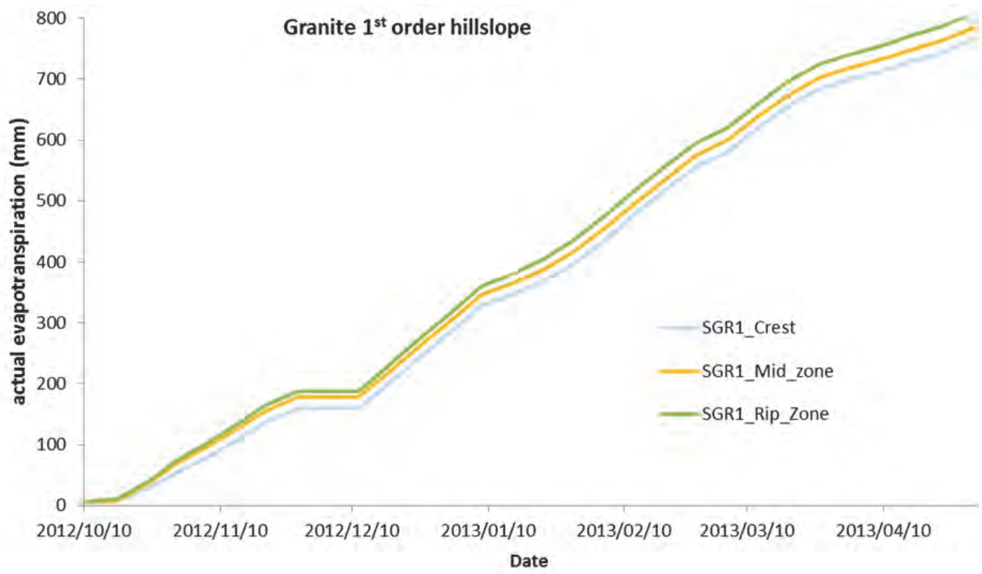

Figure 5.57: ETa per catena element for granite 1st order hillslope

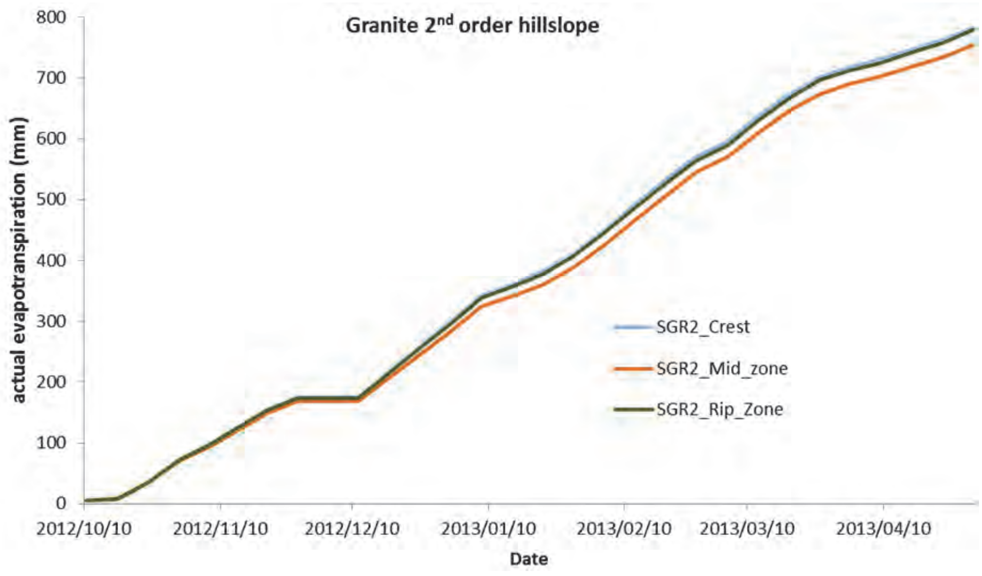

Figure 5.58: ETa per catena element for granite 2nd order hillslope

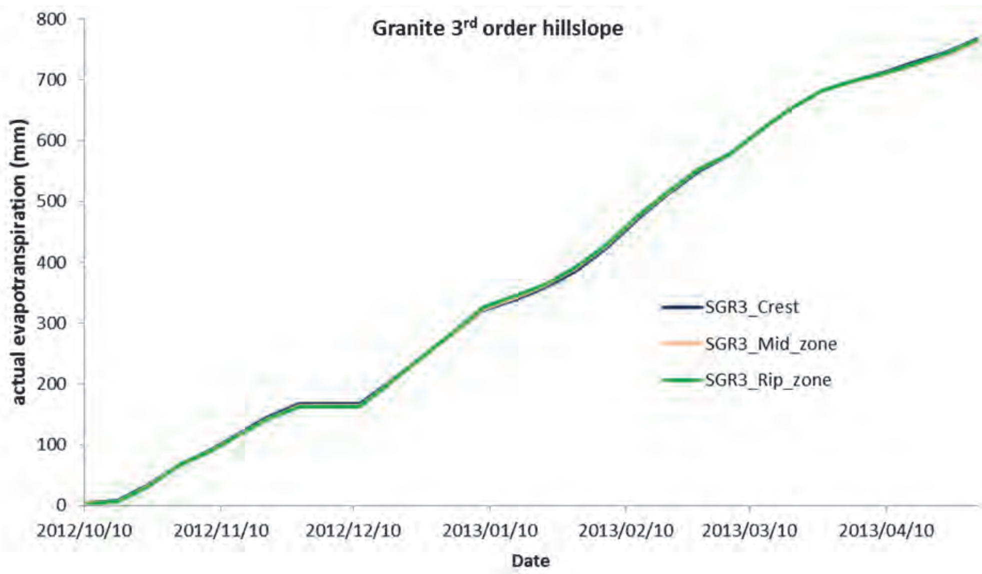

Figure 5.59: ETa per catena element for granite 3rd order hillslope

5.8.1.2 Modelled Hydrological Fluxes

As discussed in section 4.2.12.1 the objective of the modelling was to use atmospheric inputs and soil hydraulic parameters to estimate the remaining hydrological fluxes at the scale of the catena element and thereto determine their water budgets. Furthermore this was to be able to provide an upscaled understanding of hydrological processes at the hillslope scale.

5.8.1.2.1 SGR1 Simulated Results

The 1st order hillslope shows a positive change in storage of 48 mm at the crest whilst the midslope and the riparian zone are shown to be losing water. Based on soil depth, the crest was anticipated to have the least storage compared to the downslope elements since it has shallow soils. As shown in Table 5.13 the midslope and riparian have negative storage because of water loss through ET (470 mm) and (546 mm) respectively compared to the crest (294 mm). However the crest has the greatest free drainage (Figure 5.61) compared to the other downslope elements. At the hillslope scale, it is shown that more water is being lost through ET than free drainage. This is therefore indicative of how the savannah vegetation is able to extract large amounts of water when it is not limited. This was illustrated by watermark responses (Figure 5.22) by the quick drying cycles soon after rainfall events especially in the shallow and intermediate soils.

Figure 5.60 shows the modelled evaporation and transpiration fluxes from the vadose zone into the atmosphere at the 3 catena elements of the 1st order hillslope. At the riparian zone a large proportion of the ET loss is from the soil surface. This was not anticipated since the riparian is characterized by more woody cover and herbaceous vegetation. This could be attributed to uncertainty in the model set up where root depth and density might have been underestimated. The crest and midslope elements are losing water through transpiration than evaporation.

Free drainage increases moving upslope on this hillslope as illustrated on Figure 5.61. The crest has the greatest amount although this wasn't expected given the Cartref soil forms here (Table 5.10) hence the presence of an E horizon, according van Tol (2008), indicates a perched water table and also implies that flow is restricted in some areas of the lithocutanic B resulting in more lateral flow and less free drainage. The crest responds to about 5 of the rainfall events whilst the midslope only responds to 3 events and the riparian responds to only two. This modelled data shows that the majority of these soils only respond to high intensity events of approximately >100 mm/day. This means if there are seasons characterized by low to medium intensity events, there will be less or insignificant amounts of free drainage (potential recharge) especially in the lower elements of this hillslope. A similar observation was also made in a study by Peterson (2011).

Table 5.13: Catena element water budgets for 1st order granite hillslope

	SGR1 Crest	SGR1 Mid	SGR1 Rip
Unit	mm	mm	mm
P	637.6	637.6	637.6
ET	294.9	470.17	546.73
R	0	0	0
FD	294.66	178.36	108.23
ΔS	48	-11	-17

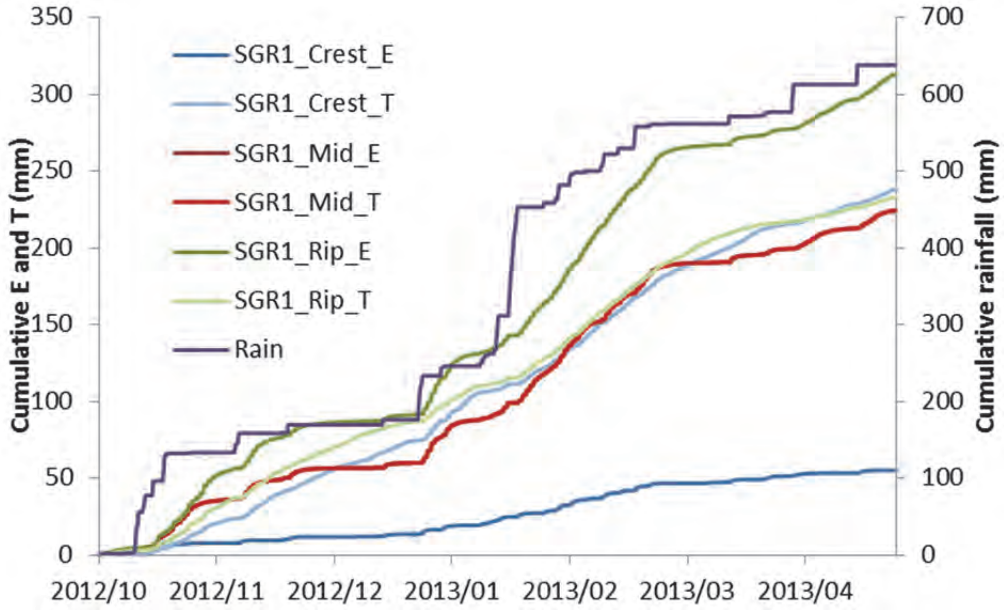

Figure 5.60: Simulated cumulative evaporation and transpiration fluxes on SGR1 hillslope catena elements

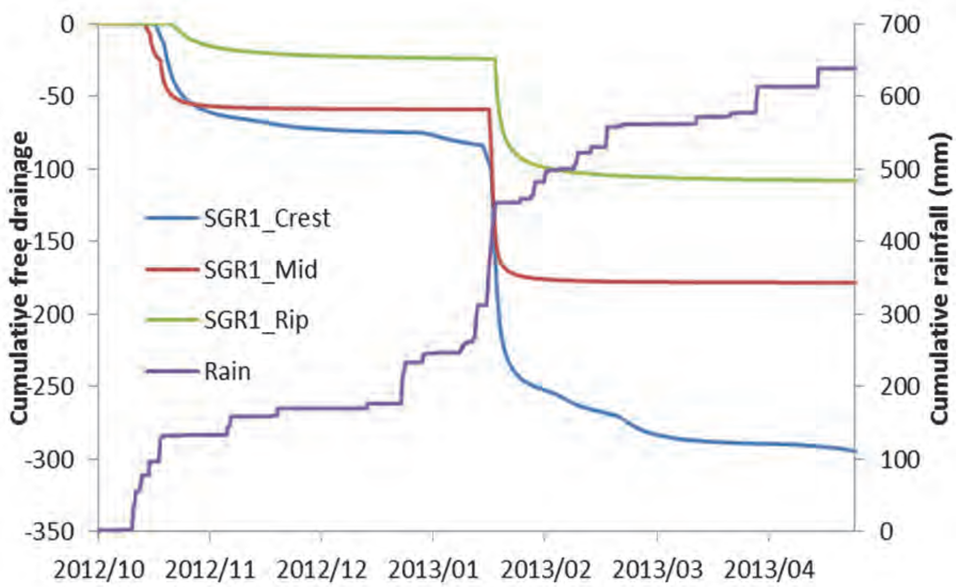

Figure 5.61: Simulated cumulative free drainage fluxes on SGR1 hillslope catena elements

5.8.1.2.2 SGR2 Simulated Results

The crest on the 2nd order hillslope has the greatest change in storage (45 mm) followed by the midslope (10 mm) whilst the riparian zone is losing water (Table 5.14). The riparian zone here lost the most amount of water due to ET as well as free drainage.

The 2nd order riparian zone is the only catena element modelled that experiences surface runoff on this hillslope (Figure 5.62). This catena element has a Cartref soil form therefore interflow is anticipated due to a flow restriction in some parts of the B horizon so this runoff will result from infiltration excess flow. Taking a closer look at the runoff responses on this catena element shows that it was responding to almost all rainfall events not just to those of high intensity impling a responsive soil. Soils at this catena element were classified as shallow interflow soils with a possibility of overland flow.

Water use was greatest on the midslope at this 2nd order hillslope which was not expected but as illustrated on Figure 5.63 losses were mainly through evaporation from the soil surface than through transpiration. Meanwhile the crest and riparian are losing most water through transpiration.

The riparian zone at the 2nd order hillslope experiences the greatest free drainage of water (Figure 5.64). In terms of free drainage responses to rainfall events, the crest and midslope only respond to high intensity events in October and January.

Table 5.14: Catena element water budgets for 2nd order granite hillslope

	SGR2 Crest	SGR2 Mid	SGR2 Rip
Unit	mm	mm	mm
P	637.7	637.6	637.6
ET	420.04	507.39	354.43
R	0	0.012	22
FD	172.69	120.05	272.4
ΔS	45	10	-11

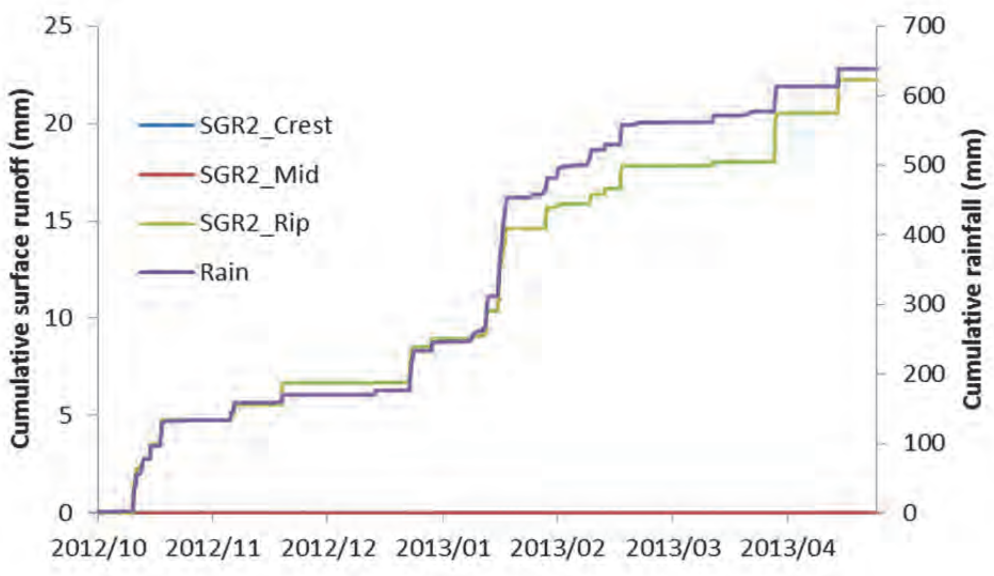

Figure 5.62: Cumulative surface runoff on SGR hillslope catena elements

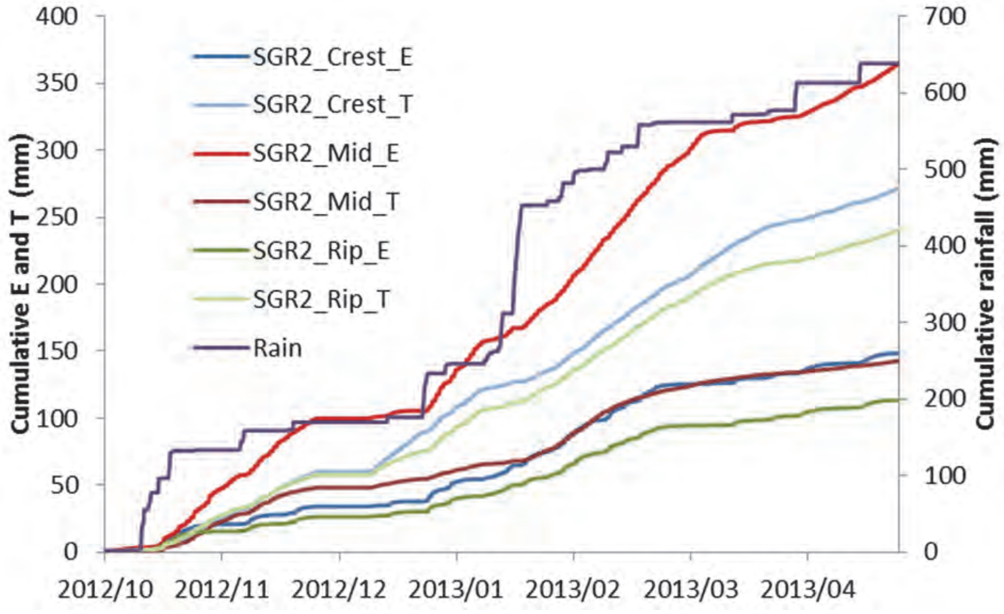

Figure 5.63: Simulated cumulative evaporation and transpiration fluxes on SGR2 hillslope catena elements

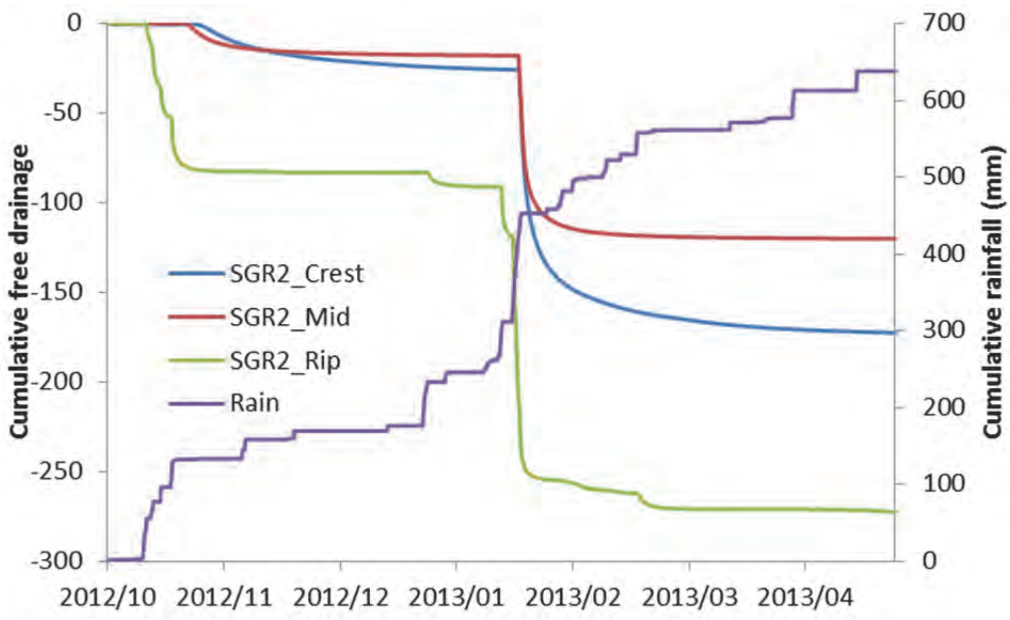

Figure 5.64: Simulated cumulative free drainage fluxes on SGR2 hillslope catena elements

5.8.1.2.3 SGR3 Simulated Results

As shown in Table 5.15 the 3rd order hillslope shows greatest storage change on the riparian (54 mm), followed by the crest (48 mm). The midslope has negative storage losing water through ET showing the highest water use compared to the other catena elements. Similar to the 1st and 2nd order hillslopes; large proportions of water are lost through ET but in terms of storage, this hillslope has the greatest storage (combined) compared to the lower order hillslopes. Factors such as area covered, soil hydraulic properties and vegetation density will be responsible for this storage.

Similar to the 2nd order hillslope, ET was greatest at the midslope of this 3rd order hillslope and at least due to this model set-up more water was lost through evaporation from the soil (Figure 5.65). Meanwhile the crest and the riparian lost more through transpiration than evaporation which was also the case on the 2nd order due to the increased density of woody cover and herbaceous plants on these elements.

Free drainage as shown on Figure 5.66 is highest at the riparian in comparison with the other elements. This augments the hydropedological classification of this catena element as a potential recharge soil. The midslope and riparian zones only respond twice to two high intensity rainfall events (October and January). The crest only responded to the January event. This data shown for the crest augments the low K_{sat} values (Table 5.12: Soil classification per catena element on granite 3rd order hillslope) on the C horizon. This means therefore that flow is restricted in this horizon implying less water will drain from this catena element but would either flow laterally at the A/B interface and some lost through ET. Similar to the 1st and 2nd order hillslope, less free drainage is anticipated under low to medium intensity events.

Table 5.15: Catena element water budgets for 3rd order granite hillslope

	SGR3 Crest	SGR3 Mid	SGR3 Rip
Unit	mm	mm	mm
P	637.6	640.8	637.6
ET	457.46	496.12	382.24
R	3	0	0
FD	129.38	152.39	201.84
ΔS	48	-8	54

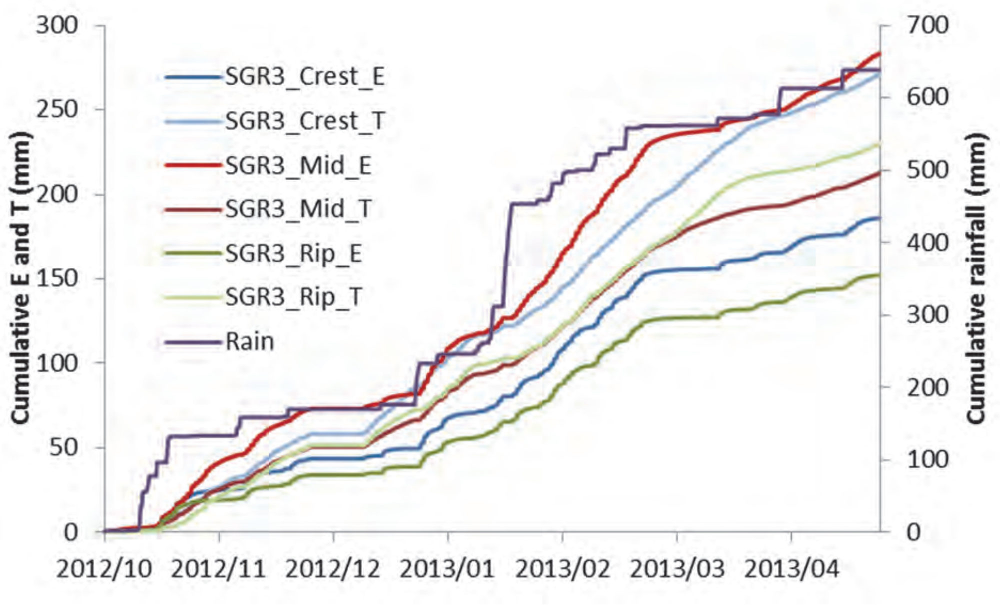

Figure 5.65: Simulated cumulative evaporation and transpiration fluxes on SGR2 hillslope catena elements

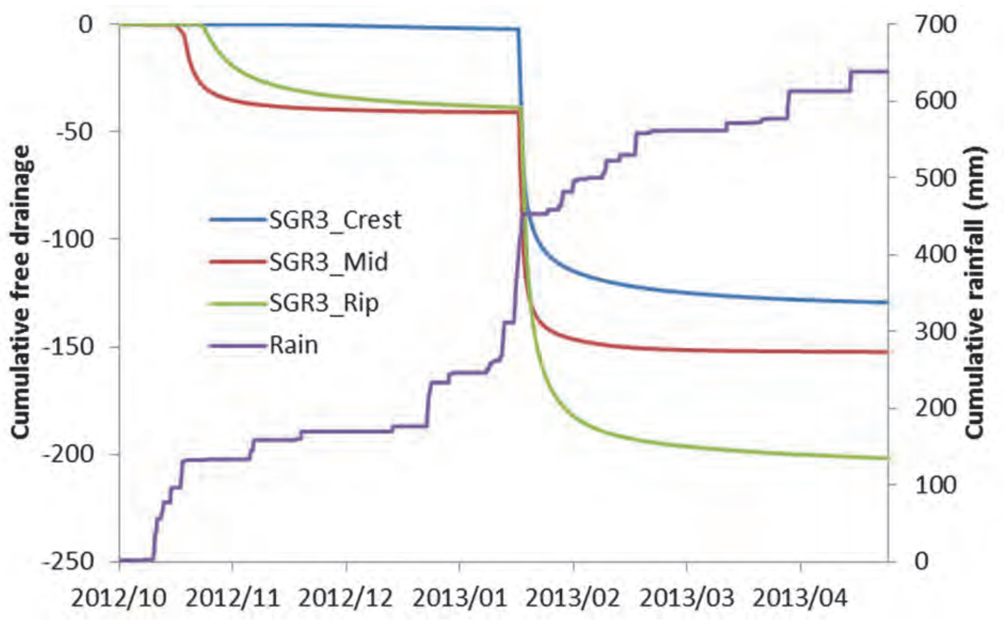

Figure 5.66: Simulated cumulative free drainage fluxes on SGR3 hillslope catena elements

5.8.1.3 Updating the conceptual hillslope models on the Southern Granites

Conceptual models were updated using both the observed data (K_{sat}, K_{unsat} and hydropedological surveys) and simulated data. Results presented below show the initial narrative concepts and the quantitative updated conceptual models derived following the Hydrus 1D modelling.

The 1st order hillslope is dominated by interflow soils (Figure 5.67). Most water leaves the soil domain in this hillslope through free drainage (potential recharge) with a lower contribution of lateral flow. The simulated results show the significance of free drainage after two high intensity events in October hence the high percentage. Therefore under low to medium intensity events, the dominant flowpath will be subsurface lateral flow with a possibility of return flow at the toeslope of this hillslope. Unlike the 2nd and 3rd order hillslopes, the 1st order hillslope shows connectivity with the adjacent 1st order stream through lateral flow.

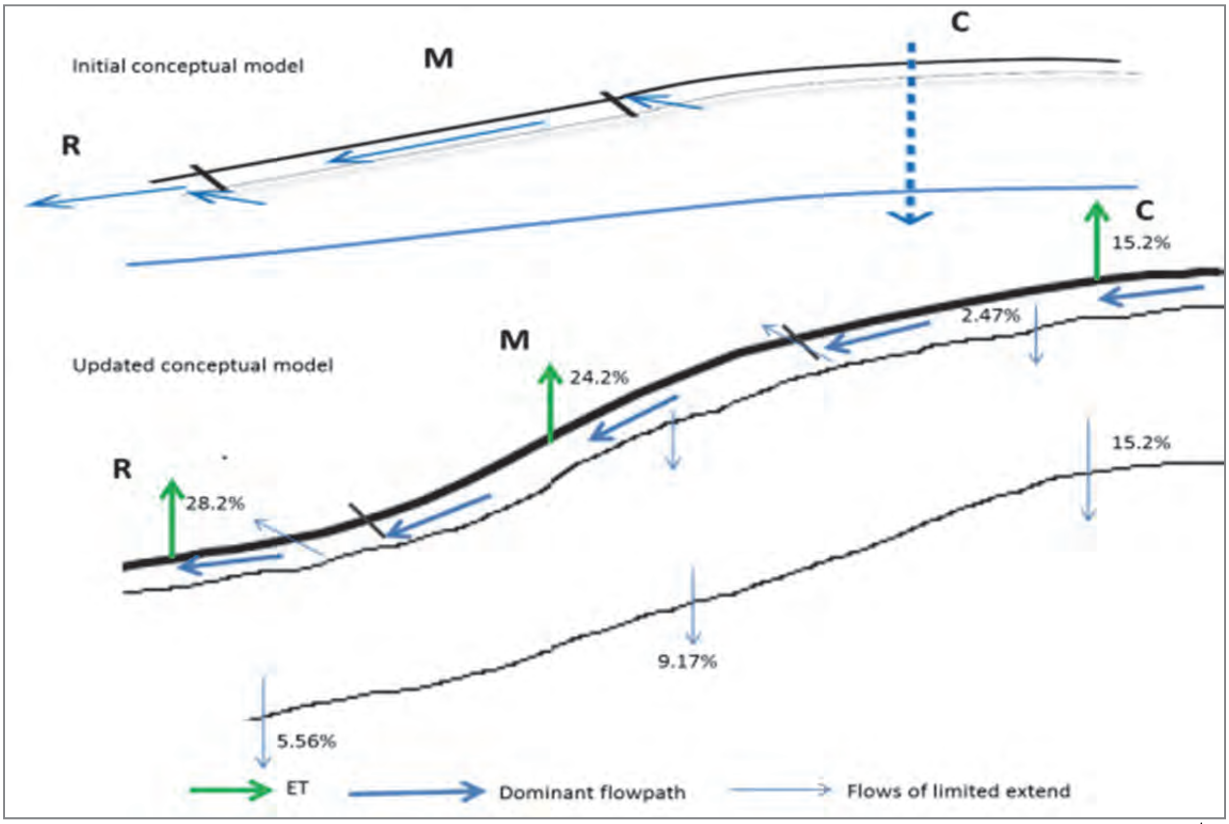

Figure 5.67: Initial and updated conceptual model of Vadose zone water balance for 1st order granite hillslope (values represent proportions of annual rainfall)

The 2nd order hillslope (Figure 5.68) is dominated by interflow (lateral). Similar to the 1st order, free drainage also shows high potential following high intensity rainfall events. Therefore under low to medium intensity rainfall events, the hydropedological interpretations are still embraced for this hillslope. The midslope was characterized as responsive but since it did not generate overland flow even after high intensity events, this implies subsurface flow interflow. Since there are duplex soils on this catena element, flow will be restricted in the B horizon resulting in interflow at the A/B interface.

The 3rd order hillslope was initially anticipated to have recharge soils and interflow (lateral) on the midslope and riparian soils (Figure 5.69). Through hydropedological surveys and conductivity data, the crest comprises interflow soils and the midslope is still classified as responsive. Similar to the 1st and 2nd order, hydropedological interpretations supported by the K data are still embraced.

A comparison of the 3 hillslopes show that a lot of water is being lost through ET with the 3rd order hillslope losing the greatest The modelled responses shows that there is free drainage only after high intensity events. This shows that a threshold rainfall amount and/or intesity is required for certain responses such as free drainage and connectivity between hillslope and stream components. Interflow is the dominant flowpath on the granite hillslopes.

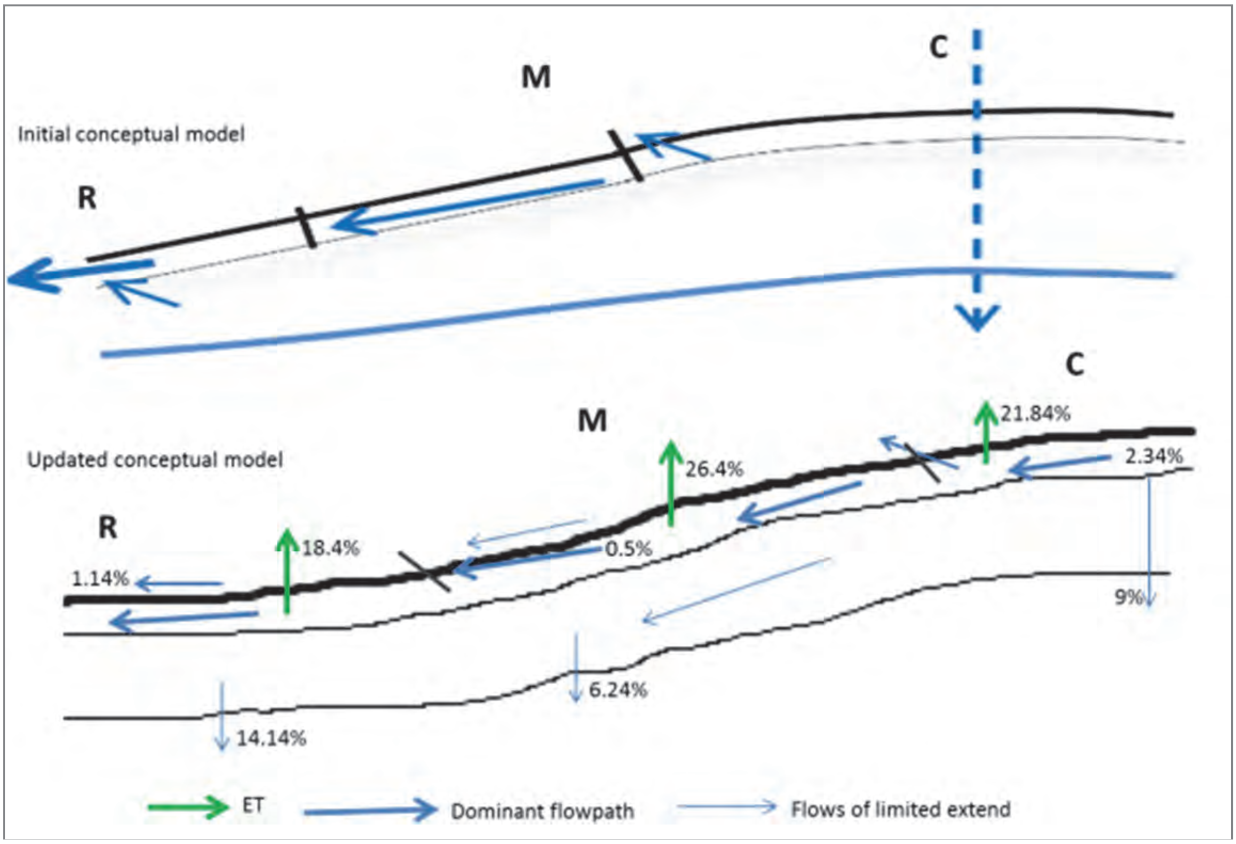

Figure 5.68: Initial and updated conceptual model of Vadose zone water balance for 2nd order granite hillslope (values represent proportions of annual rainfall)

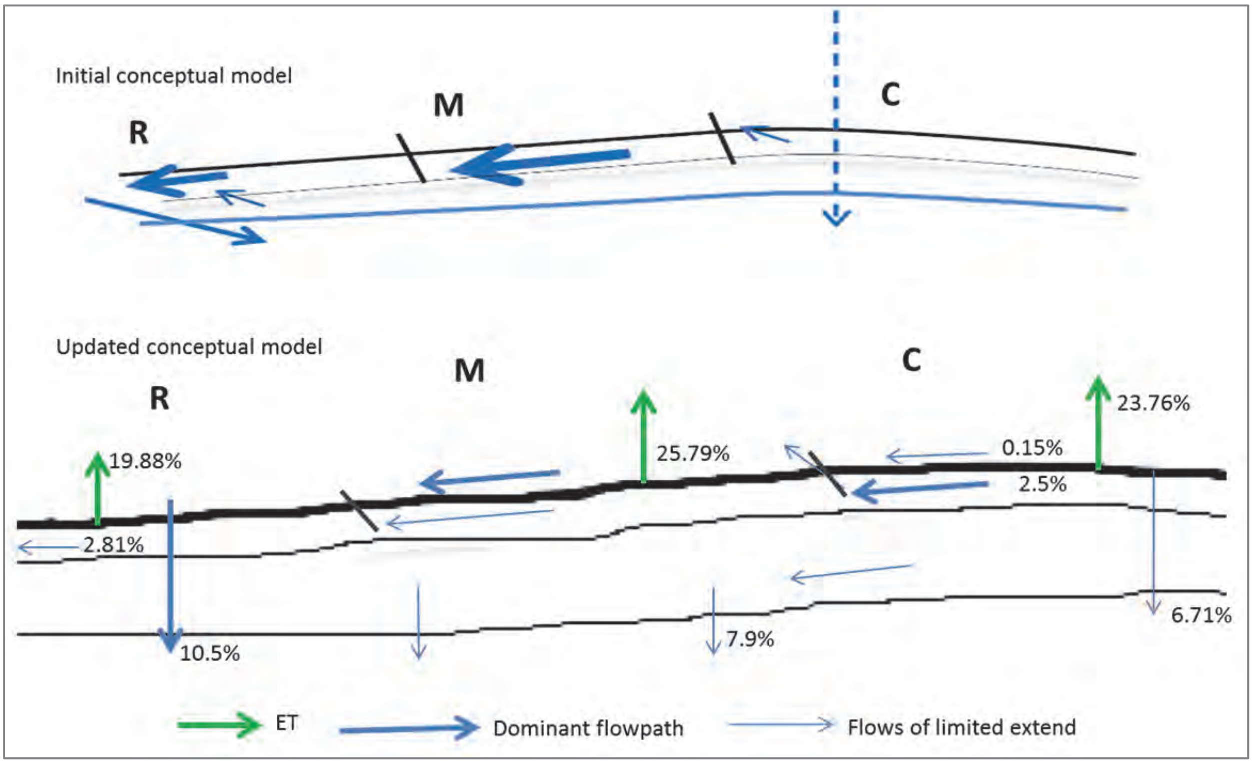

Figure 5.69: Initial and updated conceptual model of Vadose zone water balance for 3rd order granite hillslope (values represent proportions of annual rainfall)

5.8.2 Scaled Geohydrological Processes (Modflow) on the Southern Granites

5.8.2.1 Model Domain Specifications, Mesh and Layers

At the Southern Granites the model domain was defined by topography and surface water catchment boundaries in the area between coordinates 31.55, -25.11 and 31.59, -25.05. Compilation of the finite difference grid using the Groundwater Vistas graphic user interface facilitated the construction of a rectangular horizontal grid, as well as vertical geometry provided for each of the layers. The rectangular grid consisted of 3 layers with a total of 15642 cells (79 x 66 x 3 layers). The positions of the different geological boundaries are incorporated in the modelling grid. A grid of 100 m x 100 m refined to a 6.25 m cell size around the borehole network was allocated to the model. Smaller cell sizes were specified in the areas of the well field where a more accurate solution of the groundwater flow equation is required. Slightly larger cell sizes were specified in other areas. Cell size refinement across the model domain did not exceed 0.5 times the neighbouring cells.

A 3-layer, MODFLOW finite difference grid is applied to the model area as shown in Figure 5.70. The grid is more refined around borehole nests to achieve a more accurate numerical solution. The model layers are broadly defined by hydrogeological units, based on the site conceptual model. Geologic formations within the layers are listed below:

- Layer 1: Shallow groundwater system i.e. alluvium and vadose zone.
- Layer 2: Weathered rock groundwater system.
- Layer 3: Deep groundwater system i.e. consolidated hard rock
- Outflows from the model domain on the Southern Granites were represented by general head boundaries positioned down-gradient from the 3rd order catchment outflow, at an elevation representative of the projected regional groundwater elevation at that point. The MODFLOW Drain package was used instead of rivers because of the ephemeral nature of streamflows in the study site, since flows are event driven and are of limited duration. Drain cells were assigned lengths and widths in such a way that they could totally fill the entire surface area of the cell. No flow boundaries were specified in areas outside the model domain since these are a special kind of constant flux boundary where the flow is set to zero indicating their exclusion from the flow system. The drain, no flow and general head boundary conditions specified in the current model are shown in Figure 5.71.

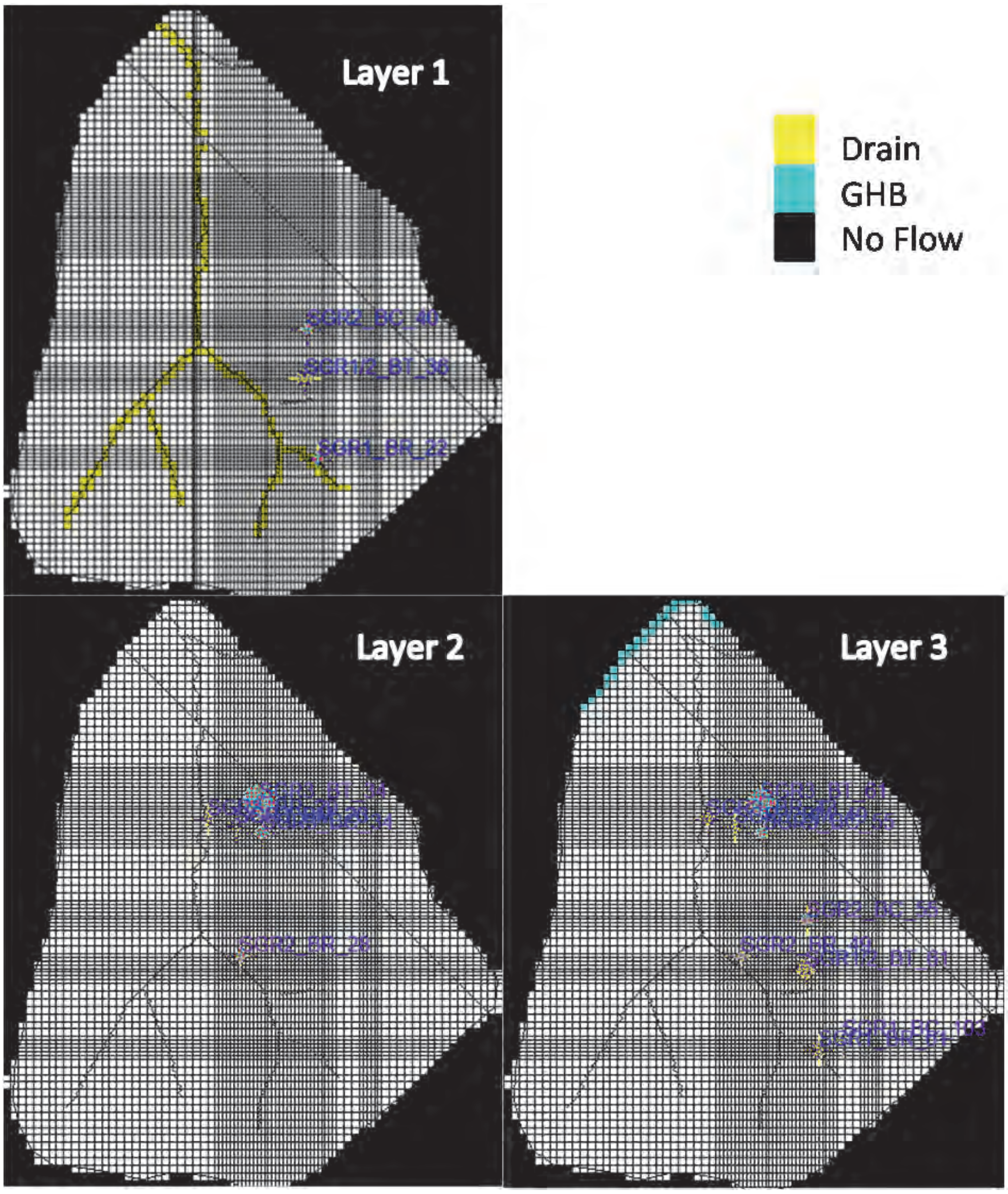

Figure 5.70: The 3 layers of the Southern Granites MODFLOW model showing the Drain, General Head (GHB) and No Flow boundary conditions.

Time parameters are relevant when modelling transient (time-dependent) conditions. They include time unit, the length and number of time periods and the number of time steps within each time period. All model parameters associated with boundary conditions and various stresses remain constant during one time period. Having more time periods allows these parameters to change in time (Kresic, 2007).

The steady state groundwater flow model was used for sensitivity analysis. In order to gain more insight into the groundwater flow system, the transient simulation was discretised into seven stress periods of one-month lengths. Each stress period was then divided into 30 time steps. Incremental time steps (Time Step Multiplier: 1.2) from a few days to several months were used.

Model input parameters for this model included hydrogeological parameters and initial conditions. The initial conditions for hydraulic properties were assigned based on the aquifer test results. The initial head conditions, specified in the steady state model, were estimated from topography. Initial transient model heads were derived from the steady state model results.

5.8.2.2 Recharge

Effective precipitation is represented in the model as distributed recharge into the saturated groundwater system (Figure 6.70). The percentage of precipitation reaching the alluvium and bedrock as recharge was adjusted during model calibration and percentage infiltration of 2% for alluvium and between 6 and 8% for the bedrock were found to be optimum.

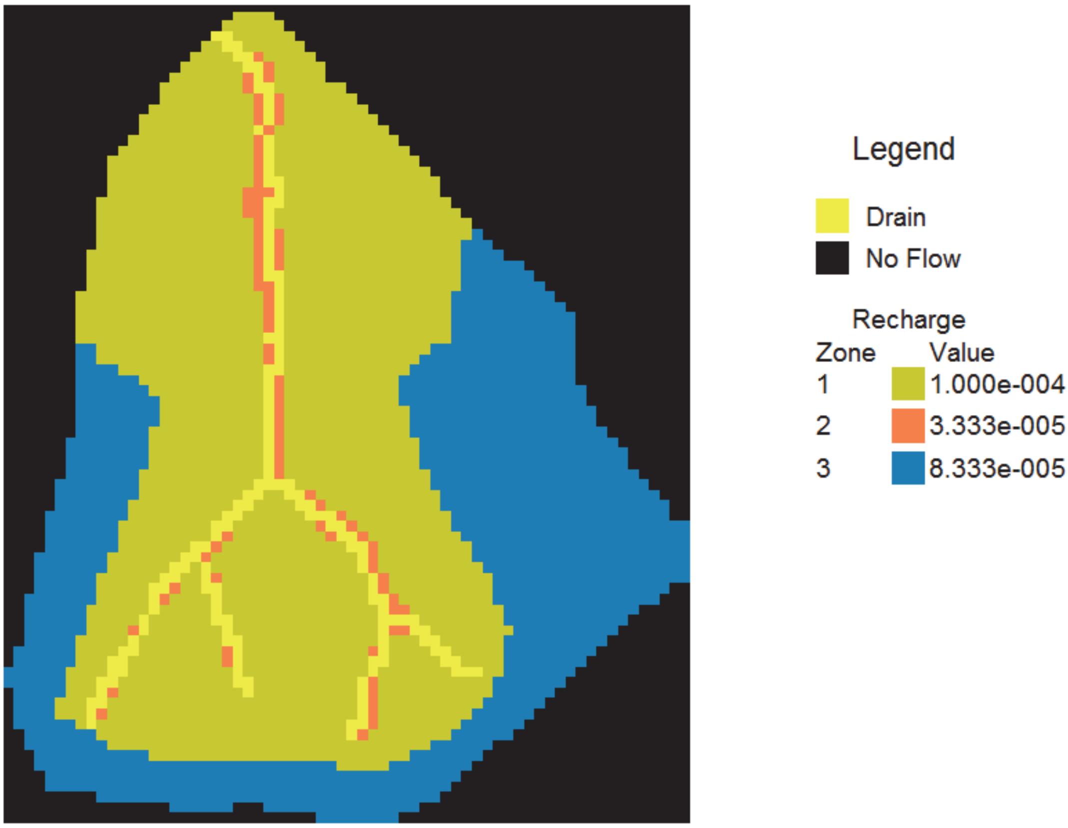

Figure 5.71: Recharge rate property in m/day for the model domain at Southern Granite site.

5.8.2.3 Hydraulic properties

Average hydraulic properties were used as initial values in the model. These properties were modified during calibration within realistic ranges.

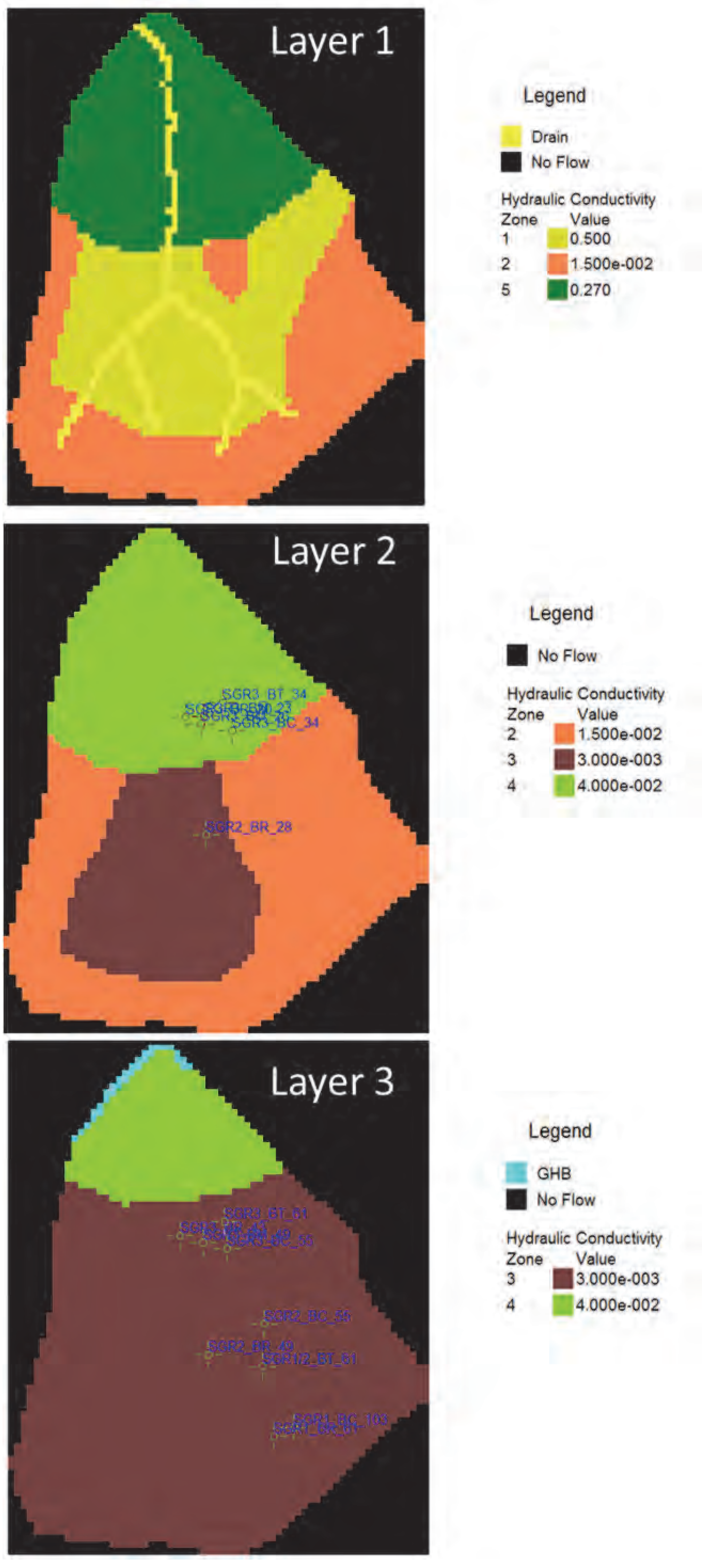

Figure 5.72: spatial distribution of 6 hydraulic property zones at Southern Granite site (K = m/day).

Table 5.16: Calibrated hydraulic conductivity property values for the Southern Granite model

Zone	Kx(m/day)	Ky(m/day)	Kz(m/day)
1	0.5	0.5	0.0005
2	0.015	0.015	0.0015
3	0.003	0.003	0.00003
4	0.04	0.04	0.004
5	0.27	0.27	0.17

5.8.2.4 Model Calibration

Calibration is the process of finding a set of boundary conditions, stresses and hydrogeological parameters that produce results that most closely matches field measurements of hydraulic heads and flows. Steady-state and transient model calibration was undertaken by a combination of manual and inverse calibration. The transient state model was also calibrated by using automated calibration using PEST, a nonlinear parameter estimator. Manual calibration entails the adjustment of boundary conditions, parameter values and stresses for each consecutive model run until the calculated model heads match the preset calibration targets.

Automated calibration minimizes uncertainties associated with the modeller's subjectivity. Computer codes for automated calibration search an optimal parameter set for which the sum of squared deviations between calculated and measured values is reduced to a minimum. The efficiency of automated calibration codes, such as PEST, coupled with the manual calibration is arguably the most appropriate calibration method available (Kresic, 2007).

For steady state conditions the groundwater flow equation 3.39 reduces to the following equation:

$$\frac{\partial}{\partial x}(K_x\frac{\partial h}{\partial x})+\frac{\partial}{\partial y}(K_y\frac{\partial h}{\partial y})+\frac{\partial}{\partial z}(K_z\frac{\partial h}{\partial z})\pm W=0$$

Equation 3.40

The numerical model calculated head distribution ($h_{x,y,z}$) is dependant upon the recharge, hydraulic conductivity and boundary conditions. For a given set of boundary conditions the head distribution across the aquifer can be obtained for a given set of hydraulic conductivity values and specified recharge values. This simulated head distribution can then be compared to the measured head distribution and the hydraulic conductivity/transmissivity or recharge values can be altered until an acceptable correspondence between measured and simulated heads is obtained.

Steady state calibration of the model area was accomplished by refining the vertical and horizontal hydraulic conductivity relative to average recharge values until a reasonable resemblance between the measured piezometric levels and the simulated piezometer levels were obtained. For the steady state model, calibration was done by using a combination of manual and inverse calibration using aquifer zone properties for all model layers.

The success rate of the calibration process is usually assessed by the following statistical quantities:

- Residual Mean (RM);
- Absolute Residual Mean (ARM);
- Root Mean Square (RMS);
- Scaled Absolute Mean (SAM); and
- Scaled RMS (SRMS).

The steady state calibration was regarded as sufficient at RM = -0.12 m, ARM = 0.96 m, RMS= 1.20 m, SAM = 8.6% and SRMS = 10.7%.

The graph in Figure 5.73 shows the relation between measured and simulated head at the end of the steady state calibration process. In case of absolute conformity, the points should create a 45-degree straight line. The level of conformity for the steady state calibration is tolerable especially when the uncertainty in spatial variation of hydraulic properties is taken into account.

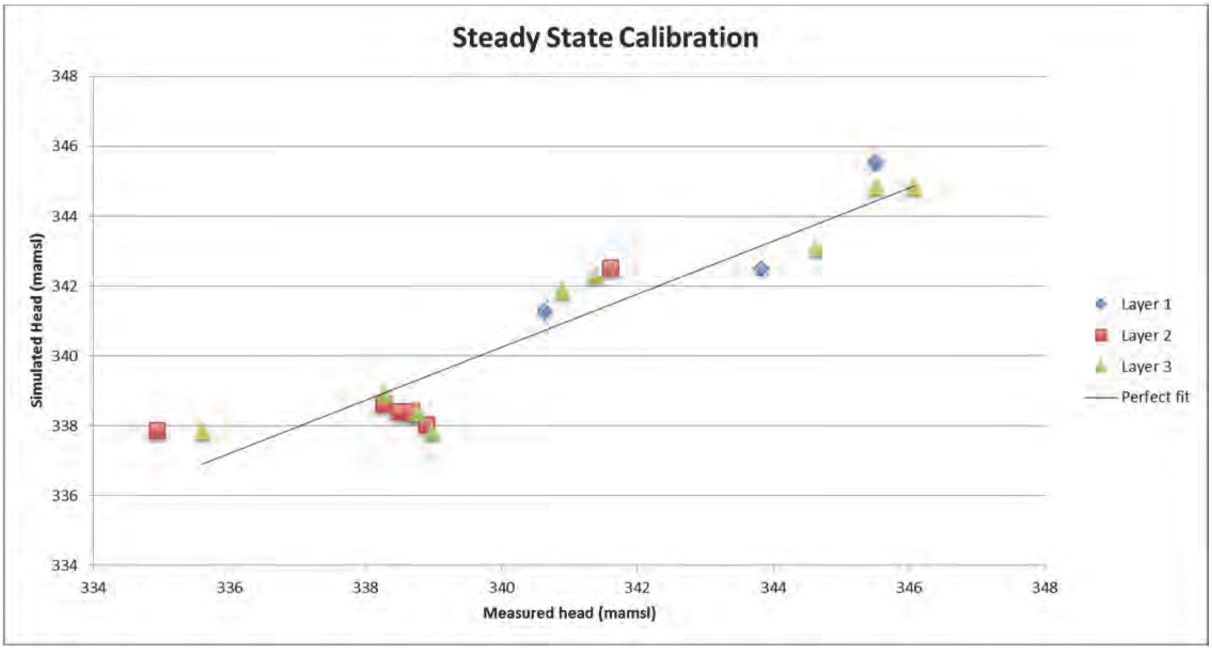

Figure 5.73: Steady state calibration results

The steady state mass balance for entire model domain presented in Table 5.16 achieved a water balance error of less than 0.0001%.

The steady state calibrated groundwater flow model was calibrated under transient conditions using water level data obtained from time series water level data collected over the study period. This calibration was performed in order to ensure that the model is sufficiently calibrated to understand the interactions between the rainfall/recharge, aquifer flow processes and discharge to the surface water. The simulated and observed water level responses are shown in Figure 5.74.

The simulated results show that the hydrogeological flow model is capable of simulating observed groundwater flow data reasonably well allowing confidence in the flow model. Simulated groundwater levels show a general increase with time with increases in the trend coinciding with recharge incidences following exceptional rainfall events. The sensitivity to recharge events is much clearer towards the shallow perched aquifer system which could not be simulated effectively due to the limited understanding of it.

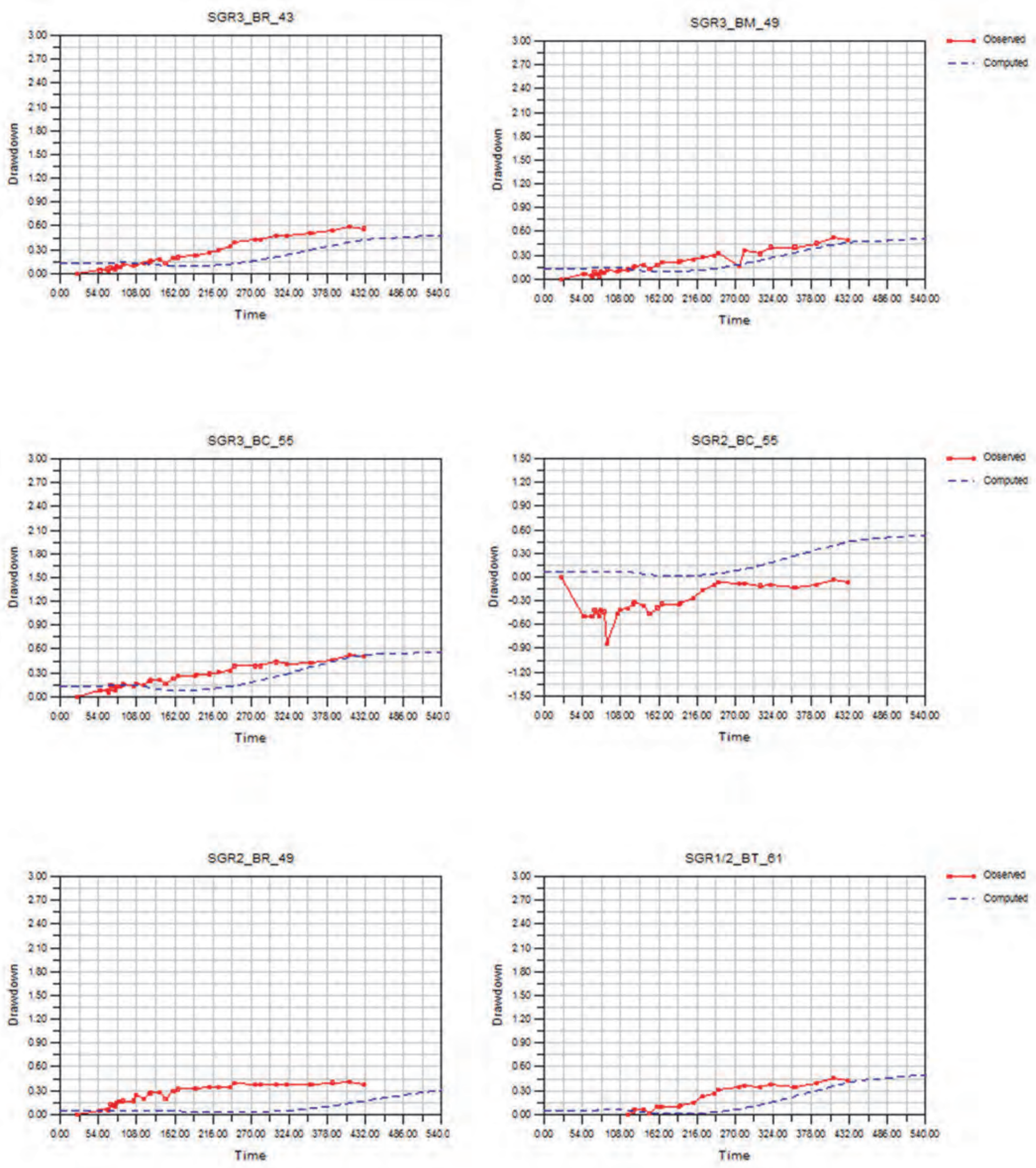

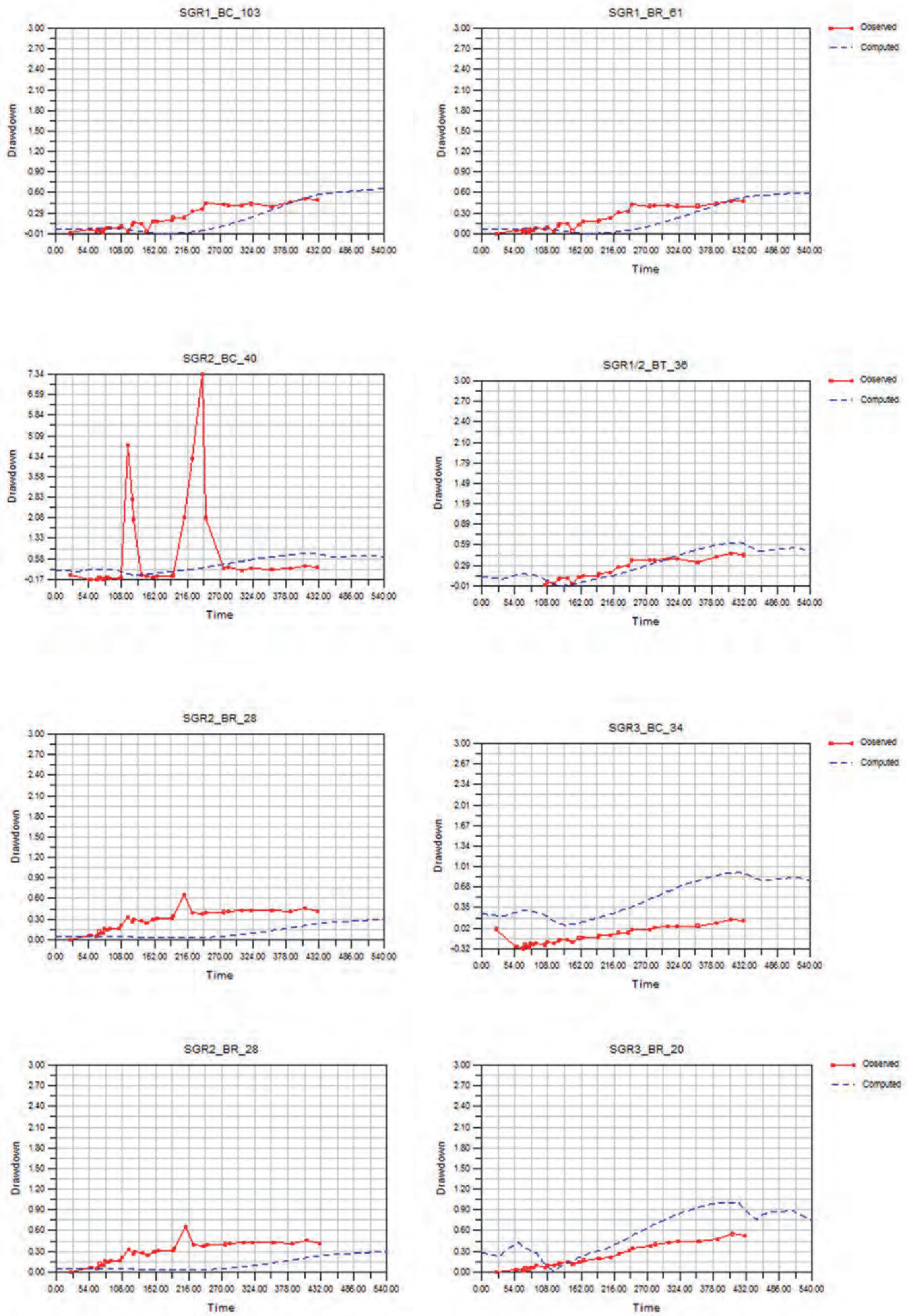

Figure 5.74: Calibrated transient groundwater flows at Southern Granite site (Time = days).

6. RESULTS – SOUTHERN BASALTS

Instrumentation of the southern basalt (SBAS) began in October 2011 with catena element soil moisture sensors and stream stage level loggers. This site was completely instrumented following the completion of groundwater monitoring boreholes by July 2013. Site names, descriptions and localities are given in Table 6.1and Figure 6.1.

Table 6.1: Hydrometric monitoring points in the Southern Basalt KNP Supersite (Site SBAS_Q3 included an ALCO 20 bottle sequential streamflow sampler)

Site_Name	Site_Description	Easting	Northing
SBAS1_C	Southern Basalt Transect 1/Crest Soil Moisture Watermark Station	31.908479	-25.212399
SBAS1_M	Southern Basalt Transect 1/Midslope Soil Moisture Watermark Station	31.908084	-25.210838
SBAS1_R	Southern Basalt Transect 1/Riparian Footslope Soil Moisture Watermark Station	31.908052	-25.210094
SBAS2_C	Southern Basalt Transect 2/Crest Soil Moisture Watermark Station	31.919532	-25.212884
SBAS2_M	Southern Basalt Transect 2/Midslope Soil Moisture Watermark Station	31.933822	-25.209041
SBAS2_R	Southern Basalt Transect 2/Riparian Footslope Soil Moisture Watermark Station	31.933749	-25.208591
SBAS3_C	Southern Basalt Transect 3/Crest Soil Moisture Watermark Station	31.955967	-25.200131
SBAS3_M	Southern Basalt Transect 3/Midslope Soil Moisture Watermark Station	31.959422	-25.204244
SBAS3_R	Southern Basalt Transect 3/Riparian Footslope Soil Moisture Watermark Station	31.960331	-25.205692
SBAS_Baro	Southern Basalt Barologger	31.574764	-25.115199
SBAS_Rain	Southern Basalt Rain	31.913912	-25.262790
SBAS_Q1	Southern Basalt 1st order Streamflow levellogger	31.919532	-25.212884
SBAS_Q2	Southern Basalt 2nd order Streamflow levellogger	31.956653	-25.211396
SBAS_Q3	Southern Basalt 3rd order Streamflow levellogger	31.963166	-25.204570
SBASMet	Southern Basalts Weather Station	31.913912	-25.262790
SBAS3_BR_80	MP190020 Southern Basalt 3rd order riparian borehole 80m	31.959264	-25.204352
SBAS3_BR_10	MP190021 Southern Basalt 3rd order riparian borehole 10m	31.959278	-25.204346
SBAS3_BC_80	MP190022 Southern Basalt 3rd order crest borehole 80m	31.956005	-25.200167
SBAS3_BC_10	MP190023 Southern Basalt 3rd order crest borehole 10m	31.956043	-25.200164
SBAS3_BT_61	MP190039 Southern Basalt 3rd order triangulation borehole 61m	31.967663	-25.203028
SBAS3_BT_4	MP190040 Southern Basalt 3rd order triangulation borehole 4m	31.967675	-25.203016
SBAS1_BR_67	MP190025 Southern Basalt 1st order riparian borehole 67m	31.908118	-25.210724
SBAS1_BR_12	MP190026 Southern Basalt 1st order riparian borehole 12m	31.908102	-25.210761
SBAS1_BT_56	MP190028 Southern Basalt 1st order triangulation borehole 56m	31.909464	-25.211996
SBAS1_BT_14	MP190029 Southern Basalt 1st order triangulation borehole 14m	31.909454	-25.212016
SBAS1_BC_61	MP190030 Southern Basalt 1st order crest borehole 61m	31.908624	-25.212862
SBAS1_BC_18	MP190031 Southern Basalt 1st order crest borehole 18m	31.908624	-25.212862
SBAS1_BC_100	MP190041 Southern Basalt 1st order crest borehole 100m	31.908616	-25.212880
SBAS2_BR_80	MP190032 Southern Basalt 2nd order riparian borehole 80m	31.933832	-25.208948
SBAS2_BR_8	MP190033 Southern Basalt 2nd order riparian borehole 8m	31.933809	-25.208952
SBAS2_BT_80	MP190034 Southern Basalt 2nd order triangulation borehole 80m	31.934533	-25.209562
SBAS2_BT_15	MP190035 Southern Basalt 2nd order triangulation borehole 15m	31.934517	-25.209578
SBAS2_BC_57	MP190037 Southern Basalt 2nd order crest borehole 57m	31.933999	-25.210579
SBAS2_BC_12	MP190038 Southern Basalt 2nd order crest borehole 12m	31.933991	-25.210599

Table 6.2: Southern Basalt Borehole in-situ hydraulic parameters following drilling (2013)

Borehole	Temperature (°C)	Specific Conductance (mS/cm)	pH	Static water level (mbc)	Blow out yield (l/s)	Transmissivity (m^2/d)	Test Type
SBAS3_BR_80	25.51	1.41	7.06	9.63	0.39	13.1	CJ
SBAS3_BC_80	24.99	1.32	7.03	9.37	0.16	0.1	CJ
SBAS3_BT_61	25.63	2.12	7.49	4.17	NA	0.22	BR
SBAS1_BR_67	25.88	2.73	7.82	18.68	0.08	0.39	BR
SBAS1_BT_56	24.97	1.59	7.36	18.05	NA	0.009	BR
SBAS1_BC_61	24.76	1.69	7	17.91	0.082	1.52	BR
SBAS1_BC_100	25.36	1.7	7.16	18	NA	5.49	BR
SBAS2_BR_80	25.04	1.95	7.2	8.21	0.92	43.54	CJ
SBAS2_BT_80	24.85	2.36	7.31	9.25	4.5	70.37	CJ
SBAS2_BC_57	24.99	3.68	7.2	11.2	NA	0.0051	BR
SBAS3_BR_10	25.73	1.3	6.9	9.48	NA	NA	NA
SBAS3_BC_10	25.12	0.97	6.9	9.24	NA	NA	NA
SBAS2_BT_15	24.07	1.69	7.48	9.48	1	63.34	CJ
SBAS2_BC_12	NA	NA	NA	dry	NA	NA	NA
SBAS2_BR_8	NA	NA	NA	7.97	NA	NA	NA
SBAS1_BC_18	NA	NA	NA	dry	NA	NA	NA
SBAS1_BT_14	NA	NA	NA	dry	NA	NA	NA
SBAS1_BR_12	NA	NA	NA	dry	NA	NA	NA
SBAS3_BT_4	NA	NA	NA	3.51	NA	0.0057	BR

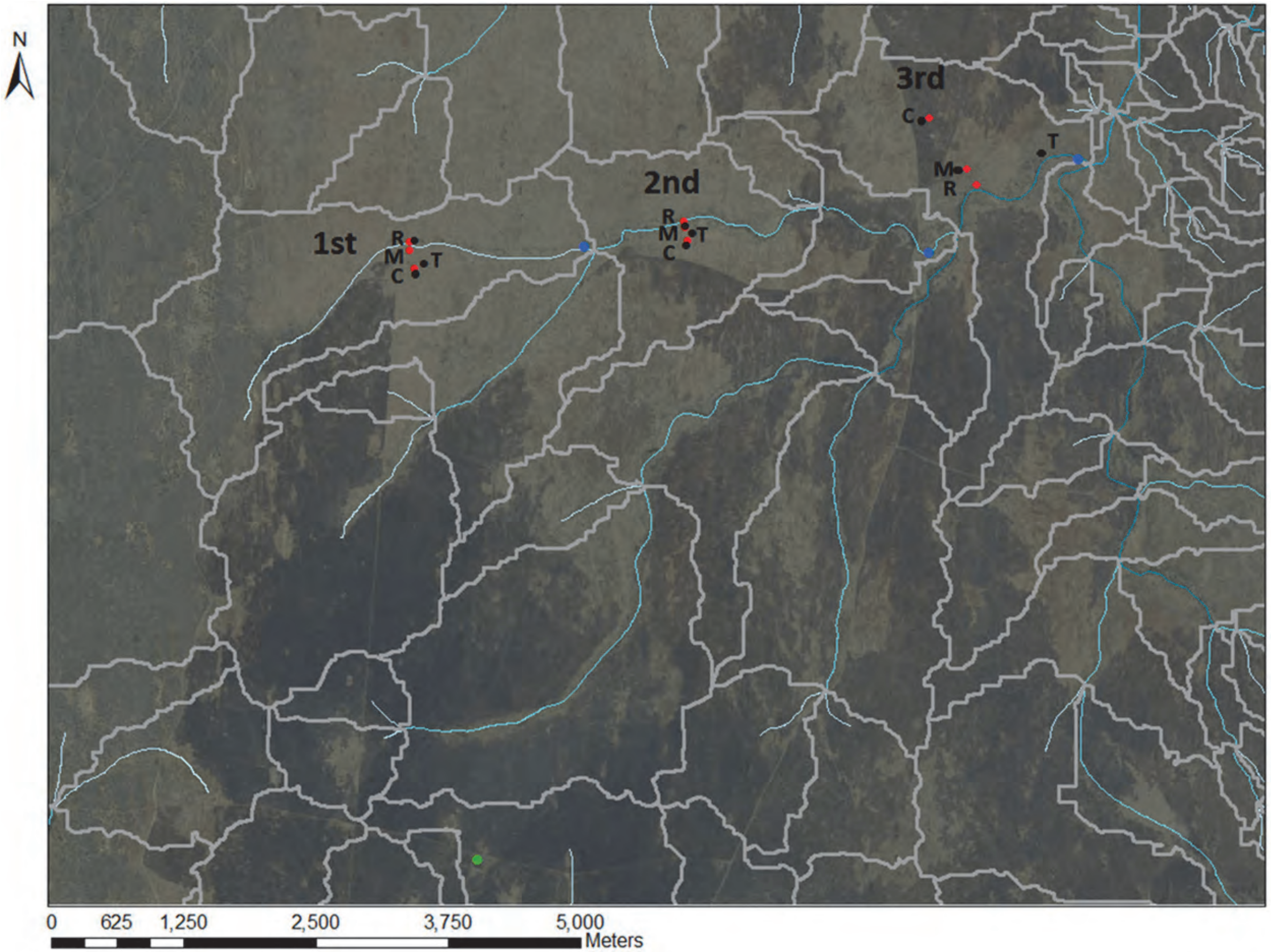

Figure 6.1: Map of installed instrumentation at the Southern Basalt (Nhlowa) Supersite (red = soil moisture station, blue = streamflow gauge, black = boreholes, green = rainfall station & Davis™ Weather Station, R = riparian, M = midslope, C = crest, T = triangulation, L = lower, U = upper).

6.1 Precipitation

The hydrological season for the southern basalt supersite commenced on 22nd October 2012 by which time stream flow observations had already commenced (late 2011) and the 3rd order boreholes had been drilled (October 2012). Meanwhile the completed multi-piezometer borehole network was drilled during June-August 2013.

NB: DATA REPORTED IN THIS CHAPTER SPANS TWO HYDROLOGICAL SEASONS FROM OCTOBER 2012 UP TO MARCH 2014.

The total precipitation for this period is 1145 mm as depicted in Figure 6.2. From the API in Figure 6.3 major precipitation sequences are perceived namely, October 2012 to May 2013 (sequence 1) and September 2013 to March 2014 (sequence 2). Sequence 1 was associated with low to high rainfall ranging 1-70 mm/day and sequence 2 was associated with low to high rainfall ranging 1-118 mm/day.

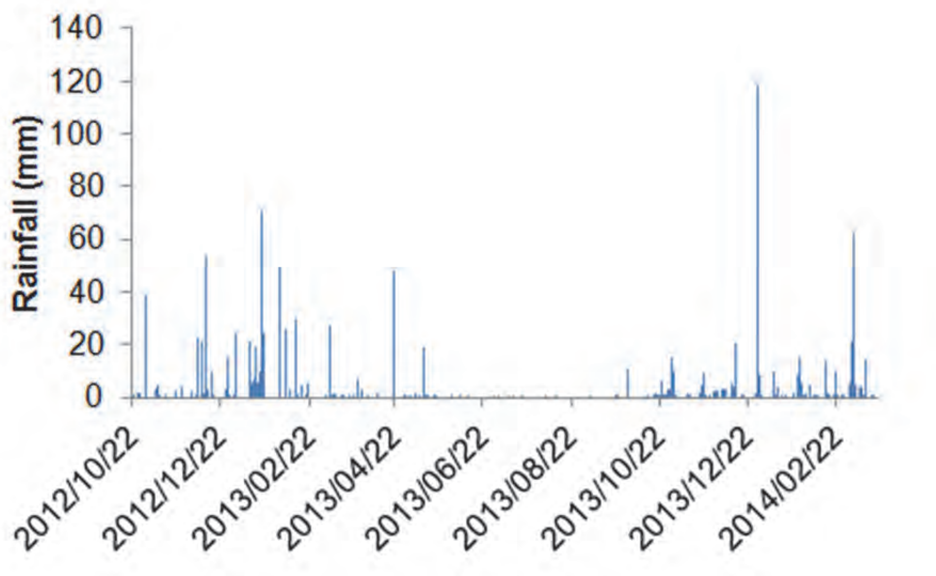

Figure 6.2: Southern basalt time series rainfall from October 2012 to March 2014.

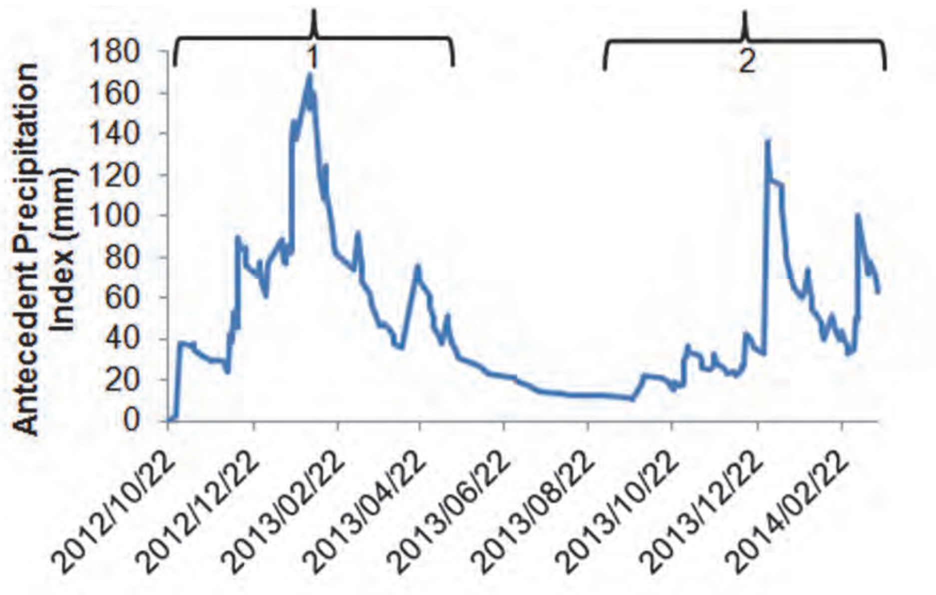

Figure 6.3: Southern basalt Antecedent Precipitation Index October 2012-March 2014

6.2 Southern Basalts Streamflows

6.2.1 Total Discharge at Southern Basalts

Event driven flows were observed for the three spatial scales from 1st to 3rd order stream reaches and these are represented as flow duration curves in Figure 6.4 and as times series in Figure 6.5 and Figure 6.6. FDCs which completely cut off at lower tails before the low-flow regime depict the ephemeral nature of runoff at the southern basalts. Rapid streamflow recessions were observed at all sites but particularly SBAS2. The 3rd order reach (SBAS3) had most persistent event-driven flows compared to lower order reaches during the period September 2012 to March 2013 and this is indicated by a low-flow exceedance probability of 45% which is higher than for both 1st and 2nd order reaches at this site (Figure 6.4).

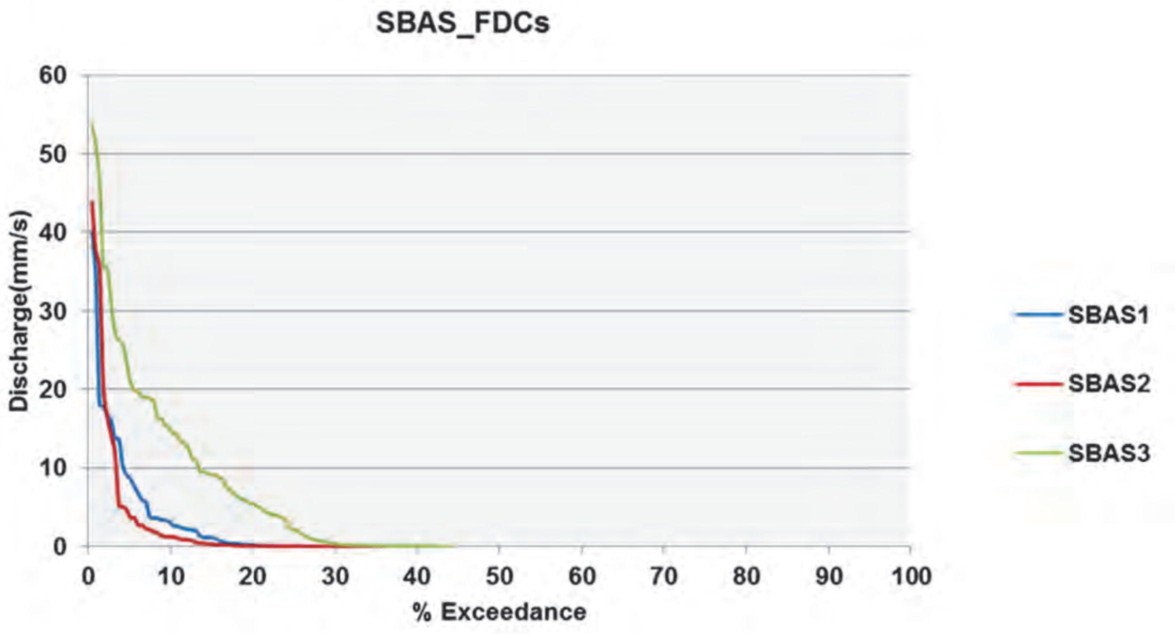

Figure 6.4: Southern Basalts (SBAS) Flow Duration Curves for the period from September 2012 to March 2013.

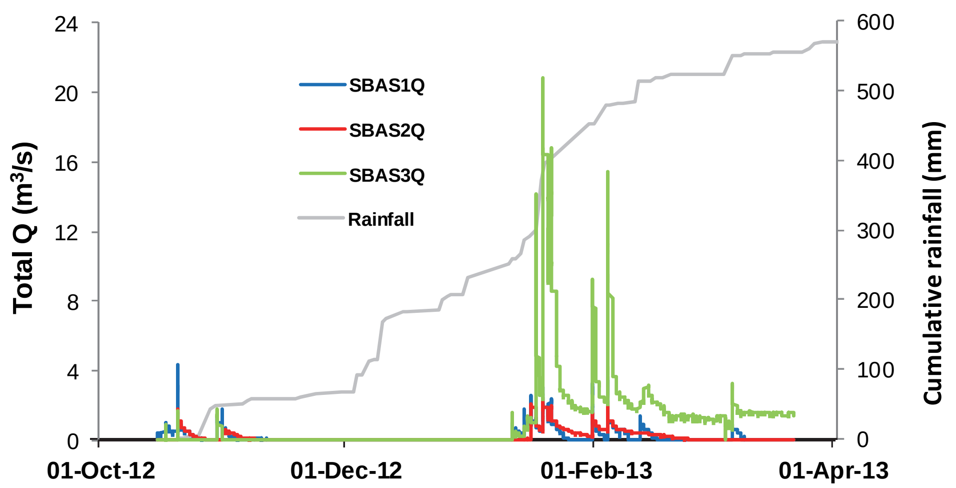

Figure 6.5: Streamflows at Southern Basalts from October 2012 to March 2013

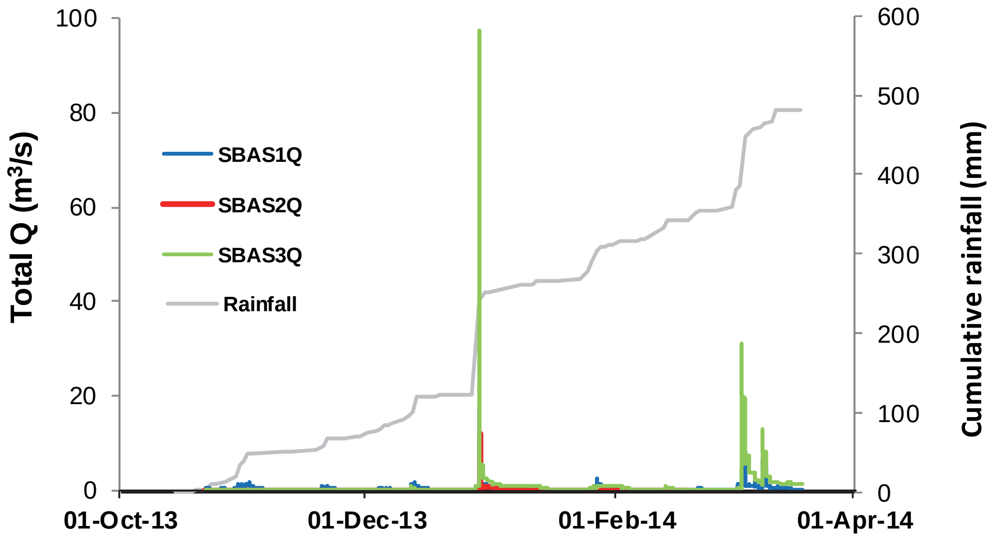

Figure 6.6: Streamflow responses at Southern Basalts from October 2012 to March 2014.

6.2.2 Southern Basalts Rainfall-Runoff Analysis: Statistical Analysis

Rainfall-runoff characteristics for the Southern Basalts site to identify relationships between hydrological parameters is presented in Table 6.3. High precipitation depth as expected was found to be positively correlated to runoff volume strongly influencing the magnitude of runoff peak discharge ($r = 0.999$; $p = 0.000$ and $r = 0.999$; $p = 0.001$, respectively). A strong dependence of runoff volume on maximum precipitation intensity was identified ($r = 0.999$; $p = 0.000$). As anticipated, high rainfall intensities resulted in short delay times and such high intensities positively correlated with short duration rainfall events ($r = -0.999$; $p = 0.003$ and $r = -0.970$; $p = 0.029$). The role of antecedent catchment conditions, represented by API, on runoff delay times and rising times was notably significant ($r = -0.994$; $p = 0.006$ and $r = 0.923$; $p = 0.001$, respectively). High APIs were revealed to cause high runoff volumes and high peak discharges ($r = 0.999$; $p = 0.001$ and $r = 0.999$; $p = 0.001$, respectively).

Table 6.3: Pearson's product moment correlation coefficient (r) with level of significance (p in parenthesis) for rainfall and runoff characteristics of three events at Southern Basalts monitored during December 2012 to February 2013.

	Precip. Duration	Precip. Amount	Precip. Int_{mean}	Precip. Int_{max}	Precip API_{-7}	Runoff Delay time	Runoff Rising Time	Catchment Area	Runoff Peak Discharge
Precip. Amount	0.919 (0.073)								
Precip. Int_{mean}	-0.313 (0.391)	0.088 (0.469)							
Precip. Int_{max}	-0.970* (0.029)	0.987* (0.012)							
Precip. API_{-7}	0.899 (0.303)	0.999 (0.068)	0.134 (0.452)	0.881 (0.102)					
Runoff Delay time	0.230 (0.314)	-0.998** (0.002)	-0.999** (0.003)	-0.928 (0.058)	-0.994** (0.006)				
Runoff Rising Time	0.076 (0.231)	-0.464 (0.445)	-0.227 (0.419)	-0.037 (0.487)	-0.923** (0.001)				
Runoff Peak Discharge	0.897 (0.076)	0.999 (0.256)	0.132 (0.330)	0.879 (0.086)	0.999** (0.001)			0.903* (0.04)	
Runoff Volume	0.999** (0.001)	0.999** (0.000)	0.089 (0.468)	0.999** (0.000)	0.999** (0.001)	-0.174 (0.438)	-0.465 (0.326)		0.999** (0.001)

**Significant at the 0.01 level
*Significant at the 0.05 level

6.2.3 Runoff Coefficients

The runoff coefficients (Rc) for the Southern Basalts are presented in Table 6.4. Increasing Rc values were observed with increasing precipitation depths for the events in question. A linear relationship across spatial scales was noted on the dates where the API_{-7} was high. This signifies the importance of antecedent conditions on connectivity of channel networks in the southern basalts. Low API_{-7} (and therefore lower soil moisture) increases infiltration capacity and subsequent infiltration losses implying less water getting to downstream reaches under these conditions. However, incidence of high intensity rainfall under low soil moisture conditions can connect channel networks due to infiltration excess.

Table 6.4: Southern Basalts Runoff Coefficients for incremental stream reaches.

EVENT DATE	SBAS1Q(Rc)	SBAS2Q(Rc)	SBAS3Q(Rc)	RAINFALL(mm)	API_{7}
2012/12/16	0.01	0.78	1.28	10	36.4
2013/01/19	0.73	2.18	2.62	70.8	108.62
2013/02/20	0.01	0.005	0.01	5.4	35.02
2014/01/17	0.0038	0.0065	0.0077	6.0	59.60
2014/01/28	0.00002	0.0025	0.0107	12.8	52.01

6.2.4 Hydrometric Analysis of Stream network and Stream-Catchment Connectivity

In order to closely link identified relationships to interactions of hydrological processes, two of the analysed events are presented in Figure 6.7 and Figure 6.8. Streamflow responses on the basalt geology are flashy as shown by sharp rising limbs and steep recession curves. Incremental changes in peak stream runoff with increasing stream orders is proof of stream network connectivity at least during and immediately following high intensity rainfall events. This reveals the influence of scale in runoff generation where larger contributing areas result in pronounced runoff responses. Field surveys revealed the presence of persistent pools along channel networks, especially at the 3rd order where there is the possibility of groundwater contribution to streamflow. These pools were observed to have water for a period exceeding two months after the last rainfall event at this 3rd order reach. Events of high intensity clearly play a pivotal role in enhancing runoff responses as well as in facilitating hydrologic connectivity. A 10 mm/15 min rainfall rate on the 19th of January 2013 corresponded to a peakflow of 8.7 m^3/s showing close correlation between rainfall and runoff response.

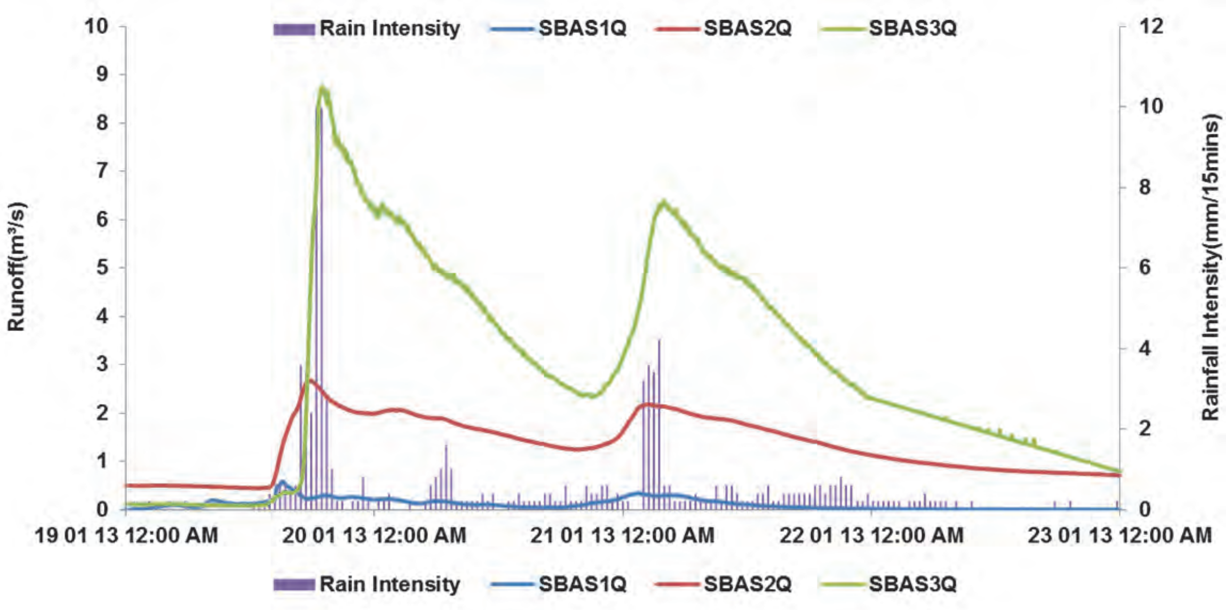

Figure 6.7: Southern Basalts streamflow responses following the rainfall event on the 19th of January 2013.

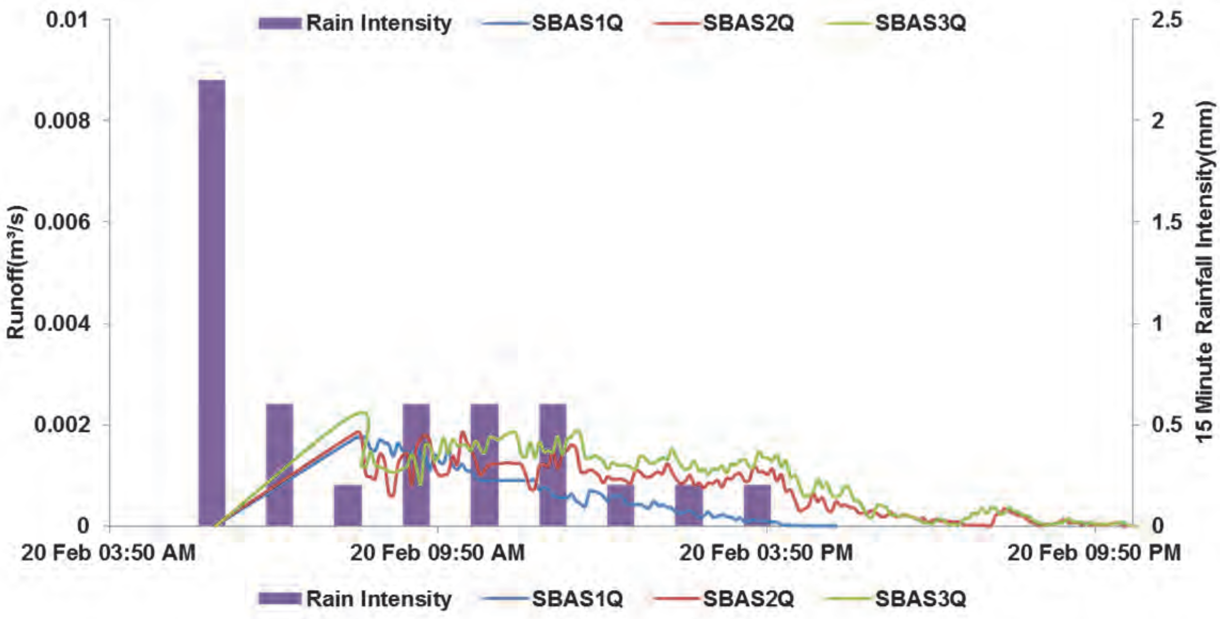

Figure 6.8: Southern Basalts streamflow responses following the 20th of February 2013 rainfall event.

No subsurface discharge rating was done at the Southern Basalts catchment since this geology is characterised by very shallow soils where subsurface fluxes were presumed to be negligible. Compounding the difficulty for free drainage is the presence of vertic soils which are characterised by very low hydraulic conductivities. The few piezometers driven into the subsurface at this catchment confirmed the insignificant role of subsurface fluxes by being dry most of the time. As such stream-aquifer interaction was only characterised between streamflow processes and the deep groundwater zones from 1st to 3rd order spatial scales.

The crest borehole water level at SBAS1 reach is higher than that of the riparian borehole and the stream, suggesting a possible hydraulic gradient towards the stream. However, the stream water level is higher than that of the riparian borehole indicating a negative gradient from the stream (Figure 6.9). It can, therefore, be inferred from hydrometric analysis that the SBAS1 reach is disconnected from the adjacent hillslope, a position that is further supported by shallow riparian boreholes and piezometers which were always dry during the monitoring period from July 2013 to March 2014.

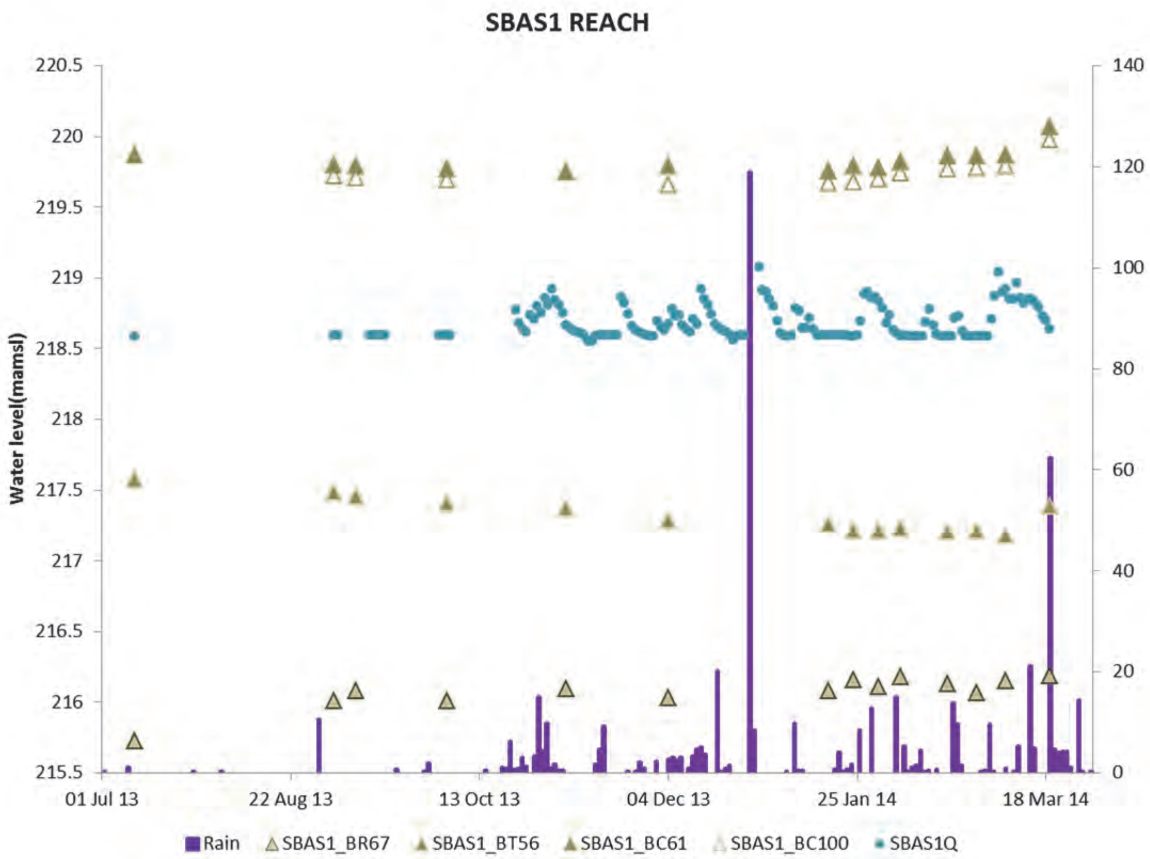

Figure 6.9: Hydraulic head of SBAS1 boreholes relative to stream water levels. (SBAS1Q = 1st order stream gauge; SBAS1_BC61 = 61 m crest borehole; SBAS1_BT56 = 56 m triangulation borehole; SBAS1_BC100 = 100 m crest borehole and SBAS1_BR67 = 67 m riparian zone borehole). *NB: Stream gauges for all 1st to 3rd order reaches are positioned at catchment outlets longitudinally further downstream. The gauges are not directly adjacent to borehole transects.*

Borehole and stream water levels at the 2nd order reach (SBAS2) indicate an approximate 10 m difference in elevation suggesting a positive hydraulic gradient towards the stream (Figure 6.10). However, whether this hydraulic gradient results in groundwater contribution to streamflow is not supported either by hydrochemistry or by isotopes ($\delta^{18}O$) (See Section 6.2.5.4). This could possibly be due to the presence of an impermeable lineament between stream and riparian zone at this point and/or the relatively impermeable vertic soils in the stream channel.

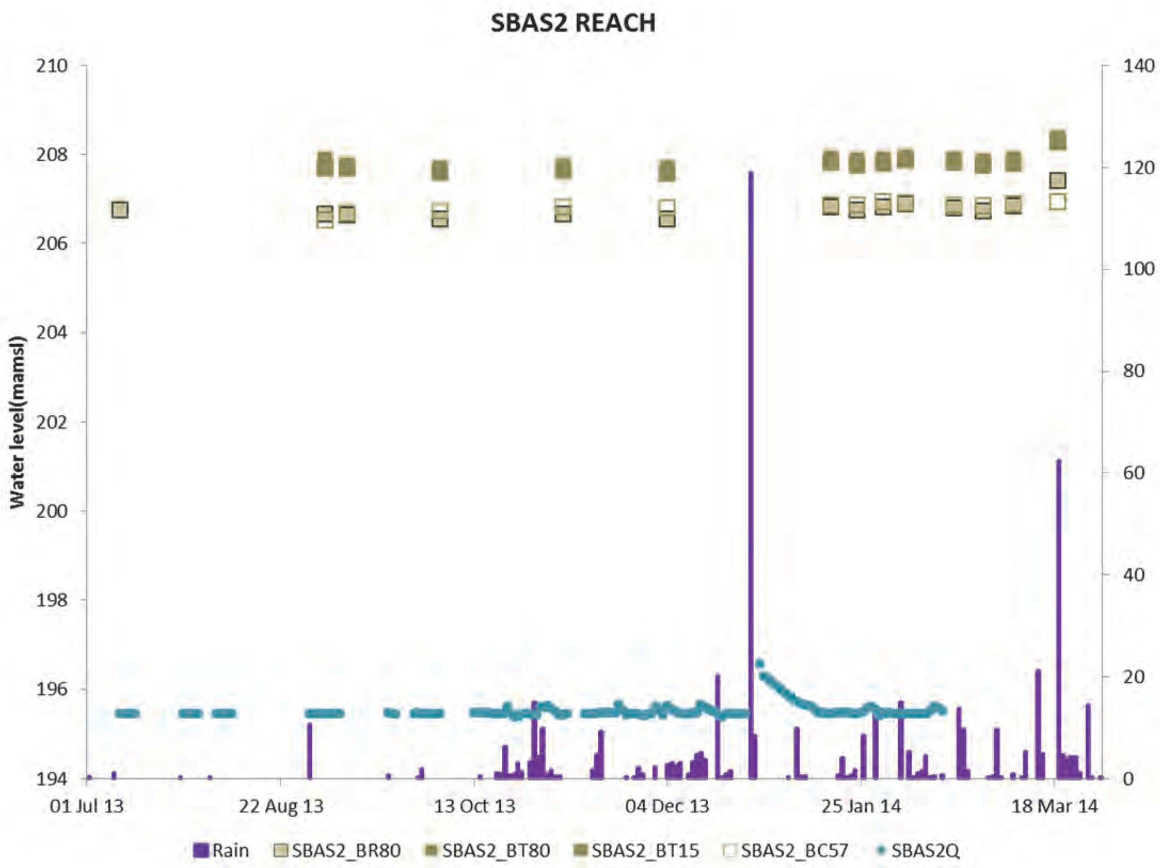

Figure 6.10: Hydraulic head of SBAS2 boreholes relative to stream water levels. (SBAS2Q = 2nd order stream gauge; SBAS2_BC57 = 57 m crest borehole; SBAS2_BT80 = 80 m triangulation borehole; SBAS2_BT15 = 15 m triangulation borehole; SBAS2_BR80 = 80 m riparian zone borehole and SBAS2_BR8 = 8 m riparian zone borehole). *NB: Stream gauges for all 1st to 3rd order reaches are positioned at catchment outlets longitudinally further downstream. The gauges are not directly adjacent to borehole transects.*

At the 3rd order reach groundwater connectivity to the stream is perceived to occur through localised fractures within the aquifer. A 9 m water level difference between crest boreholes and the stream at SBAS3 was observed during February 2013 to March 2014 which indicates a significant positive hydraulic gradient towards the stream (Figure 6.11). However, the stream water level is higher than that of the 61 m triangulation borehole (in fact close to the riparian zone of the catchment outlet, see Figure 6.1) which suggests possible losses from the stream to the aquifer further downstream. This is supported by the rise in water level following at the triangulation point following the rains of late December 2013. As such the 3rd order reach is portrayed as a gaining reach at the upstream section and as losing in some segments on its downstream end.

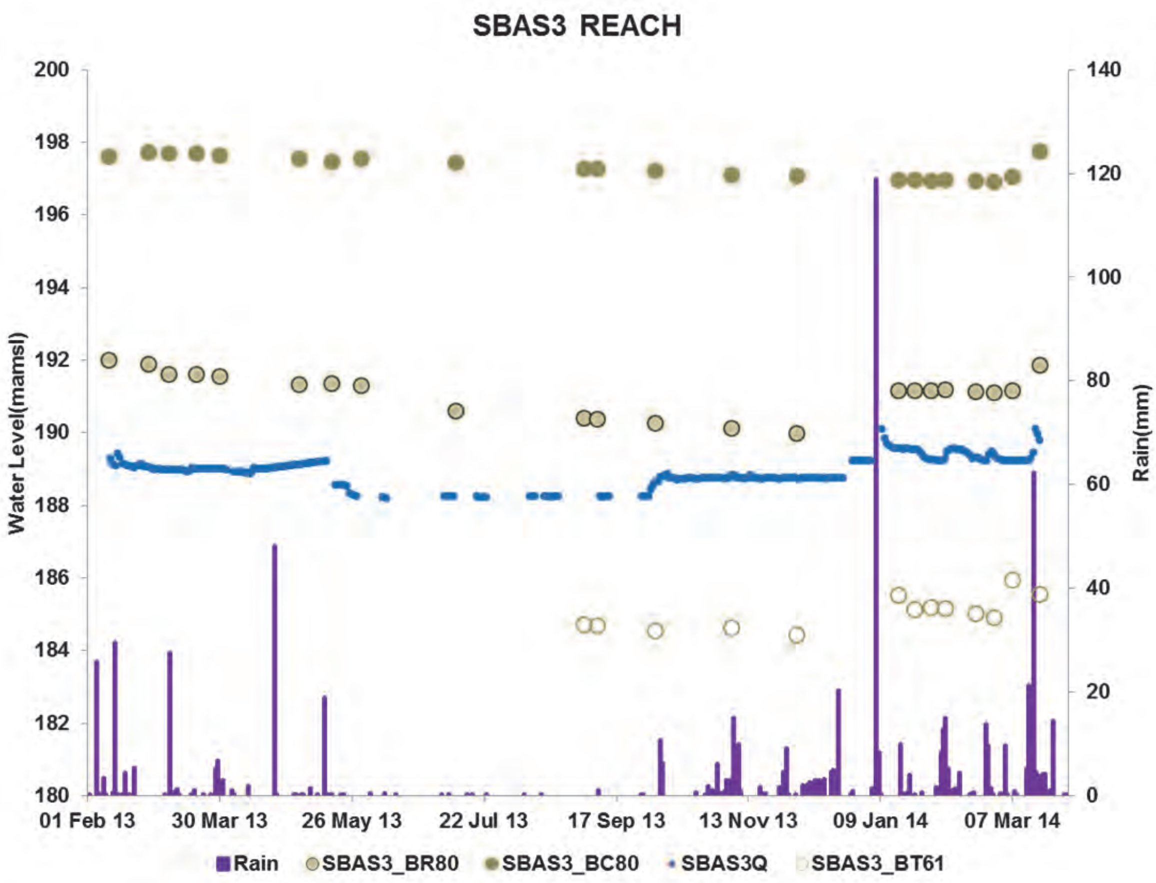

Figure 6.11: Hydraulic head differences between crest boreholes, riparian boreholes and the stream at Southern Basalts 3rd order reach during the period February 2013 to March 2014.

6.2.5 Streamflow Hydrochemistry

6.2.5.1 Isotopic trends in rainfall and surface water samples

At the Southern Basalts study site rainfall isotopic patterns generally aligned with those of stream samples with stream concentrations showing depleted signals during large rainfall events (Figure 6.12). This observation is consistent with findings by Van Wyk et al. (2012), who indicated the importance of episodic rainfall sequences which are associated with groundwater-stream connectivity in a study conducted in a semi-arid environment in South Africa. This study points out the need for a unique rainfall pattern in semi-arid regions which should occur prior to a sustainable aquifer storage-recharge condition develops. Similar stream and high intensity rainfall signatures at the Southern Basalt site were identified and these portrayed mixing between these two water sources suggesting the significance of event water contribution to ephemeral stream runoff (Table 6.5).

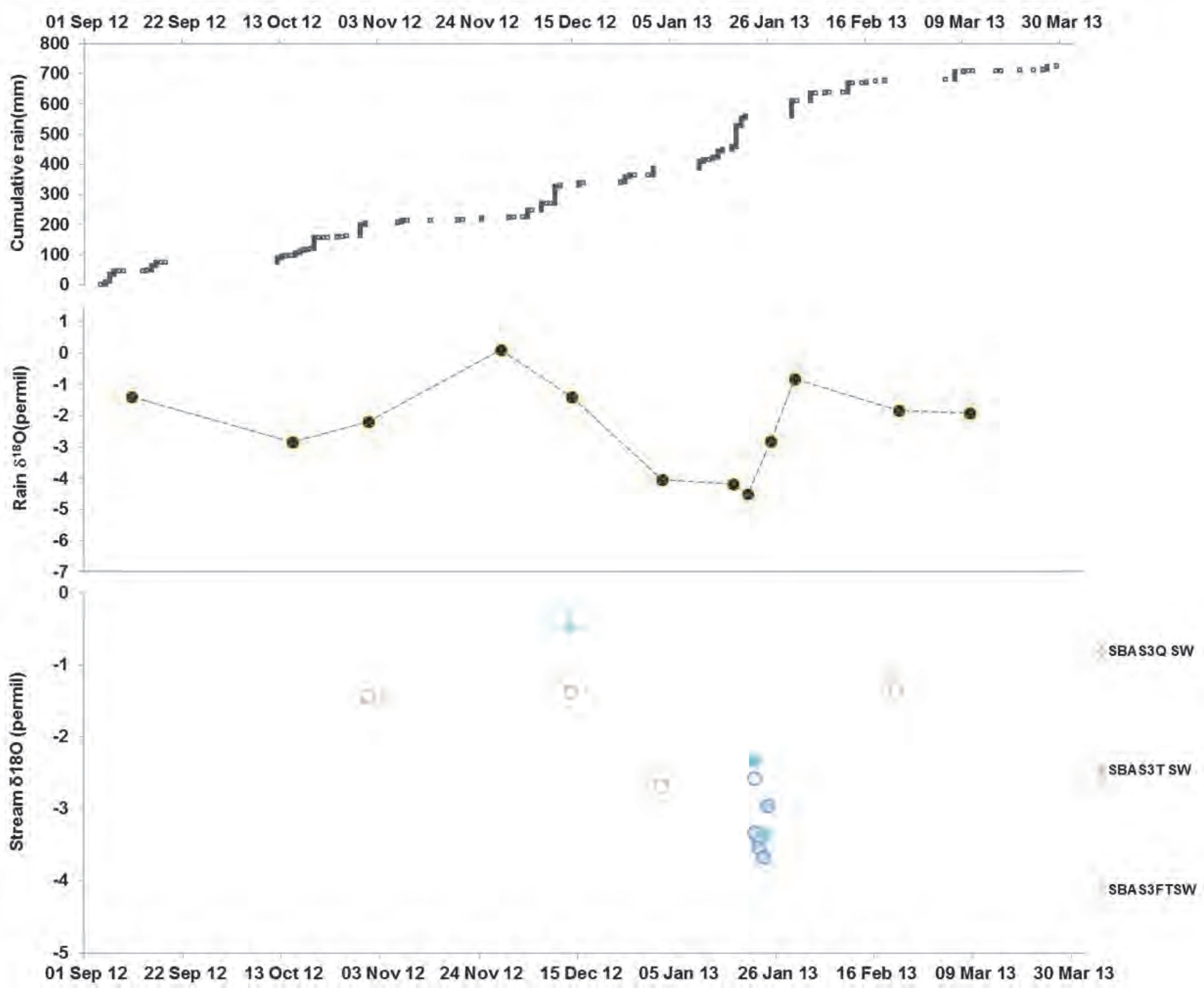

Figure 6.12: Isotopic trends in rainfall and stream samples at Southern Basalts from September 2012 to March 2013.

Table 6.5: Rainfall and stream isotopic signatures for Southern Basalts site for samples collected between December 2012 and January 2014.

Date	Location	Stream $\delta^{18}O$ (permil)	Rain δ18O (permil)
13/12/2012	SBAS3	-1.38	-1.41
21/01/2013	SBAS3	-2.58	-2.81
28/01/2014	SBAS1	-3.71	-3.73
28/01/2014	SBAS2	-3.70	-3.73
28/01/2014	SBAS3*	-3.83	-3.73

*mean of 6 automated stream samples. Most depleted sample (-4.27) was used as rain sample for hydrograph separation since no rain sample was collected on this date

Analytical error for $\delta^{18}O$ is 0.3 ‰

6.2.5.2 *Physico-chemical (EC) trends in rainfall, stream and borehole water samples*

EC values for analysed samples ranged between 62 µS/cm to 2040 µS/cm at the Southern Basalts. Highest EC values were recorded for groundwater, lowest for rain and intermediate values for stream samples (See Table 6.6). Stream EC values at this site dropped momentarily following large rainfall events (e.g. 95.7 mm on 19 January, 2013) showing pronounced dilution of solutes in the catchments during these very wet conditions. No defined trend was observable for borehole EC values.

Table 6.6: Selected typical EC, silica and chloride concentration ranges at Southern Basalts during December 2012 to January 2014.

Date	Location	Borehole			Stream			Rain		
		EC (µs/cm)	Silica (mg/L)	Cl (mg/L)	EC (µs/cm)	Silica (mg/L)	Cl (mg/L)	EC (µs/cm)	Silica (mg/L)	Cl (mg/L)
2012/02/06	SBAS3	1442	17.9	--	808	11.05	--	75.6	0	--
2013/01/19	SBAS3	1480	24.47	--	367	11.36	--	62.0	0	--
2013/02/20	SBAS3	1491	21.33	--	642	12.20	--	72.6	0	--
2014/01/28	SBAS1	2040	7.01	--	213	14.49	--	65.0	--	--
2014/01/28	SBAS2	1480	4.80	--	367	12.00	--	65.0	--	--
2014/01/28	SBAS3	1710	13.16	--	288	15.38	--	65.0	--	--

--Means no data

6.2.5.3 *Hydrochemical (silica) trends in rainfall, stream and borehole water samples.*

Silica concentrations at SBAS1 ranged between 7.01 mg/L and 24.5 mg/L while at SBAS2 these ranged between 4.8 mg/L and 24.47 mg/L (Table 6.6). No clear cut trends were observed for silica at the 1st and 2nd order reaches of the Southern Basalts study site. At SBAS3 reach silica concentration ranged from 0.0 mg/L to 24.47 mg/L with groundwater having highest concentrations followed by stream samples while lowest values were recorded in rainfall. Distinct differences in silica concentrations at SBAS3 were observed between boreholes, streams and rain samples hence using silica for hydrograph separation was possible for this 3rd order reach.

6.2.5.4 *Tracer Analysis at Southern Basalts*

The SBAS1 reach show wide differences in hydrochemical (Na & EC) and isotopic ($\delta^{18}O$) signatures between borehole and stream samples (Figure 6.13 to Figure 6.15). This further supports hydrometric observations that the stream is not connected to groundwater at this headwater reach. The narrowest margin between borehole and stream sodium concentrations for samples collected on the 28th of January 2014 was 42.5 mg/L and EC margin for the same date was 773µS/cm. On this date groundwater, stream and rain samples had $\delta^{18}O$ values of -2.76‰, -3.73‰ and -3.71‰, respectively. This indicates pronounced contribution of event water to runoff against minimal to no groundwater contribution, given an analytical accuracy of +/-0.3‰ for oxygen isotopes. Thus, at this spatial scale (SBAS1) no groundwater contribution is reflected either from hydrochemistry or isotopes, supporting our original hypothesis that hillslopes are disconnected from the stream. Boreholes had higher sodium concentrations than stream samples probably due to piston-type or translatory vertical redistribution of old-water forced downwards by younger fresh water from a series of preceding rainfall events.

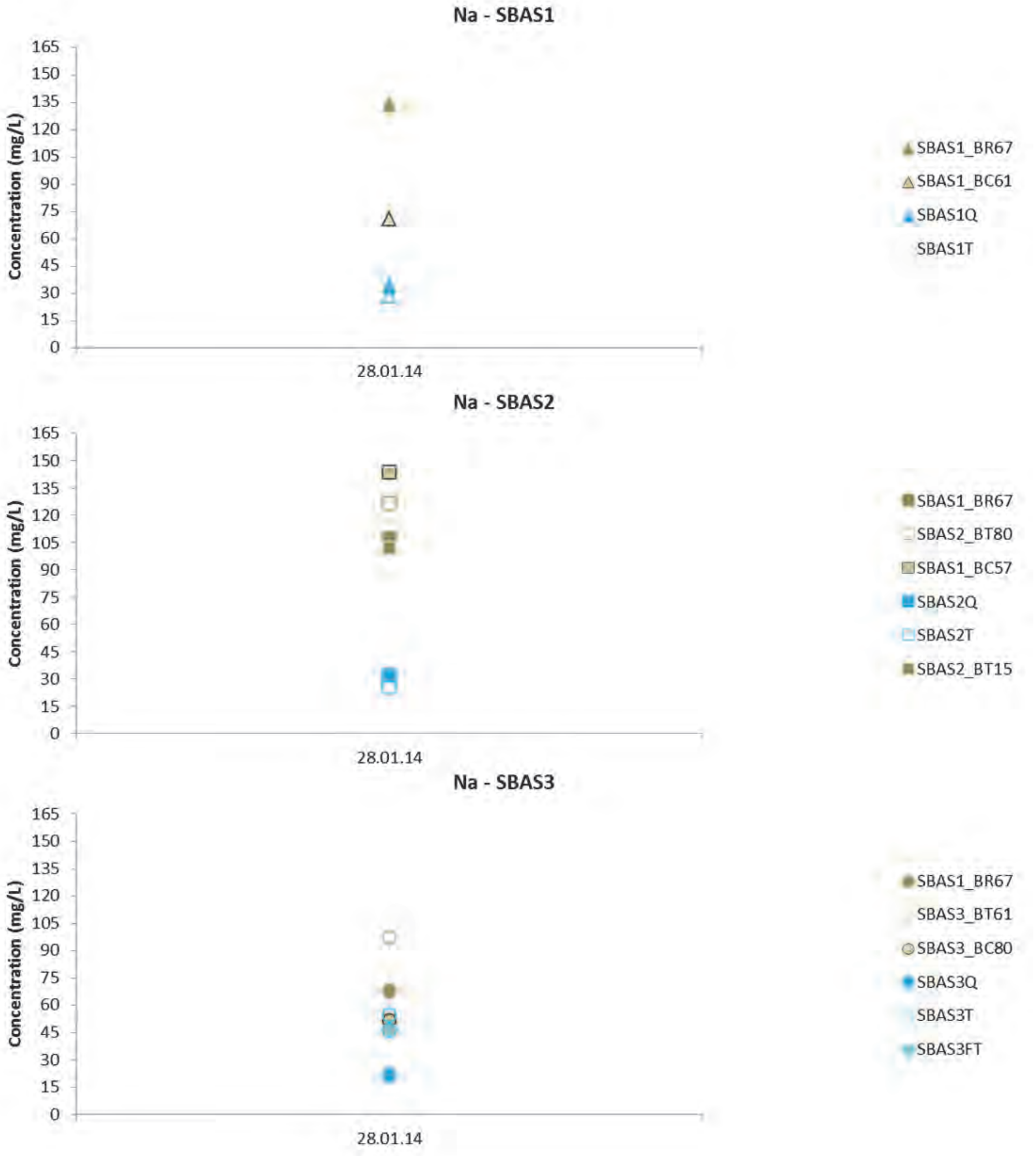

Figure 6.13: Sodium (Na) signatures in boreholes and the stream at Southern Basalts site. (SBAS1 = Southern Basalts 1st order; SBAS2 = Southern Basalts 2nd order; SBAS3 = Southern Basalts 3rd order). Greens are GW samples and blues are surface water samples (Q = catchment outlet, T = hydrometric transect).

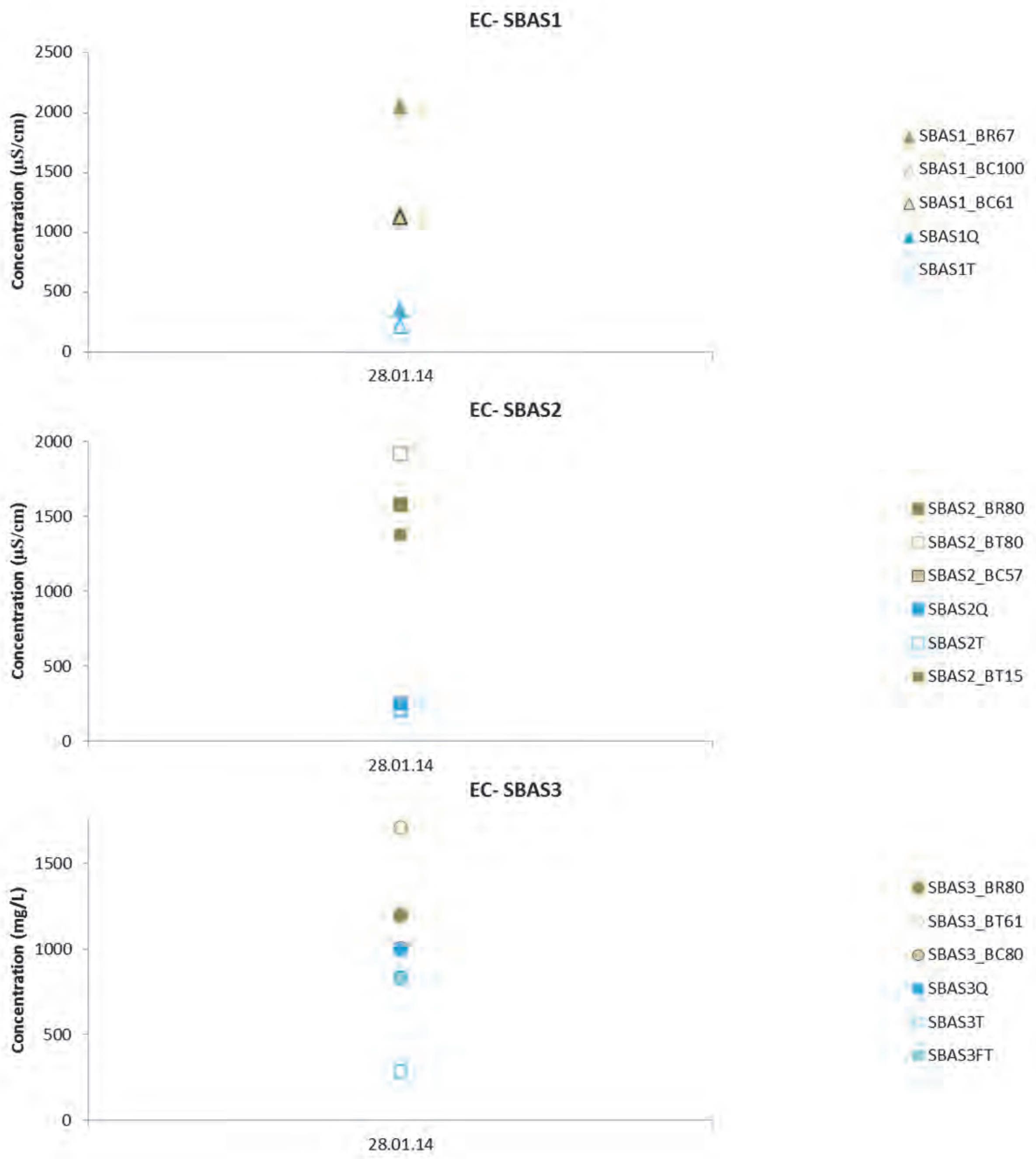

Figure 6.14: Electrical conductivity (EC) signatures in boreholes and the stream at Southern Basalts site. (SBAS1 = Southern Basalts 1st order; SBAS2 = Southern Basalts 2nd order; SBAS3 = Southern Basalts 3rd order). Greens are GW samples and blues are surface water samples (Q = catchment outlet, T = hydrometric transect).

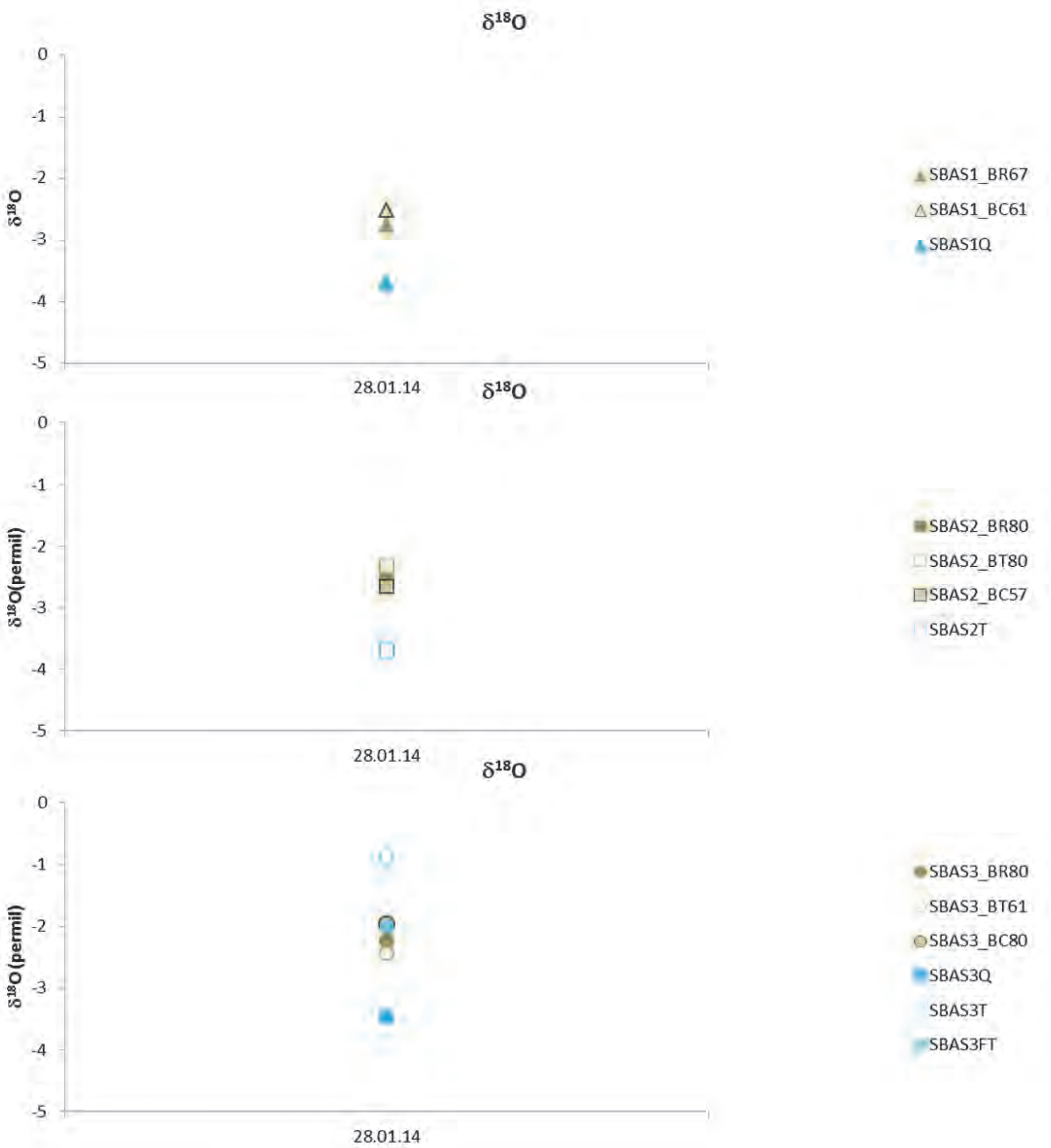

Figure 6.15: Isotope ($\delta^{18}O$) signatures in boreholes and the stream at Southern Basalts site for the event of the 28th of January 2014. (SBAS1 = Southern Basalts 1st order; SBAS2 = Southern Basalts 2nd order; SBAS3 = Southern Basalts 3rd order). Greens are GW samples and blues are surface water samples (Q = catchment outlet, T = hydrometric transect).

A similar trend of disconnection was observed from sodium signatures at this 2nd order reach (SBAS2). Groundwater sodium concentrations were higher and markedly different from those of stream samples (Figure 6.13). For instance, on the 28th of January 2014 the lowest borehole sodium concentration was 101.7 mg/L which contrasted with the highest stream sample value of only 25.58 mg/L. Isotopic signatures were less negative in boreholes (e.g. -2.66 ‰) than in the stream (e.g. -3.70 ‰) and rain samples (-3.73 ‰). Very high EC values were measured for boreholes (e.g. 1370µS/cm) while low stream EC values were observed (e.g. 213 µS/cm). These hydrochemical and isotopic data indicate that groundwater does not contribute to streamflow at this 2nd order reach supporting the original hypothesis. Similar stream and rain isotopic signatures (-3.70 ‰ and -3.73 ‰) show that event water is the dominant contributing source to stream runoff. However, time series ERT profiles for this reach (SBAS2) show lower resistivity values (3-19.7 Ω.m) at the riparian zone which are attributed to higher moisture content at the riparian zone than further away from the stream. This interpretation derives from the fact that the time series ERT were conducted using fixed probes and the same survey protocol with time as the only variable factor (See Section 5.4.1). As such these low resistivity values during the months of February and March 2014 possibly indicate transmission losses from the stream to the aquifer.

At the 3rd order reach (SBAS3) sodium concentrations and EC values reiterate findings from silica and isotopes for samples collected on the 28th of January 2014 that groundwater contributes to streamflow through localised fractured rock preferential flow (Figure 6.13 to Figure 6.15). An earlier analysis for samples collected between September 2012 and March 2013 also revealed similar tracer signatures between selected pools along the stream and groundwater samples at the SBAS3 reach (See Figure 6.16 & Figure 6.17). On the 9th of January 2013 samples collected from the stream and riparian zone boreholes respectively, had $\delta^{18}O$ values of -2.61‰ and 2.68‰, and silica concentrations of 31.94 mg/L and 32.25 mg/L (Table 6.7). Given the analytical error of +/-0.3 for both $\delta^{18}O$ and silica the stated values support that there is groundwater contribution to streamflow at SBAS3. Following the large rainfall event on the 19th of January 2013, similar isotopic signatures (-2.20‰ and -2.30‰) for groundwater and the stream respectively, further support the notion that this reach is a gaining reach from groundwater aquifers.

Table 6.7: Isotopic ($\delta^{18}O$) delta values and hydrochemical (Silica) concentrations indicating connectivity points at the 3rd order reach of Southern Basalts study site.

TRACER	DATE	LOCATION	CONCENTRATION
Silica (mg/L)	09/01/2013	SBAS3 Riparian 80(60m)	32.25
		SBAS3T	31.94
$\delta^{18}O$ (‰)	09/01/2013	SBAS3Q	-2.68
		SBAS3 Riparian 80(40m)	-2.61
	21/01/2013	SBAS3FT	-2.20
		SBAS3 Crest 80(60m)	-2.30
	24/01/2013	SBAS3Q	-2.68
		SBAS3 Crest 80(80m)	-2.59
	28/01/2014	SBAS3 Crest 80(60m)	-1.97
		SBAS3FT	-2.00
EC (µs/cm)	28/01/2014	SBAS3 Crest 80(60m)	1000.00
		SBAS3Q	996.00

Analytical error for $\delta^{18}O$ is +/-0.3‰; for Silica is +/-0.3 mg/L)

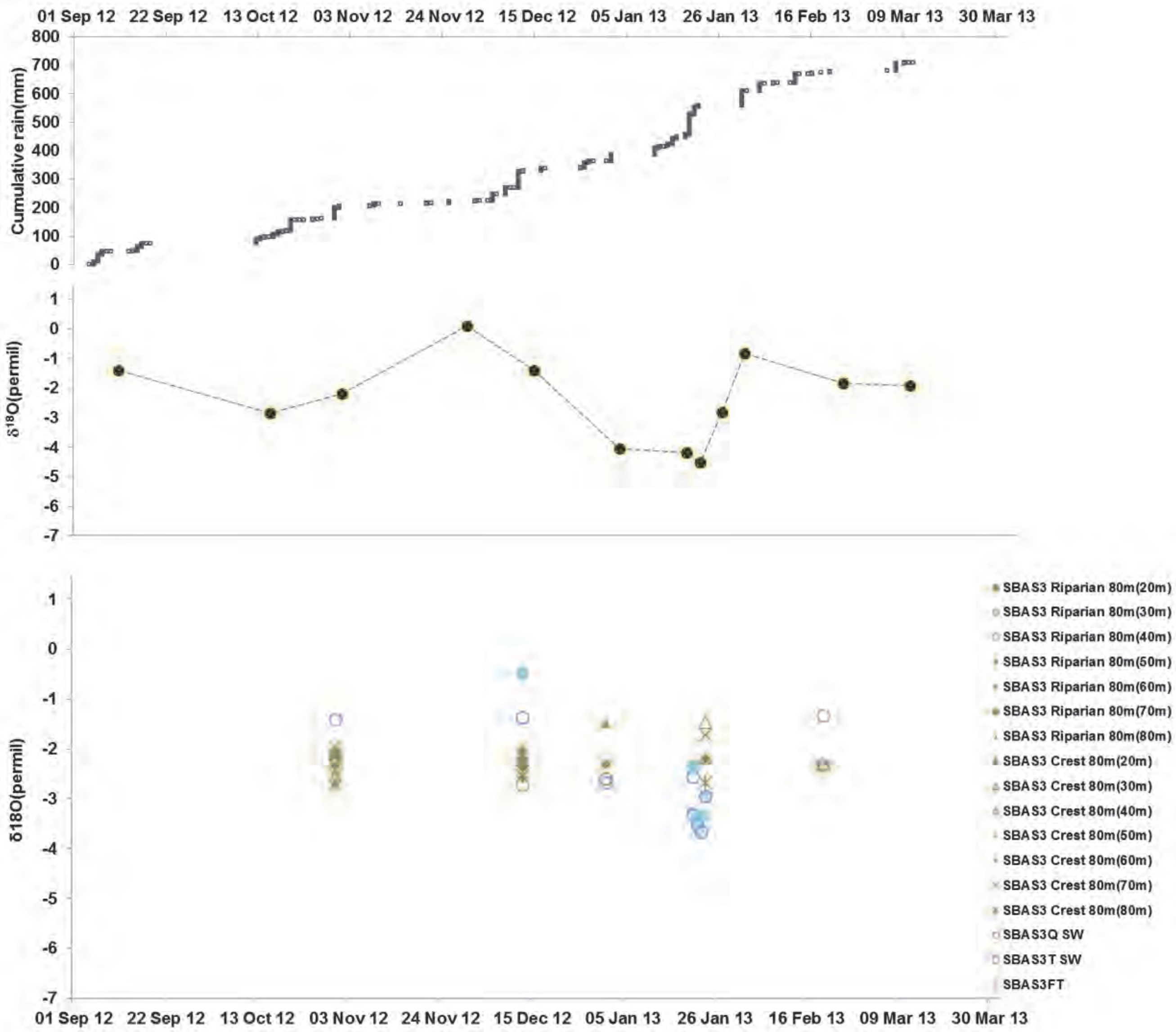

Figure 6.16: Southern Basalts time series presentation of δ^{18}O delta values for the 3rd order reach from September 2012 to March 2013. (Blue = surface water; Green = Groundwater).

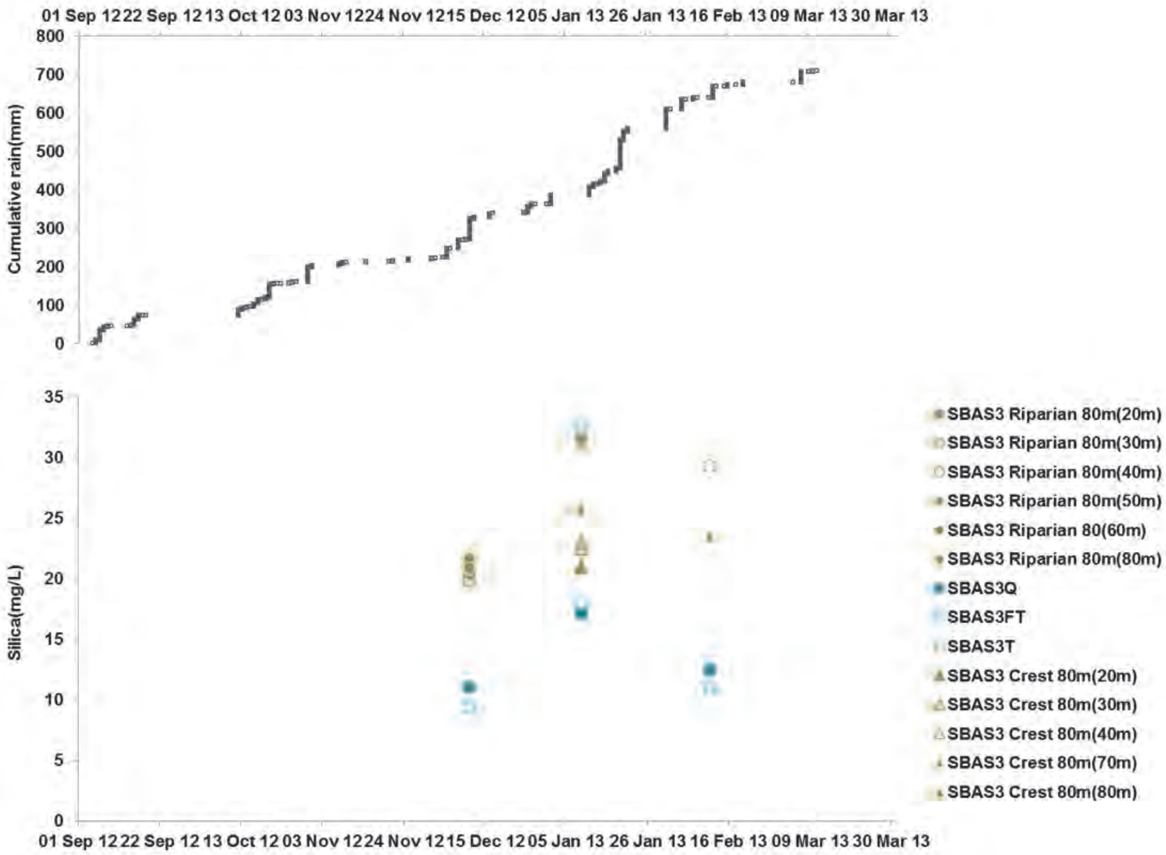

Figure 6.17: Southern Basalts time series presentation of silica concentrations from September 2012 to March 2013. (Blue = surface water; Green = Groundwater)

6.2.5.5 Quantifying contributions of different water sources to streamflow

Hydrograph separation at Southern Basalts relied on both automatic and grab sampling at the 3rd order reach while for 1st and 2nd order reaches only grab samples were used. Three high-intensity rainfall events were selected for hydrograph separation and these occurred on the 19th of January 2013, 20th February 2013 and on the 28th of January 2014. Flows from an additional event (Event 4) which occurred on the 29th of December 2013 were analysed and partitioned into component contributions for the 3rd order reach from automated samples. Peak and mean 15-minute intensities for Event 1 were 10 mm and 0.47 mm respectively, while for Event 2 these were 2.2 mm and 0.54 mm. Event 1 totalled 70.8 mm over 10 hours. Approximately 60% (44.8 mm) of the rainfall total fell within two hours. Stream discharge at the third order gauged outlet increased from 0.6 m^3/s to 2.5 m^3/s at peakflow. Event 2 lasted for 5 hours and had a total of 5.4 mm, 51% (2.8 mm) of which fell in two hours. Event 3 had duration of 1hour and 58% of the total rainfall (12.8 mm) fell within 20 minutes. Event 4 had duration of 6.5 hours and stream discharge increased from 0.042 m^3/s to 4.49 m^3/s at peak flow. Approximately 50% of the total rainfall fell within 3 hours.

6.2.5.6 *Two Component Hydrograph Separation*

6.2.5.6.1 *Event 1 (19 January 2013) at Southern Basalts 3rd Order Reach (SBAS3)*

At the 3rd order reach, surface water isotope values were closer to the rain concentration than groundwater, indicating greater event water contribution to stream runoff at the SBAS3 reach (Figure 6.18). Linear interpolation between end members estimated the contribution of event water at 63% with the remaining 37% being pre-event contribution. Mass balance calculations for a two component hydrograph separation estimated this component at 62% and 60% using $\delta^{18}O$ and EC, respectively (Figure 6.19). These results clearly show that event water is the dominant component in total stream runoff at this reach. Pre-event water contributions estimated at 37% (lumped isotopes technique) as well as 38% and 40% using mass balance calculations for water and tracer ($\delta^{18}O$ and EC) are evidence of groundwater draining into the stream.

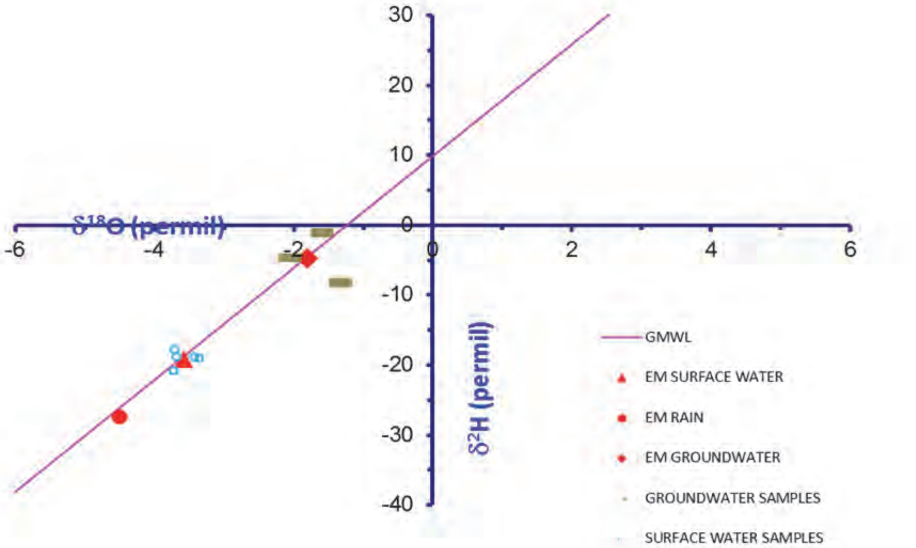

Figure 6.18: Isotope data for samples collected following the January 19, 2013 rainfall event at the 3rd order catchment of Southern Basalts study site. (EM =End Member; GMWL = Global Meteoric Water Line).

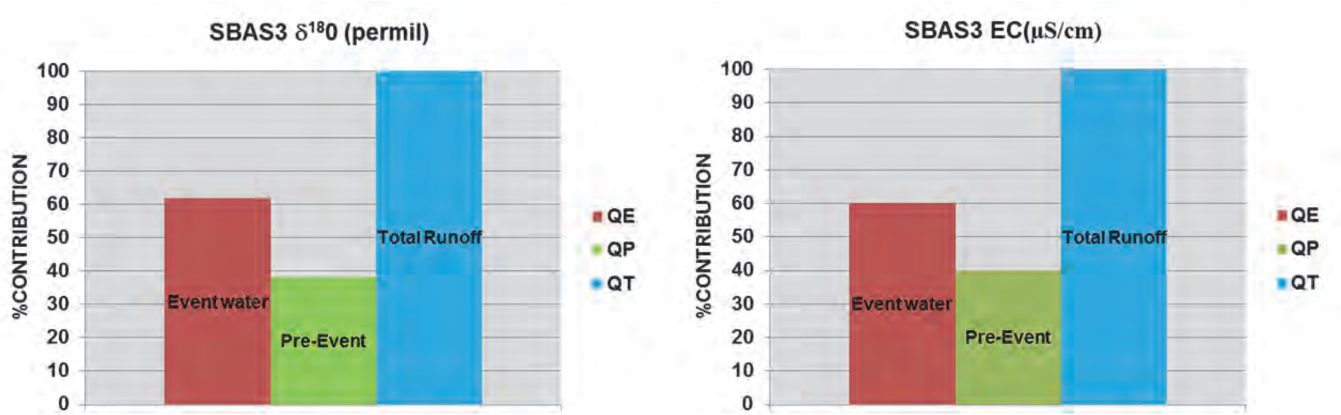

Figure 6.19: Percentage contribution of event and pre-event water to total runoff using $\delta^{18}O$ and EC as tracers for the event of 19 January 2013 at SBAS3 reach of Southern Basalts site.

6.2.5.7 Event 2 (20 February 2013) at Southern Basalts 3rd order reach (SBAS3)

Event water contribution, the dominant component was estimated at 64% using linear interpolation between end members (Figure 6.20). Mass balance calculations for a two component hydrograph separation estimated event water contribution at 51% and 60% using $\delta^{18}O$ and EC, respectively (Figure 6.21).

There is not much difference in event water contribution estimates for both events 1 and 2 at this catchment. Considerable proportions of pre-event water (49% and 40% for $\delta^{18}O$ and EC, respectively) further support that significant groundwater feeds the stream even during lower volume rain events through localised fracture flow at this reach.

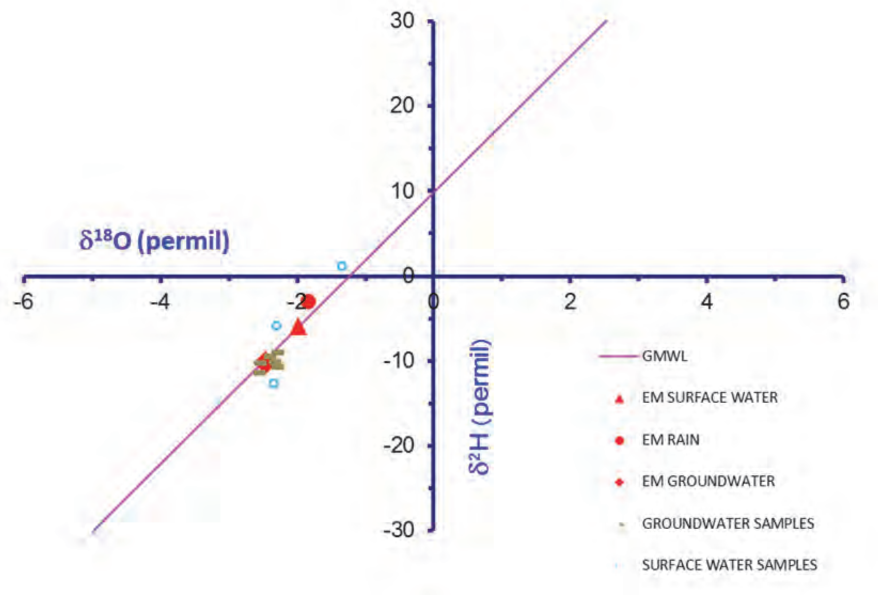

Figure 6.20: Isotope data for samples collected following the February 20, 2013 rainfall event at the 3rd order catchment of Southern Basalts study site. (EM =End Member; GMWL = Global Meteoric Water Line).

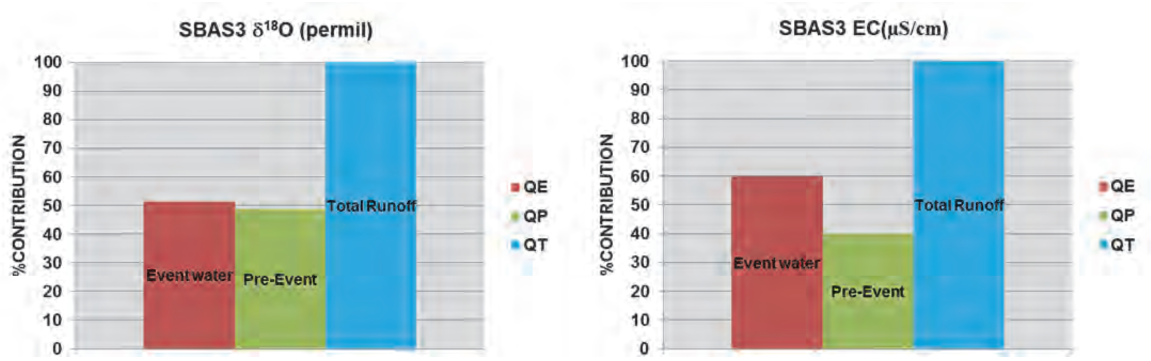

Figure 6.21: Percentage contribution of event and pre-event water to total runoff using $\delta^{18}O$ and EC as tracers for the event of 20 February 2013 at Southern Basalts study site.

6.2.5.8 Event 3 (29 December 2013) at Southern Basalts 3rd stream order.

A significant rainfall event >100 mm occurred on 29 December 2013, fortunately the automated ALCO sampler was able to capture this event. At the onset of the storm event water contribution was estimated at 56% against 44% of pre event water input to stream runoff. Twenty minutes into the storm, event water contribution reached a peak 100% and then dropped for about 15 minutes to 69% during the recession limb (Figure 5.19). These results support our original hypothesis that the 3rd order reach (SBAS3) is a gaining reach from adjacent aquifers.

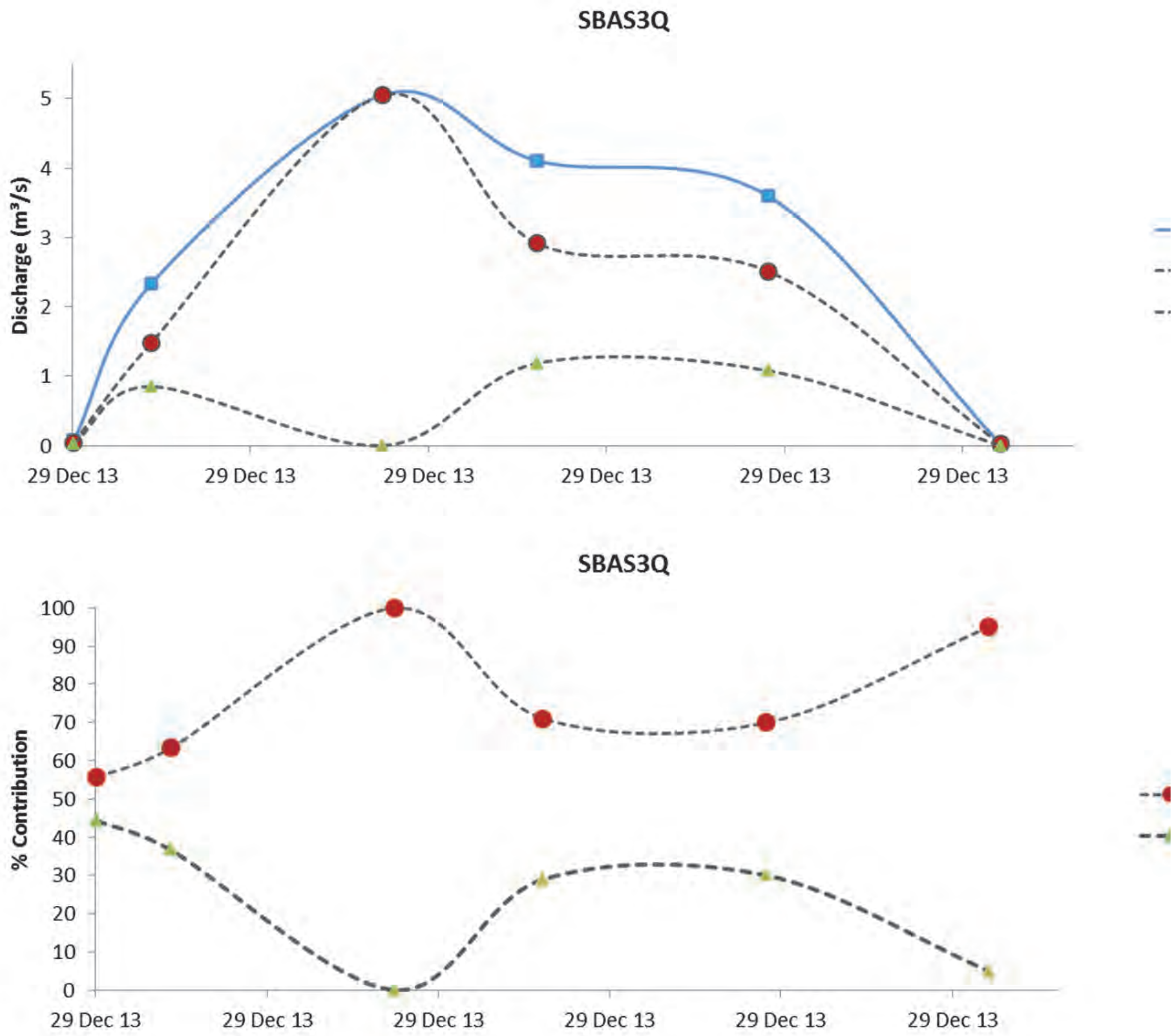

Figure 6.22: Two component hydrograph separation for Event 3 (December 29, 2013) at SBAS3 showing event and pre event components and percentage contributions of these components to the streamflow. (QT = Total discharge; QE = Event discharge; QP = Pre-event discharge; %QE and %QP = percentage contributions of event and pre-event water to total streamflow, respectively).

6.2.5.9 *Event 4 (28 January 2014) at Southern Basalts all stream orders*

Event water was revealed to be the dominant contributor to streamflow hydrographs of 1st (SBAS1) and 2nd (SBAS2) order streams at Southern Basalts study site (figure 6.23). At SBAS1 the contributions of event water and pre event water respectively, were estimated at 99.5% and 0.5%. At SBAS2 event water was estimated to contribute 92.6% while the contribution of pre event water was 7.4% (Figure 6.24). The significance of event water contribution to streamflow at these lower order reaches is further supported by the two component hydrograph separation, thus affirming our original hypotheses of disconnected hillslopes from the stream network at the lower catchment orders.

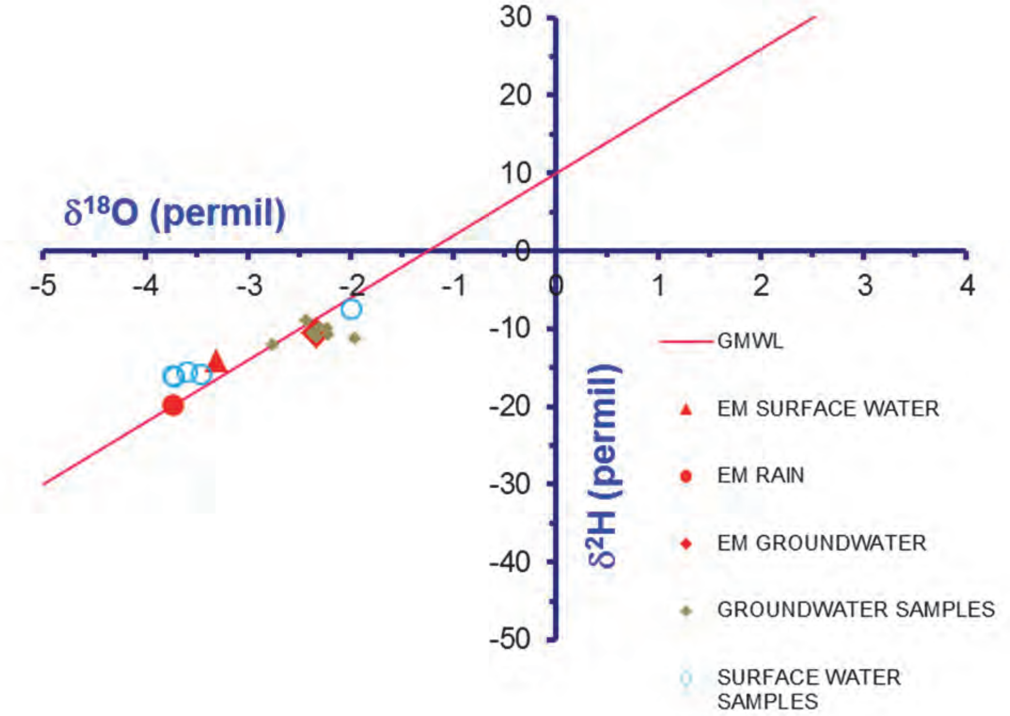

Figure 6.23: Isotope data for samples collected following the January 28, 2014 rainfall event at the 3rd order catchment of Southern Basalts study site. (EM =End Member; GMWL = Global Meteoric Water Line).

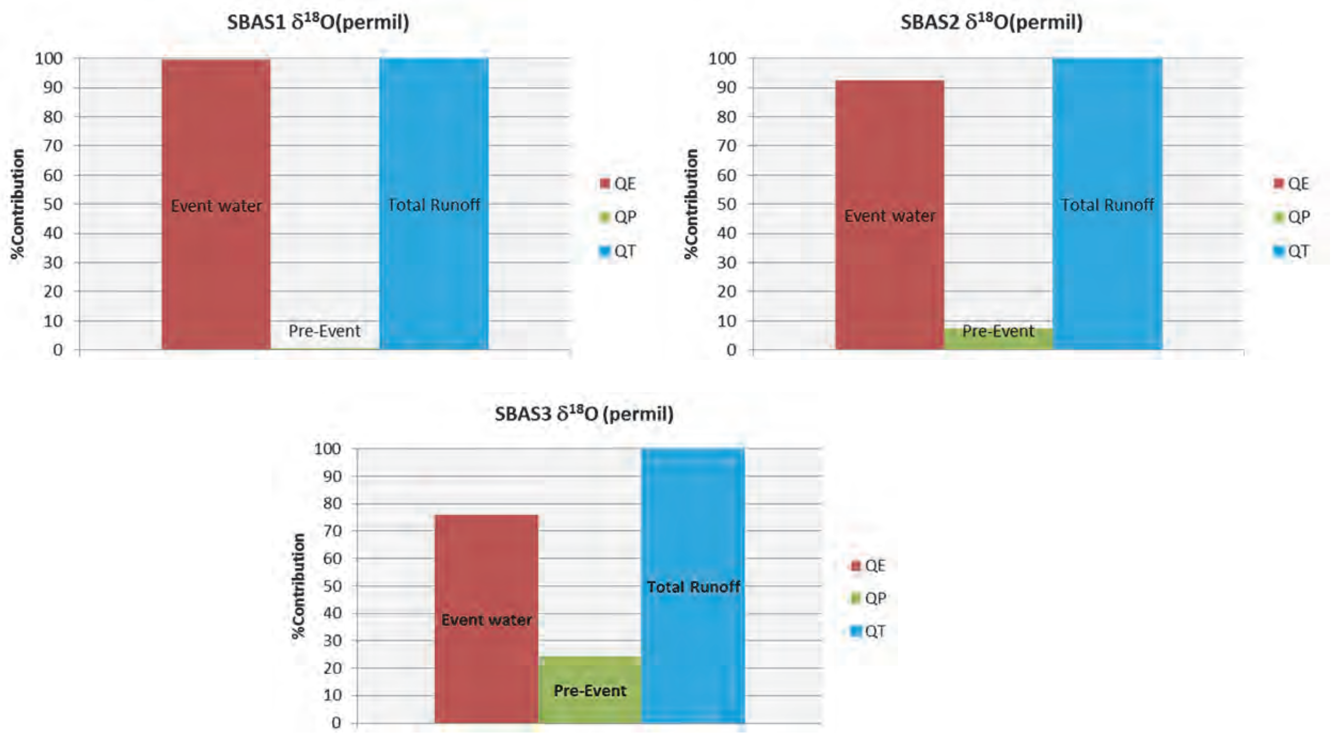

Figure 6.24: Contribution of event and pre-event water to total runoff at SBAS1, SBAS2 & SBAS3 reaches at Southern Basalts using δ18O for the event of 28 January 2014.

At the 3rd order stream samples aligned more towards rain samples implying significant event water contribution to streamflow for the 28th of January 2014 rainfall event. However, the presence of stream samples closer to some groundwater samples is indication that there was mixing of water sources in the stream. Component contributions to stream runoff using end member linear interpolations for this event were estimated at 73% event water and 27% pre-event water (Figure 5.18).

6.2.6 Stream Network Connectivity at Southern Basalts

High intensity rainfall events at Southern Basalts allow the stream network to be connected from the 1st order to all downstream reaches during threshold rainfall of >70%. Gentle recession limbs indicate sustained flows following long duration large volume/high intensity events only, indicating no sustained contributions from the hillslopes to streamflow on the southern basalts. Thus catchment scale hydrological connectivity is extremely intermittent on the southern basalts which is also driven by threshold level antecedent soil moisture conditions equivalent to an API_{-7} values of >130 mm (See section 6.1, Figure 6.3).

6.3 Southern Basalt 1st order hillslope

6.3.1 1st order Geophysics

Figure 6.25 shows the initial and revised interpretation of the 1st order geophysics traverse, where the unsaturated zone across the profile had an interpreted depth of 20 m with variable moisture contents due to the changes in low resistivity (3-19.7 Ω.m) values across the profile at shallow depths. The estimated groundwater level was expected to be approximately 8-10 m across the profile. The riparian zone was estimated to have shallower weathering which then increases in depth towards the crest due to shallower depths of high (844-2162 Ω.m) resistivity material there. Two boreholes were drilled at the riparian zone as saturated condition were expected to occur at two distinctive depths namely the weathered/unsaturated zone and hard rock/saturated zone given the difference in resistivity in the shallow (3-19.7 Ω.m) and deep (844-2162 Ω.m) subsurface. The close banding of resistivity 129-844 Ω.m at 20-35 m depth across the hillslope suggests a possible interface zone between the weathered and hard rock basalt. The crest also had two boreholes as it was estimated that two zones occur such as the high resistivity values (844-2162 Ω.m) of hard rock/saturated zone and low resistivity values (3-19.7 Ω.m) of weathered/unsaturated zone annotated on the profile.

The final interpretations following drilling revealed that the 1st order hillslope exhibits a low permeable weathered basalt and slightly higher permeable hard rock basalt aquifer at both the riparian and crest position boreholes. This is due to the shallow boreholes being drilled dry and having no record of any water level to date which suggest no shallow groundwater system. The deep boreholes had low blow out yields (0.08 l/s) and low T values which suggests an inactive deep groundwater flow system.

Figure 6.26 shows a time series geophysics analysis of the 1st order hillslope, a defined lateral band distribution of low resistivity (3-19.7 Ω.m) extends across the profile at depths of 5-10 meters which could be related to the clay soil properties and thus has capacity to retain moisture.

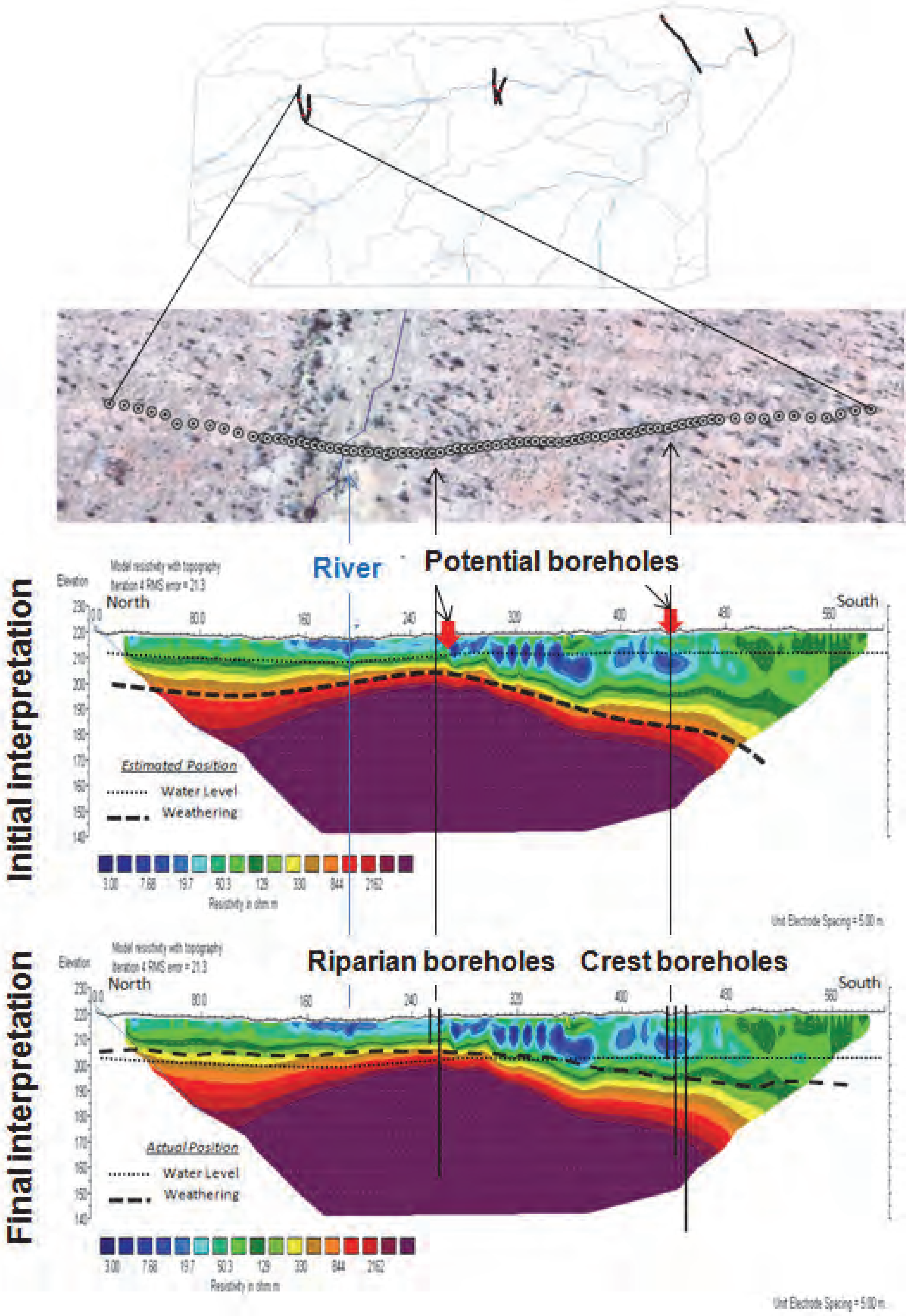

Figure 6.25: Initial and final interpretation of 2D ERT traverses coupled with topography data, satellite imagery and estimated and actual positions of groundwater level and weathering

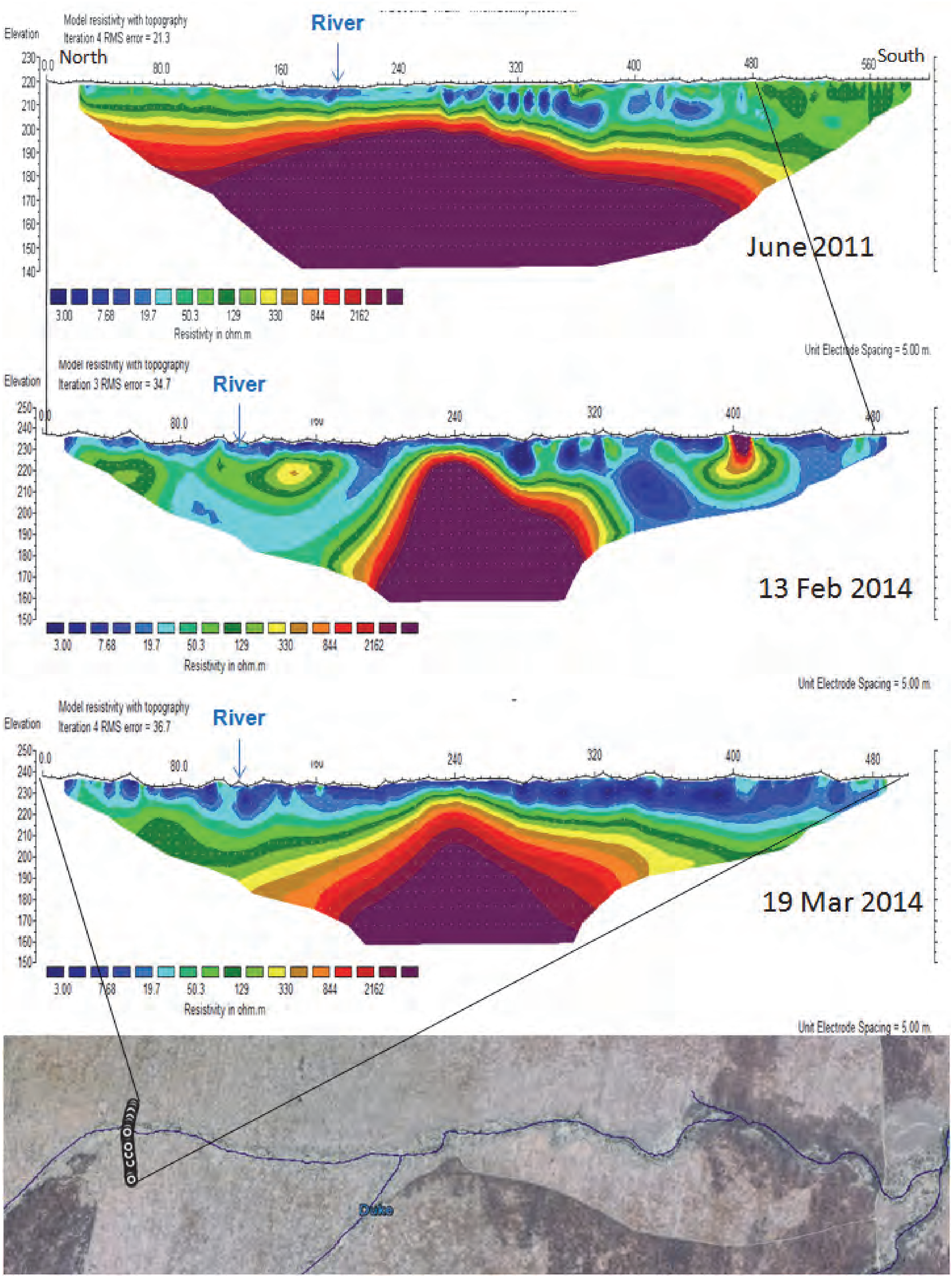

Figure 6.26: Time-series geophysics transect southern basalt 1st order hillslope

6.3.2 1st order shallow unsaturated zone characterization and responses

Characterization at the southern basalt supersite was done through K_{unsat} measurements and soil classification. K_{unsat} was measured at the surface at each catena element close to the soil moisture monitoring stations. Due to time and logistical constraints, K_{sat} could not be done.

1st Order Hillslope

High K_{unsat} (12 mm at φ =5 mm) is shown at the crest on this 1st order hillslope Figure 6.27. Values decrease moving downslope with the riparian having the least (0.4 mm at φ =5 mm). This is attributed to the presence of more clay particles on the riparian that have been gradually washed downslope over the years possibly through wind or water and possibility some contributions from river alluvium. The whole hillslope is characterized by Shortlands soil form (Table 6.8) and the red structured B horizon characteristic of this soil form is a potential recharge soil (Le Roux et al., 2013). This therefore suggests the possibility of an absence of lateral flows on the entire hillslope implying a hydrological disconnection between catena elements and also between the entire hillslope and the adjacent stream network.

Table 6.8: Soil classification per catena element on basalt 1st order hillslope

Catena Element	Taxonomical soil class	Diagnostic Horizons	Hydropedological soil type
SBAS1_Crest	Shortlands	Orthic A	Recharge
		Red Structured B	
		-	
SBAS1_Mid	Shortlands	Orthic A	Recharge
		Red Structured B	
		-	
SBAS1-Rip	Shortlands	Orthic A	Recharge
		Red Structured B	
		-	

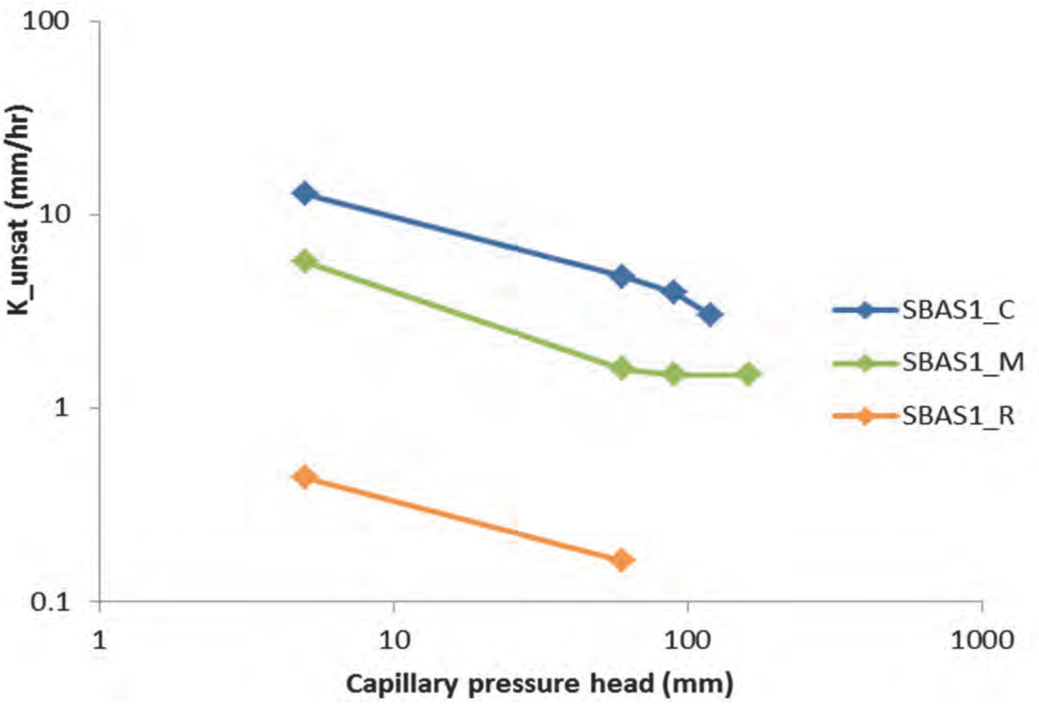

Figure 6.27: Unsaturated hydraulic conductivity on 1st order hillslope

Soil moisture responses on the 1st order hillslope (Figure 6.28), shows low potential for shallow soils on the crest in response to the first rainfall events (September 2012). The intermediate soils shows a lag of about two weeks after the first rains whilst the deeper soil layers have a 6 week lag only to respond mid October which is when there was some significant high intensity rainfall events. The deep soils respond to high intensity events only (October and January) therefore since these are Shortlands soils, the red structured B horizon is a potential recharge soil implying free draining soils. Since the deeper soils did not respond to most of the events this suggests a high ET demand therefore moisture was being taken up by plant roots and evaporation before getting deep into the profile. This catena element is generally a dry area as illustrated by the % ED data showing that they were dry (>10000 mm) for more than 80 % of the time.

The midslope also follows a more or less similar pattern to the crest whereby the shallow soils respond to the first rainfall event then the intermediate soils responds after a two week lag. Theydid not get saturated, remained relatively dry (>1000 mm) for ~85% of the time. The deeper layers show no response to first 18 weeks of the wet season only responding to the high intensity event mid January 2013 before drying up. This supports the presence of interflow from the hydropedological classification. Similar to the crest this is also a relatively dry area, more drier than the crest as illustrated by the %ED curves showing they were dry for almost 90% of the time.

The riparian soil moisture sonsors were faulty therefore data was ommitted.

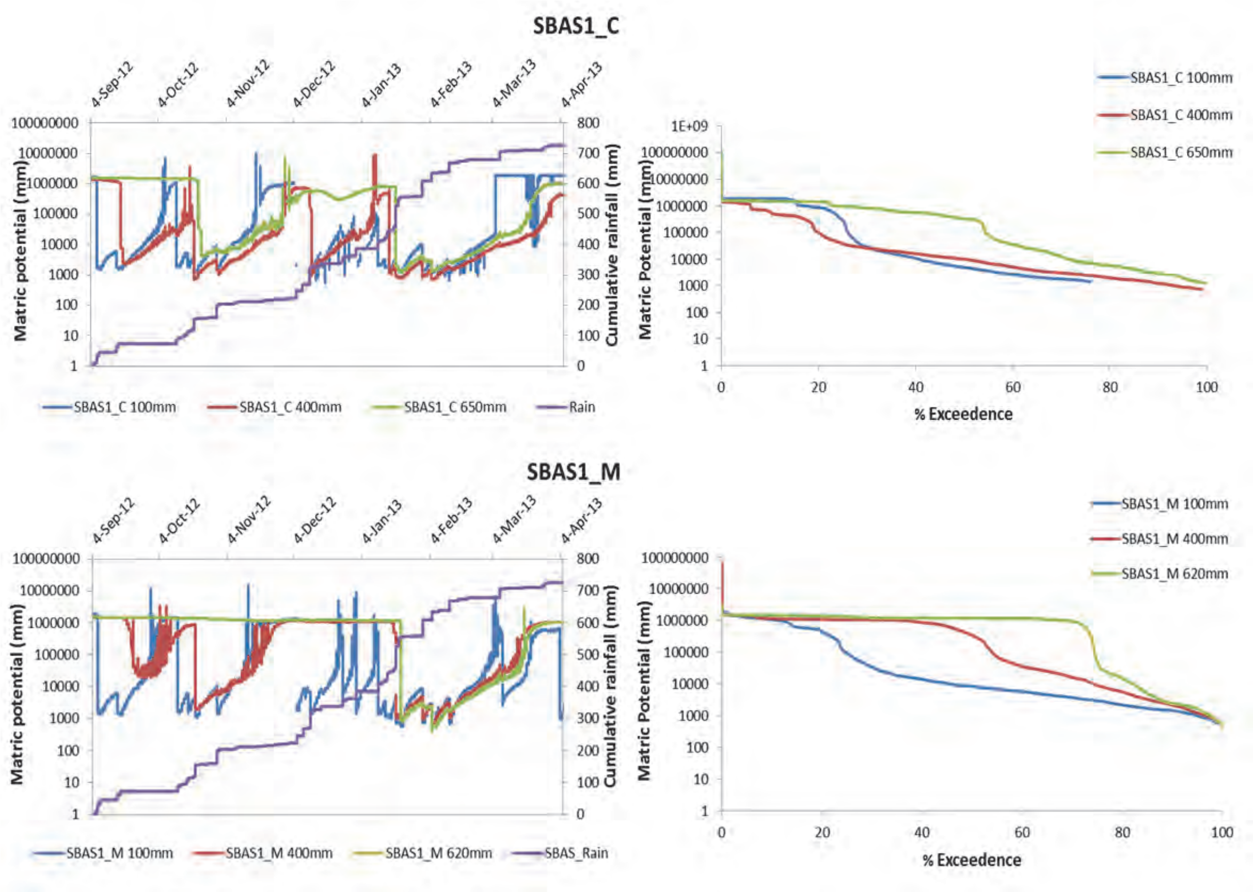

Figure 6.28: soil moisture responses and % ED curves for 1st order hillslope

6.3.3 1st order Hydrogeology: Hydraulic Responses and Parameters

To gain understanding of the trend in groundwater levels in response to rainfall, each nested piezometric (shallow and deep) borehole water level within a particular catenal element was plotted against rainfall. From this one is able to infer flow gradients and possible processes identified such as groundwater recharge, discharge and interflow.

The hard rock deep groundwater level of the 1st order riparian position 67 m borehole can be seen in Figurwe 6.29. The record of water levels is from July 2013 to March 2014 and exhibits no major response to the 2nd sequence of rainfall with a dH of 0.18 m. This occurrence suggests an inactive deep groundwater flow system at the localized hillslope scale and characteristic of a more regional groundwater flow system.

The hard rock deep groundwater level of the 1st order crest position 61 m and 100 m borehole can be seen in Figure 6.30. The record of water levels is from July 2013 to March 2014 and exhibits no major response to the 2nd sequence of rainfall with a dH of 0.26 m. However after the high intense rainfall (62 mm/day) event occurring on 2014/03/05 caused the water level in both boreholes to rise by 0.20 m. Given that the water level had not responded to the 118 mm rainfall event on 2013/12/29 suggests that possibly rainfall exceeding 60-70 mm/day provides extensive runoff and minimal infiltration hence no major contribution to groundwater.

The 1st order triangulation borehole 56 m water level record starts in October 2012 and has a decreasing trend. The dH then increases by 0.21 m as a result of the 62 mm/day rainfall event on 2014/03/05.

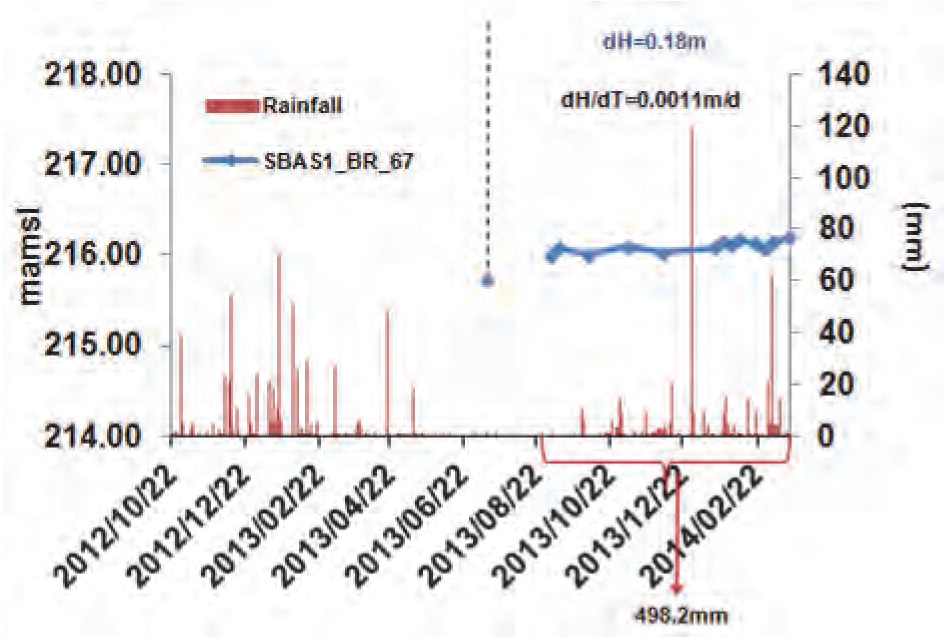

Figure 6.29: 1st order riparian position 67 m borehole water level response to rainfall over the hydrological season October 2012 to March 2014

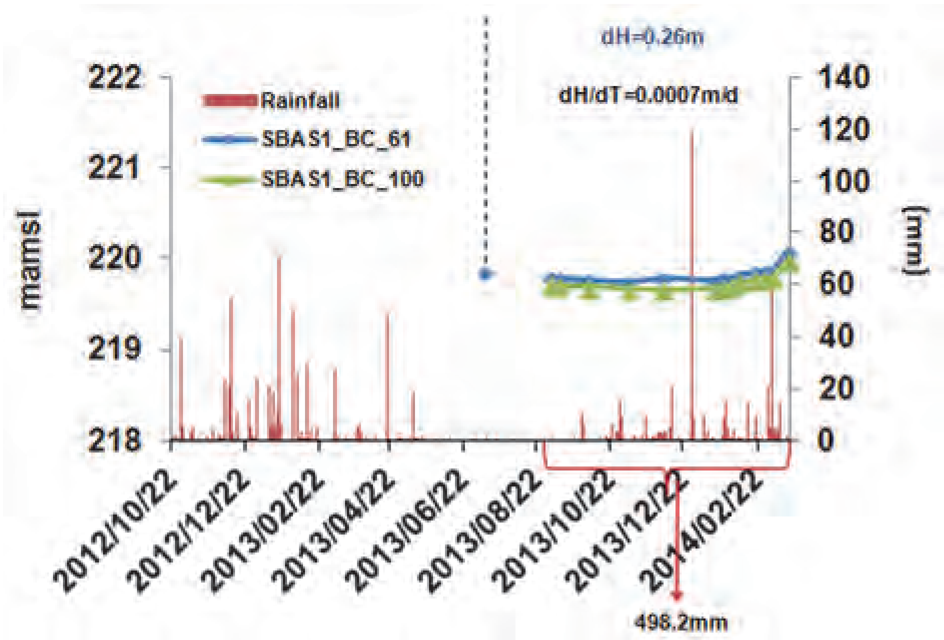

Figure 6.30: 1st order crest position 61 m and 100 m borehole water level response to rainfall over the hydrological season October 2012 to March 2014

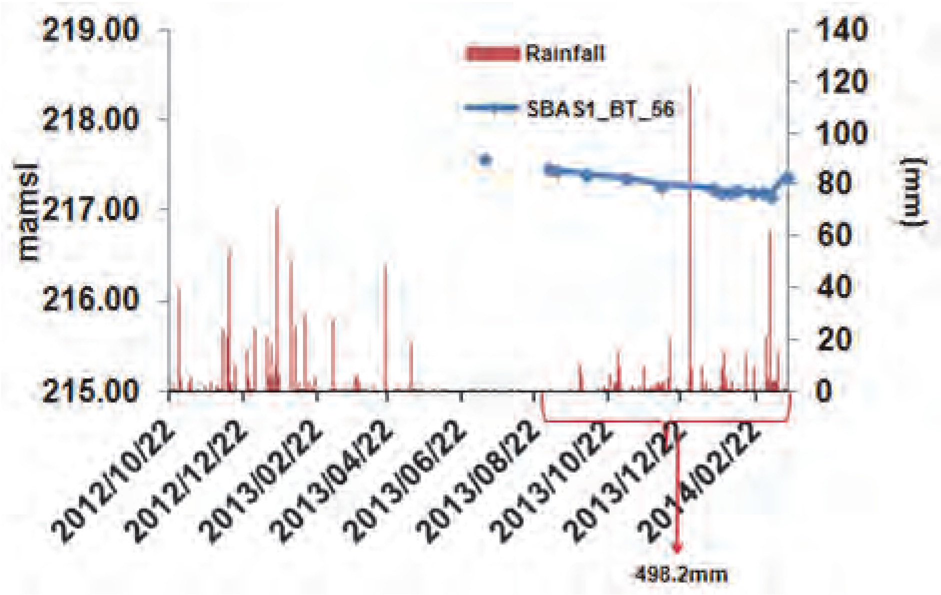

Figure 6.31: 1st order triangulation position 56 m borehole water level response to rainfall over the hydrological season October 2012 to March 2014

To gain an improved understanding of the spatial temporal distribution of groundwater at the hillslope scale and within the catchment, in-situ measurements of specific conductance (mS/cm) in groundwater at the first order scale were plotted in Figure 6.32-Figure 6.35 (see Appendix A6.1 to A6.2 for Temperature and pH). In the case of the crest 100 m and 61 m borehole specific conductance values do not change significantly over the 2 month fluid logs. This indicates that there is no active influx or mixing of fresh (low specific conductance) groundwater. Hence, there is also no rapid response in water level to the 1st and 2nd sequence of rainfall events.

The fluid logs of the 1st order 61 m crest borehole indicate a freshening of borehole water above 200 mamsl (possible fracture position) due to the deviation in the vertical distribution of specific conductance values. This can be attributed to flow through of fresher groundwater in the shallow weathered zone or fracture. In terms of the variation over the 2 fluid logs there is not much difference. This indicate that there is no active influx of fresh water (low SC) contributing to groundwater i.e. rainfall stream water.

The fluid logs of the 1st order 56 m triangulation borehole indicate no variation in the vertical distribution or over the 2 SC fluid logs. This shows that no active influx of fresh water reaching the groundwater system. The minor responses of the water level to rainfall supports a non-active groundwater flow system at this point.

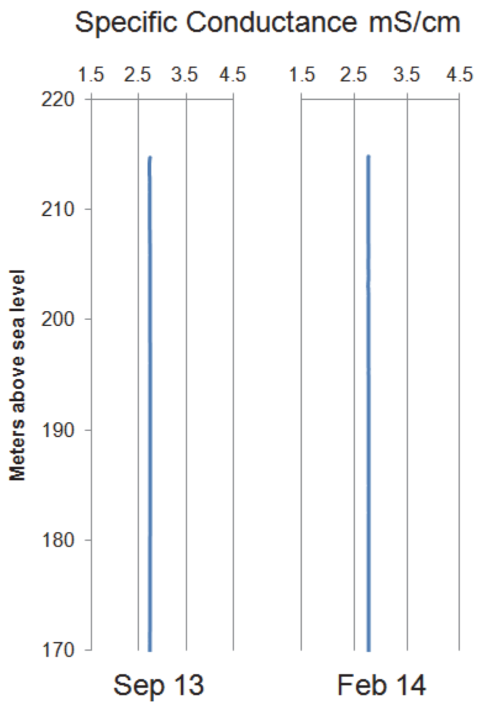

Figure 6.32: specific conductance quarterly fluid log for the 1st order riparian position 67 m borehole

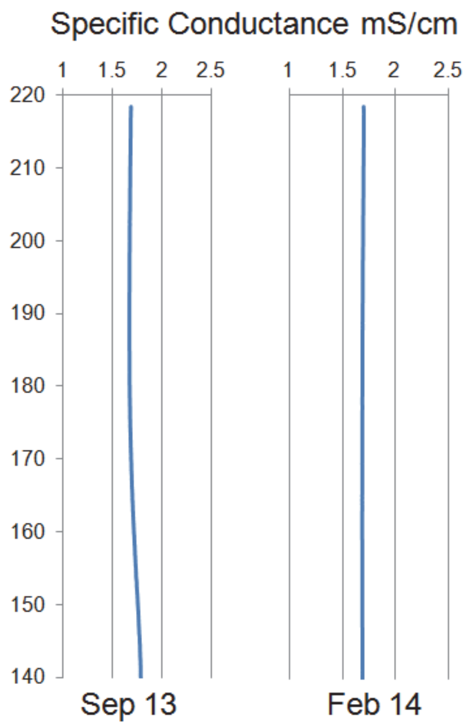

Figure 6.33: specific conductance quarterly fluid log for the 1st order crest position 100 m borehole

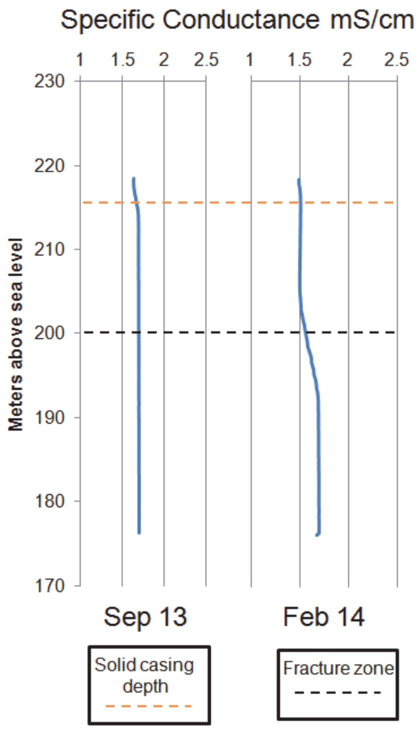

Figure 6.34: specific conductance quarterly fluid log for the 1st order crest position 61 m borehole

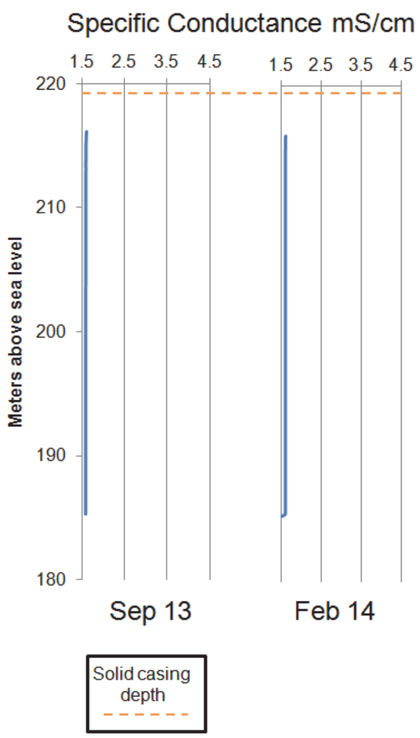

Figure 6.35: specific conductance quarterly fluid log for the 1st order triangulation position 56 m borehole

6.4 Southern Basalt 2nd order hillslope

6.4.1 2nd order Geophysics

Figure 6.36 shows the initial interpretation of the 2nd order hillslope subsurface where it was estimated that the riparian zone exhibited an 8-10 m unsaturated zone with shallow groundwater levels at 10 m due to low resistivity values (3-19.7 Ω.m) below the surface. The riparian zone was expected to have shallower weathering which increased toward the crest due to the higher (844-2162 Ω.m) resistivity values occurring at a greater depth at the crest. Two boreholes were drilled at the riparian zone to capture the expected saturated conditions at two distinctive depths namely the weathered/unsaturated zone and hard rock/saturated zone. The resistivity values suggest a low (3-19.7 Ω.m) and high (844-2162 Ω.m) resistivity zone which could be interpreted as weathered and hard rock zones respectively. The crest also had two boreholes drilled to monitor the two zones of saturation.

The final interpretation indicated that the riparian position boreholes have shallower weathering than the crest position boreholes. The high yielding (blow out yield of 0.92 l/s) deep borehole drilled into the fractured rock at the riparian is more permeable relative to the deep borehole drilled at the crest which had no blow out yield.

The time-series plots for the same hillslope shown in Figure 6.37 show some key aspects. Such as the low resistivity values encountered with an increased depth at station 160 on the February 2014 and March 2014 geophysics profile. This occurrence indicates possible contribution from the hillslope towards the stream or vice versa. When considering the increase in water levels at the riparian boreholes during this period the later seems more likely.

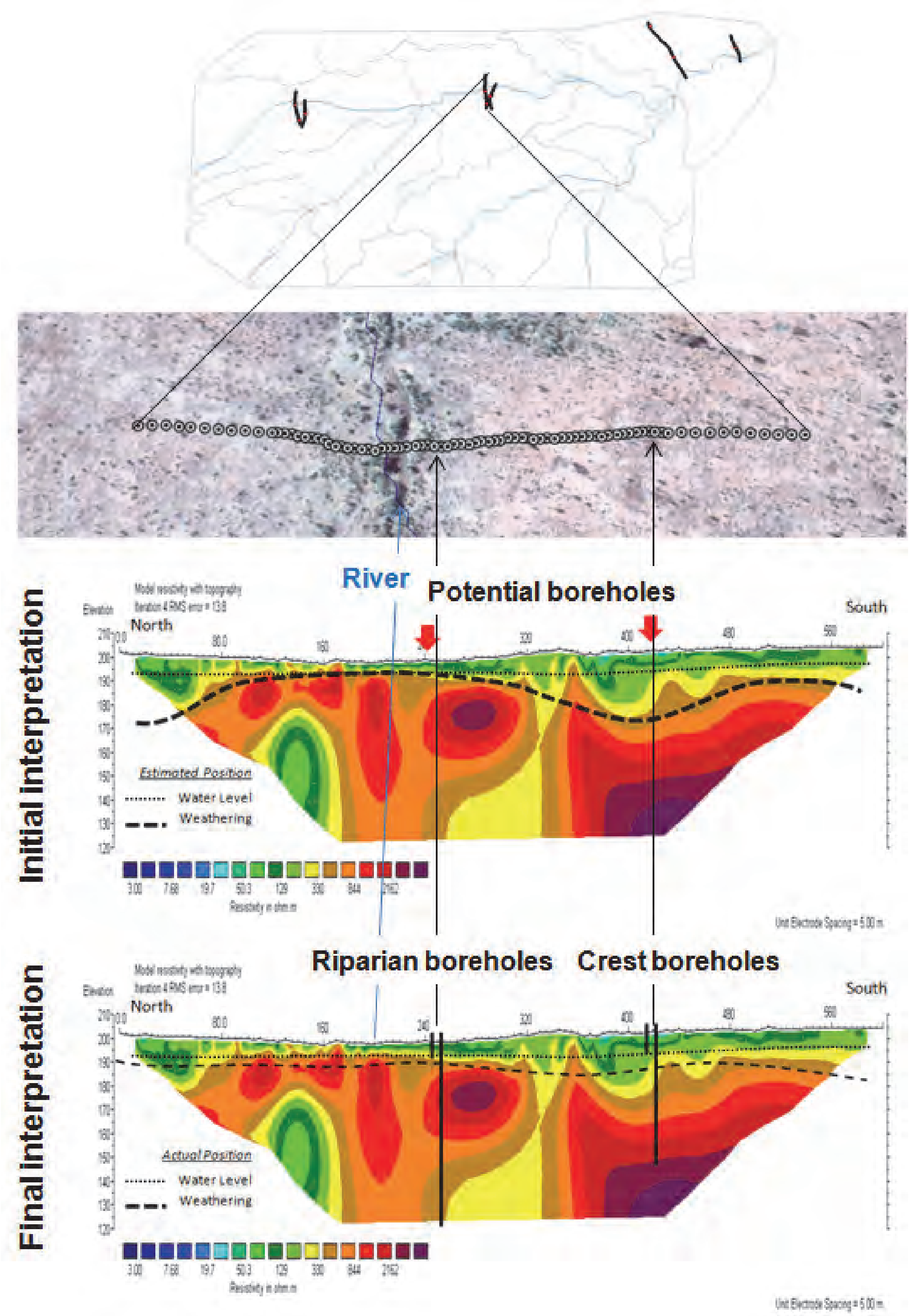

Figure 6.36: Initial and final interpretation of 2D ERT traverses coupled with topography data, satellite imagery and estimated and actual positions of groundwater level and weathering

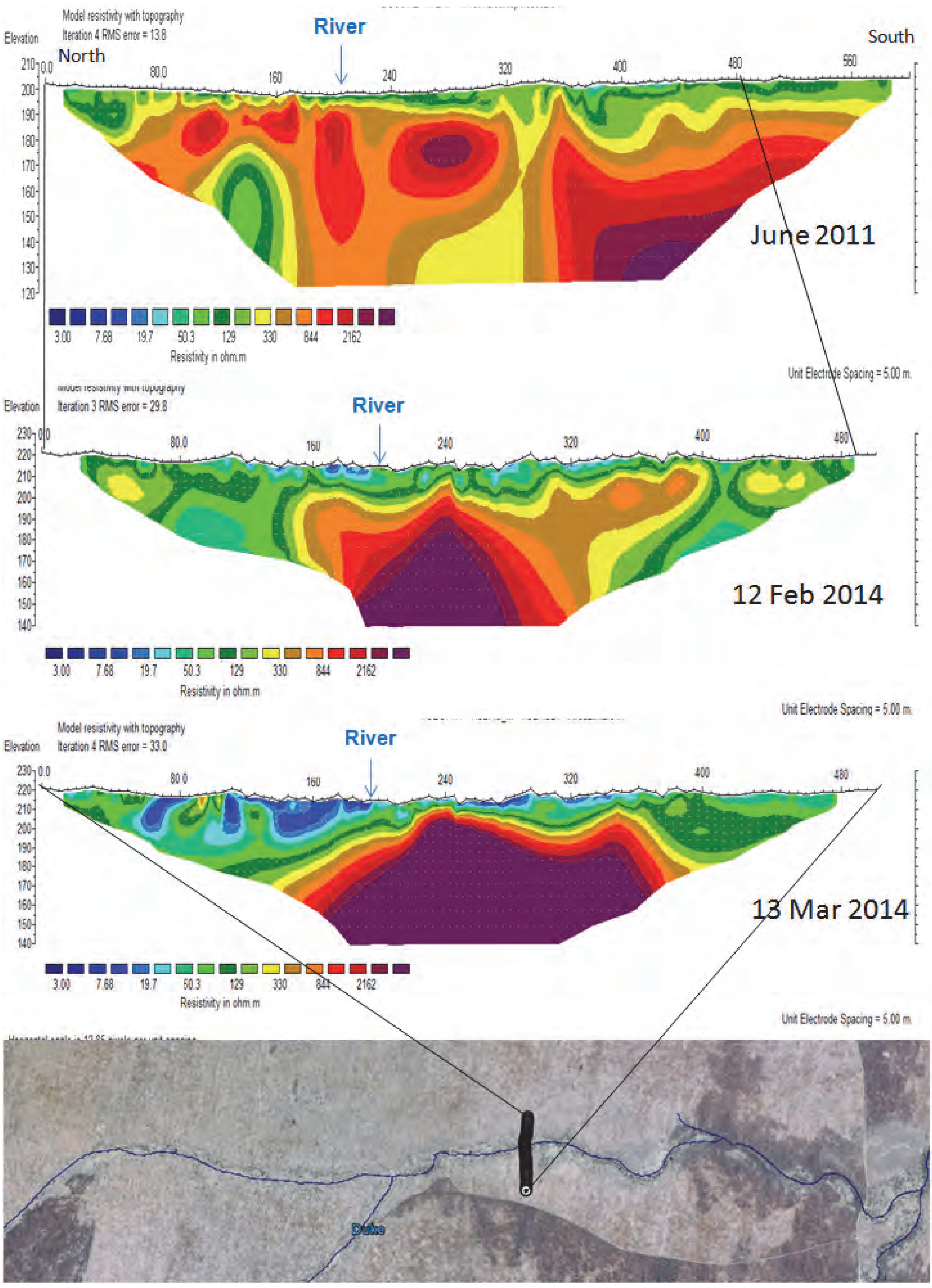

Figure 6.37: time-series geophysics transect southern basalt 2nd order hillslope

6.4.2 2nd order shallow unsaturated zone characterization and responses

Measured K_{unsat} on the 2nd order hillslope (Figure 6.38) shows the riparian zone to have the highest conductivity at lower capillary pressure head and vice versa (37 mm/hr at φ =5 mm). This suggests a high clay content since clay soils sometimes tend to have high K_{unsat} at low pressure heads (Artiola et al., 2004).This also depends on the bulk density of the soil. The crest shows low K_{unsat} at low capillary pressure head compared to the midslope and riparian. Hydropedological classification shows variability in the distribution of soils on this hillslope (Table 6.9). Due to the lack of any morphological indication of saturation within the diagnostic horizons throughout soil profiles, all the catena elements at this hillslope were classified as potential recharge soils implying no hydrological connectivity between elements and also suggesting a hydrological disconnection from the stream network.

Table 6.9: Soil classification per catena element on basalt 2nd order hillslope

Catena Element	Taxonomical soil class	Diagnostic Horizons	Hydropedological soil type
SBAS2_Crest	Glenrosa	Orthic A	Recharge
		Lithocutanic	
		-	
SBAS2_Mid	Mayo	Melanic A	Recharge
		Lithocutanic	
SBAS2_Rip	Swartland	Orthic A	Recharge
		Pedocutanic B	
		Saprolite	

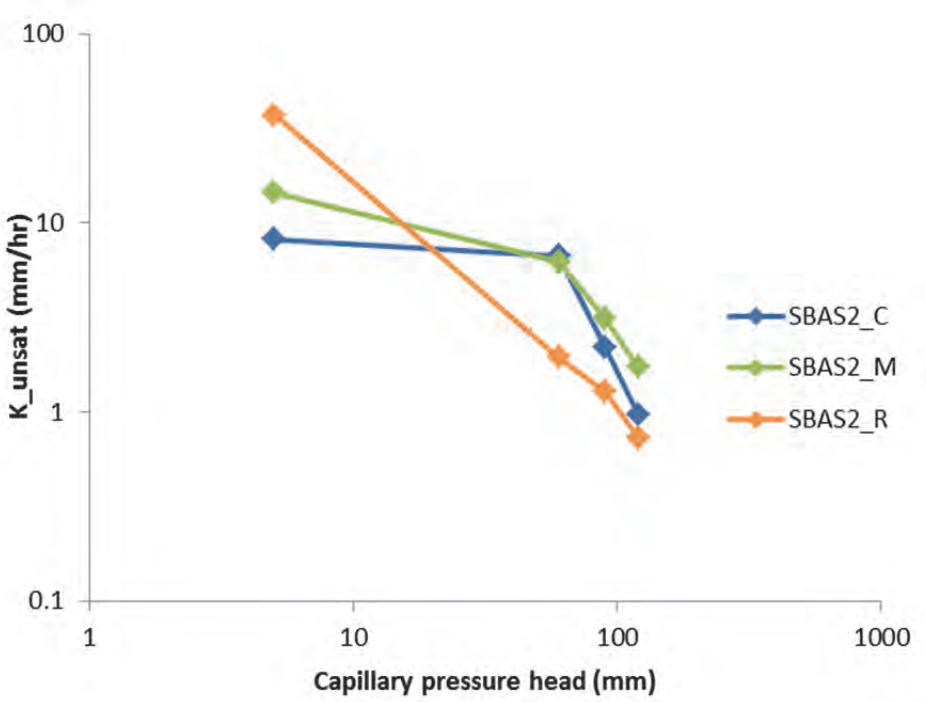

Figure 6.38: K_{unsat} on 2nd order hillslope

The data presented for the 2nd order hillslope (Figure 6.39) is for the crest and riparian catena elements, no data will be presented for the midslope since sensors were pulled out by wild animals. At the crest, shallow and intermediate soils show low potential in response to the first September rains then the deeper layers respond after a two week lag. Unfortunately the deepest sensor was pulled out just after the January events therefore only data from September to January is presented for the deep soils at this element. The shallow and intermediate soils show more or less similar wetting and drying cycles. Soils got close to saturation (<1000 mm) for almost 40% of the time as illustrated by the %ED curves. Soils here are classified as recharge and this data suggest that water does not easily infiltrate to deeper layers due to root water uptake and evaporation from the surface.

The riparian shows low potentials for both shallow and intermediate soils in response to the early September rains whilst the deep soils show a 6 week lag to the rains only to respond to the October high intensity events. The deeper soils only respond to high intensity events (October and January) but %ED curves show that this element was dry for more than 65% of the time. The similar wetting and dying cycles of the shallow soils imply some vertical subsurface flow (potential recharge) augmenting the hydropedological classification (Table 6.9) but the lag in response by the deep soils suggest water loss through ET therefore water will not get deep into the profile. Since the riparian soils are described as potential recharge, this means they are largely disconnected from the stream network.

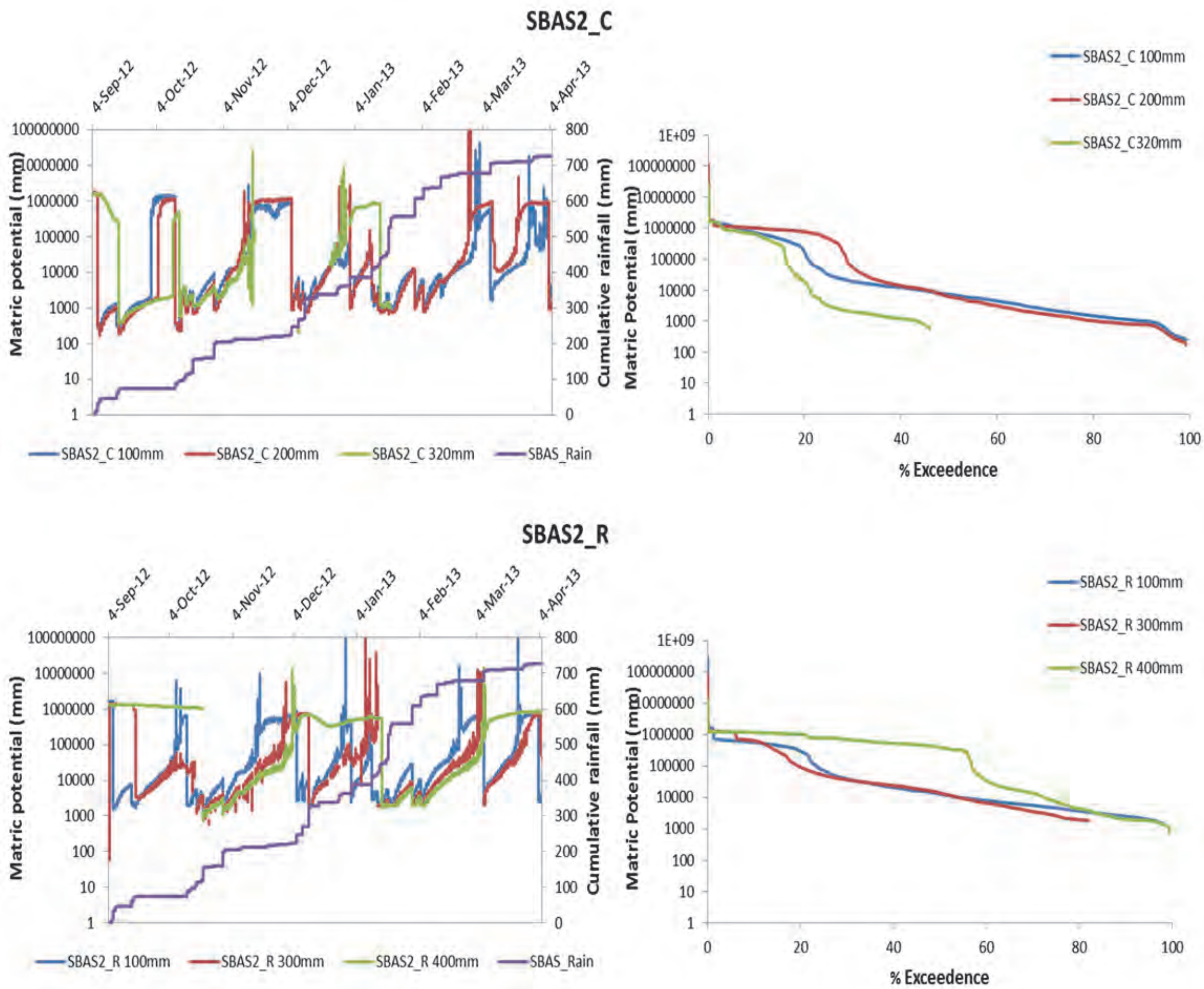

Figure 6.39: Soil moisture responses and % exceedence curves for 2nd order hillslope

6.4.3 2nd order Hydrogeology: Hydraulic Responses and Parameters

The 2nd order riparian 80 m and 8 m boreholes generally follow the same trend as each other with similar water level depths when the 8 m borehole has a water level (Figure 6.40). The 8 m borehole has a water level record as result of the high (118 mm/day) intense rainfall occurring 2013/12/29. However both boreholes do not have a major response to this event. The water level in the 80 m and 8 m boreholes had risen by 0.55 m and 0.56 m respectively as a result of the 62 mm/day rainfall event of 2014/03/05. This suggests that the high intense rainfall of 118 mm/day possibly provides more runoff than infiltration and ultimately contribution to groundwater. Whereas the 62 mm/day rainfall could be seen as a possible rainfall threshold intensity which contributes to groundwater.

The 2nd order crest position 57 m borehole drilled into the hard rock has a water level record starting from August 2013 to March 2014 (see Figure 6.41). The 12 m borehole drilled into the weathered material at this location has no record of a water level and was drilled dry. This suggests that a shallow/weathered groundwater component doesn't occur at this point. The 57 m borehole water level doesn't have a major response to the 2nd rainfall sequence yet a dH of 0.41 m from the initial to the end of the water level record. This suggests an inactive groundwater flow system at this point and probably part of a region groundwater flow system given the slow rise in water level response to the 2nd sequence of rainfall.

The 2nd order triangulation 80 m and 15 m borehole generally follow the same trend with a slight decline in depth to water level from the initial water level to before the high (118 mm/day) intensity rainfall occurring on 2013/12/29 (see Figure 6.42). The dH in the 80 m and 15 m borehole then increased by 0.23 m and 0.24 m respectively after the 118 mm/day rainfall event. The dH of the 80 m and 15 m borehole then increase by 0.55 m and 0.56 m respectively after the 62 mm/day rainfall event on 2014/03/05. This occurrence suggests that to some degree a localized response in water levels to rainfall does occur. However in the case of the 118 mm/day rainfall event less response in the water level is seen relative to the response in water levels after the 62 mm/day rainfall event. This suggests that the 118 mm/day rainfall provides more runoff than infiltration which potential contributes to the groundwater level.

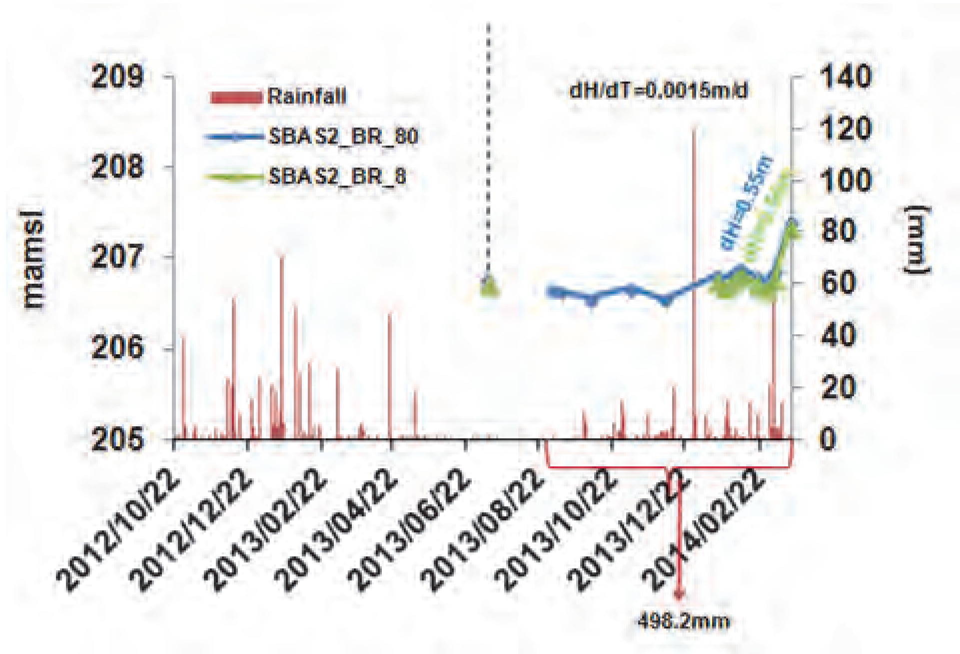

Figure 6.40: 2nd order riparian position 80 m and 8 m borehole water level response to rainfall over the hydrological season October 2012 to March 2014

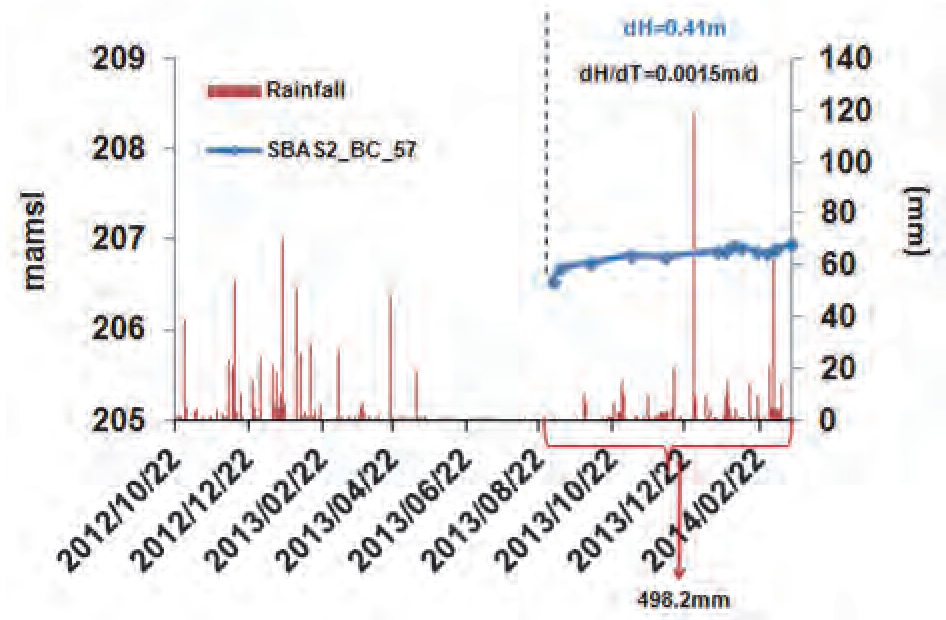

Figure 6.41: 2nd order crest position 57 m borehole water level response to rainfall over the hydrological season October 2012 to March 2014

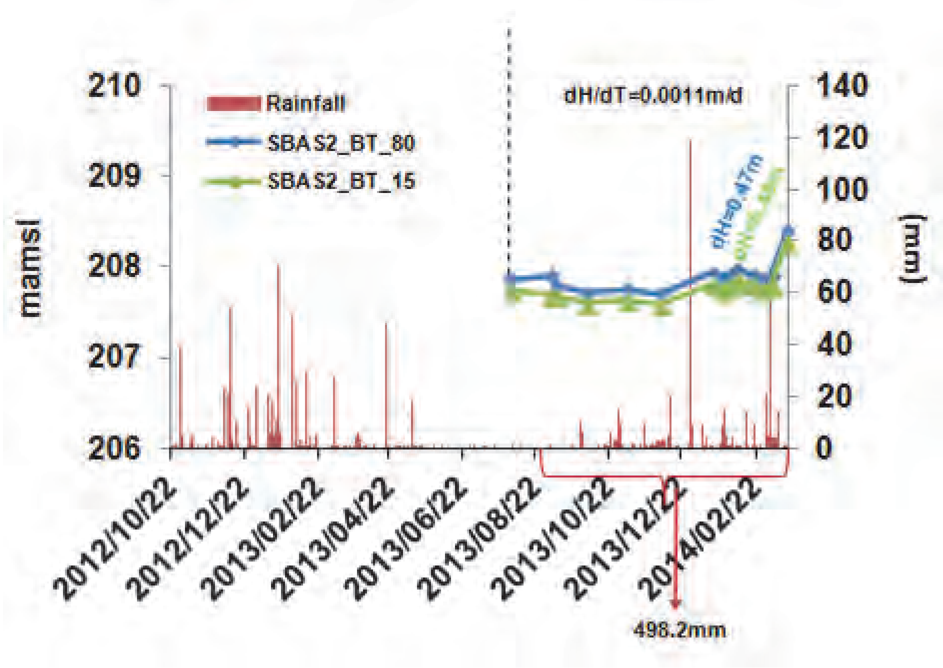

Figure 6.42: 2nd order triangulation position 80 m and 15 m borehole water level response to rainfall over the hydrological season October 2012 to March 2014

The specific conductance fluid logs for the 2nd order riparian 80 m borehole (Figure 6.43) shows an increase in value, which is possibly due to evaporated stream water contributing to the groundwater system at this point. There is also a change in gradient of the vertical distribution of SC in the Feb 14 fluid log. This is indicative of a potential fracture zone.

The variation in the vertical distribution of the SC values of the 2nd order crest 57 m borehole (Figure 6.44) does not change significantly. However at 195 mamsl there is a change in the gradient of the SC profile indicating a possible fractured zone. The SC values are high and are in the range of 3.5 mS/cm for most of the borehole profile. This indicates that no active influx of fresh water contributes to groundwater at this point.

Initially during the profile of the 2nd order triangulation 80 m borehole the vertical distribution of SC values remain low ranging from 1.5-1.8 mS and increases to 3.4 mS at a depth of 162 mamsl. This abrupt change could be indicative of a potential fracture/weathered zone feeding lower SC water through the shallow aquifer. The SC values of the 2nd order triangulation 15 m borehole do not vary significantly, however the SC values are ranging from 1.5-1.8 mS. This suggests a possible active shallow groundwater flow system which supports the higher blow out yield at this borehole of 1 l/s.

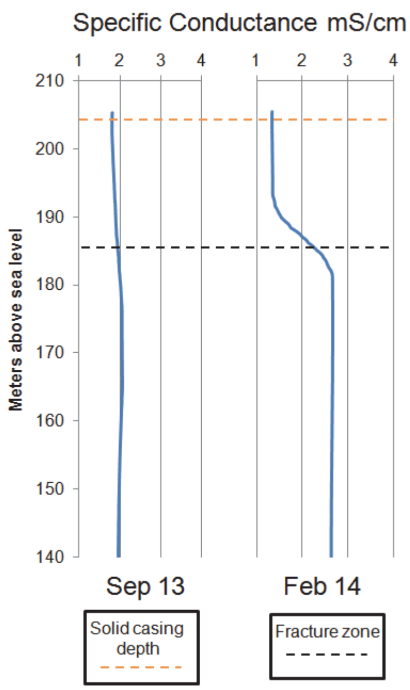

Figure 6.43: specific conductance quarterly fluid log for the 2nd order riparian position 80 m borehole

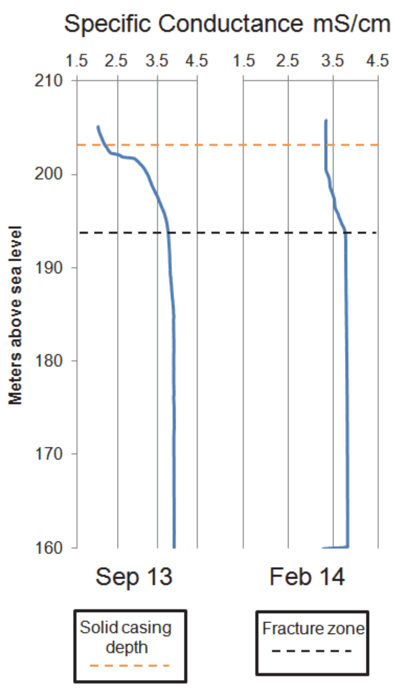

Figure 6.44: specific conductance quarterly fluid log for the 2nd order crest position 57 m borehole

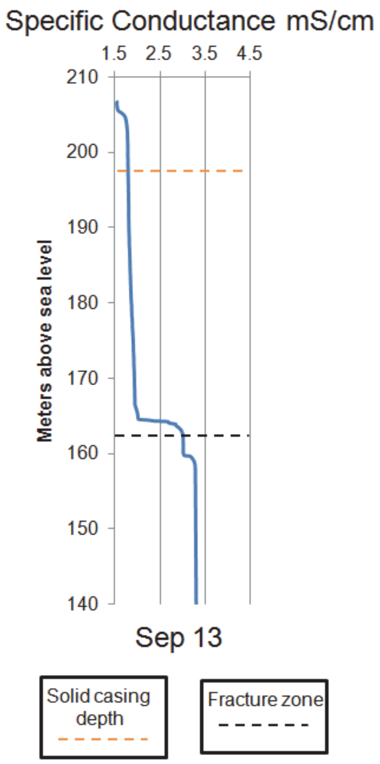

Figure 6.45: specific conductance quarterly fluid log for the 2nd order triangulation position 80 m borehole

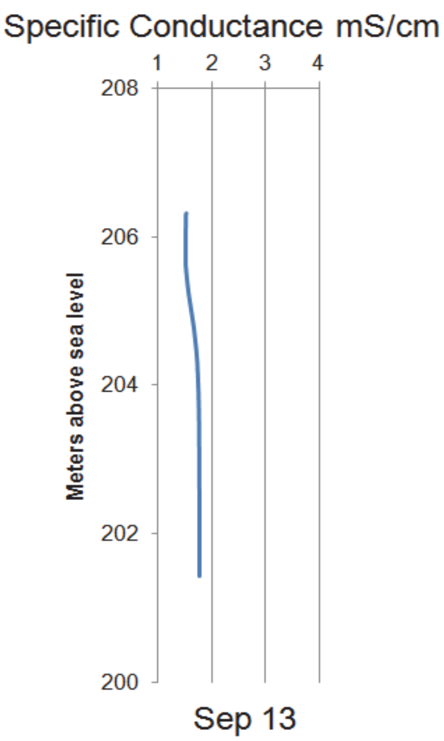

Figure 6.46: specific conductance quarterly fluid log for the 2nd order triangulation position 15 m borehole

6.5 Southern Basalt 3rd order hillslope

6.5.1 3rd order Geophysics

The initial geophysics interpretation of the 3rd order basalt hillslope (Figure 6.47) suggested that the unsaturated zone was estimated between 20-30 m deep. The water level across the profile was expected to be flat due to the consistency in low resistivity values (3-19.7 Ω.m) at shallow depths across the profile. The depth to hard rock across the profile appears to be at a similar depth due to the high (844-2162 Ω.m) resistivity values occurring at consistent depths.

Meanwhile following borehole drilling the final interpretation was as follows: The weathering depths were at 13 m for both the riparian and crest borehole positions. The blow out yield of the riparian deep borehole drilled into the hard rock was 0.39 l/s and at the crest it was 0.16 l/s. This suggests that the hard rock at the riparian borehole position is more permeable and an active groundwater flow system relative to the hard rock borehole position at the crest.

The time-series survey of the 3rd order hillslope (Figure 6.48) reveal sustained low (3-19.7 Ω.m) resistivity values at the river channel suggests a possible groundwater contribution to the steam or a stream to groundwater contribution. Between stations 400 and 720 a zone of deep weathering or a geological feature occurs. This can be seen by the extended depth of high (844-2162 Ω.m) resistivity values within this zone and the satellite imagery also provides a change in the vegetation at this zone.

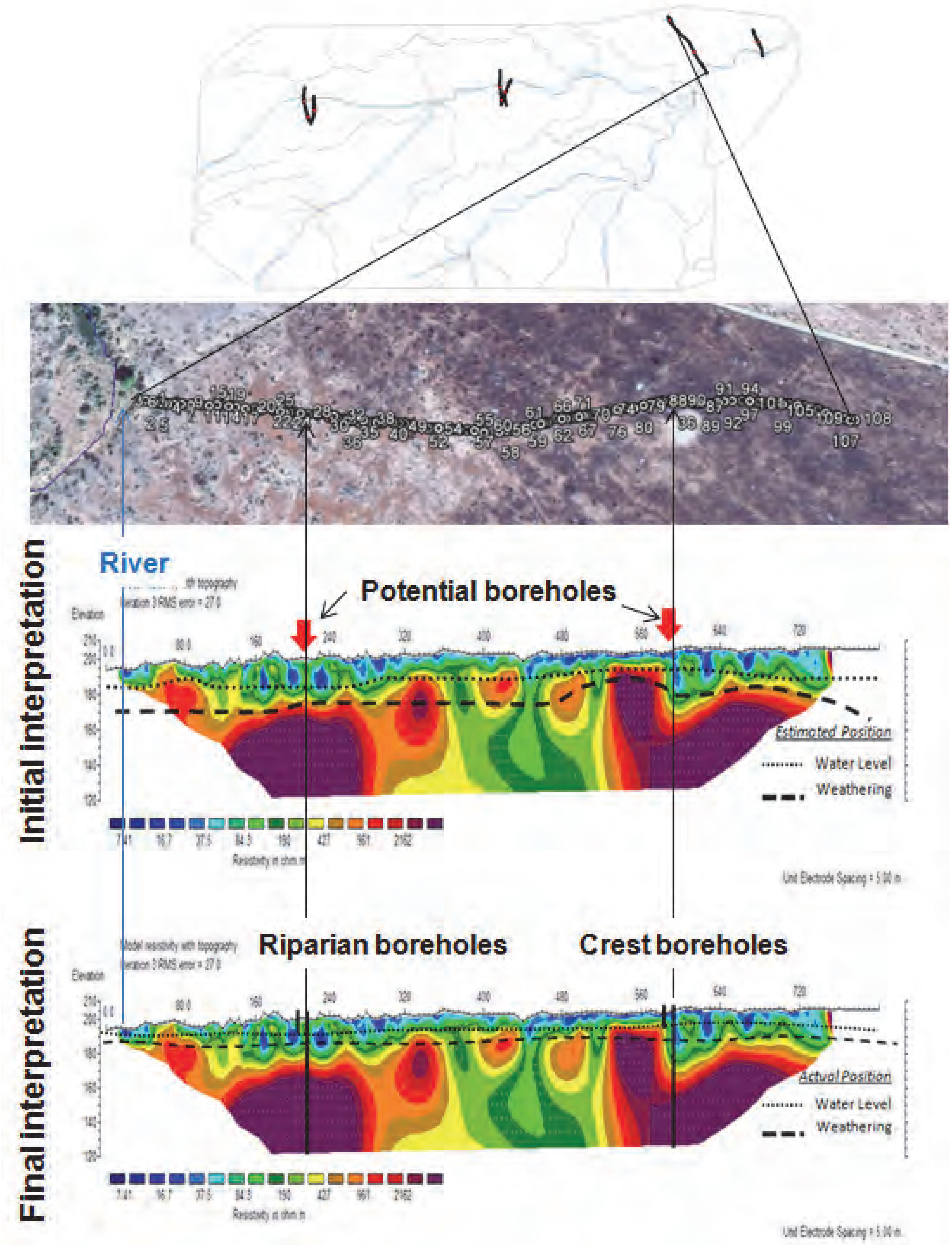

Figure 6.47: Initial and final interpretation of 2D ERT traverses coupled with topography data, satellite imagery and estimated and actual positions of groundwater level and weathering

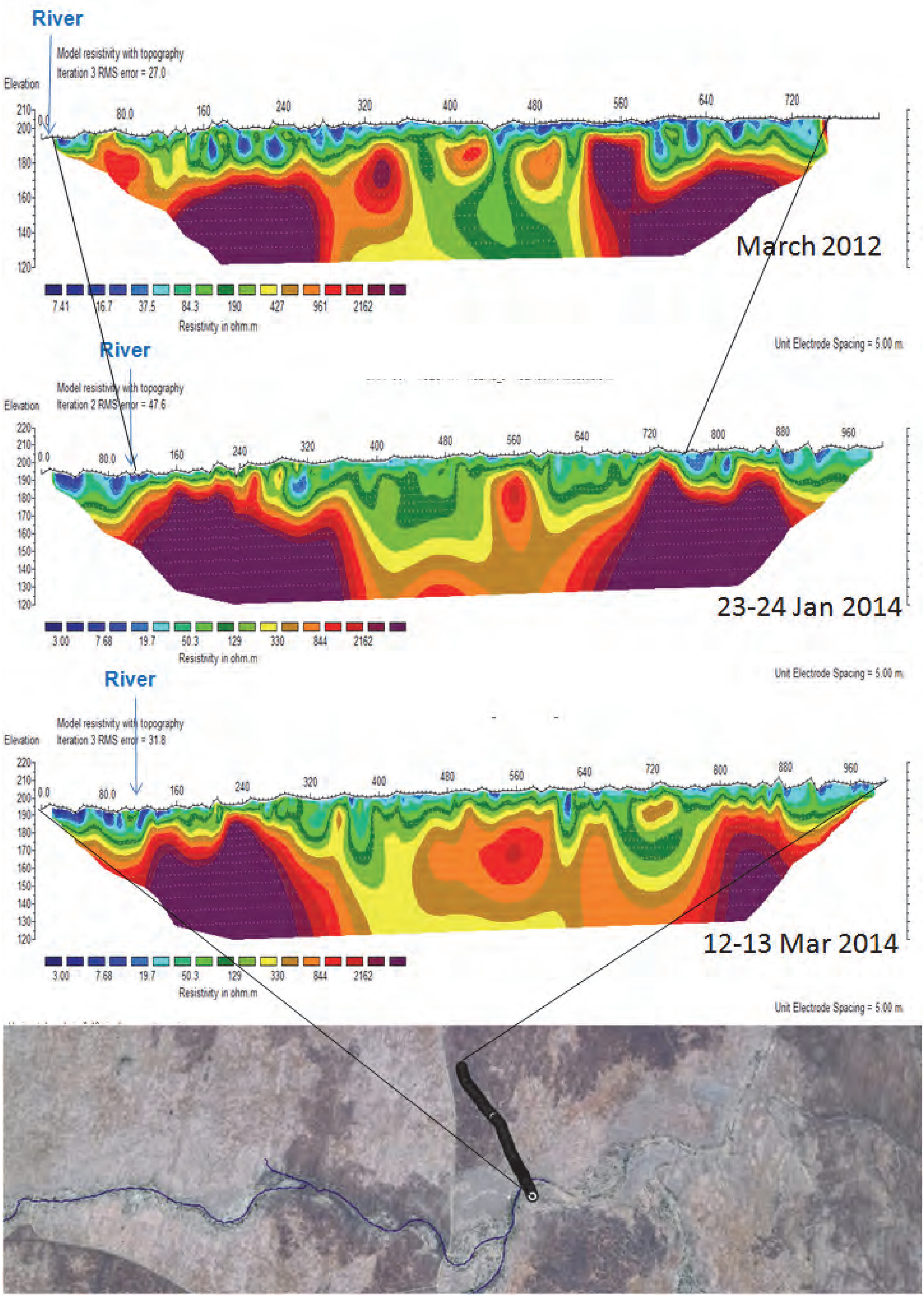

Figure 6.48: time-series geophysics transect southern basalt 3rd order hillslope

6.5.2 3rd order shallow unsaturated zone characterization and responses

Results for the 3rd order hillslope in Figure 6.49 show soils with low K_{unsat} at both low and high pressure heads on the crest (0.4-0.7 mm/hr) whilst on the contrary; the riparian zone shows high conductivity at both low and high pressure heads. K_{unsat} was expected to be low at the riparian zone due to clays being washed downslope and/or contributions through river alluvium but due to the low gradient topography on this site, it probably means there are still more clays at the crest than at the riparian zone. Hydropedological classification on this hillslope shows the Mispah soil forms (Table 6.10) which are typical responsive soils due to soil depth shallowness. This hillslope is therefore anticipated to have limited storage. Similar to the 1st and 2nd order hillslopes, this 3rd order shows no connectivity between catena elements or the adjacent stream.

Table 6.10: Soil classification per catena element on basalt 3rd order hillslope

Catena Element	Taxonomical soil class	Diagnostic Horizons	Hydropedological soil type
SBAS3_Crest	Mispah	Orthic A	Recharge
		Hard Rock	
		-	
SBAS3_Mid	Mispah	Orthic A	Recharge
		Hard Rock	
		-	
SBAS3_Rip	Mispah	Orthic A	Recharge
		Hard Rock	
		-	

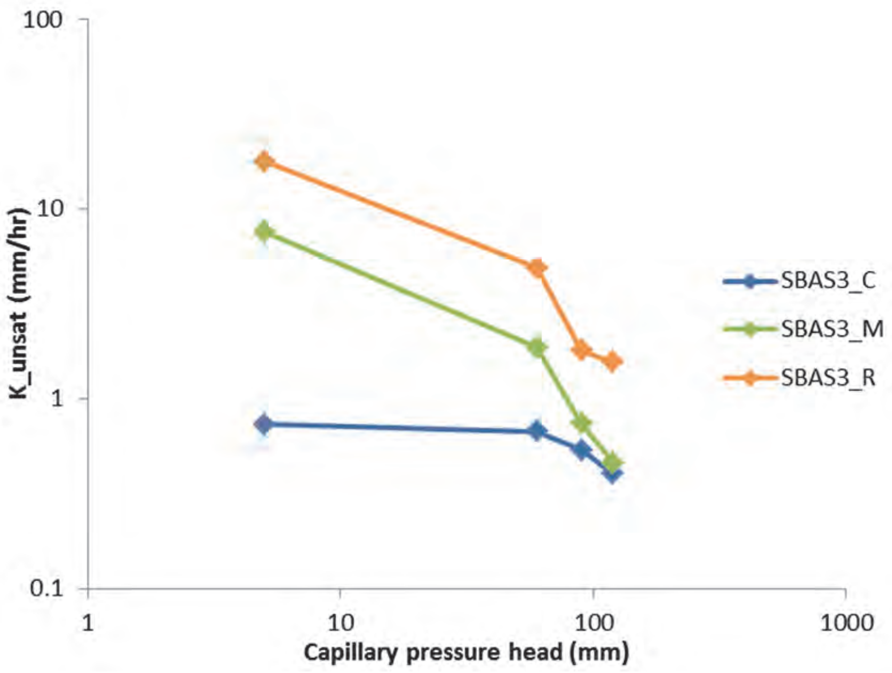

Figure 6.49: K_{unsat} on 3rd order hillslope

In conclusion, the basalt hillslopes have all shown an absence of hydrological connectivity between catena elements on each hillslope as well as between the hillslopes and their adjacent stream networks. Soil depth on these hillslopes decrease with an increase in orders therefore the 1st order hillslopes has deeper soils hence more storage is anticipated whilst the 3rd order has the least depths. There is a possibility of colluvial processes in the low order hillslopes compared to the higher orders as shown by low K_{unsat} at the riparian regions of the low order hillslopes

Sensors on this 3rd order hillslope were installed a month later after the onset of rains so data presented here is from October to April. The crest (Figure 6.50: soil moisture responses and % exceedence curves for 3rd order hillslope), shows quick responses from the shallow and intermediate soils after the first rains then the deep soil layers (depth=490 mm) respond after a week's lag. The whole profile starts drying out and the first two horizons respond to some of the events again (December) but deeper soils remained dry only to respond to the January events. This shows that the deep soil layers are only responding to high intensity events which could be attributed to a high rate of evapotranspiration whereby water is lost to the atmosphere before it gets deep into the soil. This catena element is generally a dry area as illustrated by %ED curves showing only the intermediate soils retaining moisture for about 40% of the time whilst the other layers were relatively dry (>1000 mm). These responses show free drainage in the shallow and intermediate soils but since deep soils are showing infrequent responses this means water is lost through ET thereby implying a disconnection of this element to downslope elements on this hillslope.

Low potential is shown for the midslope shallow soils in response to the early rains and intermediate soils respond a few days after then they all show a similar trend of responses until mid-November, the intermediate sensor then became faulty. Nonetheless, it shows that the soils in this region respond to some of the events but not all compared to the shallow soil responses which were also able to maintain moisture for almost 40% of the time as illustrated by %ED curves. If the shallow soils are able to retain moisture for almost 40% of the time, this means therefore that there is a possibility of high water retention from the deep and layers once they get some water from the upper horizon.

Low potentials are shown for the full profile at the riparian zone in response to the high intensity October rainfall events. The wetting and drying cycles for this catena element are similar throughout the season except for a few times in December and October where shallow soils go very close to saturation (<500 mm). This catena element is therefore able to retain moisture for longer periods (more than 50% of the time) as illustrated by the %ED curves. These responses augment the K_{unsat} data that was presented earlier (Figure 6.49: Kunsat on 3rd order hillslope) where the riparian zone is shown to have high conductivity than the other catena elements.

In conclusion, the basalt hillslopes have been shown to be characterized by recharge soils (potential) but from the majority of responses shown most of the water does not get into the deeper layers of the soil profiles. This has been attributed to water lost through ET before percolating to these deep layers. This shows that these soils require a certain threshold in the amount and intensity of rainfall received so that they can be replenished after the dry winter seasons. The absence or limited possibility of lateral subsurface flow in these soils due to low gradient topography suggests a hydrological disconnection of the catena elements from one another.

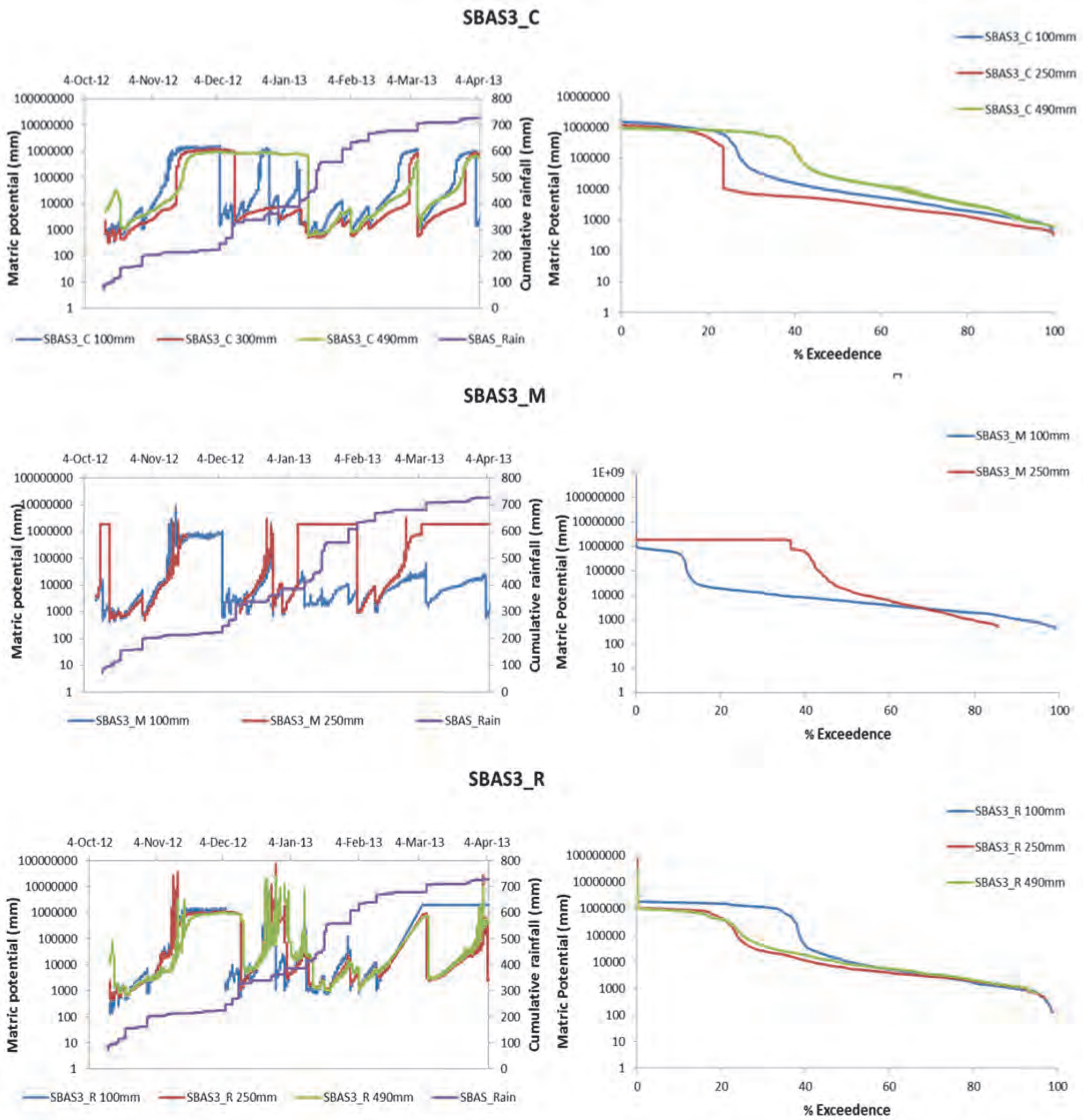

Figure 6.50: soil moisture responses and % exceedence curves for 3rd order hillslope

6.5.3 Conceptual models derived from Hydropedological interpretations on southern Basalt supersite

The basalt hillslopes comprise different soil forms including Mispah, Mayo and Shortands. From the soil surveys, the majority of the profiles have no morphological indications of saturation therefore all the soils were classified as potential recharge soils (Figure 6.51: Hydrological soil types and flow paths for basalts 1st, 2nd and 3rd order hillslopes). Due to the low gradient topography on these sites (Colgan et al., 2006), this term only refers to the vertical subsurface movement of water but not necessarily recharging to groundwater and since the water has a limited possibility of flowing laterally, it is therefore lost through evapotranspiration. Overland flow is only anticipated after exceptionally large events and this is the only time when the possibility of hydrological connectivity between catena elements on the hillslopes is anticipated.

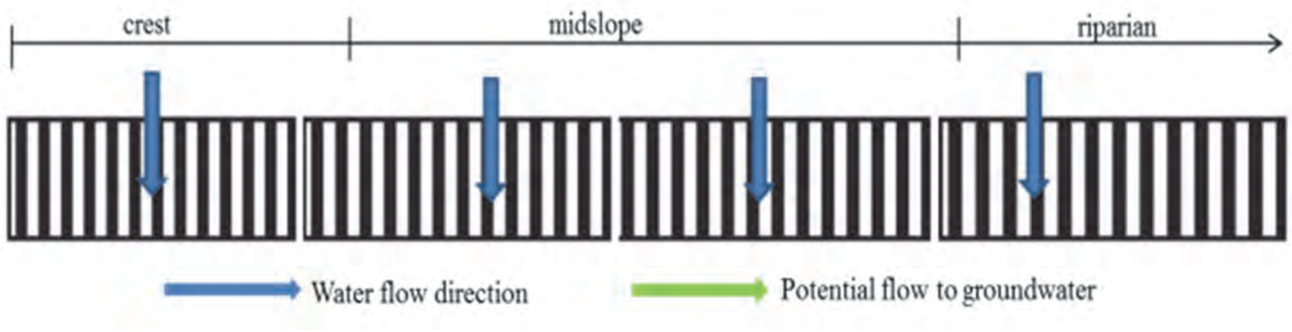

Figure 6.51: Hydrological soil types and flow paths for basalts 1st, 2nd and 3rd order hillslopes

6.5.4 3rd order Hydrogeology: Hydraulic Responses and Parameters

The 3rd order riparian 80 m and 10 m boreholes generally follow the same trend when the 10 m borehole has a water level (see Figure 6.52: 3rd order riparian position 80 m and 10 m borehole water level response to rainfall over the hydrological season October 2012 to March 2014). The 80 m borehole has an inclining trend and response to the 1st sequence of rainfall in particular to the 70 mm/day event on 2013/01/19. As a result the dH has risen by 1.49 m and the 10 m borehole had a water level. Thereafter the water levels in both boreholes declined as rainfall decreased moving into the dry season. The 10 m borehole then dried out completely after 2013/10/04. The 80 m borehole initially had a delayed response to the 2nd sequence of rainfall and increasing in dH by 0.17 m following the 118 mm/day rainfall event on 2013/12/29. The water level then follows a steady trend before increasing in dH by 0.75 m following the 62 mm/day rainfall event on 2014/03/05. As a result of this rainfall event the 10 m borehole had a water level. Given the rise in dH at this point whereby the 10 m borehole has a water level could be seen as the deep groundwater level rising. Therefore a shallow/weathered groundwater system doesn't play a role at this point. Due to the response time in water levels to the rainfall sequences a possible localized permeable groundwater flow system exists.

The 3rd order crest 80 m and 10 m boreholes generally follow the same trend as a result of the 1st sequence of rainfall in particularly following the 70 mm/day rainfall event on 2013/01/19 (see Figure 6.53: 3rd order crest position 80 m and 10 borehole water level response to rainfall over the hydrological season October 2012 to March 2014). This rainfall event caused the 80 m borehole dH to rise by 1.47 m and providing a water level in the 10 m borehole. Thereafter the water levels in both boreholes declined as rainfall decreased moving into the dry season. The dH in both boreholes continued to decline during the 2nd sequence of rainfall even after the high (118 mm/day) intense rainfall event on 2013/12/29. However following the 62 mm/day rainfall event on 2014/03/05 the 80 m and 10 m borehole dH had risen by 0.76 m and 0.81 m respectively. With the 10 m borehole dH having a greater response and responding 1st to the 62 mm/day rainfall event suggests a possible piston recharge mechanism associated at this point. Given these occurrences a possible localized response in groundwater water level to rainfall is possible at this point but confined to a particular sequence or intensity of rainfall.

The 3rd order triangulation 61 m borehole initially follows declining trend in response to the 2nd sequence of rainfall before the dH rises by 0.89 m following the 118 mm/day rainfall event on 2013/12/29 (Figure 6.54: 3rd order triangulation position 61 m and 4 m borehole water level response to rainfall over the hydrological season October 2012 to March 2014). This rainfall event also gave rise to a water level in the 4 m borehole. Both boreholes then followed a similar depth to water level declining trend before the 62 mm/day rainfall event on 2014/03/05, which after the 61 m and 4 m dH had risen by 1.04 m and 1.34 m respectively. Given these responses to rainfall a possible localized groundwater flow system exists.

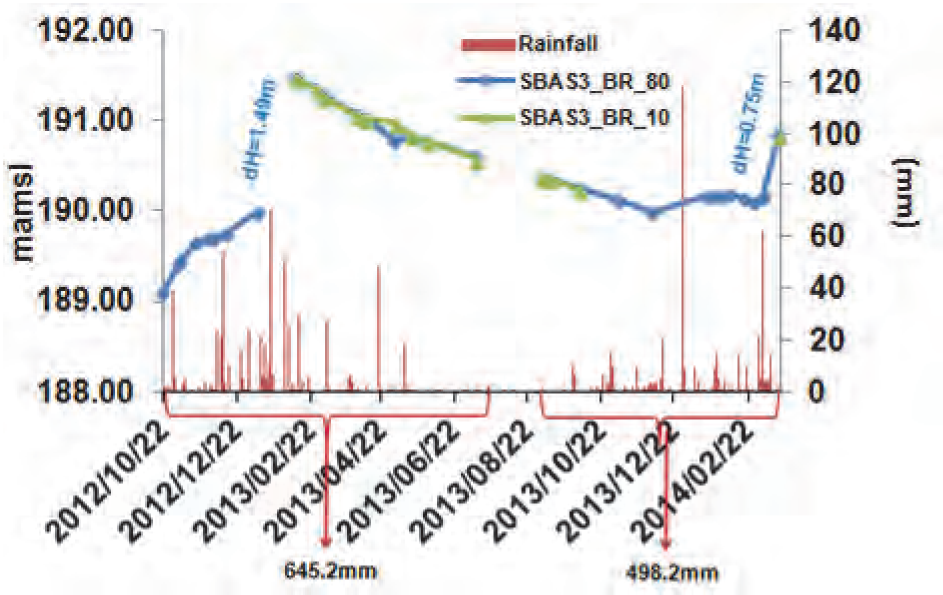

Figure 6.52: 3rd order riparian position 80 m and 10 m borehole water level response to rainfall over the hydrological season October 2012 to March 2014

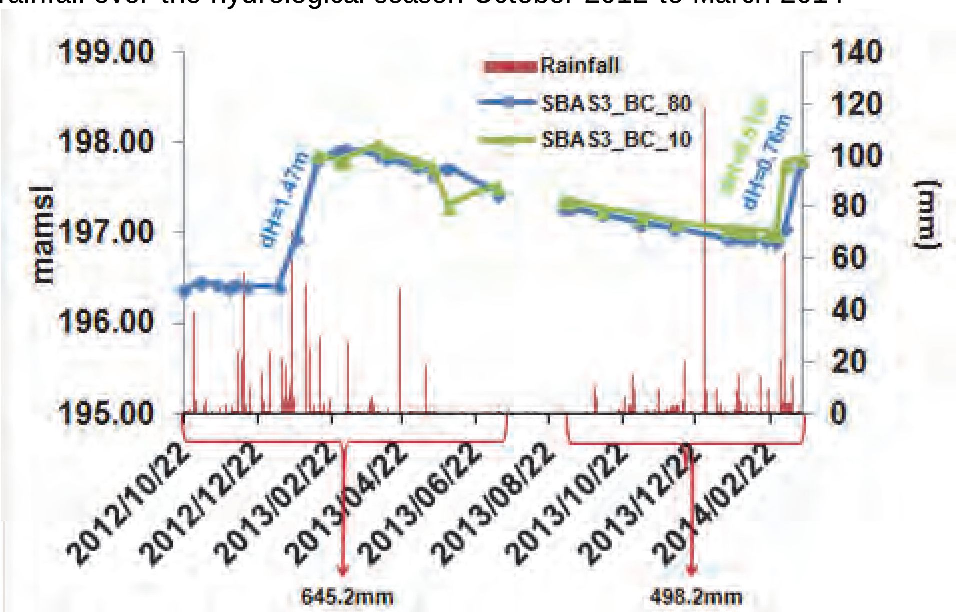

Figure 6.53: 3rd order crest position 80 m and 10 m borehole water level response to rainfall over the hydrological season October 2012 to March 2014

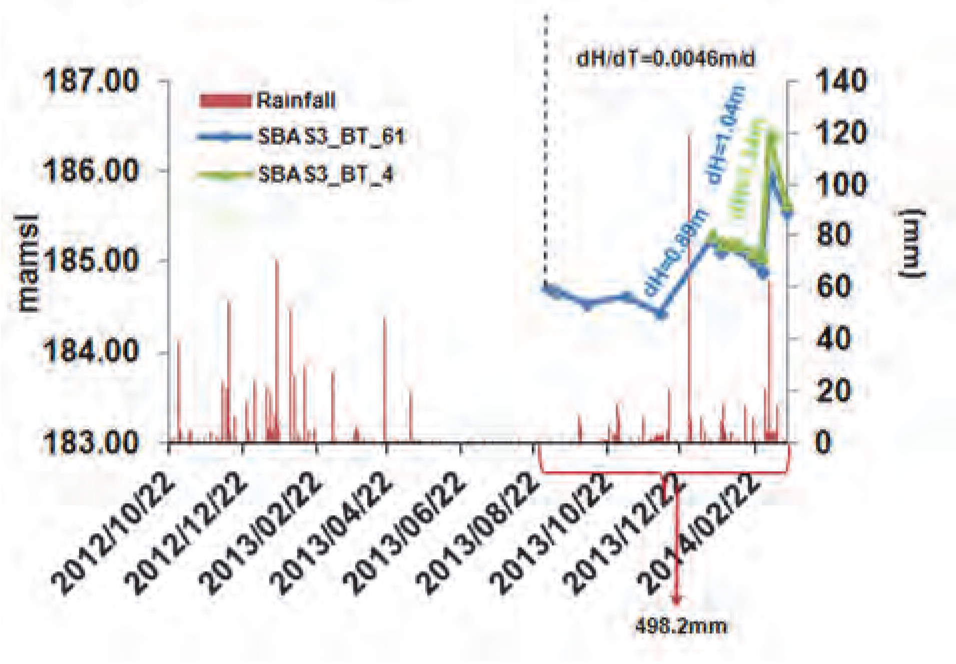

Figure 6.54: 3rd order triangulation position 61 m and 4 m borehole water level response to rainfall over the hydrological season October 2012 to March 2014

The successive fluid logs of the 3rd order riparian 80 m borehole do no change significantly over the wet and dry seasons. However the SC values are low (1.5 mS) in all fluid log profiles. This suggests that fresh water (rainfall or stream water) could be contributing to groundwater at this point. The moderate (0.39 l/s) blow out yield could suggest frequent flow through of groundwater resulting in the low SC values.

The quarterly fluid logs of the 3rd order crest 80 m borehole have increased from 1.4 mS/cm to 1.8 mS/cm from the initial log to the final log. The change in SC occurs at a depth of approximately 164 mamsl. This change in gradient could be seen as a potential fracture/weathered zone. The change in SC suggests an influx of groundwater flow and possibly at a slow to moderate rate owing to the low (0.16 l/s) blow out yield and T values.

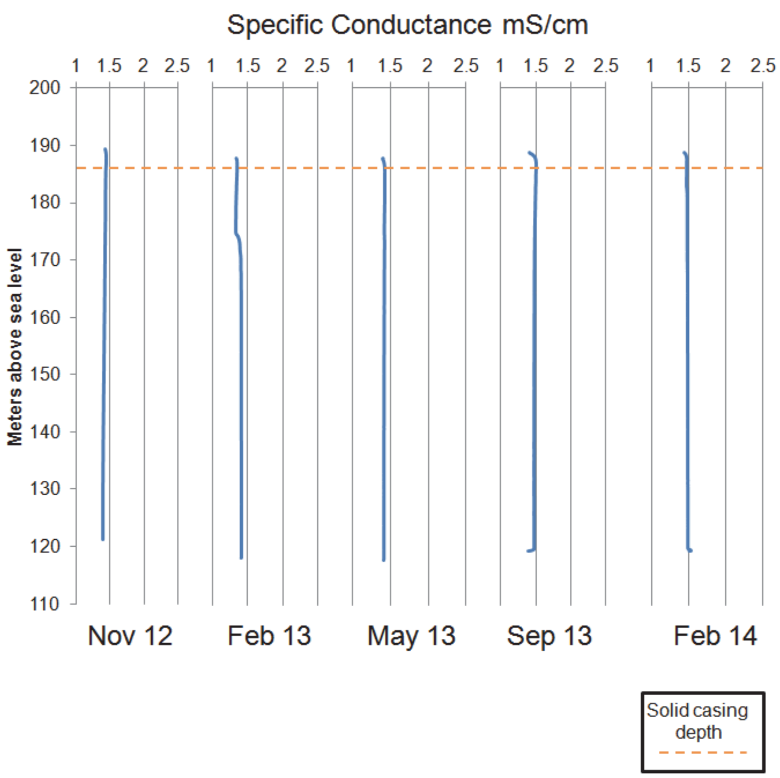

Figure 6.55: specific conductance quarterly fluid log for the 3rd order riparian position 80 m borehole

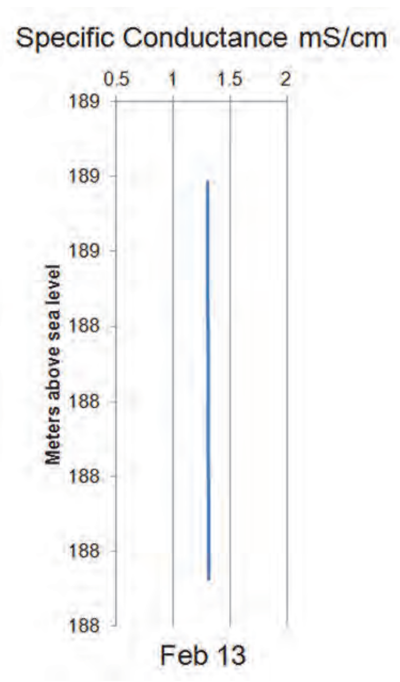

Figure 6.56: specific conductance quarterly fluid log for the 3rd order riparian position 10 m borehole

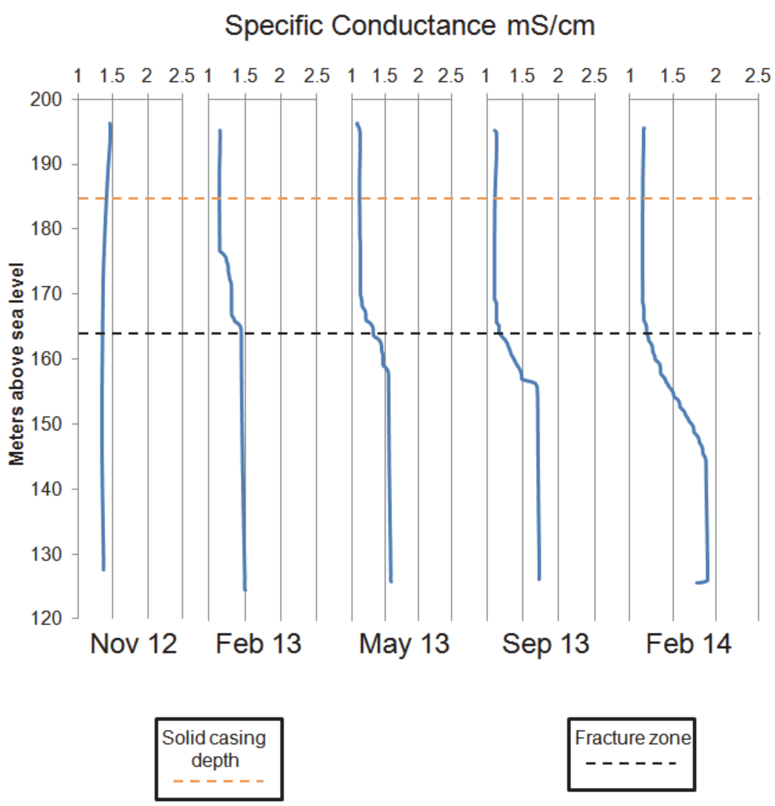

Figure 6.57: specific conductance quarterly fluid log for the 3rd order crest position 80 m borehole

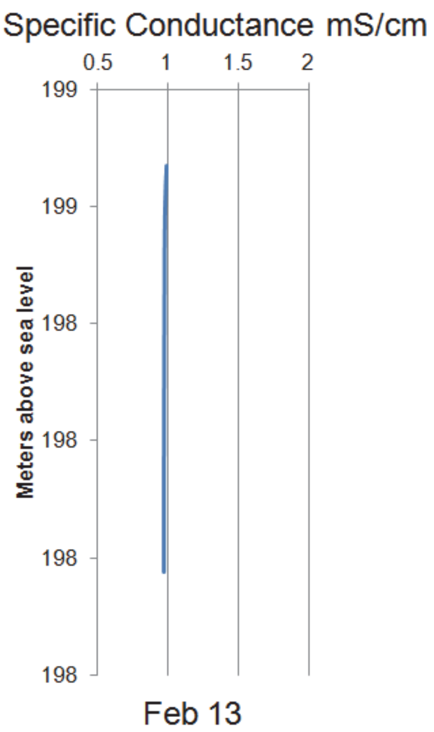

Figure 6.58: specific conductance quarterly fluid log for the 3rd order crest position 10 m borehole

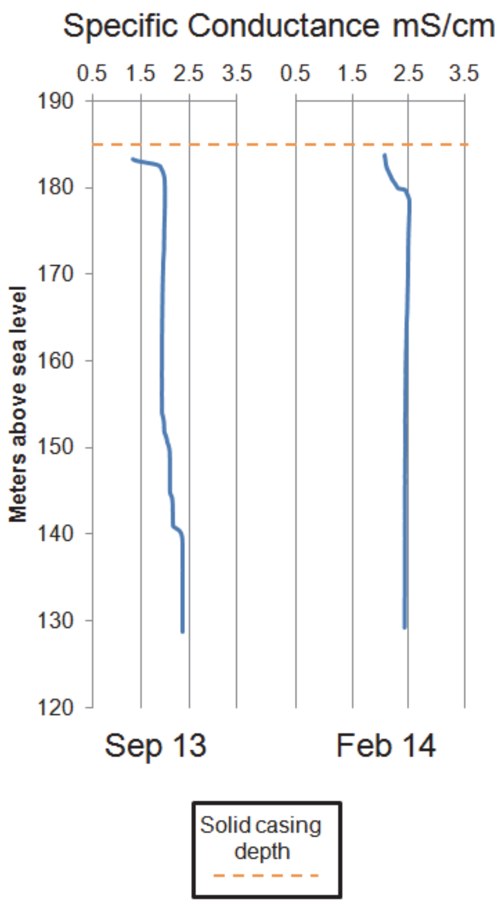

Figure 6.59: specific conductance quarterly fluid log for the 3rd order triangulation position 61 m borehole

6.6 Spatial Integration of Groundwater Data

Spatial distribution of deep groundwater head within the southern basalt supersite is shown in Figure 6.60: General groundwater contours of the deep boreholes within the southern basalt Supersite. which depicts the general flow contours of the deep boreholes. The water levels are quite shallow and the gradient is from the 1st order hillslope towards the 3rd order hillslope and roughly towards the stream. However, groundwater is only emergent at the 3rd order reach since lower order stream stage is always above the groundwater head, implying a negative hydraulic gradient. Figure 6.61: The general groundwater flow direction of the shallow boreholes within the southern basalt Supersite. No recordable water levels existed at the 1st order but sizeable water levels became more apparent at the 2nd and 3rd order hillslopes. Given that most of the shallow boreholes had no record of a water level possibly suggests that a shallow/weathered groundwater system doesn't play a role within this 3rd order catchment.

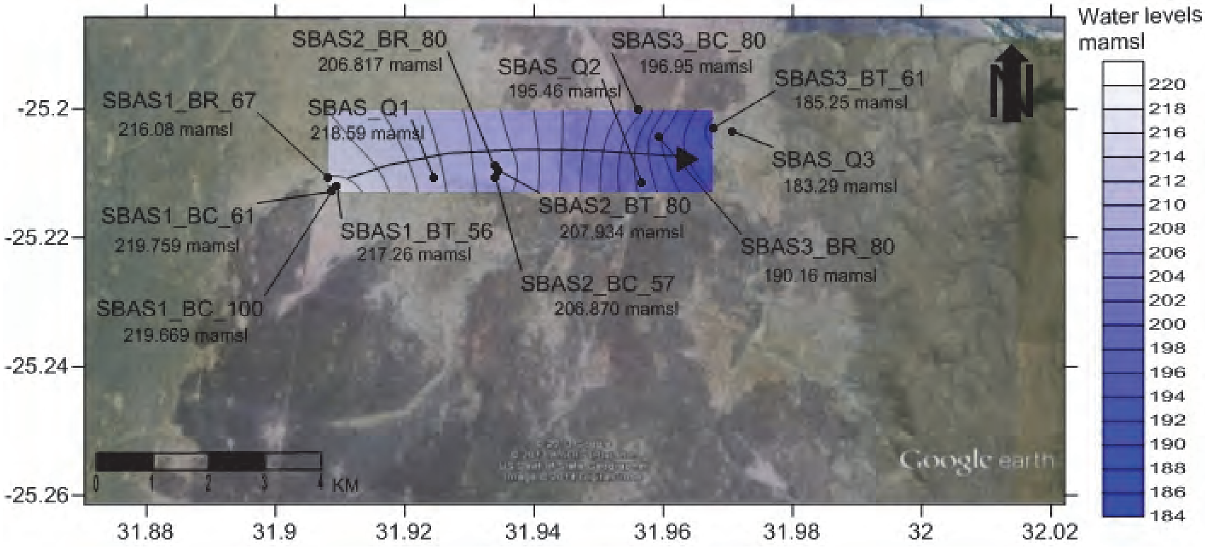

Figure 6.60: General groundwater contours of the deep boreholes within the southern basalt Supersite.

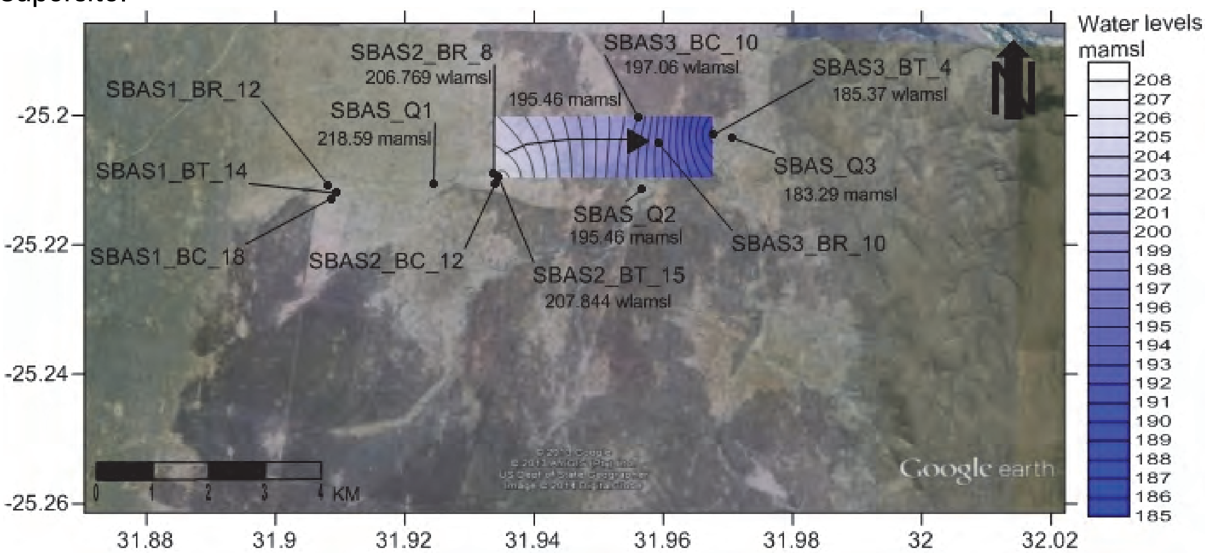

Figure 6.61: The general groundwater flow direction of the shallow boreholes within the southern basalt Supersite.

6.7 Hydrological Modelling

6.7.1 Catena Water Balances (HYDRUS)

6.7.1.1 Atmospheric Input Variables

Rainfall on the southern basalt supersite is described in section 6.1. Meanwhile in terms of aET, where on the basalts the narrow mid-slopes and crest were treated as the same, the basalt 1st order hillslope (Figure 6.62)), showed very little variation between the interfluves (mid-crest) and the riparian zone with a difference of only 4 mm in water use. The interfluvial area has 603 mm whilst the riparian has 607 mm. For the greater part of the season (October to February), the interfluve show more water use but towards the end of the season (February to April), the riparian had the greatest ET.

The 2nd order hillslope shows significant differences in water use between the interfluvial area and the riparian zone from Mid-November until April (Figure 6.63). The interfluve has 609 mm whilst the riparian zone has 573 mm. More water use is shown on the interfluves.

The 3rd order hillslope (Figure 6.64) shows some variation between the interfluves and the riparian with greatest water use shown on the interfluves. Similar to the 1st and 2nd order, the midslope and crest were combined. The very narrow riparian areas with adjacent bare regions and dry channels in the basalts may therefore explain the lower aET determined for this zone (greater resolution <30 m SEBAL data may yield different results).

A comparison of water use on the hillslopes at the basalt site shows that actual ET is greater at the low order hillslopes. This implies more storage potential since there are deeper soils compared to higher orders. (A comparison of water use between the two geologies shows that high actual ET was recorded at the southern granite supersite showing a high cumulative value of 809 mm at the 1st order riparian zone whilst the highest recorded at the basalt site is 609 mm resulting in a difference of 200 mm between the two sites).

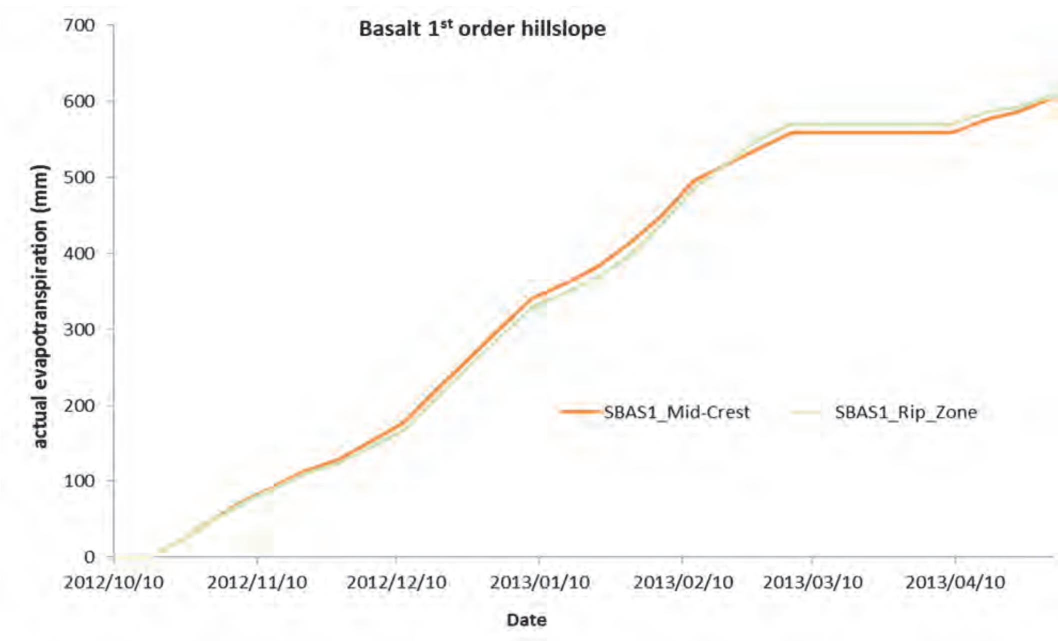

Figure 6.62: ETa per catena element for basalt 1st order hillslope

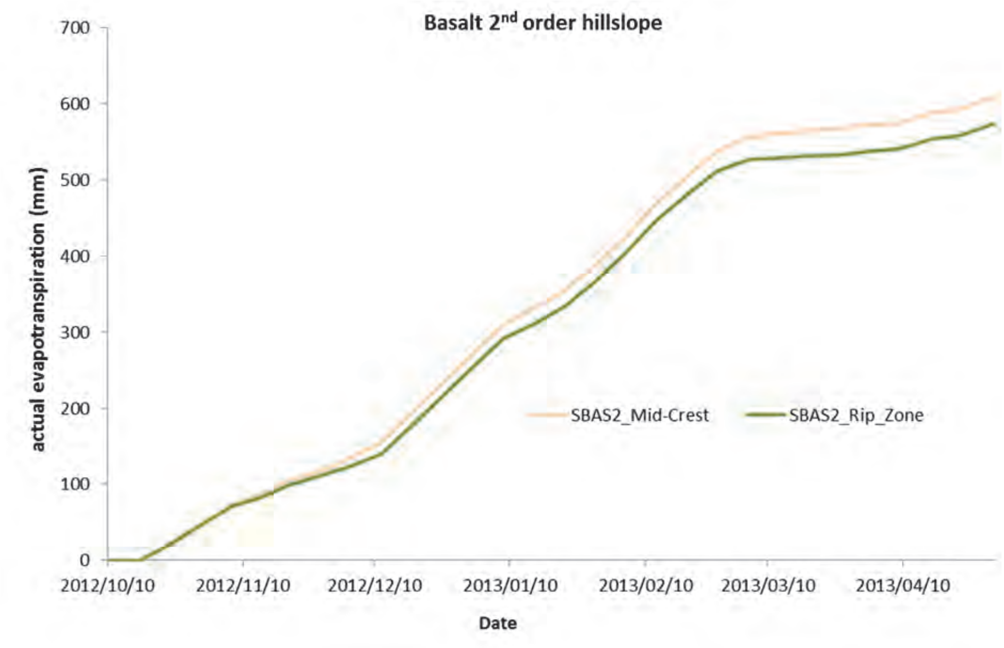

Figure 6.63: ETa per catena element for basalt 2nd order hillslope

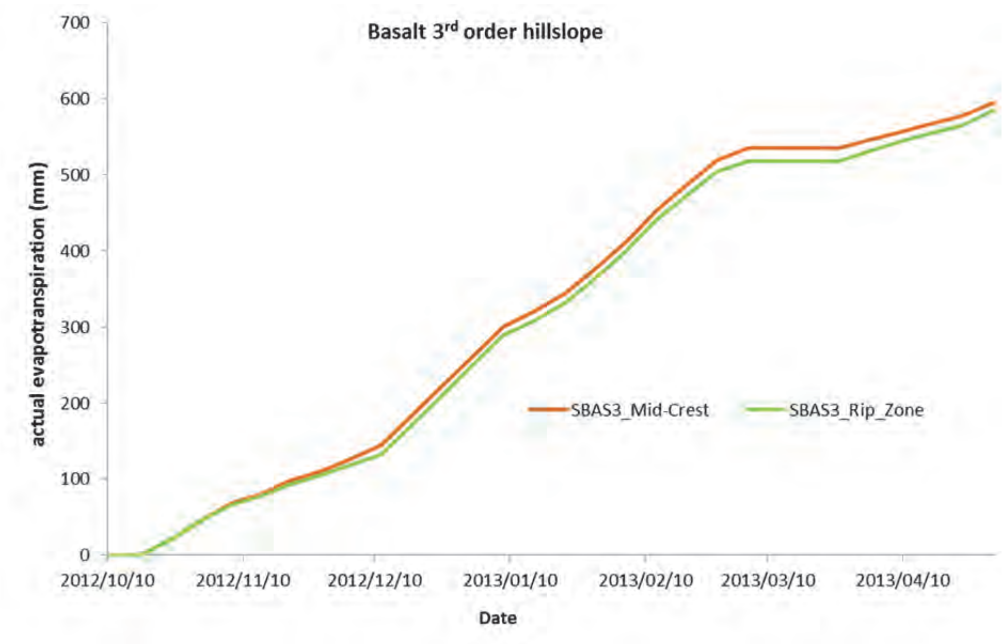

Figure 6.64: ETa per catena element for basalt 3rd order hillslope

6.7.1.2 Modelled Hydrological Fluxes

6.7.1.2.1 SBAS3 Simulated Results

The basalt 3rd order hillslope was chosen for catena element modelling as a geological contrast with the southern granite 3rd order. The basalt 3rd order riparian catena element shows the greatest ET (386 mm) and runoff (82 mm) but has the least free drainage and overall water balance compared to the other elements (Table 6.11). Meanwhile the midslope has the greatest change in water storage (102 mm). One important observation here is the runoff output by the model. Due to the low gradient topography on this site, the possibility of runoff generation is minimal. Thus were runoff resulted in the model it was considered as ponded water and therefore was not added as a downslope contribution (as was the case in the southern granite model procedure).

Table 6.11: Catena element water budgets for 3rd order basalt hillslope

	SBAS3 Crest	SBAS3 Mid	SBAS3 Rip
Unit	mm	mm	mm
P	701	701	701
ET	106.6	103.85	386.3
R	36	43.62	82
FD	532	450.6	236.83
ΔS	26	102.94	-4

Cumulative ET () showed that more water was being taken up through transpiration than evaporation at the riparian although there is not much difference from water loss through evaporation.

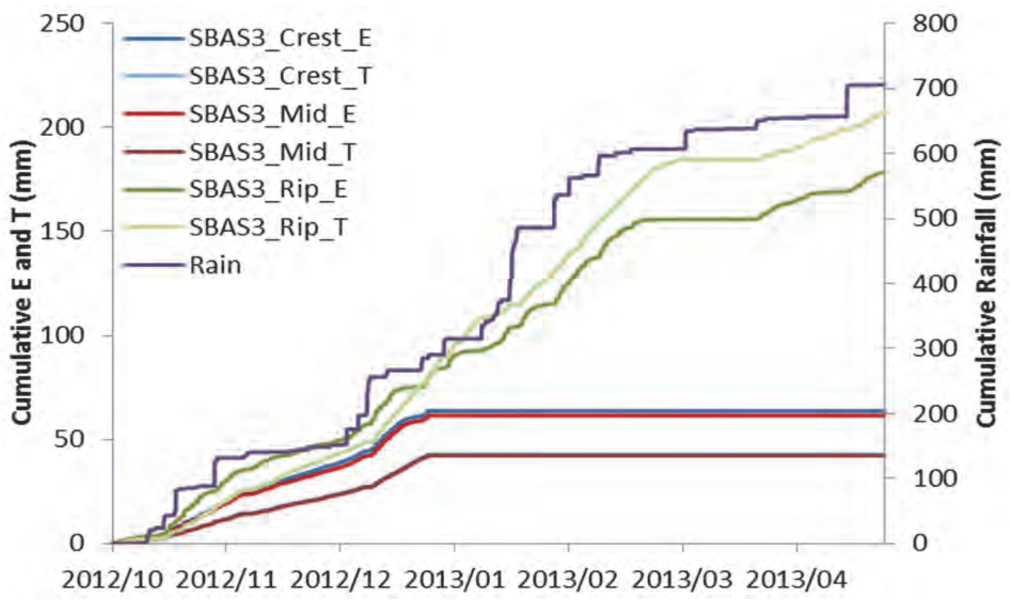

Figure 6.65: Simulated cumulative evaporation and transpiration fluxes on SBAS3 catena elements

Free drainage on this 3rd order basalt hillsope does not show much variation on the crest and midslope (Figure 6.66: Simulated cumulative free drainage fluxes on SBAS3 hillslope catena elements). The riparian zone has the least free drainage and it shows a response to only 5 rainfall events whilst the crest and midslope respond to most of the events. Due to high K_{unsat} at the riparian zone free drainage was anticipated to be high compared to the crest and midslope, although since this did not occur in the model, suggests the significant loss of water through ET.

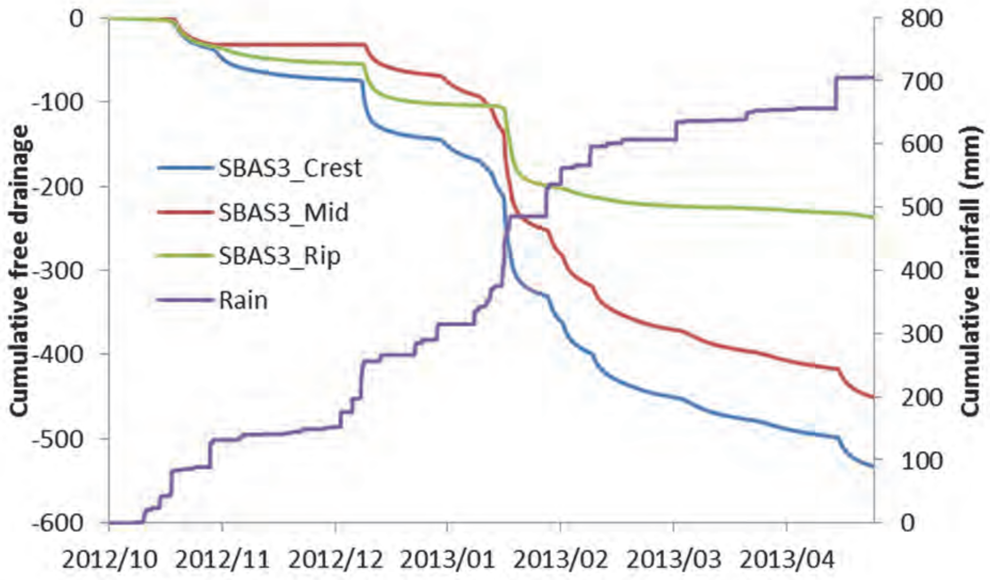

Figure 6.66: Simulated cumulative free drainage fluxes on SBAS3 hillslope catena elements

6.7.1.3 Updating the conceptual hillslope models on the Southern Basalts

Conceptual models were updated using both the observed data (K_{sat}, K_{unsat} and hydropedological surveys) and simulated data. Results presented below show the initial narrative concepts and the quantitative updated conceptual model for basalt hillslope derived following the Hydrus 1D modelling on the 3rd order hillslope.

The basalt hillslope was initially conceptualized to have potential recharge soils, through hydropedological surveys; this concept was supported numerically in this modelling with the potential for over 20% of annual rainfall to leave the soil horizon and flow to deep groundwater, primarily in the interfluvial area of the large expansive crest areas (Figure 6.67: Initial and updated conceptual model for 3rd order basalt hillslope). Meanwhile outputs from the model show that the basalt soils could be responsive as well. Overland flow was only anticipated after high intensity events but results show otherwise. Based on field observations, surface ponding was observed on the hillslopes after the January high intensity events. However the low relief of this catchments setting and the presence of vertic soils implies that this ponded water will evaporate (and this is supported through visual monitoring of these catchments).

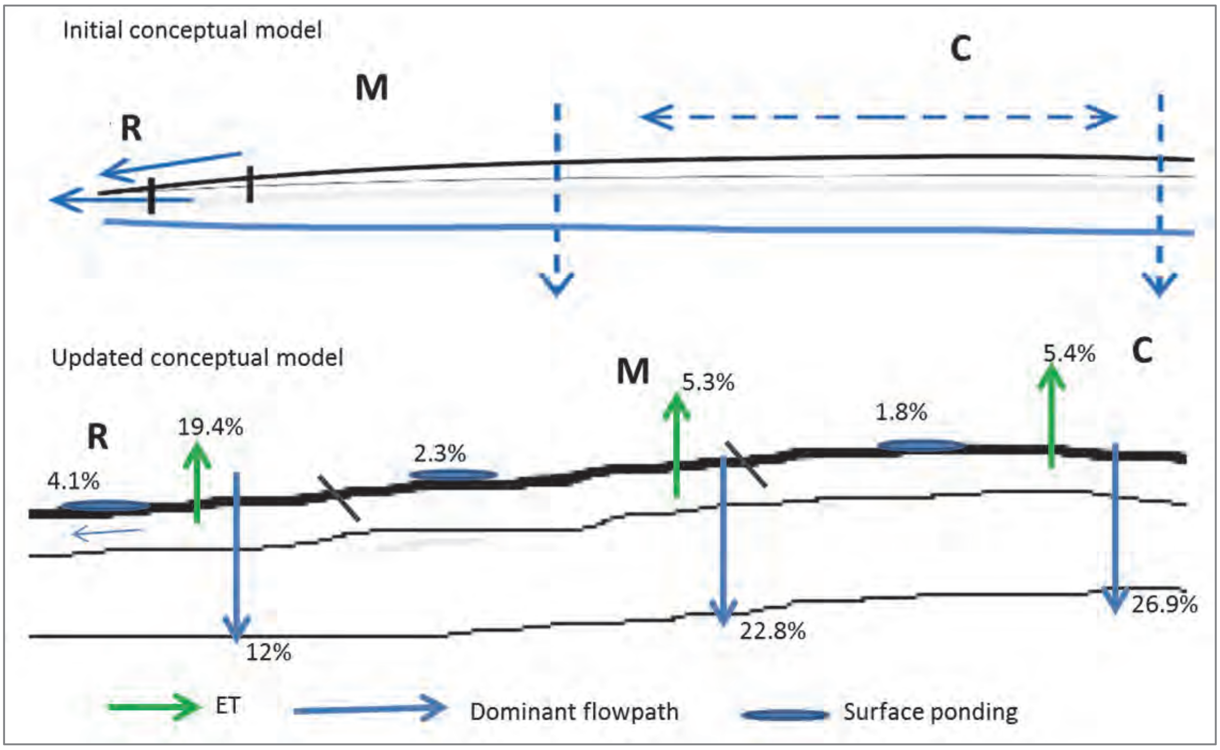

Figure 6.67: Initial and updated conceptual model for 3rd order basalt hillslope

6.7.2 Scaled Geohydrological Processes (Modflow) on the Southern Basalts

6.7.2.1 Model Domain Specifications, Mesh and Layers

At the Southern Basalts the model domain was defined by topography and surface water catchment boundaries in the area between coordinates 31.889, -25.263 and 31.979, -25.189. Compilation of the finite difference grid using the Groundwater Vistas graphic user interface facilitated the construction of a rectangular horizontal grid, as well as vertical geometry provided for each of the layers. The rectangular grid consisted of 2 layers with a total of 55632 cells (152 x 183 x 2 layers). The positions of the different geological boundaries are incorporated in the modelling grid. A grid of 100 m x 100 m refined to a 6.25 m cell size around the borehole network was allocated to the model. Smaller cell sizes were specified in the areas of the well field where a more accurate solution of the groundwater flow equation is required. Slightly larger cell sizes were specified in other areas. Cell size refinement across the model domain did not exceed 0.5 times the neighbouring cells.

A 2-layer, MODFLOW finite difference grid is applied to the model area as shown in Figure 6.68 and Table 6.12: The grid is more refined around borehole nests to achieve a more accurate numerical solution. The model layers are broadly defined by hydrogeological units, based on the site conceptual model. Geologic formations within the layers are listed below:

- Layer 1: Shallow groundwater system i.e. alluvium and weathered rock aquifer.
- Layer 2: Deep groundwater system i.e. consolidated hard rock or aquifer.
- Outflows from the model domain on the Southern Basalts were represented by drains. The MODFLOW Drain package was used instead of rivers because of the ephemeral nature of streamflows in the study site, since flows are event driven and

are of limited duration. Drain cells were assigned lengths and widths in such a way that they could totally fill the entire surface area of the cell. No flow boundaries were specified in areas outside the model domain since these are a special kind of constant flux boundary where the flow is set to zero indicating their exclusion from the flow system. The drain, no flow and general head boundary conditions specified in the current models are shown in Figure 6.69.

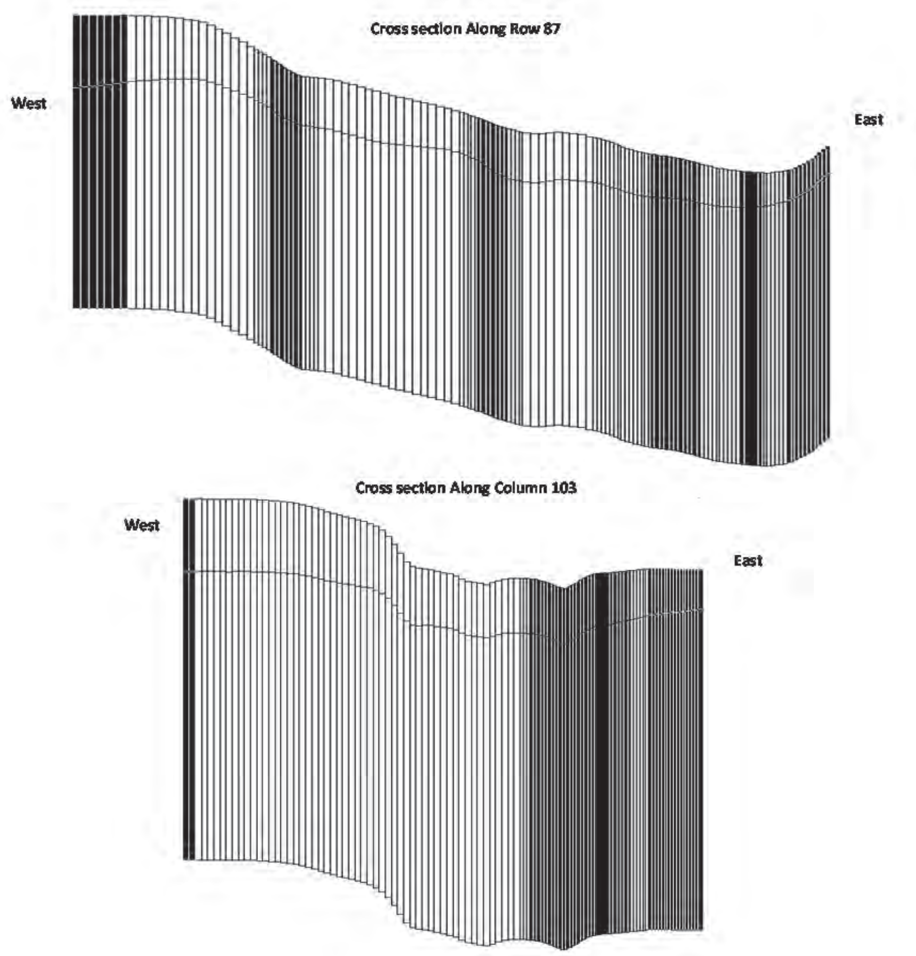

Figure 6.68: The vertical cross-sections of the Southern Basalts model.

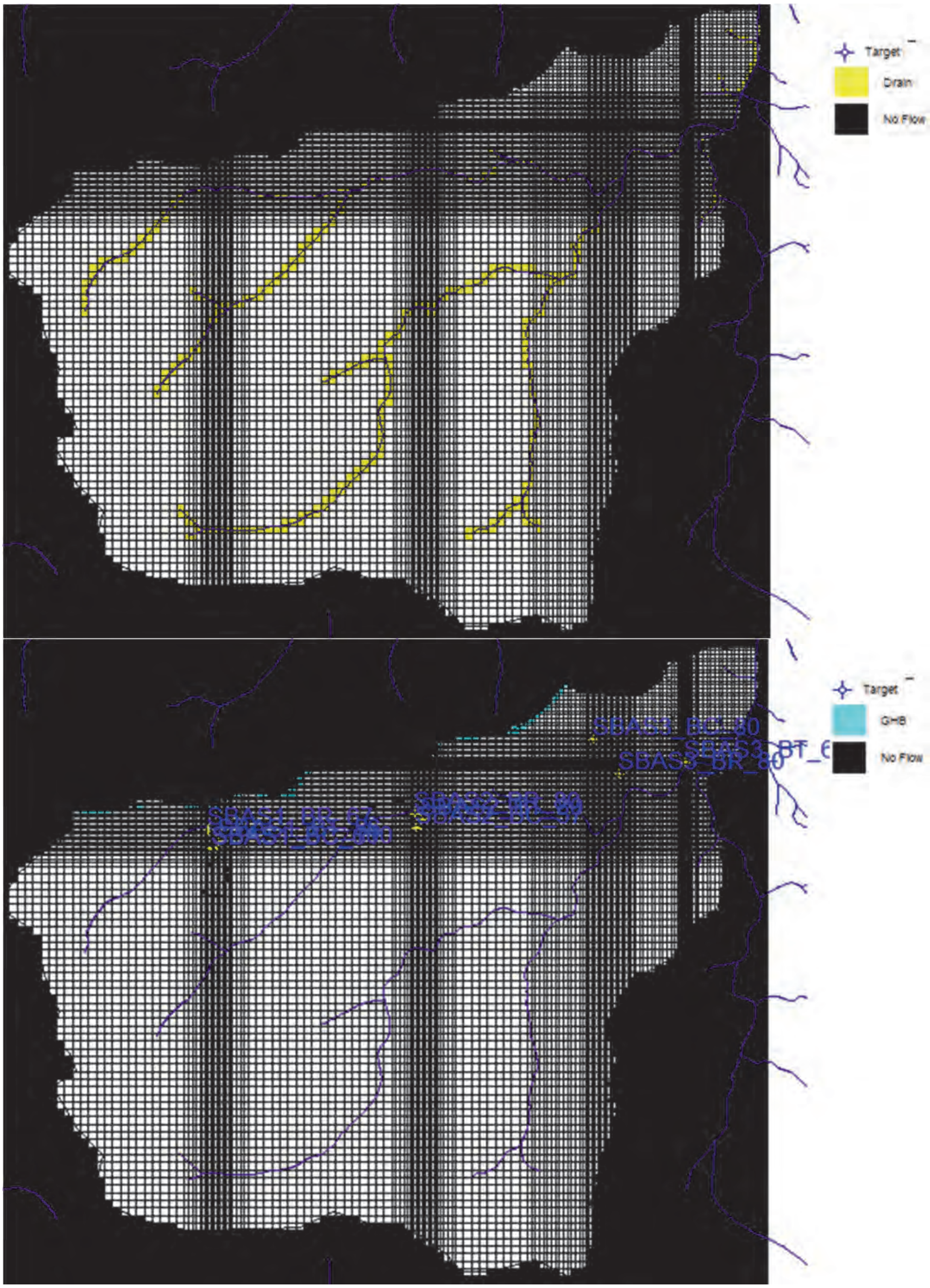

Figure 6.69: Maps showing No flow boundary, head targets, Drain boundary (Top map) in Layer 1 and General Head Boundary (GHB) (Bottom map), in Layer 2 for the Southern Basalts model.

Table 6.12: Model layer elevations and thicknesses

<table>
<tr><th>Model</th><th>Model Layer</th><th>Hydro-lithological unit</th><th>Layer top elevation</th><th>Layer bottom elevation</th><th>Thickness (m)</th></tr>
<tr><td rowspan="7">Southern Basalts</td><td rowspan="3">1</td><td>Unconsolidated alluvium
SBAS1 Reach</td><td rowspan="3">Topographic map</td><td>Base of alluvium</td><td>Topography minus base elevation</td></tr>
<tr><td>SBAS2 Reach</td><td rowspan="2">Topographic surface minus 10 m</td><td rowspan="2">1</td></tr>
<tr><td>SBAS3 Reach</td></tr>
<tr><td rowspan="4">2</td><td>Consolidated Aquifer</td><td rowspan="4">Bottom of upper layer</td><td rowspan="4">Layers 2: Base of upper layer minus 70 m</td><td rowspan="4">70</td></tr>
<tr><td>SBAS1 Wells</td></tr>
<tr><td>SBAS2 Wells</td></tr>
<tr><td>SBAS3 Wells</td></tr>
</table>

6.7.2.2 Time Discretization

Time parameters are relevant when modelling transient (time-dependent) conditions. They include time unit, the length and number of time periods and the number of time steps within each time period. All model parameters associated with boundary conditions and various stresses remain constant during one time period. Having more time periods allows these parameters to change in time more often (Kresic, 2007). The model was run for the period 01/10/2012 to 01/03/2014.

The steady state groundwater flow model was used for sensitivity analysis (See Appendix A9.3).

6.7.2.3 Recharge

Effective precipitation is represented in the model as distributed recharge into the saturated groundwater system (Figure 6.70). The percentage of precipitation reaching the alluvium and bedrock as recharge was adjusted during model calibration and percentage infiltration of 6% for alluvium and 4% for the bedrock were found to be optimum.

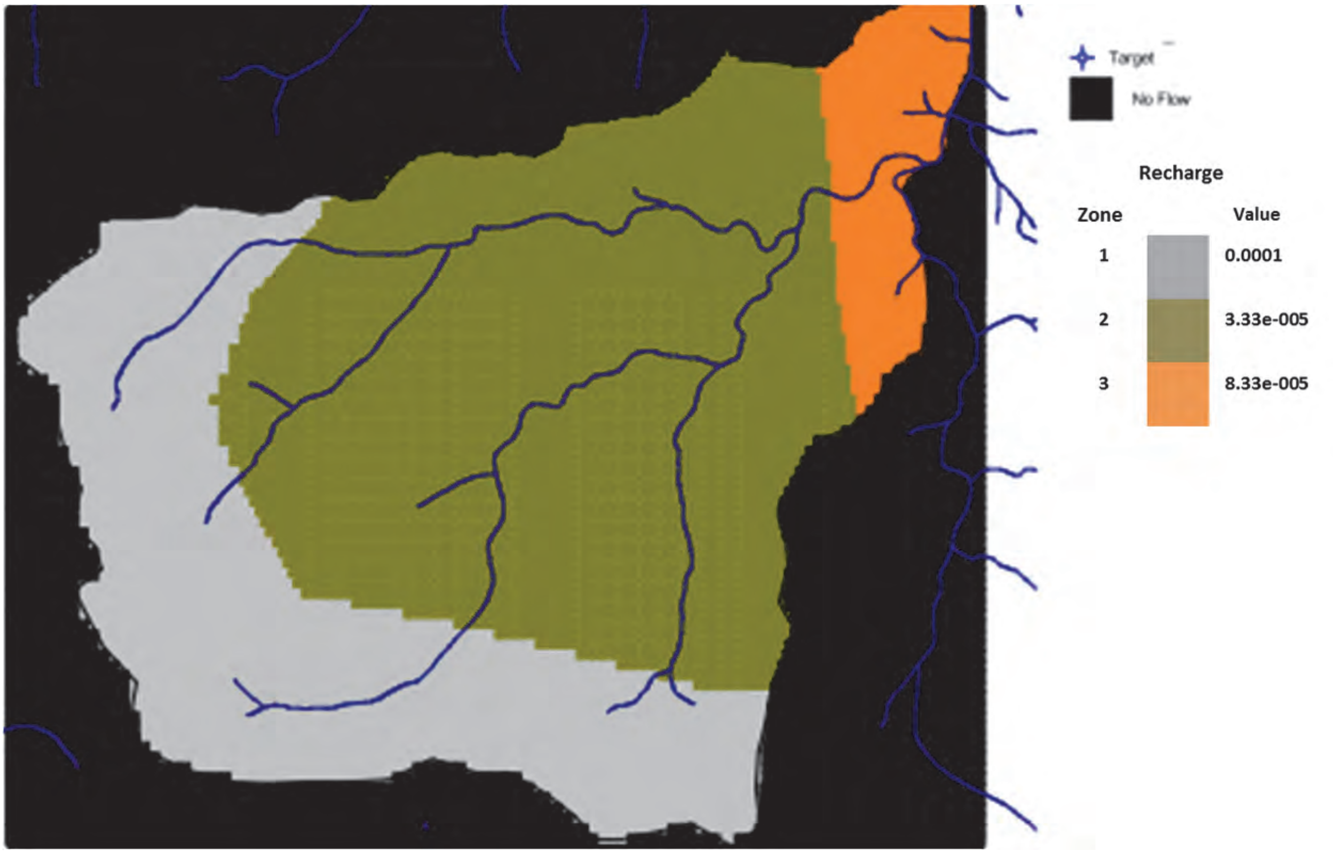

Figure 6.70: Recharge rate property in m/day for the model domain at Southern Basalts site.

6.7.2.4 *Hydraulic properties*

Average hydraulic properties were used as initial values in the model. These properties were modified during calibration within realistic ranges.

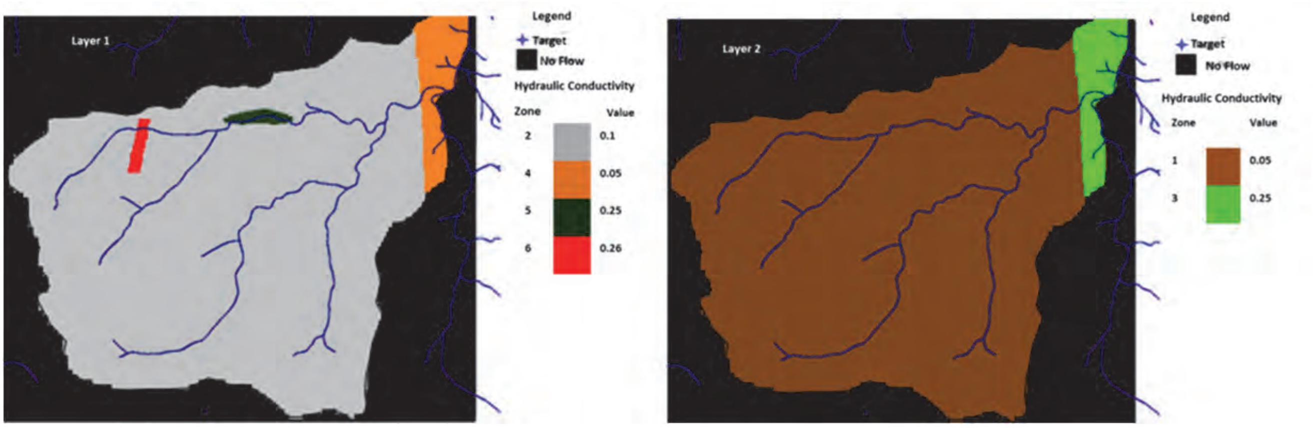

Figure 6.71: spatial distribution of 6 hydraulic property zones at Southern Basalts site (K = m/day).

Table 6.13: Calibrated hydraulic conductivity property values for the Southern Basalts model

Zone	Kx(m/day)	Ky(m/day)	Kz(m/day)
1	0.025	0.025	0.03
2	0.1	0.1	0.03
3	0.25	0.25	0.02
4	0.1	0.1	0.01
5	0.05	0.05	0.02
6	0.26	0.26	0.02

6.7.2.5 Steady State Model calibration results

Figure 6.72 shows observed versus modelled water levels for the Southern Basalts model. The straight line represents the ideal condition where field observations and model results are identical. In general, these steady state calibration results show a good match with the observed water levels.

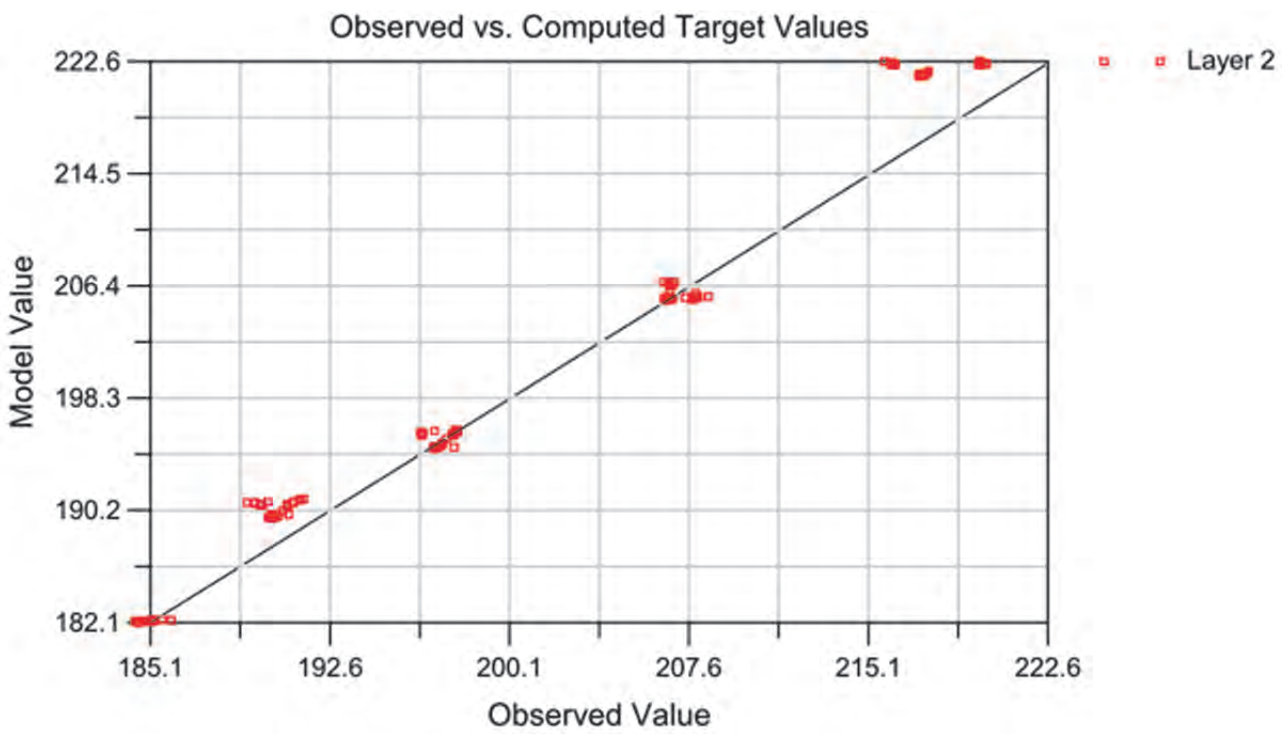

Figure 6.72: Simulated versus observed head targets in mamsl at Southern Basalts study site

The Southern Basalts steady state model calibration statistics for hydraulic head presented the mean error, absolute mean and the RMS errors as -5.8 m, 2.64 m and 3.29 m respectively. All of these error margins are acceptable statistics for a groundwater model. This Scaled Mean Absolute error represents 4.2% of the scaled total head difference measured between the boreholes used for the steady state calibration. The typical target value for calibrated models is <10%. Thus the statistics show that the model has been calibrated in steady state with relatively low errors.

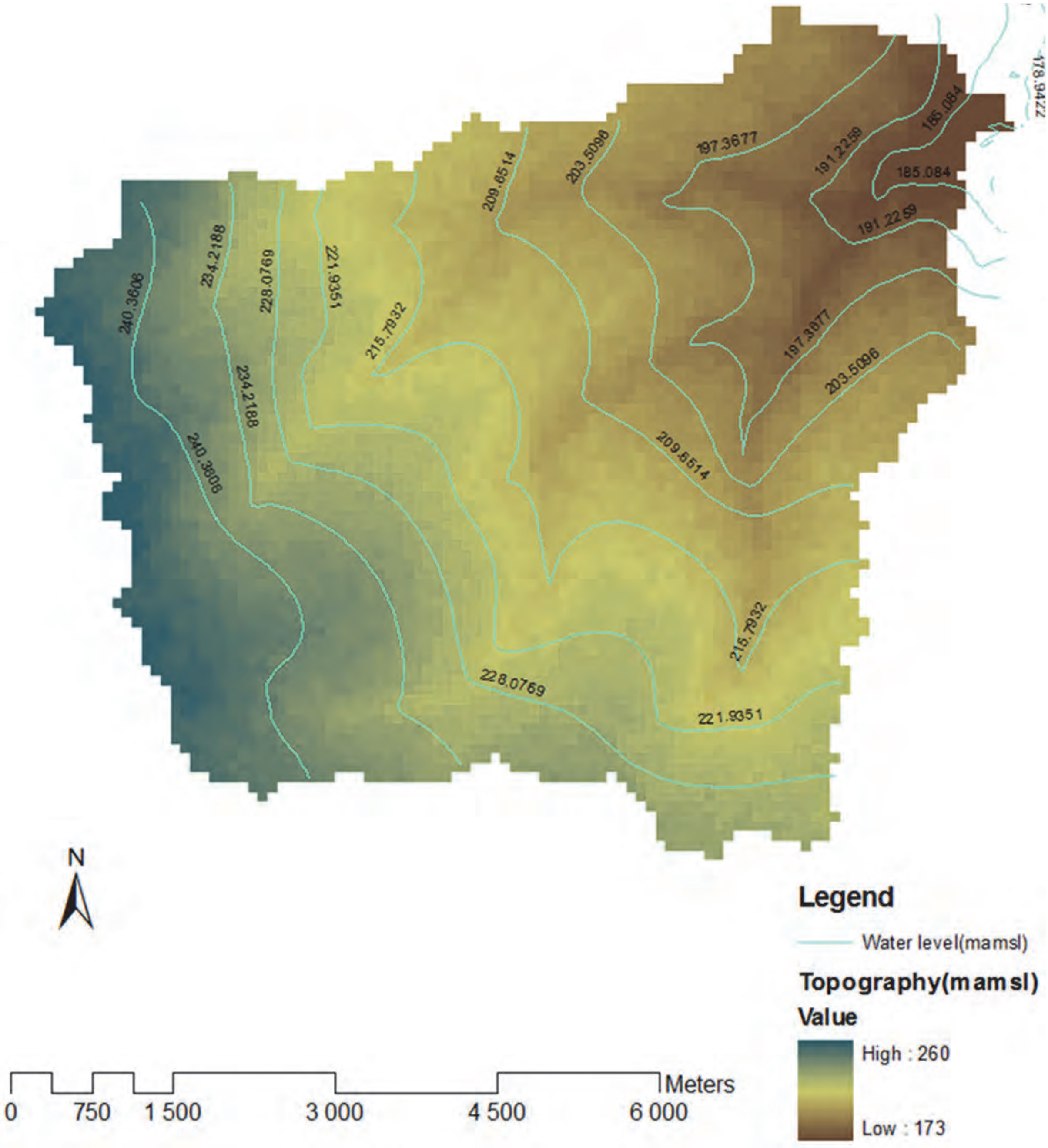

Figure 6.73: Water level contours after steady calibration of the Southern Basalts model.

6.7.2.6 Transient Model calibration results

The groundwater flow model was calibrated under transient conditions using time series water level data collected over the study period. This calibration was performed understand the interactions between the rainfall/recharge, aquifer flow processes and discharge to the surface water. The simulated and observed water level responses are shown in Figure 6.74.

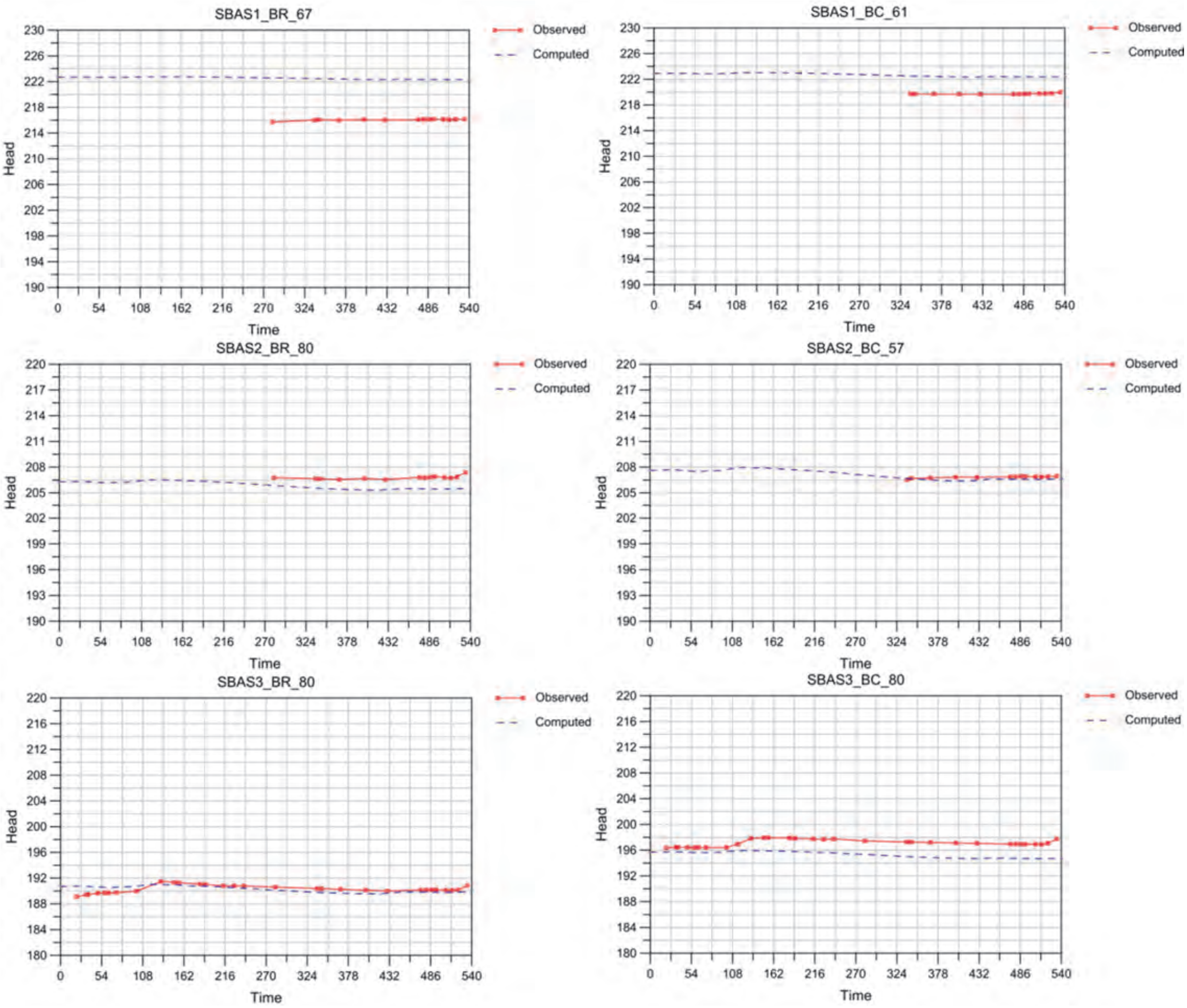

Figure 6.74: Calibrated transient groundwater flows at Southern Basalts site (Time = days).

It is clear from the simulated results obtained that the hydrogeological flow model is capable of simulating observed groundwater flow data reasonably well allowing confidence in the flow model. Simulated groundwater levels show a general decrease with time except for isolated occasions which should coincide with recharge incidences following exceptional rainfall events. Hydrometric findings documented in Petersen (2012) attest to the conceptual understanding that groundwater levels have since been decreasing with time in the Kruger National Park. The sensitivity to recharge events is much clearer towards higher stream orders as the aquifer gets shallower. A summary of calibrated recharge values used in the transient flow model are presented in Table 6.14.

Table 6.14: Calibrated values of effective recharge compared to monthly precipitation from October 2012 to March 2014.

Date	Calibrated value of effective recharge (m/day)			Monthly precipitation (mm)
	Zone 1	Zone 2	Zone 3	
2012-10-01	1.31E-04	4.36E-05	1.09E-04	130.8
2012-11-01	1.68E-05	5.60E-06	1.40E-05	16.8
2012-12-01	1.42E-04	4.73E-05	1.18E-04	141.8
2013-01-01	2.46E-04	8.21E-05	2.05E-04	246.2
2013-02-01	7.06E-05	2.35E-05	5.88E-05	70.6
2013-03-01	4.66E-05	1.55E-05	3.88E-05	46.6
2013-04-01	5.18E-05	1.73E-05	4.32E-05	51.8
2013-05-01	2.24E-05	7.47E-06	1.87E-05	22.4
2013-06-01	1.20E-06	4.00E-07	1.00E-06	1.2
2013-07-01	8.00E-07	2.67E-07	6.67E-07	0.8
2013-08-01	4.00E-07	1.33E-07	3.33E-07	0.4
2013-09-01	1.20E-05	4.00E-06	1.00E-05	12
2013-10-01	2.18E-05	7.27E-06	1.82E-05	21.8
2013-11-01	5.22E-05	1.74E-05	4.35E-05	52.2
2013-12-01	1.75E-04	5.83E-05	1.46E-04	174.8
2014-01-01	4.74E-05	1.58E-05	3.95E-05	47.4
2014-02-01	6.36E-05	2.12E-05	5.30E-05	63.6
2014-03-01	1.27E-04	4.25E-05	1.06E-04	127.4

7. REFERENCES

Aldridge, BN, and Garrett, JM. 1973. Roughness coefficients for stream channels in Arizona. United States Geological Survey Open-File Report, p87.

Ali, GA, and Roy, AG. 2009. Revisiting Hydrologic Sampling Strategies for an Accurate Assessment of Hydrologic Connectivity in Humid Temperate Systems. Geography Compass Journal Volume 3, Issue 1: 350-374.

Amoozegar, Abit, SM, A, Vepraskas, MJ and Niewoehner, CP. (2008) Solute transport in the capillary fringe and shallow groundwater: Field evaluation. Vadose Zone Journal 7(3): 890-898.

Ankeny, MD, Ahmed, M, Kaspar, TC and Horton, R. 1991. Simple field method for determining unsaturated hydraulic conductivity. *Soil Science of America Journal* 55: 467- 470.

Artiola J, Pepper IL and Brusseau ML (Eds). (2004) Environmental monitoring and characterization. Elsevier Academic Press, San Diego

Baskaran, S, Ransley, T, Brodie, RS and Baker, P. 2009. Investigating groundwater-river interactions using environmental tracers. Australian Journal of Earth Sciences 56, 1: 13-19.

Bastiaanssen, WGM, Menentia, M, Feddesb, RA, and Holtslagc, AAM. 1998a. A remote sensing surface energy balance algorithm for land (SEBAL) 1. Formulation. Journal of Hydrology 212-213:198-212.

Baxter, C, Hauer, F R, and Woessner, WW. (2003) Measuring Groundwater-Stream Water Exchange: New Techniques for Installing Minipiezometers and Estimating Hydraulic Conductivity. Transactions of the American Fisheries Society,132,(3): 493-502.

Ben-Shahar, R. (1990). Soil nutrients distribution and moisture dynamics on upper catena in a semi-arid nature reserve. Vegetatio, 89(1), 69-77. doi:10.1007/BF00134435

Beven, KJ, and Hornberger, GM. 1982. Assessing the effect of spatial pattern of precipitation in modeling stream flow hydrographs. Journal of the American Water Resources Association 18: 823-829.

Beven KJ, and Germann PF. 1982. Macropores and water flow in soils. Water Resources Research 18:1311-1325.

Bloschl, G, Sivapalan, M, Wagener, T, Viglione, A, and Savenije, H. 2013. A synthesis framework for runoff prediction in ungauged basins. In: eds. Bloschl, G, and Sivapalan, M, Runoff Prediction in Ungauged Basins. Cambridge University Press. Cambridge, UK.

Bohte, R, Mul, ML, Bogaard, TA, Savenije, HHG, Uhlenbrook, S, and Kessler TC. 2010. Hydrograph separation and scale dependency of natural tracers in a semi-arid catchment. Hydrol. Earth Syst. Sci. 7: 1343-1372

Bouwer, H. and Rice, RC. 1976. A Slug Test for Determining Hydraulic Conductivity of Unconfined Aquifers with Completely or Partially Penetrating Wells. Water Resources Research. Vol. 12, No.3

Blume, T, Zehe, E and Bronstert, A. 2010. Rainfall-runoff response, event-based runoff coefficients and hydrograph separation, Hydrological Sciences Journal, 52:5, 843 862, DOI: 10.1623/hysj.52.5.843

Birkhead, AL., James, CS and Olbrich, BW (1995) Monitoring the bank storage dynamics component of the riparian water balance in the Sabie River, Kruger National Park. Water SA, 21 (3), 211-220

Bohte, R, Mul, ML, Bogaard, TA, Savenije, HHG, Uhlenbrook, S, and Kessler TC. (2010) Hydrograph separation and scale dependency of natural tracers in a semi-arid catchment. Hydrol. Earth Syst. Sci. 7: 1343-1372

Bracken, L. and Croke, J. 2007. The concept of hydrological connectivity and its contribution to understanding runoff-dominated geomorphic systems. Hydrological Processes 21: 1749-1763.

Bredenkamp, DB., Botha, LJ., Van Tonder, GJ., and Van Rensburg, HJ (1995). Manual on quantitative estimation of groundwater recharge and aquifer storativity. Water Research Commission Report TT 73/95

Buttle, JM, PJ Dillon, GR Eerkes (2004) Hydrologic coupling of slopes, riparian zones and streams: an example from the Canadian Shield. Journal of Hydrology 287 (1-4) 161-177

Brink, A.B.A. and Bruin, R.M.H. (ed). (1990). Guidelines for soil and rock logging in South Africa. Proceedings of the Geoterminology Workshop. Association of Engineering Geologists, South African Institution of Civil Engineering, and South African Institute for Engineering and environmental Geologists. 2nd impression, 2002.

Burns, DA, McDonnell, JJ, Hooper, RP, Peters, NE, Freer, 1, Kendall, C and Beven, K. 2001. Quantifying contributions to storm runoff through end-member mixing analysis and hydrologic measurements at the Panola Mountain Research Watershed. Hydrological Processes 15: 1903-1924

Cey, EE, Rudolph, DL, Parkin, GW. and Aravena, R. 1998. Quantifying discharge to a small Perennial stream in southern Ontario, Canada. Journal of Hydrology 210, 21-37.

Cooper, H.H. and Jacob, C.E. (1946). A generalized graphical method for evaluating formation constants and summarizing well field history. American Geophysical Union Transactions 27: 526-534. Available from: (http://core.ecu.edu/geology/spruill/spruill/Groundwater%20Notes%20No.%207.pdf)

Courault, D, Seguin, B, and Olioso, A. 2005. Review on estimation of evapotranspiration from remote sensing data: From empirical to numerical modelling approaches, Irrigation and drainage systems. 19: 223-249.

Cowan, WL. 1956. Estimating hydraulic roughness coefficients: Agricultural Engineering, 377,p 473-475.

Colvin, C., Everson, C., Gush, M., Maherry, A., Clulow, A., Schaschtschneider, K., Dzikiti, S. (2011) Groundwater Dependent Ecosystems in the Northern Kruger Park – assessing complex plant water-use. Presentation to the 9th Savanna Science Network Meeting, Skukuza, Kruger National Park, March 2011.

Costa, AC, Foerster, S, De Araújo, JC, and Bronstert, A. 2012. Analysis of channel transmission losses in a dryland river reach in north-eastern Brazil using streamflow series, groundwater level series and multi-temporal satellite data. Hydrol. Processes10,1002: 9243.

Cullum, C., Rogers, KH. (2011) A FRAMEWORK FOR THE CLASSIFICATION OF DRAINAGE NETWORKS IN SAVANNA LANDSCAPES. Water Research Commission Report No K5/1790

Du Toit, W.H. (1998). Geohidrologie van die Nasionale Krugerwildtuin gebaseer op die evaluering van bestaande boorgatinligting. Volume 1 (Teks). Department of Water Affairs and Forestry. Directorate Geohydrology internal report GH 3798. Pretoria. pp284

Du Toit, WH., Verster H., Smit I (2009) unpublished SANParks Project Progress Report (Aug 09) pp37.

Dunham, KM., Robertson, EF., Grant, CC (2004) Rainfall and the decline of a rare antelope, the tsessebe (Damaliscus lunatus lunatus), in Kruger National Park, South Africa, Biological Conservation, 117(1), 83-94

Everson, CS., Burger, C., Olbrich, BW., Gush, MW (2001) VERIFICATION OF ESTIMATES OF WATER USE FROM RIVERINE VEGETATION ON THE SABIE f RIVER IN THE KRUGER NATIONAL PARK. Water Research Commission Report No 877/1/01

February, EC., Higgins, SI., Newton, R., West, AG. (2007) Tree distribution on a steep environmental gradient in an arid savanna, Journal of Biogeography, 34(2), 270-278

Fischer, S., Witthüser, KT., Birke, M., Leyland, RC., Schneider, M. (2009) Regional description of the groundwater chemistry of the Kruger National Park (KNP) using multivariate statistics. Groundwater Conference 2009, Somerset West, South Africa.

Fryirs, K. A., Brierley, G. J., Preston, N. J., and Kasai, M. (2006) Buffers, barriers and blankets: The (dis)connectivity of catchment-scale sediment cascades, Catena, 70(1), 49-67.

Grant, CC & de Buys, A. (2004) Northern Plains Programme. Internal SANParks report pp20

Grootjans, AP., Grundling, P-L., Grundling, A., Lindström, A., Engelbrecht, J., Price, JS. (2010) Spring mires fed by hot artesian water in Kruger National Park, South Africa. Mires and Peat, 6, 1-10

Harbaugh, AW, ER Banta, MC Hill, MG McDonald (2000) MODFLOW-2000, the US Geological Survey modular ground-water model: User guide to modularization concepts and the ground-water flow process

Hartshorn, A., Chadwick, O., Khomo, L., Rogers, K. Heimsath, A (2007). Landscape Chromatography along a Semiarid Catena. Presentation to ASA-CSSA-SSSA November 4-8 2007, New Orleans, Louisiana

Harvey, WJ, Wagner, BJ, and Bencala, KE. 1996. Evaluating the reliability of the stream tracer approach to characterise stream-subsurface water exchange. Water Resources Research 32, 8: 2441-2451.

Herron, N, and Wilson, C.2001. A water balance approach to assessing the hydrologic buffering potential of an alluvial fan, Water Resources Research, 37(2), 341-351, doi:10.1029/2000WR900253.

Herschy, RW. 1985. Streamflow Measurement (2nd Ed.) Elsevier Applied Science Publishers.p240

Hillerislambers, R, Rietkerk, M, van den Bosch, F, Prins, H, and de Kroon, H. 2001. Vegetation pattern formation in semi-arid grazing systems, Ecology, 82, 50-61.

Ivkovic, KM. 2008. A top-down approach to characterise aquifer-river interaction processes. Journal of Hydrology 365, 2009: 145-155

Jacobs, SM et al. (2007) Nutrient Vectors and Riparian Processing: A Review with Special Reference to African Semiarid Savanna Ecosystems, Ecosystems, 10(8), 1231-1249

Jencso, KG, and McGlynn, BL. 2011. Hierarchical controls on runoff generation: Topographically driven hydrologic connectivity, geology, and vegetation. Water Resources Research 47, W11527: 16.

Kalbus, E, Reinstorf, F, and Schirmer, M. 2006. Measuring methods for groundwater, surface water and their interactions: a review. Hydrol. Earth Syst. Sci. 3: 1809-1850.

Katz, B. JS Catches, TD Bullen, RL Michel (2000) Changes in the isotopic and chemical composition of ground water resulting from a recharge pulse from a sinking stream Journal of Hydrology 211(1-4) 178-207

Khomo, LM., Rogers, KH (2005) Proposed mechanism for the origin of sodic patches in Kruger National Park, South Africa, African Journal of Ecology, 43 (1), 29-34

Kirchner, WJ, Feng, X and Neal, C. 2001. Catchment scale advection and dispersion as a mechanism for fractal scaling in stream tracer concentrations. Journal of Hydrology 254,82-101.

Kohler, M. A. and Linsley, R. K.: Predicting the runoff from storm rainfall. Weather Bureau, US Department of Commerce, Washington, Research Paper No. 34, p. 9, 1951.

Kotschy, K., Rogers, K. (2008). Reed clonal characteristics and response to disturbance in a semi-arid river. Aquatic Botany, 88(1), 47-56. doi:10.1016/j.aquabot.2007.08.006

Kresic, N. (2007). Hydrogeology and groundwater modelling. 2nd edition. CRC press. Taylor and Francis group, LLC.

Kulmatiski, A., Beard, KH., Verweij, RTH., February, EC (2010), A depth-controlled tracer technique measures vertical, horizontal and temporal patterns of water use by trees and grasses in a subtropical savanna., The New phytologist, 188 (1), 199-209

Kutsch, WL et al. (2008) Response of carbon fluxes to water relations in a savanna ecosystem in South Africa, Biogeosciences, 5(6), 1797-1808

Kruseman, G.P. and De Ridder, N.A. (1994). Analysis and Evaluation of Pumping Test Data. 2nd ed. Available from: http://content.alterra.wur.nl/Internet/webdocs/ilripublicaties/publicaties/Pub47/Pub47.pdf (Accessed: 21 March 2012).

Larned, S.T. Datry, T. Arscott, D.B., Tockner, K (2010) Emerging concepts in temporary-river ecology. Freshwater Biology 55, 717-738

Le Roux, PAL., van Tol, JJ., Kuenene, BT., Hensley, M., Lorentz, SA., Everson, CS., van Huyssteen, CW., Kapangaziwiri, E., Riddell, E. (2011) Hydropedological interpretations of the soils of selected catchments with the aim of improving the efficiency of hydrological models. Water Research Commission Report No. 1748/1/10

Le Roux, PAL, du Plessis, MJ, Turner, DP, van der Waals, J and Booyens, HB (2013) South African Soil Surveyors Organisation Field Book for classification of South African soils. Reach Publishers, Wandsbeck, South Africa. ISBN 978-0-620-55039-0.

Leibundgut, C, Maloszewski, P and Kulls, C. (2009) Environmental Tracers, in Tracers in Hydrology, John Wiley & Sons, Ltd, Chichester, UK. doi:10.1002/9780470747148.ch3

Levick, SR et al. (2010) Regional insight into savanna hydrogeomorphology from termite mounds., Nature communications, 1(6), 1-7.

Leyland, RC., Witthuser, KT (2008) Regional Description of the Groundwater Chemistry of the Kruger National Park. WRC Project No. K8/758 October 2007. pp18

Lin, H, Bouma, J, Pachepsky, Y, Western, A, Thompson, J, Van Genuchten, R, Vogel, HJ, and Lilly, A. 2006. Hydropedology: Synergistic Integration of Pedology and Hydrology. Water Resources Research 42, W05301:4085

Loke, MH. (1999) Electrical imaging survey environment and engineering studies: A practical guide to 2-D and 3D surveys: Geometrics, San Jose.

Loke, M. H. (2004) Tutorial: 2-D and 3-D electrical imaging surveys, available at: www.geoelectrical.com

Loke, M. H. (2008) Res2dinv 2-D Resisitivity and IP inversion, Geotomo Software, Malaysia, available at: www.geoelectrical.com

Lorentz, S., Riddell, E., Koning, B., Grant, R.(2006) The Influence of Catena Soil Water Dynamics on the Vegetation Patch Structure in the Northern Plains, KNP. HydroEco 2006, Karlovy Vary, Czech Republic, 11-14 September

Lorentz, SA., Riddell, ES., Koning, B. (2007) Hydrological Lessons Learned from the Sabie and Letaba Exclosure Transects. 5th KNP Annual Science Networking Meeting, Skukuza, April 2007 – Theme: Water in the landscape pattern and processes

Lorentz, S, Bursey K, Idowu, O, Pretorius, C, and Ngeleka, K. 2008. Definition and Upscaling of Key hydrological Processes for Application in Models. Report to the Water Research Commission No 1320/1/08. School of Bioresources Engineering and Environmental Hydrology, University of Kwa-Zulu Natal.

MacKenzie, JA, Jacoby, DL, and Rogers, KH. 2003. Modelling of Terrestrialisation and Technology Transfer to Enable Management of Kruger National Park Rivers. Report to the Water Research Commission Number 1063/1/03. Centre for Water in the Environment, University of Witwatersrand, South Africa.

MacKinnon, D, and Tetzlaff, D. 2009. Conceptualising Scale in Regional Studies and Catchment Science – Towards an Integrated Characterisation of Spatial Units. Geography Compass 3, 2009: 1749-8198.

McDonnell, JJ, Sivapalan, M, Vache, K, Dunn, S, Grant, G, Haggerty, R, Hinz, C, Hooper, R, Kirchner, J, Roderick, ML, Selker, J, and Weiler, M. (2007) Moving beyond heterogeneity and process complexity: A new vision for watershed hydrology. Water Resources Research, 43, W07301: 1029.

McGlynn, BL, McDonnell, JJ and Brammer, DD. (2002) A review of the evolving perceptual model of hillslope flow paths at the Maimai catchments, New Zealand, J. Hydrology 257:1-26.

McGuire, KJ and McDonnell, JJ. (2010) Hydrological connectivity of hillslopes and streams: Characteristic time scales and nonlinearities. Water Resources Research, Vol. 46, W10543, doi: 10.1029/2010WR009341.

Malcolm, IA, Soulsby, C, Youngson, AF, Hannah, DM. 2005. Catchment-scale controls on groundwater-surface water interactions in the hyporheic zone: Implications for salmon embryo survival. River Research Applications 21: 977-989.

Mansell, M.G and Hussey, S.W. 2005. An investigation of flows and losses within the alluvial sands of ephemeral rivers in Zimbabwe. Journal of Hydrology 314 (2005) 192-203

McCartney, MP, Neal, C, and Neal, M. 1998. Use of deuterium to understand runoff generation in a headwater catchment containing a dambo. Hydrological and Earth System Sciences 2,1: 65-76.

McDonnell, JJ, McGuire, K, Aggarwal, P, Beven, KJ, Biondi, D, Destouni, G, Dunn, S, James, A, Kirchner, J, Kraft, P, Lyon, S, Maloszewski, P, Newman, B, Pfister, L, Rinaldo, A, Rodhe, A, Sayama, T, Seibert, J, Solomon, K, Soulsby, C, Stewart, M, Tetzlaff, D, Tobin, C, Troch, P, Weiler, M, Western, A, Worman, A, and Wrede, S. 2010. How old is streamwater? Open questions in catchment transit time conceptualization, modelling and analysis. Hydrol. Process. 24: 1745-1754.

McGlynn, BL, and McDonnell, JJ. 2003. Quantifying the relative contributions of riparian and hillslope zones to catchment runoff. Water Resources Research 39, 11: 1310.

McLoughlin, C., Deacon, A., Sithole, H., & Gyedu-Ababio, T. (2011). History, rationale, and lessons learned: Thresholds of potential concern in Kruger National Park river adaptive management. Koedoe – African Protected Area Conservation and Science, 53(2), 1-27. doi:10.4102/koedoe.v53i2.996

Michaelides, K, and Chappell, A. 2009. Connectivity as a concept for characterising hydrological behaviour. Hydrological Processes 23: 517-522.

Nadeau, TL, and Rains, MC. 2007. Hydrological Connectivity Between Headwater Streams and Downstream Waters: How Science Can Inform Policy. Journal of the American Water Resources Association 43,1:118-133.

Noguchi, S, Tsuboyama, Y, Sidle, RC and Hosoda, I. 1999. Morphological Characteristics of Macropores and the Distribution of Preferential Flow Pathways in a Forested Slope Segment. Soil Sci. Soc. Am. Journal 63: 1413-1423.

Nuttle, WK. 2002. Is ecohydrology one idea or many? Hydrological Sciences Journal 47,5: 805.

O'Keefe, J., Rogers, KH (2003) Heterogeneity and Management of the Lowveld Rivers. In Du Toit, J. T., Rogers, K. & Biggs, H. C. (Eds.) The Kruger Experience. Ecology and Management of Savanna Heterogeneity. Washington DC, Island Press.

Ogunkoya, OO. and Jenkins, A.1993. Analysis of storm hydrograph and flow pathways using a three component hydrograph separation model. Journal of Hydrology, Volume 142,71-88.

Parsons, M., McLoughlin, C. Rountree, MW., Rogers, KH (2006) The biotic and abiotic legacy of a large infrequent flood disturbance in the Sabie River, South Africa. River Research and Applications, 22(2), 187-201. doi:10.1002/rra.905

Petersen, R. (2011) Pers Comm relating to unpublished data for MSc in Geohydrology at the University of Western Cape

Praamsma, T, Novakowski, K, Kyser, K, Hall, K . 2009. Using stable isotopes and hydraulic head data to investigate groundwater recharge and discharge in a fractured rock aquifer. Journal of Hydrology 366: 35-45.

Pringle, C. 2003. What is hydrologic connectivity and why is it ecologically important? Hydrological Processes Journal 17: 2685-2689.

Renshaw, C. 2010. HydroToolBox Excel Add-in, version 1.4. www.dartmouth.edu/renshaw/hydrotoolbox/

Riddell, ES, Everson, C, Clulow, A, and Mengistu, M. 2013. The hydrological characterisation and water budget of a South African rehabilitated headwater wetland system. Water SA 39, 1: 0378-4738.

Rivers-moore, NA., Jewitt, GPW (2004). Intra-annual thermal patterns in the main rivers of the Sabie Catchment , Mpumalanga , South Africa. Water SA, 30(4), 445-452.

Rodriguez-Iturbe, I (2000) Ecohydrology: A hydrologic perspective of climate-soil-vegetation dynamies, Water Resources Research, 36(1)

Rogers, KH., O'Keeffe, J (2003) River Heterogeneity: Ecosystem Structure, Function & Management. In Du Toit, J. T., Rogers, K. & Biggs, H. C. (Eds.) The Kruger Experience. Ecology and Management of Savanna Heterogeneity. Washington DC, Island Press.

Sankaran M et al. (2005) Determinants of woody cover in African savannas., Nature, 438, (7069), 846-9

Schroder, B. 2006. Pattern, process, and function in landscape ecology and catchment hydrology – how can quantitative landscape ecology support predictions in ungauged basins? Hydrol. Earth Syst. Sci. 10: 967-979.

Šimůnek, J, Šejna, M, Saito, H, Sakai M, and van Genuchten, MTh. (2013) The HYDRUS-1D Software Package for Simulating the Movement of Water, Heat, and Multiple Solutes in Variably Saturated Media, Version 4.17, HYDRUS Software Series 3, Department of Environmental Sciences, University of California Riverside, Riverside, California, USA, pp. 342.

Sophocleous, M. 2002. Interactions between groundwater and surface water: the state of the science. Hydrogeology Journal 10:52-67.

Soulsby, C, Neal, C, Laudon, H, Burns, DA, Merot, P, Bonell, M, Dunn, SM, and Tetzlaff, D. 2008. Catchment data for process conceptualization: simply not enough? Hydrological Processes Journal 22: 2057-2061.

Sklash, MG, and Farvolden, RN. 1979. The Role of Groundwater in Storm Runoff. Journal of Hydrology 43: 45-65.

Sivapalan, M. 2005. Process, Pattern and Function: Elements of a Unified Theory of Hydrology at Catchment Scale. In: ed. Anderson, MG, Encyclopaedia of Hydrological Sciences, John Wiley and Sons. Crawley, Australia.

Smit, I.P.J., Riddell, E.S., Cullum, C. & Petersen, R., 2013, 'Kruger National Park research supersites: Establishing long-term research sites for cross-disciplinary, multiscaled learning', Koedoe 55(1), Art. #1107, 7 pages. http://dx.doi.org/10.4102/koedoe.v55i1.1107

Smithers J and Schulze RE. (1995) ACRU Agrohydrological Modelling System User Manual. WRC Report TT 70/95, Water Research Commission, Pretoria.

Smithers, JC., Schulze, RE., Pike, A., Jewitt, GPW (2001). A hydrological perspective of the February 2000 floods : A case study in the Sabie River Catchment. Water SA, 27(3), 325-332.

Shanley, JB, Kendall, C, Smith, TE, Wolock, DM, and McDonnell, JJ. 2002. Controls on old and new water contribution to streamflow at some nested catchments in Vermont, USA. Hydrological Processes Journal.16, 589-609.DOI: 10.1002/hyp.312.

Tetzlaff, D, Carey, SK, Laudon, H, McGuire, K. 2010. Catchment processes and heterogeneity at multiple scales – benchmarking observations, conceptualization and prediction. Hydrological Processes 24: 2203-2208.

Tetzlaff, D, Waldron, S, Brewer, MJ, and Soulsby, C. 2007. Assessing nested hydrological and hydrochemical behaviour of a mesoscale catchment using continuous tracer data. Journal of Hydrology 336: 430-443.

Uhlenbrook, S. and Hoeg, S.2003. Quantifying uncertainties in tracer-based hydrograph separations: a case study for two-, three- and five-component hydrograph separations in a mountainous catchment. Hydrological Processes. Hydrol. Process. 17, 431-453.

Uhlenbrook, S, Wenninger, J, and Lorentz, S. 2005. What happens after the catchment caught the storm? Hydrological processes at the small, semi-arid Weatherley catchment, South-Africa. Advances in Geosciences, 2, 237-241.

USGS. (2008) Standard operating procedure for continuous measurement of discharge. NPDES CM 1000. USGS Publication.

Van der Scheur, W (2001) Characterisation of soil-water-plant-dynamics of plant ecotopes on the Northern Plains in the Kruger National Park. Unpublished MSc Thesis, Wageningen University, The Netherlands, October 2001 pp112

van Genuchten, MT, Leij, FJ and Yates, SR. (1991) The RETC code for quantifying the hydraulic functions of unsaturated soils. EPA/600/2-91/065. RS Kerr Environmental Research Laboratory, US environmental Protection Agency, Oklahoma, USA.

van Tol, (2008) Soil indicators of hillslope hydrology in the Bedford and Weatherly catchments. Personal Communication relating to unpublished data for MSc in Agriculture at the University of Free State.

Van Tol, JJ, Le Roux, PAL, Lorentz, SA, Hensley, M. (2013) Hydropedological Classification of South African Hillslopes. Vadose Zone Journal. doi:10.2136/vzj2013.01.0007

Van Wyk, E, Van Tonder, GJ and Vermeulen, D. 2011. Characteristics of local groundwater recharge cycles in South African semi-arid hard rock terrains – rainwater input. Water SA Vol. 37 No. 2.

Van Wyk, E, Van Tonder, GJ and Vermeulen, D. 2012. Characteristics of local groundwater recharge cycles in South African semi-arid hard rock terrains: Rainfall-groundwater interaction. Water SA Vol. 38 No. 5.

Venter, FJ (1990) A classification for land management planning in the Kruger National Park. PhD Thesis. Pretoria, University of South Africa. pp394

Venter, FJ, Scholes, RJ and Eckhardt, HC. 2003. The abiotic template and its associated vegetation pattern. In: eds. Du Toit, JT, Rogers, KH and Biggs, HC, *The Kruger experience: Ecology and management of savanna heterogeneity*, Ch. 5, 83-129. Island Press, Washington, D.C., USA.

Wagener, T, Sivapalan, M, and McGlynn, B. 2008. Catchment Classification and Services – Toward a New Paradigm for Catchment Hydrology Driven by Societal Needs. In: Anderson, MG, Encyclopaedia of Hydrological Sciences. John Wiley & Sons. New York, USA.

Walter, H. (1971) Ecology of tropical and subtropical vegetation. Oliver and Boyd, Edinburgh, UK.

Waters, R, Allen, R, Bastiaanssen, W, Tasumi, M and Trezza, R. 2002. SEBAL-Surface Energy Balance Algorithm for Land, Advanced Training and User's Manual. Funded by a NASA EOSDIS/Synergy grant from the Raytheon Company through The Idaho Department of Water Resources.

Weddepohl, JP (1998) as cited in Schulze, RE., Schmidt, EJ., Smithers, JC (1993) SCS-SA User Manual: University of Natal, Pietermaritzburg, Department of Agricultural Engineering.

Wenninger, J, Uhlenbrook, S, Lorentz, S, and Leibundgut, C. 2008. Identification of runoff generation processes using combined hydrometric, tracer and geophysical methods in a headwater catchment in South Africa Hydrological Sciences Journal 53(1).

Winter, TC.2007. The role of groundwater in generating streamflow in headwater areas and in maintaining base flow. Journal of the American Water Resources Association, Vol. 43, Number 1, 102-115.

Uchida, T, Van Meerveld, IT, McDonnell, JJ. 2005. The role of lateral pipe flow in hillslope runoff response: An intercomparison of non-linear hillslope response. Journal of Hydrology 311: 117-133.

Yokoo, Y. Sivapalan, M. (2011) Towards reconstruction of the flow duration curve: development of a conceptual framework with a physical basis. *Hydrology and Earth System Science* 15 2805-2819

Younger, PL. 2006. Groundwater in the Environment: An Introduction. Blackwell. Newcastle Upon Tyne.

Zhang, L. (2002) Modelling and prediction. Hydrological Processes 13: doi:10.1006/rwas.2002.0172. University of Nevada – Las Vegas, Department of Geoscience, Las Vegas, NV 89154, USA.